ISSN 2542-2049

Saint-Petersburg State University

15 International School-Conference

Magnetic resonance and its applications

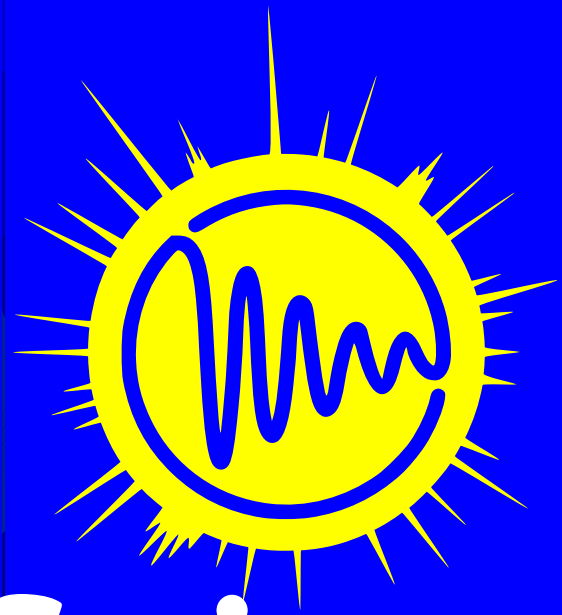

Spinus

1 — 6 April 2018

Saint-Petersburg, Russia

SAINT PETERSBURG STATE UNIVERSITY
Department of Nuclear Physics Research Methods

15th International School-Conference

MAGNETIC RESONANCE AND ITS APPLICATIONS

Abstracts

an AMPERE event

April 1-6, 2018
Saint Petersburg, Russia

Magnetic resonance and its applications. Spinus - 2018.
Abstracts book. Sant Petersburg State University, 2018. 280 pp.

ISSN 2542-2049

Schola **Spinus**

15th International School-Conference
MAGNETIC RESONANCE AND ITS APPLICATIONS
SPINUS-2018

ORGANIZING COMMITTEE

Chairman	Dr. Sci. Denis Markelov, associate professor, SPSU
Vice-chairman	Alexander Ievlev, researcher, SPSU
Committee members	Dr. Andrey Egorov, associate professor, SPSU Dr. Andrey Komolkin, associate professor, SPSU Andrei Chudin, assistant researcher, SPSU Dr. Pavel Kupriyanov, engineer, SPSU Konstantine Tutukin, senior teacher, SPSU Timofey Popov, SPSU
Layout of Abstracts Book	Aleksandr Levantovskii

CONTACTS

1, Ulyanovskay st., Peterhof, 198504, St. Petersburg, Russia
Department of Nuclear Physics Research Methods
St. Petersburg State University

Tel.	+7-953-350-0640
Fax	+7-812-428-7240
E-mail	spinus@spinus.spb.ru
Website	http://spinus.spb.ru/

PROGRAM COMMEETEE

SCIENTIFIC ADVISER OF THE SCHOOL-CONFERENCE

Vladimir Chizhik	Honored scientist of Russia, Professor, SPSU

ADVISORY BOARD

V. Balevicius	Professor, Vilnius, Lithuania
Yu. M. Bunkov	Professor, Kazan Federal University, Russia
V. I. Chizhik	Professor, St. Petersburg State University, St. Petersburg, Russia
S. V. Dvinskikh	Professor, Royal Institute of Technology, Stockholm, Sweden
J. Fraissard	Professor, University Pierre and Marie Curie, Paris, France
L. Yu. Grunin	Associate Professor, CEO, Resonance Systems, Russia
E. Lahderanta	Professor, Lappeentanta Technical University, Finland
D. Michel	Professor, Leipzig University, Germany
B. Rameev	Professor, Gebze Technical University, Turkey
N. R. Skrynnikov	Professor, St. Petersburg University, Russia, Purdue University, USA
M. S. Tagirov	Professor, Kazan Federal University, Russia
S. Vasiliev	Professor, University of Turku, Finland

Spinus

Contents

Schedule of Spinus-2018

	01.04.18 Sunday	02.04.18 Monday	03.04.18 Tuesday	04.04.18 Wednesday	05.04.18 Thursday	06.04.18 Friday	07.04.18 Saturday
08:45 – 10:00		**BREAKFAST**				**9:10-10:30 BREAKFAST**	**BREAKFAST**
10:00 – 11:30		**Registration 30** **Opening 10** **Chizhik 30** ***GROUP PHOTO 20***	**Fujara 40** Privalov 20 Chertkov 15 Ryzhov 15	***Excursion day***	**Cabal 40** Svyatova 15 Mikhailovskaya 15 Drozdov 20	**Vasiliev 40** Mozzhukhin 20	**Departure**
11:30 – 12:00		**COFFEE BREAK**			**COFFEE BREAK**		
12:00 – 14:00		**Papavassiliou 40** **Varela 40** **Dvinskikh 40**	**Fraissard 40** **Michel 40** **Rameev 40**		Schepkens 20 Dallons 20 Kumaravel 20 **Skrynnikov 40** Kharkov 20	Atta 20 Krylova 15 Pokochueva 15 Marchenko 15 Ievlev 15 Babanova 20 Okrugin 20	
14:00 – 15:30		**LUNCH**			**LUNCH**		
15:30 – 17:00		Bystrov 15 Baranauskaite 15 Shuvarakova 15 Dolgorukov 15 Mamadazizov 15 Zorin 20	Oral blitz reports of young scientists (5min x 14) Lahderanta 20		Oral blitz reports of young scientists (5min x 18)	Dolgushev 20 Shpotya 20 Zinkevich 20 Kosenkov 15 Neronov 15	
17:00 – 17:30	**Registration of participants**	**COFFEE BREAK**			**COFFEE BREAK**		
17:30 – 19:00		Izmailov 15 Rabdano 15 Semisalova 20 Grunin 20 Kachala 20	**POSTER SESSION I**		**POSTER SESSION II**	Kulagina 20 **Samoson 40** **Awarding Closing**	
19:00 – 20:00	**Welcome**	**DINNER**				**DINNER**	
20.00		**Cultural and sporting activities**		**Round table Chairman: Sergeyev**	**CONFERENCE DINNER**		

Schedule

15-th International School-Conference

«Magnetic Resonance and its Applications. Spinus-2018»

April 01-06, 2018

St. Petersburg

SUNDAY – 01 April 2018	
14:00 – 15:30	**LUNCH**
15:30 – 19:00	**REGISTRATION OF PARTICIPANTS**
19:00 –	**WELCOME PARTY «*EVENING IN KARELIA*»**

	MONDAY – 02 April 2018
08:45 – 10:00	**BREAKFAST**
10:00 – 10:30	**Registration**
10:30 – 10:40	**Opening**
10:40 – 11:10	**Vladimir I. Chizhik (St. Petersburg, Russia)** **Lecture:** Some Problems of Quantitative Analysis by NMR Method
11:10 – 11:30	***GROUP PHOTO***
11:30 – 12:00	**COFFEE BREAK**
12:00 – 12:40	**Georgios Papavassiliou (Athens, Greece)** **Lecture:** Freezing Polarons and the Quantum Liquid-Crystal Phase in Ferromagnetic Metallic Manganites. A combined NMR and HRTEM study in the temperature range 3.2K to 1000K
12:40 – 13:20	**Luis Miguel Varela (Santiago de Compostela, Spain)** Lecture: Computer simulation of ionic liquids
13:20 – 14:00	**Sergey V. Dvinskikh (Stockholm, Sweden)** **Lecture:** Strategies for measuring 13C-15N dipole-dipole couplings in liquid crystalline samples with natural isotropic abundance
14:00 – 15:30	**LUNCH**
15:30 – 15:45	**Sergei S. Bystrov (St. Petersburg, Russia)** Influence of residual water on NMR-relaxation in ionic liquids on basis of [bmim]+ cation
15:45– 16:00	**Valeriia E. Baranauskaite (St. Petersburg, Russia)** NMR studies of the 'water-in-salt' ternary LiCl-CsCl-D2O system
16:00– 16:15	**Ekaterina I. Shuvarakova (Novosibirsk, Russia)** EPR study of electron-acceptor sites during dehydrochlorination of 1-chlorobutane over metal oxides
16:15– 16:30	**Gleb Dolgorukov (Kazan, Russia)** Atomic-scale probing of paramagnetic centers in nanodiamonds by 3He NMR at low temperature
16:30– 16:45	**Sultonazar Mamadazizov (Kaliningrad, Russia)** Multiexponential distribution of 14N NQR relaxation times in tetrazole derivatives
16:45– 17:05	**Vadim Zorin (Santiago de Compostela, Spain)** Global Spectrum Deconvolution and its applications in NMR spectroscopy

17:05 – 17:30	**COFFEE BREAK**
17:30 – 17:45	**Sergei A. Izmailov (St. Petersburg, Russia)** EPR spectra simulation from MD data using Redfield theory and direct propagation method
17:45 – 18:00	**Sevastyan O. Rabdano (St. Petersburg, Russia)** Dynamic modes in spin-labeled protein revealed by MD simulations: experimental and computed EPR spectra
18:00 – 18:20	**Anna S. Semisalova (Drezden, Germany)** Ferromagnetic resonance study of FeRh thin films near the antiferromagnetic-ferromagnetic phase transition
18:20 – 18:40	**Leonid Y. Grunin (Yoshkar-Ola, Russia)** Fast Technique for Crystallinity Estimation of Solids by the Transverse Magnetization and Double Quantum Relaxation
18:40– 19:00	**Vadim V. Kachala (Moscow, Russia)** How to optimize NMR approach for structure elucidation of small molecules on Bruker spectrometers
19:00 – 20:00	**DINNER**
20:00 –	**CULTURAL AND SPORTING ACTIVITIES**

	TUESDAY – 03 April 2018
08:45 – 09:45	**BREAKFAST**
10:00 – 10:40	**Franz Fujara (Darmstadt, Germany)** Lecture: 1H NMR at Larmor frequencies down to 3 Hz by means of Field-Cycling
10:40 – 11:00	**Alexei F. Privalov (Darmstadt, Germany)** Fast Field cycling as a tool for studying molecular dynamics in solids
11:00 – 11:15	**Vyacheslav A. Chertkov (Moscow, Russia)** Vibration effects in NMR spectroscopy for studies of ultra fast conformational dynamics
11:15 – 11:30	**Vyacheslav A. Ryzhov (St. Petersburg, Russia)** Magnetic phase separation and its temperature evolution in porous carbon-based nanomaterials doped by Au and Co
11:30 – 12:00	**COFFEE BREAK**
12:00 – 12:40	**Jacques Fraissard (Paris, France)** **Lecture**: NMR studies of metal particles
12:40 – 13:20	**Dieter Michel (Leipzig, Germany)** **Lecture:** Solid State NMR in nanosized systems: MAS NMR studies in combination with pulsed field gradient techniques
13:20 – 14:00	**Bulat Rameev (Gebze, Turkey)** **Lecture**: Combination of Microwave & NMR Techniques for Effective Detection of Dangerous Materials
14:00 – 15:30	**LUNCH**
15:30 – 16:40	Oral blitz reports of young scientists (5min x 14); see speakers below in the list of **POSTER SESSION I**
16:40–17:00	**Erkki Lahderanta (Lappeenranta, Finland)** Masters Degree Programme in Lappeenranta
17:00 – 17:30	**COFFEE BREAK**
17:30 – 19:00	**POSTER SESSION I**
19:00 – 20:00	**DINNER**
20:00 –	**CULTURAL AND SPORTING ACTIVITIES**

	WEDNESDAY – 04 April 2018
08:45 – 09:45	**BREAKFAST**
	EXCURSION DAY
19:00 – 20:00	**DINNER**
20:00 –	**Round table:** "PROBLEM BOOKS ON NMR SPECTROSCOPY" **Chairman: Nickolai M. Sergeyev (Moscow, Russia)**

	THURSDAY – 05 April 2018
08:45 – 09:45	**BREAKFAST**
10:00 – 10:40	**C. Cabal Mirabal (Havana, Cuba)** **Lecture**: MRI basics and application
10:40 – 10:55	**Alexandra Svyatova (Novosibirsk, Russia)** In situ NMR/MRI of Hyperpolarized Molecules
10:55 – 11:10	**Anna Mikhailovskaya (St. Petersburg, Russia)** An inductively-coupled volumetric resonator based on wire metamaterials for local sensitivity enhancement on a 3 T MRI system
11:10 – 11:30	**Andrey A. Drozdov (St. Petersburg, Russia)** Evaluation the delayed contrast enhancement as a tool for the differential diagnostics between brain metastases and neurotoxoplasmosis
11:30 – 12:00	**COFFEE BREAK**
12:00 – 12:20	**Corentin Schepkens (Mons, Belgium)** In vitro and in vivo applications of 1H-NMR spectroscopy in the biological field
12:20 – 12:40	**Matthieu Dallons (Mons, Belgium)** Study of the metabolic doxorubicine-induced alterations in H9C2 cells and the effect of preincubation with dexrazoxane, a cardioprotective agent
12:40 – 13:00	**Kaliaperumal Kumaravel (Guangzhou, China)** Isolation and Characterization of Bioactive Secondary Metabolites from the Deep Sea Derived Fungi *Penicillium* sp. SCSIO.XWFO1254
13:00 – 13:40	**Nikolai R. Skrynnikov (West Lafayette, USA)** **Lecture:** Many faces of disulfide bond
13:40 – 14:00	**Boris Kharkov (St. Petersburg, Russia)** Skin-Effect Compensated Optimal Control Pulses for Excitation in a Conductive Medium
14:00 – 15:30	**LUNCH**
15:30 – 17:00	Oral blitz reports of young scientists (5min x 18); see speakers below in the list of **POSTER SESSION II**
17:00 – 17:30	**COFFEE BREAK**
17:30 – 19:00	**POSTER SESSION II**
20:00 –	**CONFERENCE DINNER**

	FRIDAY – 06 April 2018
09:10 – 10:30	**BREAKFAST**
10:30 – 11:10	**Sergey A. Vasiliev (Turku, Finland)** **Lecture**: DNP of shallow donors in silicon at ultra-low temperatures
11:10 – 11:30	**Georgy V. Mozzhukhin (Gebze, Turkey**) Low Field 14N Nuclear Magnetic Resonance Detection of Liquid Substances
11:30 – 12:00	**COFFEE BREAK**
12:00 – 12:20	**Ramadan Atta (Damietta, Egypt)** Physical and transport properties of the novel dense membranes based on Polysulfone/Pluronic F127 composite
12:20– 12:35	**Ekaterina Krylova (St. Petersburg, Russia)** Dehydration/rehydration processes in sodium- and copper-exchanged mordenites studied by TGA and NMR
12:35 – 12:50	**Ekaterina V. Pokochueva (Novosibirsk, Russia)** NMR signal enhancement in hydrogenation reactions with parahydrogen
12:50 – 13:05	**Sergei A. Marchenko (St. Petersburg, Russia)** Complete assignment in 1H NMR spectra and conformational analysis of some modified triterpenoids in solution.
13:05 – 13:20	**Alexandr V. Ievlev (St. Petersburg, Russia)** Analysis of NMR spectra of ionic liquid EAN with the addition of inorganic salts
13:20 – 13:40	**Olga A. Babanova (Ekaterinburg, Russia)** Dynamical properties of novel imidazolate borohydrides: NMR studies
13:40 – 14:00	**Boris M. Okrugin (St. Petersburg, Russia)** Influence of the charged peptide dendrigrafts topology on the large-scale properties and their internal structure
14:00 – 15:30	**LUNCH**
15:30 – 15:50	**Maxim Dolgushev (Paris, France)** NMR relaxation of fractal macromolecules
15:50 – 16:10	**Valeriya A. Shpotya (Moscow, Russia)** Determination of the structure of hyperbranched polyester boltorn and its derivatives with l-lactide and methyl ether of polyethylene glycol using NMR-spectroscopy methods
16:10 – 16:30	**Tatiana Zinkevich (Karlsruhe, Germany)** 7Li diffusion in solid electrolytes as studied by NMR spectroscopy

16:30 – 16:45	**Denis D. Kosenkov (St. Petersburg, Russia)** NMR relaxometer for the estimation of the spin-spin proton relaxation time of the living tissue
16:45 – 17:00	**Yuriy I. Neronov (St. Petersburg, Russia)** An estimate of the change in the spin-spin relaxation time of protons of living tissue upon its cooling
17:00 – 17:30	**COFFEE BREAK**
17:30 – 17:50	**Tatiana P. Kulagina (Chernogolovka, Russia)** Topological Structure and Mobility of Polymer Chains in Branched Poly(meth)acrylates Studied by NMR
17:50 – 18:30	**Ago Samoson (Tallinn, Estonia)** **Lecture**: New MAS Technologies
18:30 – 19:00	**AWARDING CLOSING**
19:00 – 20:00	**DINNER**

	SATURDAY – 07 April 2018
08:45 – 09:45	**BREAKFAST**
	DEPARTURE

POSTER SESSION I (Tuesday, 17:30 – 19:00)		
1*	Ganina Tatyana	Dynamic Structure of Noradrenalin According to NMR Data and Quantum Mechanical Calculations
2*	Avila Salazar Dahiana Andrea	Structure-dissolution relationships in Co(II)-containing phosphate glasses
3*	Khusnutdinova Naira	Analysis of correlation functions by method of molecular dynamics
4*	Bogdanov Dmitrii	Fe/Ag bimetallic system supported on mordenites: EPR, NMR and Mössbauer study
5*	Filippova Anna	Synthesis of sulfonated phthalocyanine complexes having triazole and naphthyl fragments
6*	Beshanov Vsevolod	Molecular dynamics simulations of alkylammonium nitrate ionic liquids. The effect of nitrate-anion model parameters
7*	Matsidon Maria	Hydrogen/deuterium isotope effects on water molecule mobility. A molecular dynamics simulation study
8*	Agureeva Angelina	Influence of polysaccharide shell on magnetic resonance relaxation and colloidal stability of SPIONs nanosuspension
9*	Kostin Mikhail	Quantum-mechanical calculations of hydrogen-bonded complexes of phosphine oxide H3PO with various proton donors
10*	Efimova Aleksandra	MRI study of the influence of superparamagnetic iron oxide nanoparticles (SPIONs) entrapped in cellulose microbeads on the relaxation properties of water in agarose matrix
11*	Kerner Anastasiya	Synthesis of phthalodinitriles having bifunctionally-substituted fragments
12*	Edinach Elena	Aluminum and gallium nuclei as microscopic probes for pulsed ENDOR diagnostics in garnet ceramics doped with paramagnetic ions
13*	Dmitriev Alexander	Ultra-narrow low-field nuclear spin resonance in NV centers in bulk diamond crystal

14*	Likerov Rodion	Investigation of neodymium doped YVO4 with EPR method
15*	Ovcherenko Sergey	The Dynamics of Lactaptin in solution by NMR
16*	Vladislav Stanishevsky	High Resolution NMR Spectra and Dynamic Structure of Vinylcyclopropane
17*	Knapkiewicz Magdalena	Collective dynamics in various antiferroelectric liquid crystal mesophases probed by NMR relaxometry
18	Kupriyanova Galina	71Ga, 77Se, 115In MAS NMR study of TlGaSe2 and TlInSe2 powder
19	Pavchenko Maxim	Determination of the fine structure of the spiro-carboheterocycle using NMR spectroscopy and X-ray diffraction analysis
20	Khusnutdinov Rustem	The possibility of nuclear quadrupole resonance for distinguishing paracetamol different manufacturers and different forms (parties) from the same manufacturer of the spectral characteristics
21	Kukin Nikolay	Definition of the NV-centers orientations relatively to the crystal plane
22	Deriglazov Vladimir	Characterization of complex superparamagnetic colloids by electron magnetic resonance (EMR) and second-harmonic magnetic response (M2)
23	De Luca Deborah, Tagliatti Vanessa, and Delsinne Virginie	The application of the metabonomic approach to predict drug-induced liver injury: the case of acetaminophen and its non-toxic isomer
24	Solonинin Alexey Viktorovich	NMR study of reorientational motion in borohydrides of Mg(BH4)2
25	Tertyshnaya Yulia	Molecular mobility of polylactide investigated by electronic paramagnetic resonance
26	Kupriyanov Pavel	Neutralization of fluctuations in resonance conditions during registration of NMR spectra in the Earth's magnetic field

* *Oral blitz reports of young scientists before POSTER SESSION I*

POSTER SESSION II (Thursday, 17:30 – 19:00)		
1*	Mulloyarova Valeriya	Cyclic trimers of phosphinic acids: symmetry, chirality, proton transfer and H/D isotope effects on NMR chemical shifts
2*	Salikov Vladislav	Optimization of bacterial expression of MdmX N-terminal domain for NMR studies
3*	Kuzminova Anna	Novel mixed –matrix membrane based on composite PVA - carboxyfullerene: preparation and characterization
4*	Vasin Semen	Preparation and Characterization of Polysulfone/Pluronic F127 ultrafiltration membranes
5*	Garkavyi Stanislav	Inhomogeneous magnetic state in mechanochemically synthesized nanopowder sample of CuFeS2 according to 63,65Cu NMR spectrum in the local field
6*	Bogdan Andrey	Comparison of MRS and PET data in neurodegenerative disoders.
7*	Dorian Maroil	Exploration of the hypothyroidic effect of Sunitinib, a tyrosine kinase receptor inhibitor, by metabolomic approach, in the rat
8*	Muradova Anna	Definition of the NV-centers orientations relatively to the crystal plane
9*	Korchevaya Irina	Definition of the NV-centers orientations relatively to the crystal plane
10*	Dmitrenko Mariia	Investigation and characterization of mixed–matrix membranes based on composite PVA - fullerenol
11*	Ovcherenko Sergey	The determination of the relaxation properties of the emulsion consisted of proxyl type nitroxide radicals proposed as MRI contrast agent
12*	Nikitina Anastasia	Investigation of MRI contrast efficiency and aggregation stability of magnetic nanoparticles by NMR-relaxometry
13*	Pichugina Alina	1H NMR and ESR studies of the mechanism of gallstones formation

14*	Popova Elena	Effect of dendrimer generation on the kinetics of peptide complex formation
15*	Mershiev Ivan	14N NQR with Frank sequence excitation
16*	Belyakov Denis	Development of a standard base for the "medium" and "strong" constant field's magnetic induction measurement
17*	Pelipko Vasilii	1H, 13C, 15N NMR spectroscopy in the study of the structure of alkyl 3-nitropropanoates containing one asymmetric carbon atom in the structure
18*	Lushpinskaya Irina	Calculation of the magnetic shielding tensor on 125Te and 207Pb nuclei in PbTe
19*	Sheveleva Nadezhda	Study of Local Orientation Mobility in Lysine Dendrimers by NMR method
20*	Ubovich Milosh	Small-angle x-ray scattering profile of the two-domain Pax-5 protein in aqueous solution by molecular dynamics simulations
21*	Ievleva Svetlana	DWI/PWI Techniques of MRI
22*	Shavykin Oleg	Influence of the asymmetry of branching on the structural properties of dendrimers. Brownian dynamics simulation
23	Tsyro Larisa	Research of kern of an electronic spin resonance method
24	Demidov Viktor	Investigation of the electron-rich binuclear Pt(II) 1,10-phenanthrocyanine [(py)2Pt(μ-phencyanine—)Pt(py)2]Cl3 by the ESR method. Localization of PSC in temperature accessible electron-excited radical states
25	Bogachev Yury	55 Years of EPR laboratory at St.-Petersburg Electrotechnical University “LETI”
26	Drozdovskii Andrey	Investigation of spin-wave oscillators

* *Oral blitz reports of young scientists before POSTER SESSION II*

Spinus

Welcome to the School-Conference "Spinus" of Saint Petersburg State University

The St. Petersburg State University (SPbSU) holds International School-Conference "Magnetic resonance and its application" Spinus-2018 in the 15th time. "Spinus" is organized in according to the subjects of researches and master's degree programs, which are developed and implemented in the SPbSU. In modern physics, the term "magnetic resonance" refers to a set of phenomena accompanied with the emission or absorption of electromagnetic waves of the radiofrequency diapason by quantum systems (nuclei, electrons, atoms, molecules, etc.). These phenomena, the physical nature of which is of independent interest, provided the basis of radiospectroscopic methods for studying the structure of matter and physical-chemical processes in it. They are also used for the creation of quantum generators, amplifiers, and magnetometers. For the development of ideas and applications of magnetic resonance six Nobel Prizes were awarded in the areas of physics, chemistry, biology, physiology and medicine (the latter was in 2003).

Primarily, magnetic resonance methods are:

- Nuclear Magnetic Resonance (NMR)
- Electron Paramagnetic Resonance (EPR)
- Nuclear Quadrupole Resonance (NQR)

These methods, being contactless, do not destroy an object under a study, that makes them unique and in demand not only in physics and chemistry, but also in medicine, geology, biology, archeology. Now, any medical center with high reputation has a magnetic resonance imaging (MRI). In Russia, NMR is used in oil well logging, laboratory analysis of the productivity of oil-bearing reservoirs, analysis of oil content and moisture of seeds; EPR technique is used for geological research, non-destructive control of precious stones; there are NQR applications for remote detection of solid explosives and narcotics. Magnetometry methods based on magnetic resonance are indispensable for carrying out archaeological researches.

The designation "school-conference" means that, on the one hand, the organizers include in the program the lectures, which reflect the basics of magnetic resonance and current state of knowledge and experience in this field, and, on the other hand, as well as at any conference it is expected to discuss new results, obtained by young scientists, using magnetic resonance techniques. It should be emphasized that our school-conference aims not only to researchers specializing in the field of magnetic resonance, but also to representatives of other sciences, where these methods can be successfully applied.

Earlier the school organizers worked at the Department of quantum magnetic phenomena (QMPh) of the St. Petersburg State University, which was founded in 1993 on the initiative of Professor V. I. Chizhik on the basis of the laboratory, created in the 50s of the last century by F. I. Skripov at the Department of Radio Physics (the branch "Quantum Radiophysics"). On January 1, 2014, the Department of QMPh joined the united Department of nuclear-physics research methods (Head of the Department is Corresponding Member of the Russian Academy of Sciences, Professor Mikhail Kovalchuk). The QMPh collective has a number of priority works in the field of nuclear magnetic resonance. One of the most significant achievements was the first in the world implementation (in 1958) of the Fourier transform of a free induction signal in order to obtain a NMR spectrum. Concurrently with the research activity, the staff of the department are actively involved in the development of practical applications of magnetic resonance. The department graduates work not only in Russia and the CIS, but also in Sweden, USA, New Zealand, England, Germany, France, Italy, occupying positions from a highly advanced operator of radiospectrometers to a professor.

The main research areas developing in the team of quantum magnetic phenomena:

- Nuclear magnetic relaxation in liquids;
- Nuclear magnetic resonance in solids, including magnetically ordered materials;
- NMR in liquid crystals;
- NMR in heterogeneous systems;
- MRI in weak magnetic fields;
- Electron paramagnetic resonance;
- Nuclear magnetic resonance in the magnetic field of the Earth;
- The quantum magnetometry in archeology.

It is evident from the above that the scope of our research interests is quite wide. We are always open for the collaboration with researchers from various fields of science.

Our team has published a series of monographs, textbooks and training manuals on Magnetic Resonance. For example:

1. Vladimir I. Chizhik, Yuri S. Chernyshev, Alexey V. Donets, Viatcheslav Frolov, Andrei Komolkin, Marina G. Shelyapina. Magnetic Resonance and Its Applications. 2014, Springer-Verlag. 782 pp. *(Now about 25000 downloads).*
2. Квантовая радиофизика: магнитный резонанс и его приложения. Учеб. пособие. 2-е изд., перераб. Под ред. В. И. Чижика. – СПб.: Изд-во С.-Петерб. ун-та, 2009. 700 с.
3. В. И. Чижик. Ядерная магнитная релаксация. Учеб. пособие. 3-е изд. – СПб.: Изд-во С.-Петерб. ун-та, 2004. 388 с.
4. Практикум по магнитному резонансу. Учебное пособие. Под ред. В. И. Чижика. – СПб.: Изд-во С.-Петерб. ун-та, 2003. 184 с.

The Organizing committee
of the 15th School-conference
"Magnetic resonance and its applications" Spinus-2018

Lectures

Kinetics studies of complex biomedical process by Magnetic Resonance. Cuban experiences

Carlos Cabal Mirabal[1,2], Adolfo Fernandez Garcia[1], Manuel Lores Guevara[1], Evelio Gonzalez[2], Leonardo Oramas Diaz[2]

[1]Medical Biophysics Center, University of Oriente, Cuba.
[2]Center for Genetic Engineering and Biotechnology, Cuba.

The potentials of the Magnetic Resonance (MR) methods in the research of biomedical system have been demonstrated during the 70 years of their existence. The Cuban experiences concerning to quantitative MR associated with molecular, preclinical and clinical studies of significant diseases and the drug development are presented.

MR "in vitro" and "in vivo" studies of Sickle Cell disease (SCD), the Diabetic Foot Ulcer (DFU), the Brain Tumor Response and the Pharmacokinetics of Magnetic Nano Particles (PK-MNP), as illustration are presented. Furthermore, contributions and limitations of the MR methods to diagnostics and selection of therapeutic pathways are discuses.

A common purpose of these investigations were to set up the necessaries methodologies for the MR quantitative studies of complexes pathological scenario.

Entirely the present studies were reviewed and approved by the ethics Committee of the different medical Institutions and of the research centers involve in, according to the ethical principles of the Word Medical Association (Declaration of Helsinki). In all the cases written the informed consent were obtained of the healthy volunteers and the patient before their inclusion. The main common idea of all these works is optimize the experiments keeping, as constant as possible, all the conditions including the position of the biological sample. During the kinetics studies, in each case have been establish different well characterized external and internal markers or references, in order to have a control of the subject position and biological changes.

"In vitro" and "in vivo" MR data gave a unique complementary information related to the kinetics studies of complex biomedical process. MR have been contribute to the discovery of new pathways and drugs for treatment and to introduce modification on its. Furthermore, MR bring information to during long treatment time in order to delimit the treatment conduct and contribute in the understanding of bio physiological process associated with of action of the drugs.

Some Problems of Quantitative Analysis by NMR Method

Vladimir Chizhik

Saint Petersburg State University,
Russian Federation

Abstract

In the Saint-Petersburg State University the fundamental researches in the area of magnetic resonance have been carrying out since the beginning of the 50-ies of the last century. Basing on them, a number of practical applications have been developed, and the overview of the results will be given in the report.

Despite the evidence of the possibility of non-invasive (and non-destructive) quantitative analysis by NMR, its practical realizations are related with certain methodological difficulties. Here, the examples of NMR quantitative analysis techniques in a variety of industrial applications and some prospects for new developments are reported:

(i) The analysis of sodium and aluminum content in solutions of the technological process of aluminum production on the basis of the ^{23}Na and ^{27}Al resonances. In this case an analysis of components in the mixture Al_2O_3 – NaOH – H_2O is required. The main problem is the dependence of NMR signals on electrical conductivity of samples, that violates the instrument calibration using external standards. The original method of calibration of signal amplitudes was realized using the ^{81}Br resonance. Sensors with flowing fluids were also tested.

(ii) The state of liquid phase in heterogeneous systems (like sea ice and cement mixes). In particular, the stability of concrete samples (water saturated) under the multiple temperature cycling was investigated. Some comments on the possible errors of the NMR method in evaluating the productivity of rocks – reservoir of oil and gas – are formulated (on the basis of the comparison of ^{1}H and ^{2}H relaxation data).

(iii) Errors of the determination of characteristic times of molecular reorientation via the interpretation of NMR relaxation data are discussed (on the example of ionic liquids).

(iv) A few possibilities of NMR in the Earth's magnetic field for the quantitative analysis.

The work is partly supported by the Russian Foundation for Basic Research (grant No. 17-03-00057a).

Biography

Vladimir Chizhik, Professor of the Saint Petersburg State University, was born in 1937 in Leningrad (now Saint Petersburg), graduated from Leningrad University in 1959; 1966 – Ph D.; 1982 – Dr. Sci. (specialities: Radiophysics and Molecular Physics). In the Saint Petersburg (Leningrad) State University he consistently held the positions of junior researcher, senior researcher, professor. In 1993 V. Chizhik organized the new "Chair of Quantum Magnetic Phenomena" and was the Head of it for 20 years. The scientific areas of V. Chizhik are NMR in condensed matter, NMR-relaxation, microstructure of liquid systems. He is a member of Committee of the European Groupement AMPERE (Atomes et Molécules Par Études Radio-Électriques).

Strategies for measuring ^{13}C-^{15}N dipole-dipole couplings in liquid crystalline samples with natural isotropic abundance

S. V. Dvinskikh[1,2]

[1]*Department of Chemistry, KTH Royal Institute of Technology, SE-10044 Stockholm, Sweden*
[2]*Laboratory of Biomolecular NMR, St. Petersburg State University,*
St. Petersburg, 199034, Russia
E-mail: sergeid@kth.se

We present natural abundance nitrogen-15 (NAN15) NMR spectroscopy in thermotropic liquid crystals. It is demonstrated that high resolution NAN15 NMR spectra in mesophases can be accurately recorded in non-spinning samples with a high orientational molecular order and strong anisotropic spin interactions [1]. In this technique, due to low demand on radio-frequency decoupling power, standard solution-state probes can be used, which generally provide superior sensitivity and spectroscopic resolution in comparison to solid-state probes. We show that ^{15}N chemical shift anisotropy can be used as a sensitive parameter to characterise molecular orientational dynamics in liquid crystals. Since the nitrogen spectra are obtained from the molecules constituting the mesophase rather than from probe molecules, the information is direct and the analysis and interpretation is straightforward.

Structural information in rigid and soft solids can be obtained by NMR spectroscopy through the measurement of dipole-dipole spin couplings, which are very sensitive to interatomic distances. The dipolar interaction is also orientation dependent and, thus, reports on molecular dynamics at the atomic level [2]. Experimental detection of ^{15}N-^{13}C dipolar splitting at the natural isotopic abundance level is challenging since both rare isotopes should be simultaneously present in a molecule. The fraction of the molecules containing ^{15}N-^{13}C pairs and giving rise to satellite signals is only $4 \cdot 10^{-5}$. New experimental strategies to sensitively record ^{15}N-^{13}C dipolar spectra in liquid crystalline samples with natural isotropic abundance will be presented.

The work is supported by the RFBR grant 17-03-00057.

References

1. L. Jackalin, S. V. Dvinskikh. Natural Abundance Nitrogen-15 NMR in Thermotropic Liquid Crystals With Cyano-Group. *Z. Phys. Chem.* **231**, 795-808 (2017)
2. S. V. Dvinskikh, D. Sandström, H. Zimmermann, A. Maliniak. Carbon-13 NMR spectroscopy applied to columnar liquid crystals. *Progr. Nucl. Magn. Reson. Spectrosc.* 48, 85-107 (2006).

NMR Studies of Metal Particles

Jacques Fraissard

University P. and M. Curie, ESPCI, Laboratory LPEM, Paris, France

The chemical and petroleum industries rely upon metal catalysts for the manufacture of a wide range of essential products. Metal clusters or crystallites in the catalysts are studied by several techniques: gas adsorption isotherms, electron microscopy, EXAFS, Mössbauer spectroscopy, etc., but their number proves that none of them is able to characterise these particles correctly.

The magnetic properties of these latter should depend on their size, at least when they are sufficiently small, whence the interest of NMR. There are, *a priori*, several ways of applying NMR to such a problem:

– Detection of the metal nucleus (Slichter *et al*., Van der Klink *et al.*). However, this method cannot be generalised to all metal catalysts, since few metals can be detected by NMR. Moreover, the experimental conditions are particularly difficult and require very experienced physicists.

– The use of a probe which can be detected by NMR and adsorbed on the particles. This is an indirect measurement, much easier, which we have developed by using the ^{1}H and ^{129}Xe nuclei.

1. ^{195}Pt–NMR studies of platinum catalysts

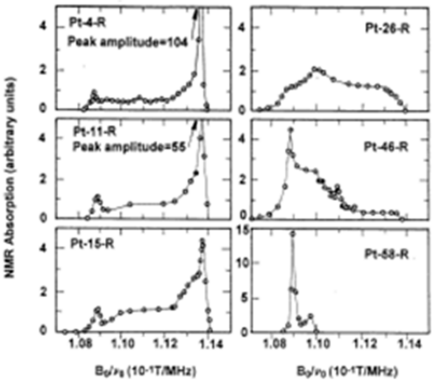

Figure 1. NMR absorption versus B_0/ν_0 for untreated samples. Value of x in Pt-x is % dispersion. As expected, the results show that the intensity of line b increases with the metal dispersion at the expense of lines a and c

^{195}Pt is a suitable nucleus for the study of metal particles: *ca.* 34% of natural isotopic abundance, reasonably high gyromagnetic ratio (9 MHz in 10 KG) and a spin I of ½. Slichter *et al.* employed the spin-echo technique which essentially removes the effect of inhomogeneous broadening by refocusing the nuclear magnetisation into an echo. The NMR lines are very broad. For this reason the line-shape is obtained point by point, by measuring the area of the spin echo at different values of B_0 for fixed ν_0. Three components are generally detected, corresponding to: *a*- Pt nuclei in the interior of the particle, far from the surface, in an environment like that of bulk Pt (Knight shift, Figure 1, B_0/ν_0 = *ca.* 1.135); *b*- Pt nuclei near the surface with a smaller shift which depends on the nature of adsorbed molecules

(B_0/ν_0 =1.09); *c*- Pt nuclei in interior layers near the surface with an intermediate shift (1.09< B_0/ν_0 <1.135).

2. ^{1}H- and ^{129}Xe-NMR studies of hydrogen and xenon adsorbed on metals. Application to the dispersion

2.1. Adsorption on platinum particles

When a very small amount of hydrogen is chemisorbed, the NMR spectrum consists of two lines: *i*- one, ***a***, with a chemical shift, δ_a(H), close to zero (TMS reference), due to the OH groups of the support, and which can be used as an internal reference; *ii*- a second one, ***b***, very much upfield, δ_b(H), characteristic of hydrogen chemisorbed on Pt.

When the number N of chemisorbed H_2 molecules (or the coverage θ_H) increases, line ***b*** grows but its chemical shift, δ_b, is roughly constant up to a coverage of about 0.50 if the sample is monodispersed, *i.e.* if the particle size is roughly homogeneous (segment AB, Fig. 2).

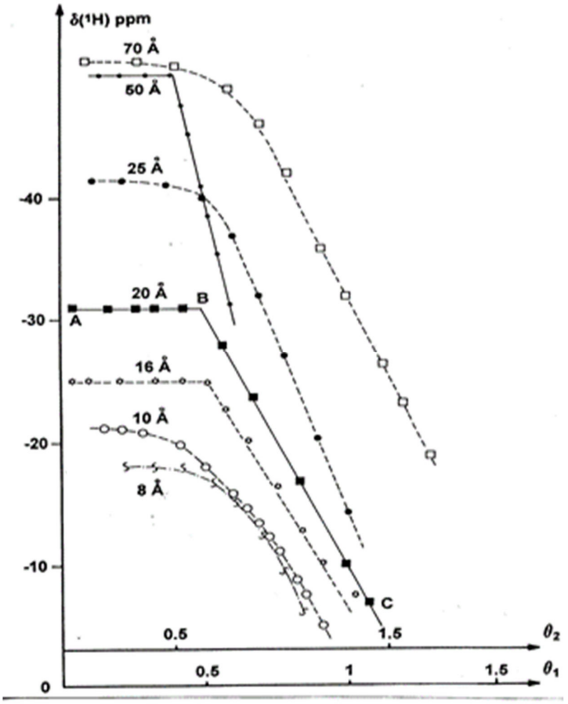

Figure 2. δ_b(H) ppm of hydrogen chemisorbed on platinum, at 26°C, versus the hydrogen coverage

This Figure shows that the position of the plateau AB depends on the particle size. θ1 and θ2 refer to the total hydrogen adsorption and to the chemisorption component, respectively. δb(H) depends also on the hydrogen concentration. Along the plateau AB hydrogen is chemisorbed at room temperature with a constant coverage θB corresponding to point B. The NMR of co-adsorbed xenon confirms this special spatial distribution.

Xe NMR of adsorbed xenon can also be used to determine the distribution of Pt particles in the microporous solids such as zeolites.

2.2. Adsorption on a palladium particle

Very different results are obtained from the ^{1}H-NMR of H_2 sorbed on supported Pd since several species are identified in the presence of this metal: H_2 gas, chemisorbed hydrogen H_S, and hydrogen in α- and β-hydrides (H_α and H_β, respectively).

The ^{1}H-NMR spectra of the Pd-H system show:

– An upfield (negative shift) signal S_1 for low hydrogen concentration, due to rapid exchange between H_S and H_α. At 26°C, the $\delta_1 = f(\theta)$ plot becomes horizontal for $\theta = 1$ and the maximum concentration of Pd-H_α hydride.

– A downfield signal S_2 for hydrogen concentrations corresponding to a coverage greater than unity, due to Pd-H_β in equilibrium with H_S. The intensity of S_2 increases with N at the expense of S_1.

– The $\delta_1 = f(\theta)$ plots are independent of the dispersion. The continuous variation of δ_1 with θ proves that the H_α and H_S concentrations increase homogeneouly throughout all the particles.

– H_S concentration controls the formation of the Pd-H_α and Pd-H_β hydrides.

– The equilibrium: $H_\alpha \Leftrightarrow H_S$ is displaced to the right when the temperature increases.

^{1}H NMR at Larmor frequencies down to 3 Hz by means of Field-Cycling techniques

Benjamin Kresse[a], Manuel Becher[a], Alexei F. Privalov[a], Marius Hofmann[b], Ernst A. Rössler[c], Michael Vogel[a], Franz Fujara[a]

[a]*Institut für Festkörperphysik, TU Darmstadt, Germany,*
[b]*Department of Chemistry, Louisiana State University, Baton Rouge, USA,*
[c]*Experimentalphysik II, Universität Bayreuth, Germany*

I will present Field-Cycling (FC) NMR experiments carried out at ^{1}H Larmor frequencies down to about 3 Hz (Fig. 1). This could be achieved by fast switching a high polarizing magnetic field down to a low evolution field which is tilted with respect to the polarization field. Then, the low frequency Larmor precession of the nuclear spin magnetization about this evolution field is registered by means of FIDs in a high detection field. The crucial technical point of the experiment is the stabilization of the evolution field, which is achieved by compensating for temporal magnetic field fluctuations of all three spatial components. I will also report on a couple of basic low field experiments such as the simultaneous measurement of the Larmor frequency and the spin-lattice relaxation time in such small fields as well as the irradiation of oscillating transversal magnetic field pulses at low frequencies as a novel method for field calibration in low field FC NMR. Our set up also allows for zircular polarized irradiation thereby evidencing resonance only if the correct polarization component is chosen. Most of the work got recently published [1].

The potential of low field FC is finally exemplified by the ^{1}H relaxation dispersion of water at frequencies below about 2 kHz stemming from slow proton exchange processes and the study of slow polymer dynamics [2]. If time permits I will also talk about these applications.

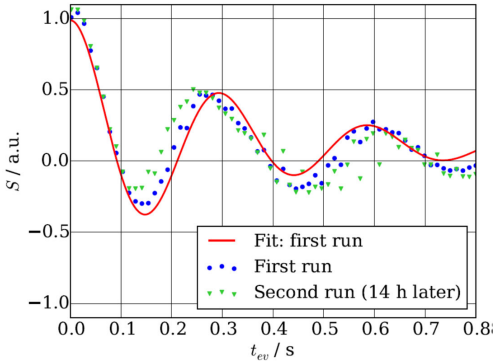

Figure 1. Precession of the magnetization vector M about the evolution field Bev at a ^{1}H Larmor frequency of 3.4 Hz, measured in tetradecane at room temperature

References

1. B. Kresse, M. Becher, A. F. Privalov, M. Hofmann, E. A. Rössler, M. Vogel, F. Fujara, ^{1}H NMR at Larmor frequencies down to 3 Hz by means of Field-Cycling techniques, J. Magn. Res. 277, 79-85 (2017)
2. B. Kresse, M. Hofmann, A. F. Privalov, N. Fatkullin, F. Fujara, E. A. Rössler, All polymer diffusion regimes covered by combining field-cycling and field-gradient ^{1}H NMR, *Macomolecules* 48, 4491-4502 (2015)

Solid State NMR in nanosized systems: MAS NMR studies in combination with pulsed field gradient techniques

Dieter Michel and Jürgen Haase

Leipzig University, Faculty of Physics and Earth Sciences, Felix-Bloch-Institute for Solid State Physics, Linné-Strasse 5, 04103 Leipzig, Germany
E-mail: michel@physik.uni-leipzig.de; Phone: +49 341 97 32683

Structure and mobility of molecules adsorbed in porous media and systems with restricted geometry has been widely investigated by means of NMR spectroscopy. Limitations occur for the study of these systems due to the presence of random local magnetic fields. For nuclear spins like ^{13}C and ^{15}N still a sufficient spectral resolution can be achieved because of the relatively large chemical shifts. In case of proton NMR spectroscopy, however, the applicability of NMR spectroscopy to these heterogeneous systems is often limited due to the poor spectral resolution. Hence, neither the advantages of modern more dimensional NMR spectroscopy for liquid-like systems nor the advanced techniques for solid-state NMR spectroscopy are fully accessible. In this presentation we show that a notable enhancement in the spectral resolution for adsorbed and interface systems may be achieved by the application of MAS techniques. NMR measurements of molecules adsorbed in these systems are often characterized by the fact that the resolution in the chemical shifts is not limited due to a strongly restricted molecular mobility but due to random local magnetic fields. A typical situation is the so-called susceptibility broadening. It occurs in these systems that the local fields in these systems are essentially not partially averaged out by the local reorientational motions but may be (partially) averaged out by longer-distance translational motions of the molecular species. The time scale of the latter motions may strongly differ from that of the (rapid) local motions and often in the same order of magnitude as for magic-angle spinning (MAS). Thus, this technique may be a powerful tool to enlarge the spectral resolution in the heterogeneous systems as considered.

The aim of the lecture will be

– to introduce into the fundamentals of MAS NMR in nanosized porous systems (e.g. zeolites and other molecular sieves, metal organic frameworks, silicas, porous glasses) and to treat the influence of thermal motions of molecules in these systems in competition to coherent averaging due to magic angle spinning: We describe advantages and shortcoming of these techniques. It will be shown that the studies may be broadly applied if a well-defined preparation *under conditions of vacuo* may be achieved for samples suitable for MAS.

– to show that MAS NMR techniques may be combined with measurements by means of NMR pulsed field gradient techniques to study self-diffusion processes in spectra with resolved lines. Special experimental requirements will be discussed. Thus, selective measurements of self-diffusion coefficients may be possible by using the various resonance lines in the MAS NMR spectra.

– to mention briefly two special applications: It will be discussed how the information on thermal mobility derived from the side-band analysis in ^{1}H MAS NMR experiments for these systems may be combined with the study of proton spin relaxation over a wider temperature range. Furthermore, the applicability of two-dimensional NMR of adsorbed molecules is discussed when the spectral resolution is enlarged by means of MAS NMR studies.

Polaron freezing and the quantum liquid-crystal phase in Ferromagnetic Metallic Manganites. A NMR and HRTEM study in the temperature range 3.2 – 1000K

Georgios Papavassiliou[1], Nikos Panopoulos[1], Michael Fardis[1], Michael Pissas[1], Nikos Boukos[1], Saeed Alhassan[2], Yasser AlWahedi[2], Jamal Hassan[2], Hae Jin Kim[3], Jin-Gyu Kim[3], Seung Jo Yoo[3]

[1]Institute of Nanoscience and Nanotechnology, NCSR Demokritos, 15310 Aghia Paraskevi, Attiki, Greece
[2]Khalifa University of Science and Technology, Abu Dhabi, United Arabic Emirates
[3]Korea Basic Science Institute,350-333, Daejeon, Republic of Korea
E-mail: g.papavassiliou@inn.demokritos.gr; http://www.inn.demokritos.gr

The remarkable electronic properties of Colossal Magnetoresistive Manganites are widely believed to be caused by the competition between a ferromagnetic metallic state and an antiferromagnetic insulating state with complex spin, charge, and orbital ordering. However, the physics underlying their magnetotransport properties is still not clear, especially the role of correlated Jahn-Teller polarons, which depending on temperature and doping, might form a liquid, glass or stripe polaron state. This question touches one of the most fundamental problems in the physics of doped Mott insulators, i.e. understanding the mechanism that chemical doping makes an insulator becoming superconductive as in the case of cuprates, or exhibiting the Colossal Magnetoresistance, as in the case of manganites. Here, by using ^{139}La NMR and high resolution transmission electron microscopy in the temperature range 3.2 K to 1000 K, we have monitored the formation and evolution of CE-type polarons in optimally doped $La_{0.67}Ca_{0.33}MnO_3$ (Figure 1). While NMR experiments show that correlated polarons dominate electron spin dynamics in the ferromagnetic phase, at very low temperatures they appear to form a quantum liquid-crystal (QLC) ferromagnetic phase, embedded into a ferromagnetic matrix with 3D polaron correlations (Figure 2). This is evidence that similarly to high Tc cuprates, quantum soft phases underlie the exotic physical properties of Colossal Magnetoresistive Manganites.

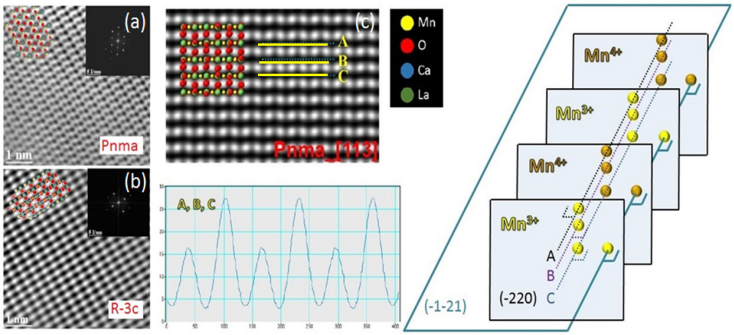

Figure 1. (a), (b) HRTEM of the Pnma (293K) and R-3c (800K) crystal structures. (c) Calculated HRTEM image parallel to the [113]$_{Pnma}$ zone axis at 293K. The line profiles along the A, B, C rows, perpendicular to the (-220)$_{Pnma}$ plane, show alternating intensity levels at the position of the Mn ions (indication of Mn^{4+} and Mn^{3+} ion ordering). This is evidence of the presence of CE-type polarons at RT

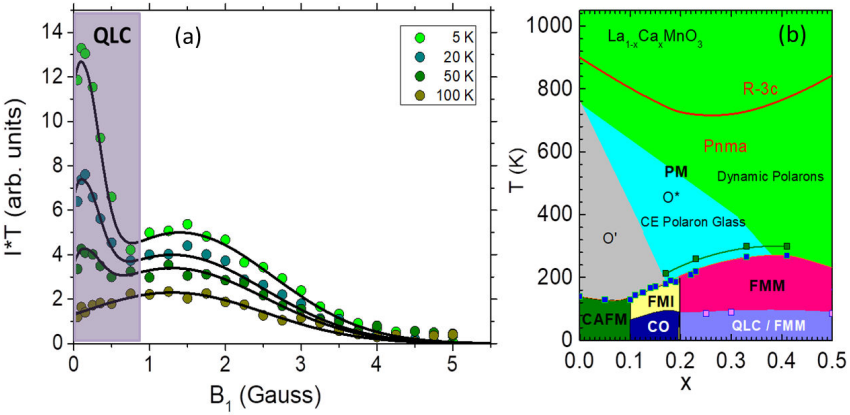

Figure 2. (a) ^{139}La NMR radiofrequency (rf) enhancement of $La_{0.67}Ca_{0.33}MnO_3$, in zero external magnetic field, as function of the rf field B_1 at various temperatures. The weak B_1 component belongs to a spin Quantum Liquid Crystal (QLC) phase. (b) The T-x phase diagram of $La_{1-x}Ca_xMnO_3$. A QLC region is observed in the Ca doping region $0.2<x<0.5$

References

1. D. Koumoulis, N. Panopoulos, A. Reyes, M. Fardis, M. Pissas, A. Douvalis, T. Bakas, D. Argyriou and G. Papavassiliou – *Phys. Rev. Letters* ***104****, 077204 (2010).*
2. N. Panopoulos, M. Pissas, H. J. Kim, Jin-Gyu Kim, S. J. Yoo, J. Hassan, Y. AlWahed, S. Alhassan, M. Fardis, N. Boukos, G. Papavassiliou – *npj Quantum Materials* (accepted for publication), (2018).

Many faces of disulfide bond

Sevastyan O. Rabdano[1], Sergei A. Izmailov[1], Dmitry A. Luzik[1], Olga N. Rogacheva[1,2], Irina I. Tyuryaeva[1,3], Olga G. Lyublinskaya[3], Ivan S. Podkorytov[1], Nikolai R. Skrynnikov[1,4]

[1]Laboratory of Biomolecular NMR, St. Petersburg State University, St. Petersburg 199034, Russia.
[2]Department of Biology, St. Petersburg State University, St. Petersburg 199034, Russia.
[3]Institute of Cytology, Russian Academy of Sciences, St. Petersburg 194064, Russia.
[4]Department of Chemistry, Purdue University, West Lafayette, Indiana 47907, USA.
E-mail: nikolai@purdue.edu

Disulfide bonds are a major determinant of protein structure and a modulator of protein function. In our first project, we have investigated formation of non-native disulfide bonds in the sample of RRM2 domain from neuropathological protein TDP-43 under the effect of oxidative stress. We have shown that the resultant disulfide-bonded dimers are not unstable per se. However, their ability to spontaneously fold is compromised. Consequently, they become vulnerable to large thermal fluctuations, which ultimately leads to misfolding, aggregation and proteolysis. In our second project, we have developed the algorithm to model formation of disulfide bridges *in silico* as a part of regular MD simulation. The new algorithm entails minimal modifications to the original force field, is virtually perturbation-free, retains the same speed as conventional MD simulations, and allows one to easily adjust the rate of disulfide formation. It has been applied to investigate oxidative folding of hormonal peptide guanylin. The results indicate that oxidative folding of guanylin occurs under kinetic control. Furthermore, the simulations produced a high-quality model of isomer 2(B) of guanylin, which is superior to the corresponding experimental structure obtained from the sample of the truncated peptide. Finally, in our third project we have focused on the cytotoxic effects of the cysteine-containing peptides. We have investigated the presumed antitumor peptide GO, which has been designed as a selective inhibitor of dimerization of the epithelial glycoprotein mucin 1. We have shown that cytotoxic activity of GO is unrelated to the level of expression of mucin and, in fact, extends to normal cells. Furthermore, we have designed a number of new cysteine-containing peptides with even higher level of cytotoxic activity. These results suggest the cytotoxic mechanism of cysteine-containing peptides is related to their activity of (weak and weakly specific) disulfide oxidoreductases. This hypothesis was directly validated using the lysozyme folding assay conducted *in vitro*. The combination of different approaches used in our work – from MD simulations to NMR measurements to cell-culture experiments – shed new light on the immensely important physiological role of disulfide bonds.

This work was supported by the RSF grant 15-14-20038.

Combination of Microwave & NMR Techniques for Effective Detection of Dangerous Materials

B. Rameev[1,2], İ. Ünver[2], B. Çolak[3], G. V. Mozzhukhin[2]

[1]E. Zavoisky Physical-Technical Institute, 420029 Kazan, Russian Federation
[2]Gebze Technical University, 41400 Gebze/Kocaeli, Turkey; rameev@gyte.edu.tr
[3]Alanya Alaaddin Keykubat University, 07450 Alanya/Antalya, Turkey

Detection of liquid energetic/illicit substances is a very important problem due to rapidly increasing number of terrorist attacks based on use of so-called home-made explosives, made from commercially available chemical materials.

The techniques providing unique, chemical-specific information on a scanned substance looks especially advantageous with respect their potential applications in security [1, 2]. Among such techniques, the low-field nuclear magnetic resonance (NMR) is considered as a prospective bulk detection method for a broad range of various liquids, including energetic, flammable, dangerous and toxic materials [3]. Time-domain (TD) NMR (or NMR relaxometry) looks attractive due to its good selectivity and relatively low device/maintenance expenses. Unfortunately, the classical ^{1}H NMR relaxometry based on the measurements of T_1 and T_2 relaxation constants does not provide a requested level of discrimination in a large group of liquid substances. Therefore, additional parameters for measurements (e.g., the complex permittivity or the ^{14}N NMR signal) are needed. Another issue is quite long times of measurements using classical NMR sequences. In this work, possible approaches to obtain additional information on a liquid content and to make the liquid scanning process faster are discussed.

The ^{1}H NMR sequences with short total measurement times which could be applied for detection of some flammable liquids or explosive precursors are analyzed. Another NMR approach, based on the detection of ^{14}N NMR signal as a fast liquid scanning protocol and additional discrimination parameter, is also studied. The dielectric spectroscopy in microwave range for detection of explosive and illicit substances is reviewed as well. Various possible sensors for bottle scanning applications (e.g. microstripes, a partially shielded dielectric resonators, ring resonators, semi-circular dielectric waveguides, etc.) are discussed.

This work is supported by NATO Science for Peace and Security Programme (NATO SPS grant No. 985005 [G5005]). Authors also acknowledge a partial support by East Marmara Development Agency (MARKA, project No. TR42/16/ÜRETİM/0013) and by Research Fund of Gebze Technical University (grants Nos. BAP 2015-A-19 and BAP 2017-A-105-44).

References

1. Rameev B.Z., Mozzhukhin G.V., Aktas B., eds.: Magnetic Resonance Detection of Explosives and Illicit Materials, Appl. Magn. Reson. **43**, no. 4, 463-467 (2012).
2. Apih T., Rameev B., Mozzhukhin G., Barras J., eds.: Explosives Detection using Magnetic and Nuclear Resonance Techniques, NATO Science for Peace and Security Series B: Physics and Biophysics, Dordrecht, Netherlands: Springer, 2014.
3. Burnett L.J., Liquid Explosives Detection, Proc. SPIE **2092**, 208-217 (1994).

New MAS Technologies

Ago Samoson, Andres Oss, Mai-Liis Org, Kalju Vanatalu

[1]*Institute of Health Technologies, Tallinn University of Technology*
[2]*NMR Institute*
Tallinn, Estonia
E-mail: ago.samoson@yahoo.com
http://www.nmri.eu

Further (solid state) NMR progress is tightly coupled to a sample spinning technology. The rotation rates are presently available over 150 kHz (Fig 1), reducing homogeneous line broadenings in a typical portein to a 0.2 ppm and below.

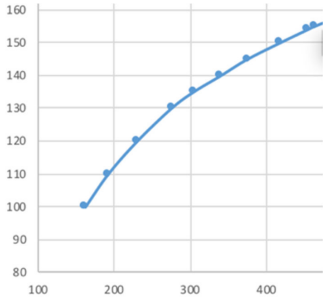

Figure 1. Rotation speed (kHz) vs drive pressure (kPa, vertical axis)

This enables an inverse detection and adaptation of various high-resolution methods for the coherence transfer. As evidenced by the measurement of protein linewidth (Fig. 2), average homogeneous T2' increases to 4 ms which is critical improvement for INEPT transfer process. High speed MAS NMR can be expected to fill, at least to some extent, a badly missing gap in analytical methods for membrane and other large biomolecular systems. We shall discuss also other technologies of MAS NMR, enhancing studies of the highest interest: heterogeneous catalyses and energy storage materials. Several convenience accessories, like multi-mode MAS controller, for a practical operation of the probes will be introduced.

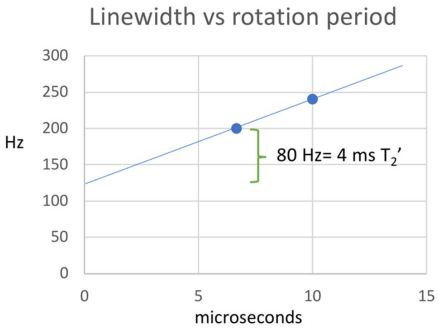

Figure 2. Experimental average proton [1]H linewidth at speeds 100 and 150 kHz

Computer simulation of ionic liquids

L. M. Varela

Grupo de Nanomateriales, Fotónica y Materia Blanda, Departamento de Física de Partículas, Facultade de Física, Universidade de Santiago de Compostela, Campus Vida s/n, E-15782 Santiago de Compostela, Spain
E-mail: luismiguel.varela@usc.es

Abstract

I report a review of the computational techniques mainly used for the analysis of the structure and dynamics of ionic liquids (ILs) and their mixtures with cosolvents and inorganic salts, both in bulk conditions and close to the electrochemical interface, focusing specifically on their capability of predicting NMR properties. I review briefly the foundations of density functional theory (DFT) calculations, molecular dynamics (MD) and ab initio MD, as well as some of the main results previously reported using those techniques. Using MD simulations, I review some of my group's latest activity [1-5] on the structure and dynamics (radial distribution functions, hydrogen bonds, vibrational densities of states and velocity autocorrelation functions, etc.) of bulk ILs and several of their mixtures, as well as properties of these media at the electrochemical interface (density and potential of the mean force profiles of the different species in solution, vibrational density of states of the solute molecules or ions, pattern transitions on the lateral structure of the layers closest to the walls…). Moreover, MD predictions of NMR properties of ILs (rotational correlation functions of hydrogens and carbons) are reported. Some recent DFT simulations of the interaction of an IL with the electrochemical interface (structure, charge transfer…) are also reported, including predictions of spectroscopic and NMR properties of ILs and their mixtures with electrochemically relevant salts (lithium, magnesium, aluminum).

Acknowledgements

The financial support provided by the Spanish Ministry of Economy and Competitiveness (MAT2014-57943-C3-1-P, MAT2014-57943-C3-2-P, MAT2017-89239-C2-1-P and MAT2017-89239-C2-2-P) is gratefully acknowledged. Moreover, this work was funded by the Xunta de Galicia (AGRUP2015/11 and GRC ED431C 2016/001). All these research projects were partially supported by FEDER. Funding from the European Union (COST Action CM 1206) and by the Galician Network on Ionic Liquids, REGALIs (ED431D 2017/06) is also acknowledged, as well as the support of the Galician Supercomputing Centre (CESGA).

References

1. T. Méndez-Morales, J. Carrete, M. Pérez-Rodríguez, O. Cabeza, L. J. Gallego, R. M. Lynden-Bell, L. M. Varela, Phys. Chem. Chem. Phys., 16, 13271–13278, 2014.
2. V. Ivaništšev, T.Méndez-Morales, R. M. Lynden-Bell, O. Cabeza, L. J. Gallego, L. M. Varela, M. V. Fedorov, Phys. Chem. Chem. Phys. 18, 1302–1310, 2016.
3. B. Docampo-Álvarez, V. Gómez-González, H. Montes-Campos, J. M. Otero-Mato, T. Méndez-Morales, O. Cabeza, L. J. Gallego, R M. Lynden-Bell, V. B. Ivaništšev, M. V. Fedorov, L. M. Varela, J. Phys Cond. Matter 28, 464001, 2016.
4. V. Gómez-González, B. Docampo-Álvarez, T. Méndez-Morales, O. Cabeza, V. B. Ivaništšev, M. V. Fedorov, L. J. Gallego, and L. M. Varela, Phys. Chem. Chem. Phys.,2017, 19, 846.
5. H. Montes-Campos, J.M. Otero-Mato, T. Méndez-Morales, O. Cabeza, L. J. Gallego, A. Ciach, L.M. Varela, Phys. Chem. Chem. Phys., 2017, 19, 24505

DNP of shallow donors in silicon at ultra-low temperatures

Sergey Vasiliev[1], Jarno Järvinen[1], Janne Ahokas[1], Sergey Sheludyakov[1], Denis Zvezdov[1,2], Yutaka Fujii[3], and Leonid Vlasenko[4]

[1]Wihuri Physical Laboratory, Department of Physics and Astronomy, University of Turku, 20014 Turku, Finland
[2]Institute of Physics, Kazan Federal University, 18 Kremlyovskaya St., 420008 Kazan, Russia
[3]Research Center for Development of Far-Infrared Region, University of Fukui, 3-9-1Bunkyo, Fukui 910-8507, Japan
[4]A. F. Ioffe Physico-Technical Institute, Russian Academy of Sciences, Russia
E-mail: servas@utu.fi

We report on experimental study of dynamic nuclear polarization (DNP) in P and As doped silicon. The samples of natural silicon (4.6% of ^{29}Si, I= 1/2) with P concentration of 3 - 6.5*10^{16} cm^{-3} were studied in a strong 4.6 T magnetic field and temperatures below 1 K, when the donor electron spins are fully polarized and the relaxation times of electrons and nuclei are very long.

Utilizing an Overhauser effect for the donor nuclei we obtained DNP of ^{31}P donors exceeding 98% by saturating the high field ESR line with very low RF powers (<1 μW) in 20 minutes [1]. An inverse sign polarization of the donors nuclear spins was created by pumping the low field lines. We observed non-exponential behavior of DNP of ^{31}P with fast initial part followed by slow exponential increase. From the DNP evolution, we extracted the data on the relaxation rates of forbidden transitions with simultaneous flips of electron and nuclear spins of ^{31}P. We performed measurement of nuclear relaxation of ^{31}P and found that it follows bi-exponential function of time. We explain these peculiar DNP and relaxation behavior by the influence of ^{29}Si nuclear magnetic moments surrounding ^{31}P donor [1]. Similar DNP and relaxation experiments were performed with the ^{75}As donors [2].

Due to strong interactions of the ^{31}P or ^{75}As donors with ^{29}Si nuclei, the electronic polarization of the donors can be effectively transferred to ^{29}Si. We performed classical hole burning experiments in the ESR lines of ^{31}P and ^{75}As, which are inhomogeneously broadened due to the interactions with surrounding ^{29}Si nuclei. We obtained very narrow holes with the width defined by the transversal relaxation rate of the donor electrons. In addition to the hole a narrow peak was observed on the right from the hole. We explain the hole and the peak shapes by the nuclear polarization of ^{29}Si via the Overhauser effect. We realized DNP of ^{29}Si via the resolved solid effect by pumping the ^{31}P-^{29}Si forbidden electron-nuclear transitions [3]. A pattern of narrow holes and peaks observed in the ESR spectrum corresponds to polarization of ^{29}Si in the specific lattice sites, resolved by the strength of the super-hyperfine interactions. This opens a way for creating entangled states of ^{29}Si spins, and realization of quantum operations with large ensembles of identical nuclei.

References

1. J. Järvinen, et al., Efficient dynamic nuclear polarization of phosphorus in silicon in strong magnetic fields and at low temperatures, Phys. Rev. B **90**, 214401 (2014)
2. J. Järvinen, et. al., Dynamic Polarization and Relaxation of ^{75}As Nuclei in Silicon at High Magnetic Field and Low Temperature, Appl. Magn. Reson., **48**(5) 473 (2017).
3. J. Järvinen, *et al*., Microscopic control of ^{29}Si nuclear spins near phosphorus donors in silicon, Phys. Rev. B **92**, 121202(R) (2015).

Oral Reports

Physical and transport properties of the novel dense membranes based on Polysulfone/Pluronic F127 composite

R. Atta[1,3], A. Penkova[1], T. Plisko[2], A. Zolotarev[1], M. Dmitrenko[1], A. Mazur[1], S. Vasin[1]

[1]Saint Petersburg State University, Saint Petersburg, Russia.
[2]Institute of Physical Organic Chemistry of the National Academy of Sciences of Belarus, 13 Surganov street, 220007 Minsk, Belarus.
[3]Damietta University, Damietta, Egypt.
Email: ramadanatta75@du.edu.eg

Nowadays, the essential improvement of the transport properties of polymer membranes can be achieved by polymer matrix modification by the introduction of polymer additives to the casting solution that yields in the development of the novel blend membranes. The introduction of the polymer additive to the polymer matrix of the membrane allows attaching additional functional properties. Blend membranes prepared by dispersing a polymer additive in the polymeric matrix offer the possibility to overcome the trade-off between the permeability and selectivity of the polymer membranes. Polymer blend membranes combine the simplicity of processing with the superior transport properties due to the incompatibility and micro phase separation of two polymers upon phase inversion process when membrane is formed. Block copolymers of polyethylene glycol and polypropylene glycol (Pluronic) attract the attention of researchers in the field of membrane technology because of their amphiphilic properties that cause good dispersion in different polymer matrices.

In the present work the novel dense membranes based on polysulfone modified by Pluronic F127 (from 0.5 to 20 wt. %) were prepared. The formation of the Polysulfone/Pluronic F127 composite was confirmed by nuclear magnetic resonance. The additional study of the composite structure was performed by water contact angle measurements, scanning electron microscopy, small-angle X-ray scattering and atomic force microscopy. Pervaporation performance of the developed membranes was investigated in the process of the separation of water-ethyl acetate mixtures.

It was shown that maximum concentration of Pluronic F127 in the casting solution that led to the improved transport properties was 5 wt. %. This membrane possessed better flux and selectivity as compared to other studied membranes.

This work was supported by Russian Foundation for Basic Research [grant No. 17-58-04067 and Belarussian Republican Foundation for Fundamental Research (grant №X17PM-083).The experimental work was facilitated by equipment from Resource Centers: for Nano technology, Magnetic Resonance Research Centre, X-ray Diffraction Methods, Thermal Analysis and Calorimetry, Chemical Analysis and Materials Research Centre and GEOMODEL at St. Petersburg State University.

Dynamical properties of novel imidazolate borohydrides: NMR studies

Olga A. Babanova[1,*], *Roman V. Skoryunov*[1], *Alexei V. Soloninin*[1], *Fabrice Morelle*[2], *Alexander V. Skripov*[1], *Yaroslav Filinchuk*[2]

[1]*M.N. Mikheev Institute of Metal Physics of the Ural Branch of the Russian Academy of Sciences, S. Kovalevskaya St. 18, 620108 Ekaterinburg, Russia*
[2]*Institute of Condensed Matter and Nanosciences Université Catholique de Louvain, Place L. Pasteur 1, 1348 Louvain-la-Neuve, Belgium*
[*]*E-mail: babanova@imp.uran.ru*

Introduction

Complex hydrides, especially borohydrides, are considered as promising materials for hydrogen storage due to their exceptional volumetric and gravimetric hydrogen densities [1]. However, their practical use is hindered by their stability with respect to thermal decomposition and poor reversibility of hydrogen absorption – desorption. Apart from the practical relevance, these compounds are of considerable interest as model systems for studying the correlation between atomic dynamics and crystal structure. Borohydrides consist of metal cations and tetrahedral anions $[BH_4]^-$, thus the reorientational motion of BH_4 groups can be represented by rotations around three 2-fold axes and four 3-fold axes. Elucidation of atomic dynamics in borohydrides may contribute to improving their hydrogen storage properties. A large number of borohydride-based systems have been synthesized recently in attempts to make their properties more favorable for practical use [2]. Among the most interesting systems are the new hybrid compounds containing both an organic ligand imidazolate Im = $[C_3H_3N_2]^-$ and the BH_4 group. Recently synthesized compounds $Li_2(Im)(BH_4)$ and $Li_2(bIm)(BH_4)$ (where bIm is the benzimidazolate) are the first materials in which the organic imidazolate-based ligand and the inorganic borohydride ion are combined; these compounds have a unique crystal structure and a strong orientational disordering of the BH_4 groups [3, 4].

In this work, we report the results of the first nuclear magnetic resonance study of dynamical properties of BH_4 groups in the new hybrid compounds: lithium imidazolate-borohydride $Li_2(Im)(BH_4)$ and lithium-benzimidazolate $Li_2(bIm)(BH_4)$. Measurements of the ^1H and ^{11}B NMR spectra and spin-lattice relaxation rates were performed over wide ranges of temperatures (5 – 305 K) and resonance frequencies (14 – 90 MHz). NMR appears to be especially effective for studies of atomic motion in borohydrides, because nuclear spin-lattice relaxation rates in these compounds do not contain any significant contributions not related to atomic motion (such as the conduction-electron contribution in metallic systems). This allows us to trace the atomic jump rates in borohydrides over the wide dynamic range (10^5 – 10^{12} s^{-1}) [5].

Experimental methods

Samples of $Li_2(Im)(BH_4)$ and $Li_2(bIm)(BH_4)$ were synthesized by Y. Filinchuk's group at the Université Catholique de Louvain (Belgium). For NMR experiments, the samples were sealed in a glass ampoule under a nitrogen pressure of ~ 0.5 bar. NMR measurements were performed on a modernized Bruker SXP pulse spectrometer with quadrature phase detection at the frequencies $\omega/2\pi$ = 14, 28 and 90 MHz for ^1H, 14 and 28 MHz for ^{11}B. The magnetic field was provided by a 2.1 T iron-core Bruker magnet. A home-built multinuclear continuous-wave NMR magnetometer working in the range 0.32 – 2.15 T was used for field stabilization. The nuclear spin-lattice relaxation rates were measured using the saturation – recovery method. NMR spectra were recorded by Fourier transforming the solid echo signals (pulse sequence $\pi/2_x - t - \pi/2_y$).

Results and discussion

The results of the ^{1}H spin-lattice relaxation measurements for $Li_2(Im)(BH_4)$ are presented in Figure 1. The dominant feature of the data is the frequency-dependent $R_1^H(T)$ peak that is typical of the spin-lattice relaxation due to motionally modulated dipole-dipole interaction between nuclear spins [6]. The $R_1^H(T)$ maximum is expected to occur at the temperature, at which the H jump rate τ^{-1} becomes nearly equal to the resonance frequency ω. Thus, the H jump motion represented by the reorientations of the BH_4 groups is very fast, i.e. the H jump rates reach values of ~ 10^8 s^{-1} already near 135 K. At a temperature near 150 K, a sharp change in the H jump rates due to the structural phase transition is revealed. Therefore, the $R_1^H(T)$ data should be separately approximated in the regions above and below the transition point. It is assumed that in both the low-T and high-T phases $\tau_i^{-1}(T)$ is governed by the Arrhenius law with the activation energy E_{ai} for reorientational motion in the ith phase (i = 1, 2 for the low-T and high-T phases, respectively). The observed frequency dependence R_1^H at the low-temperature slope is weaker than the ω^{-2} dependence predicted the standard theory [6]; this indicates a distribution of H jump rates. In order to describe the experimental $R_1^H(T)$ data in the low-T phase, the model based on a Gaussian distribution of the activation energies was used [7], while the data on the $R_1^H(T)$ in the high-T phase can be described by the standard model [6]. The mean activation energy and the activation energy of the reorientational motion of the BH_4 groups for the low-T and high-T phases are 151 (7) meV and 129 (3) meV, respectively. The behavior of the ^{11}B spin-lattice relaxation rate, $R_1^B(T)$, dependence resembles that of $R_1^H(T)$. In particular, the $R_1^B(T)$ maximum is observed at nearly the same temperature as the corresponding $R_1^H(T)$ maximum, and the $R_1^B(T)$ peak shows distinct signs of 'folding' related to the phase transition. These features indicate that the measured ^{11}B spin-lattice relaxation rates for $Li_2(Im)(BH_4)$ originate from the same reorientational jump process as the ^{1}H relaxation rates. The ^{1}H NMR line width at half-maximum remains nearly constant (changing from 35 kHz at 5 K to 29.5 kHz at 297 K) over the entire temperature range. Such a behavior of the ^{1}H NMR line width suggests that, at least for a fraction of protons, the reorientational motion with H jump rates exceeding ~10^5 s^{-1} survives down to very low temperatures. A closer inspection of the data indicates that a broader component is present in the spectra for the temperature range 5 – 68 K, giving rise to the 'wings' of the observed lines; this is typical of the systems with broad distributions of the reorientational jump rates [8].

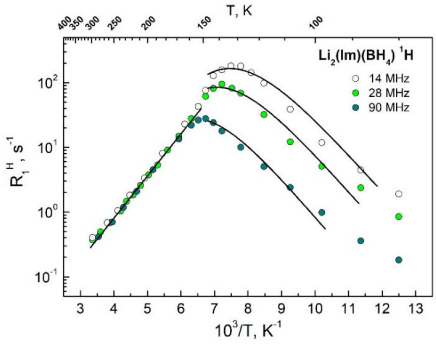

Figure 1. Proton spin-lattice relaxation rates for $Li_2(Im)(BH_4)$ as functions of the inverse temperature

The results of our ^{1}H NMR measurements for $Li_2(bIm)BH_4$ differ qualitatively from those for $Li_2(Im)(BH_4)$. Two reorientational processes occurring at different frequency scales have been revealed. In the temperature range of 80 – 305 K, the proton spin-lattice relaxation data are governed by thermally-activated reorientations of the BH_4 groups. This motional process is characterized by the activation energy of 270 (3) meV, and the corresponding reorientational jump rate reaches ~ 10^8 s^{-1} near 270 K. The second reorientational process is consistent with very fast H motion down to low temperatures. Below 60 K, the relaxation data are governed by the extremely fast process of BH_4 reorientations that are not 'frozen out' at the NMR frequency scale down to 5 K. It should be noted that the $R_1^H(T)$ peak occurs at unusually low temperature (for example, at the frequency of 14 MHz, the peak is observed near 28 K). Thus, the standard interpretation of the peak in terms of thermally-activated reorientational motion [5] would mean that the H jump rate reaches ~ 10^8 s^{-1} at 28 K. However, a closer inspection of the data shows that the frequency dependence of $R_1^H(T)$ in the region of the peak is considerably weaker than that predicted by the standard model for thermally-activated atomic motion [5]. Furthermore, the measured ^{1}H NMR spectrum for $Li_2(bIm)BH_4$ does not exhibit any changes related to motional narrowing over the broad temperature range, i.e. even at 6 K, the ^{1}H NMR line width is considerably smaller than that expected for the 'rigid' lattice remaining nearly constant (~ 30 kHz) in the temperature range 6 – 305 K. These features of the NMR data suggest a possibility of rotational tunneling of BH_4 groups in $Li_2(bIm)BH_4$ [9]. The experimental results in this range are described in terms of a gradual transition from the regime of low-temperature quantum dynamics (rotational tunneling of BH_4 groups) to the regime of classical jump reorientations of BH_4 groups with the activation energy of 44.1 meV. The rotational tunneling has been extensively studied for CH_3 and NH_4 groups in various compounds [10]; however, to the best of our knowledge, it has not been reported so far for BH_4 groups.

Acknowledgements

The research was carried out within the state assignment of FASO of Russia (theme "Spin" No. AAAA-A18-118020290104-2), supported by Grant of the President of the Russian Federation for state support of young Russian scientists (project No. MK-1692.2017.2).

References

1. S. Orimo, Y. Nakamori, J.R. Eliseo, A. Züttel, C.M. Jensen. *Chem. Rev* **107**, 4111 (2007).
2. M. Paskevicius, L.H. Jepsen, P. Schouwink, R. Černý, D.B. Ravnsbæk, Y. Filinchuk, M. Dornheim, F. Besenbacherf, T.R. Jensen*. Chem. Soc. Rev* **46 (5)**, 1565 (2017).
3. F. Morelle, V. Ban, A. Miglio, G. Hautier, R. Skoryunov, O. Babanova, A. Soloninin, A. Skripov, B. Fleutot, R. Janot, Y. Filinchuk. *To be published.*
4. F. Morelle, N. Tumanov, A. Skripov, T. Udovic, Y. Filinchuk. *To be published.*
5. A.V. Skripov, A.V. Soloninin, O.A. Babanova. *J. Alloys Compd.* **509***,* S535 (2011).
6. A. Abragam. *The Principles of Nuclear Magnetism*, Clarendon Press: Oxford, 1961.
7. J.T. Markert, E.J. Cotts, R.M. Cotts. *Phys. Rev. B* **37**, 6446 (1988).
8. A.V. Soloninin, A.V. Skripov, Y. Yan, A. Remhof. *J. Alloys Compd.*, **555**, 209 (2013).
9. A.J. Horsewill. *Prog. Nucl. Magn. Reson. Spectrosc.* **35**, 359 (1999).
10. M. Prager. A. Heidemann, *Chem. Rev.* **97**, 2933 (1997).

NMR Studies of the "Water-in-Salt" Ternary LiCl-CsCl-D_2O System

Valeriia Baranauskaite[1], Olga Pestova[1], Vladimir Matveev[2]

[1]Insitute of Chemistry, SPbSU, Saint-Petersburg, Russia
[2]Faculty of Physics, SPbSU, Saint-Petersburg, Russia
E-mail: valeriiebar@gmail.com

Introduction

Concentrated electrolyte solutions always drew attention of researchers due to their wide use in the different chemical, biological and technological processes [1]. Besides, in recent paper [2] it was shown that the highly concentrated, "water-in-salt", solution of lithium bis(trifluoromethane sulfonyl)imide, can be a perspective electrolyte for the electrochemical devices of new generation. It is possible to expect that this solution is not the single example of such kind, and the study of other similar highly-concentrated systems will allow one to find new types of electrolytes combining high performance and ecological properties. Keeping in mind above mentioned, a purpose of this investigation was the detailed study of the components mobility in the ternary LiCl-CsCl-D_2O system. The system contains common anion and two cations with sufficiently different properties concerning the cation-water interaction. Namely Li^+ is a "hydrophilic" type cation while Cs^+ is a "hydrophobic" one [3]. Therefore it is natural to expect some complex combinations of ions and solvent in the situation when there is lack of water molecules to solvate both cations [4].

Using NMR method we have measured temperature dependencies of T_1 and T_2 in the highly concentrated 17*m*LiCl-X*m*CsCl solutions in D_2O (X=1—8*m*). The T_1 and T_2 values were determined for ^2H, ^7Li and ^{133}Cs nuclei in wide range of temperature from 25^0C to the freezing point of each sample.

The detailed analysis of the temperature and concentration dependencies allowed us to reveal the major factors and influences on relaxation in each concentration region. For some concentrations the dispersion region was reached and the correlation times were determined and compared with the numerical values for the double systems. The temperatures of minimum and correlation times were found to depend mostly on the viscosity of the solutions. In addition an investigation of self-diffusion coefficients at 25^0C was performed in order to compare with the values for the double systems and to clarify the dynamics of the solutions.

Acknowledgements

NMR measurements were carried out in the Research park of St. Petersburg State University, Center for Magnetic Resonance

References

1. A.S. Arico, P. Bruce, B. Scrosati, J.-M. Tarascon, W. van Schalkwijk, - *Nat. Mater.* **4** 366–377 (2005).
2. L. Suo, O. Borodin, T. Gao, M. Olguin, J. Ho, X. Fan, Ch. Luo, Ch. Wang, K. Xu. – *Science*, **350**, 938-943 (2015).
3. Samojlov O.Ya. Struktura vodnyh rastvorov i gidrataciya ionov. – M.: Izd-vo AN SSSR, 1957.
4. L. Lilich, M. Khripun Rastvory kak himicheskie sistemy. Donorno-akceptornye reakcii v rastvorah (In Russian), - SPbSU, SPb, 2010.

Influence of residual water on NMR-relaxation in ionic liquids on basis of $[bmim]^+$ cation

S. S. Bystrov, V. V. Matveev, Yu. S. Chernyshev, V. I. Chizhik

Faculty of Physics, Saint-Petersburg State University, Department of Nuclear-Physics Research Method, Russian Federation
E-mail: barigapunk@gmail.com

Ionic liquids (ILs) are ionic compounds that are characterized by a melting point below 100°C. Cations mainly determine physical properties of IL (melting point, viscosity, density), whereas anions determine chemical properties. Since the physical and chemical properties of ILs can be adapted to the specific conditions by careful selection of types of cations and anions, ILs have become widely used in many scientific and industrial applications (electrochemistry, synthesis, processing) [1]. This study is directed to clarifying the difference in molecular mobility of ionic liquids: BMIM (butyl-methyl imidazolium) with 7 different anions (Cl, Br, I, BF4, TfO, NO3, Ac), as well as to the determination of the effect of water on the molecular mobility in the indicated ILs using NMR techniques. As examples, Fig. 1 and Fig. 2 show the standard numbering of atoms and temperature dependences of spin-lattice relaxation rates, respectively, for the dry IL $[bmim]^+ Cl^-$.

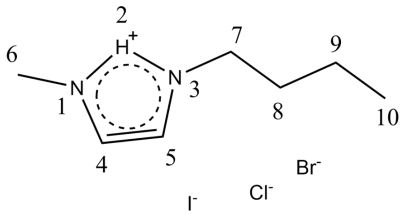

Figure 1. Numbering of atoms in IL of [bmim] type

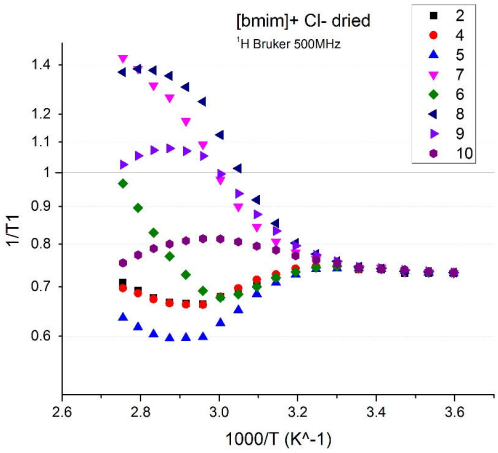

Figure 2. Temperature dependences of proton spin-lattice relaxation rates in dry IL

The investigation is based on the comparison and analysis of temperature dependences of the spin-lattice relaxation rates ($1/T_1$) and diffusion coefficients in non-aqueous (dried) ILs and water-containing ones. Fig. 3 shows temperature dependences of the diffusion coefficients for series of dried samples. The measurements were done using the capabilities of the Center for Magnetic Resonance, St. Petersburg State University: Bruker AVANCE III 500 MHz spectrometer equipped with a broadband inverse (BBI) probe. The measurements were performed in standard 5 mm NMR tubes. The temperature stability was ± 0.2˚C.

For the correct estimation of reorientation times of molecular groups the method developed in the work [2] was used. The drying process involved the use of a forvacuum pump, a heater and nitrogen traps, samples were dried at a temperature of 70˚C.

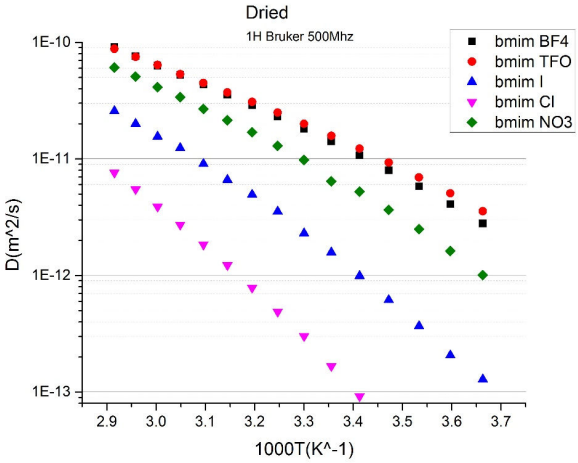

Figure 3. Temperature dependences of diffusion coefficients in various dry ILs

This part of work covers the revealing of the influence of water residues on relaxation behavior of the aforementioned system as well as identification of the physical and chemical properties of these ILs and comparison them among each other.

Acknowledgements

The work is supported by the RFFI grant 17-03-00057.

References

1. Pino V., Yao C., Anderson J. L. Micellization and interfacial behavior of imidazolium-based ionic liquids in organic solvent – water mixtures // Journal of Colloid and Interface Science. 2009. Vol. 333, no. 2. Pp. 548–556.
2. V.V. Matveev, D.A. Markelov, E.A. Brui, V.I. Chizhik, P. Ingman, E.Lahderanta. ^{13}C NMR relaxation and reorientation dynamics in imidazolium-based ionic liquids: revising interpretation. Physical Chemistry Chemical Physics. 2014, vol. 16, N 22, pp. 10480-10484.

Vibration effects in NMR spectroscopy for studies of ultra fast conformational dynamics

Vyacheslav A. Chertkov[1], *Tatyana A. Ganina*[1], *Dmitriy A. Cheshkov*[2], *Vladislav V. Stanishevskiy*[1], *Alla K. Shestakova*[2]

[1]*Department of Chemistry, Moscow State University, Moscow, Russia*
[2]*State Research Institute of Chemistry and Technology of Organoelement Compounds, Moscow Russia*
E-mail: *chertkov@org.chem.msu.ru*

Introduction

Dynamic behavior of molecular systems is regularly associated with some sort of chemical reactions. There are still numerous examples of extremely rapid dynamics, which can't be sufficiently evaluated in terms of classical kinetic parameters. Accurate structure studies of open-chain compounds and saturated four- and five-membered cycles imply solving specific problem of quantitative description of dynamic processes with no or very low barriers [1].

Methods

In recent time, quantum molecular dynamics methods [2] based on the large-amplitude vibration model have been widely used to describe various spectral and photochemical properties of organic molecules. Proper consideration of the internal rotation dynamics improves the accuracy and reliability of prediction of spectral parameters, in particular spin–spin coupling constants [3], which could provide key information for solving structural organic chemistry problems. These methods enable quantitative simulation of such fast processes as restricted internal rotation and inversion, which opens new prospects for conformational analysis of various acyclic systems, four-, five- and seven-membered rings, etc [4].

We developed a practical method for evaluation of the parameters of conformational dynamics in terms of vibrations with large amplitude. The method based on: (i) complete analysis of high resolution NMR spectra, (ii) ab'initio calculations of a reaction paths and surfaces of spin-spin coupling constants, (iii) a numerical solution of vibration problem and (iv) refinement for the parameters of the potentials based on the best fit of experimental and calculated spin-spin couplings (see e.g. [4-6]).

Results

Advantages of the technique demonstrated on studies of pseudorotation in four- and five-membered cycles and internal rotation in acyclic systems: vinylcyclopropane, styrene, cynnamic aldehyde and azobenzene. The dynamic structure of natural endogenic hormones adrenalin and noradrenalin as well as chemical warfare agent soman have been studied with the goal of obtaining accurate structural information to simulate molecular mechanisms of their action in living systems.

References

1. J.I. Steinfeld, J.S. Francisco, W.L. Hase – *Chemical Kinetics and Dynamics*, Englewood Cliffs, NJ: Prentice- all (1989).
2. F. Gatti, Ed. – *Molecular Quantum Dynamics: From Theory to Applications*, Heidelberg: Springer (2014).
3. R.D. Wigglesworth, W.T. Raynes, S. Kirpekar, J. Oddershede, S.P.A. Sauer – *J. Chem. Phys*., **112**, 3735-3745 (2000).
4. A.V. Chertkov, O.I. Pokrovsky, A.K. Shestakova, V.A. Chertkov – *Chem. Heterocycl. Comp.,* **44**, 782-784 (2008).
5. T.A. Ganina, V.A. Chertkov – *Russ. J. Org. Chem*., **52**, 489-498 (2016).
6. T.A. Ganina, D.A. Cheshkov, V.A. Chertkov – *Russ. J. Org. Chem*., **53**, 12-23 (2017).

Study of the metabolic doxorubicine-induced alterations in H9C2 cells and the effect of preincubation with dexrazoxane, a cardioprotective agent

Matthieu Dallons, Vanessa Tagliatti

Department of Human Biology and Toxicology, Faculty of Medicine and Pharmacy, University of Mons, Belgium
E-mail: Matthieu.Dallons@umons.ac.be
http://www.umons.ac.be

Introduction

Currently, doxorubicin anti-cancer treatment is limited by its irreversible cardiotoxicity [1]. The gravity of the toxicity depends on cumulated doxorubicin doses and can range from subclinical myopathy to patient's death [2]. The main toxicological mechanism is the production of reactive oxygen species (ROS), which lead to an oxidative stress impairing mitochondrial function and membrane integrity. It results in cardiomyocytes death by apoptosis and necrosis, clinically expressed by a progressive heart failure [3]. Nowadays, the main strategy to deal with this cardiotoxicity is the co-administration of dexrazoxane, a cardioprotective agent that acts by reducing ROS production through iron chelation. However, this strategy shows limited efficacy and there is a need for new cardioprotective strategies [1]. The goal of this research is to studying doxorubicin-induced metabolic alterations and the possible protective role of dexrazoxane. This strategy should help in highlighting possible new targets to counteract doxorubicin cardiotoxicity.

Material and methods

Cell culture, exposure and samples collection

Rat cardiomyoblasts H9C2 (2-1) (ECACC 88092904) were cultured in DMEM according to ECACC guidelines. For all exposure procedures, cells were first seeded with a density of 30.000 cells/cm^2 and were kept growing during 48 hours before any exposure. For metabonomic investigations, cells were randomly assigned into 4 groups (n=6): a control group (CTR), a 0,3 µM doxorubicin-exposed group (DOX), a 3 µM dexrazoxane-exposed group (DEX) a group pre-incubated with 3 µM of dexrazoxane during 30 min before 0,3 µM doxorubicin exposure (DEX-DOX). After 24 hours of incubation, culture medium was collected and stored at -80°C. Then, cells were washed with D-PBS and collected in 6 ml of cold methanol by scrapping and quickly frozen in liquid nitrogen before storage at -80°C.

Samples preparation for ^{1}H-NMR, spectra acquisition and treatment

A chloroform-methanol-water extraction was carried out with collected cells to extract intracellular metabolites. Briefly, cells were lysed by sonication and the addition of the 3 solvents allowing separation of hydrophilic and lipophilic intracellular metabolites. The methanol-water phase was collected and evaporated with a speed vacuum. Polar metabolites and culture media were mixed to phosphate buffer and TSP (external reference necessary for spectral calibration) into 5 mm NMR tubes. ^{1}H-NMR spectra were acquired by a Bruker Avance 500,16 Mhz spectrometer with a 5 mm PABBO BB- probe and a NOESYPRESTAT-1D sequence (256 scans). For each spectrum, a baseline correction, a phase correction and a TSP reference calibration to 0,00 ppm were carried out. Spectral area from 0,08 to 10 ppm was subdivised into sub-regions of 0,04 ppm wide. Each subregion was then integrated. The water peak (4,20 to 5,32 ppm), was deleted and each subregion integral was normalized to spectrum total area.

Multivariate data analysis, metabolites identification and statistical tests

Data were analysed by projection to latent structure discriminant analysis (PLS-DA) modeling with 4 defined classes corresponding to the 4 exposure groups. R^2_{cum} and Q^2_{cum} parameters, p-value of CV-ANOVA were determined. Variables with a VIP value > 0,8 were selected as most discriminant variables. Corresponding metabolites were identified with several databasis (« in house » databasis and HMDB) and by the use of Chenomix Profiler software. Statistical signifiance of identified metabolites was determined by integrating the ^{1}H-NMR peaks of each metabolite. Integrals were normalized to spectral total area. For normal and homoscedastic variables, signifiance was determined using a one-way ANOVA. For non-normal or heteroscedastic variables, signifiance was determined using Dunn test.

Results

A PLS-DA modeling was performed on both cell extract and medium spectra to highlight discriminant metabolites between the four exposure groups. Scores plots (Fig. 1) of both cell extracts and culture media show a clear separation between the 4 groups, indicating 4 different metabolic profiles.

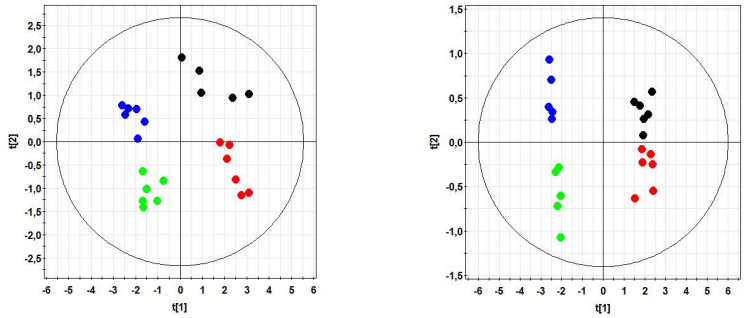

A **B**

*Figure 1. **A**: Scores plot of PLS-DA performed on cellular extracts. Parameters: R^2_{cum} = 0,59 Q^2_{cum} = 0,54, Hotteling's T2 = 0,95, P-value (CV-ANOVA) < 0,05.*
***B**: Scores plot of PLS-DA performed on culture media. Parameters: R^2_{cum} = 0,59 Q^2_{cum} = 0,52, Hotteling's T2 = 0,95, P-value (CV-ANOVA) < 0,05.*
Legend: CTR group (•), DOX group (•), DEX group (•), DEX-DOX group (•)

Single comparisons between CTR group and DOX or DEX group were carried out to highlight metabolic changes induced by doxorubicin or dexrazoxane exposure. A single comparison was also made between DOX group and DEX-DOX group to highligh metabolic changes due to dexrazoxane pre-incubation. Metabolic changes are shown in table 1.

Discussion

The metabonomic study highlighted some metabolic alterations due to doxorubicin exposure: a switch from mitochondrial aerobic energy metabolism to cytosolic anaerobic metabolism (increase of lactate, phosphocreatine and glutamine production and secretion, decrease of UDP-glucose level), a cell response to oxidative stress by an increased intracellular taurine level [4], modification of amino acids metabolism. The metabonomic study also highlighted metabolic effects of dexrazoxane pre-incubation: recovery of mitochondrial aerobic metabolism (decrease in lactate, glutamine levels and increase in UDP-glucose level), activation of choline metabolism (phosphocholine, glycerophosphocholine and serine increased levels, activation of creatine phosphorylation and an increased secretion of succinate.

Interestingly, choline metabolism activation may be linked to cell survival and growth pathways as well as succinate secretion may promote proliferation pathways by simulating GPR91 receptor [5]. Thus, choline metabolism and GPR91 could be potential targets for improving cardioprotection during doxorubicin exposure.

*Table 1. Identified discriminant metabolites. Metabolite concentration changes in DOX group and DEX group compared to CTR group and changes in DEX-DOX group compared to DOX group are indicated by arrows. VIP values are indicated between brackets. One way ANOVA or Dunn test: * p-value < 0,05, ** p-value < 0,01 *** p-value < 0,001*

Metabolites	Cell extracts			Culture media		
	DOX	DEX	DEX-DOX	DOX	DEX	DEX-DOX
Alanine	=	↓ (3,91)**	↓ (1,67)	-	-	-
Glucose	-	-	-	↓ (6,62)	↓ (2,38)	↓ (2,68)
Glutamate	=	↑ (1,05)**	↑ (1,38)	-	-	-
Glutamine	↑ (2,69)**	=	↓ (1,72)	↑ (2,49)***	=	↓ (0,13) *
Glycerophospho-choline	=	↑ (3,28)***	↑ (1,32)***	-	-	-
Glycine	=	↑ (1,23)*	↑ (2,17)*	-	-	-
Guanidoacetate	=	↑ (1,05)**	=	-	-	-
Isoleucine	↑ (1,09)	=	=	↑ (1,07)	↓ (2,19)	↑ (1,24)
Lactate	↑ (5,38)*	↓ (5,75)***	↓ (5,63)***	↑ (7,03)	↓ (11,74)***	↓ (12,00)***
Leucine	↑ (1,09)	=	↑ (1,02)	-	-	-
Methionine	↑ (5,06)	=	↓ (1,58)	-	-	-
Phosphocholine	=	↑ (3,28)***	↑ (1,32)***	-	-	-
Phosphocreatine	↑ (0,93)*	=	↑ (1,21)***	-	-	-
Proline	↑ (1,13)	↑ (1,52)	↓ (1,61)	-	-	-
Pyruvate	-	-	-	↓ (0,80)	↓ (0,17)**	=
Serine	=	↑ (8,82)***	↑ (8,79)***	=	↑ (3,91)***	↑ (2,71)***
Succinate	-	-	-	↑ (0,81)	↑ (2,66)**	↑ (2,80)*
Taurine	↑ (5,38)***	↓ (4,15)***	↓ (4,90)***	-	-	-
UDP-glucose	↓ (0,88)	↑ (4,95)*	↑ (1,44)	-	-	-
Valine	-	-	-	↑ (1,27)	↓ (1,60)	-

Acknowledgements

We sincerely thank the department of General, Organic and Biomedical Chemistry (Faculty of Medicine & Pharmacy, University of Mons) for the technical support related to the ^{1}H-MRN spectrometry.

References

1. Chung W-B, Youn H-J. Pathophysiology and preventive strategies of anthracycline-induced cardiotoxicity. The Korean Journal of Internal Medicine. 2016 Jul 1;31(4):625–33.
2. Groarke JD, Nohria A. Anthracycline cardiotoxicity: a new paradigm for an old classic. Circulation. 2015 Jun 2;131(22):1946–9.
3. Damiani RM, Moura DJ, Viau CM, Caceres RA, Henriques JAP, Saffi J. Pathways of cardiac toxicity: comparison between chemotherapeutic drugs doxorubicin and mitoxantrone. Archives of Toxicology. 2016 Jun 25.
4. Jong CJ, Azuma J, Schaffer S. Mechanism underlying the antioxidant activity of taurine: prevention of mitochondrial oxidant production. Amino Acids. 2012 Jun;42(6):2223–32.
5. Ariza AC, Deen PMT, Robben JH. The Succinate Receptor as a Novel Therapeutic Target for Oxidative and Metabolic Stress-Related Conditions. Frontiers in Endocrinology. 2012;3.

Atomic-scale probing of paramagnetic centers in nanodiamonds by ^{3}He NMR at low temperatures

Gleb Dolgorukov[1], Vyacheslav Kuzmin[1], Kajum Safiullin[1], Andrey Stanislavovas[1], Egor Alakshin[1], Timur Safin[1], Boris Yavkin[1], Sergei Orlinskii[1], Alexander Klochkov[1] and Murat Tagirov[2]

[1]Institute of Physics, Kazan Federal University, 420008 Kazan, Russian Federation
[2]Institute of Applied Research, Tatarstan Academy of Sciences, 420111 Kazan, Russian Federation
E-mail: Sasha_chayan@mail.ru

Introduction

The broad spectrum of potential applications of nanodiamonds initiated a large number of scientific studies of their properties. Recently it was demonstrated that some types of paramagnetic centers in nanodiamonds (NV-centers) can be successfully used as nanoscale sensors of the surrounding environment in NMR [1]. That requires the accurate determination of location of paramagnetic centers in nanodiamonds.

Here we present a new original technique that provides detailed information on the spatial distribution of paramagnetic impurities in nanodiamonds [2]. It is based on the measurement of relaxation times of adsorbed ^{3}He separated from the sample surface by variable thickness of preadsorbed layer of an inactive gas.

Materials and methods

Powder of detonation nanodiamonds with nearly spherical particles with sizes of 3-10 nm was used as a sample. Electron paramagnetic resonance (EPR), transmission electron microscopy (TEM), powder X-ray diffraction and nitrogen adsorption techniques were used for the detailed sample characterization.

Adsorbed ^{3}He NMR experiments were performed using a home-built pulsed NMR spectrometer [3] in the temperature range of 1.5-4.2 K at 5-19 MHz resonance frequencies. In our experiments ^{3}He was adsorbed either on a clean sample surface or onto preadsorbed layers of nitrogen. Preadsorption of the sample with a certain amount of nitrogen layers was performed during the slow cooling from room temperature down to 4.2 K.

Results and discussion

We performed NMR measurements of adsorbed ^{3}He on nanodiamonds with clean surface and with preadsorbed nitrogen layers. In these experiments we also used various monolayer coverage fractions of ^{3}He (it varied from 0.45 to 1.0). Measured ^{3}He longitudinal magnetization recovery and transverse magnetization decay curves are described well by single exponential functions.

The obtained temperature dependencies of adsorbed ^{3}He spin-lattice relaxation rates show nonlinear behavior with maxima values $T_1^{-1}{}_{max}$ (Fig. 1). The temperature T_{max} of the maxima relaxation depends on the ^{3}He monolayer coverage. It was found that the value of the maximum relaxation rate $T_1^{-1}{}_{max}$ strongly depends on the amount of preadsorbed nitrogen layers (Fig. 2), i.e. on the distance between the adsorbed ^{3}He and nanodiamond surface. The closer adsorbed ^{3}He is to the nanodiamond surface, the faster relaxation occurs.

EPR measurements on this sample revealed a high concentration of paramagnetic centers (order of 10^{20} per gram). It is also known that paramagnetic centers in detonation nanodiamonds are located in nanodiamond shell [4], which is consistent with performed sample characterization.

Taking into account these facts we suggest the ^{3}He relaxation model [2], which implied that ^{3}He relaxation is governed by paramagnetic centers and intrinsic dipolar relaxation in

adsorbed ^{3}He film. The fits of experimental data by this model provide distance to paramagnetic centers (Fig.2). The obtained average distance between paramagnetic centers of nanodiamonds and its surface is 0.5±0.1 nm. This value is in a good agreement with the fact that paramagnetic centers are located in the nanodiamond shell.

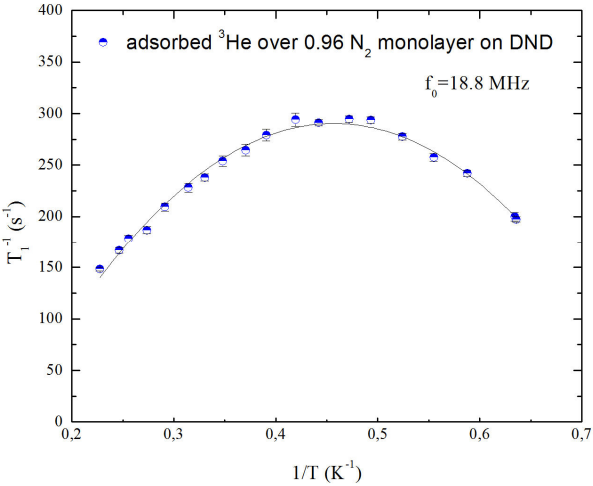

Figure 1. Temperature dependences of ^{3}He spin–lattice relaxation rate T_1^{-1} at monolayer coverage of the nanodiamond powder sample preplated with nitrogen layer (N = 0.96). Solid line represent fit by the parabolic function

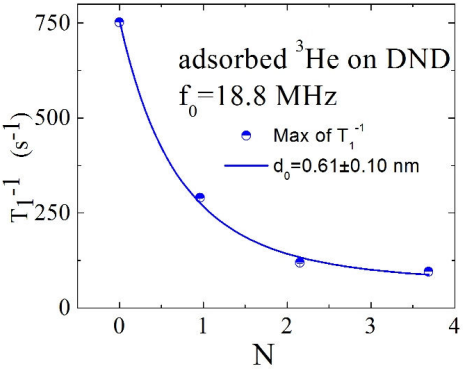

Figure 2. The dependence of ^{3}He spin-lattice relaxation rate adsorbed on nanodiamonds (full monolayer coverage) on amount of preadsorbed nitrogen layers at 18.8 MHz resonance frequency

Conclusion

The NMR measurements of adsorbed ^{3}He on nanodiamonds have been performed at low temperatures. The suggested relaxation model explains obtained experimental data on ^{3}He relaxation and allows to determine the location of near-surface paramagnetic centers in

nanodiamonds quantitatively with a high precision. According to the relaxation model and the obtained experimental results, the average distance between paramagnetic centers and surface of nanodiamonds is 0.5±0.1 nm. This value is consistent with the information on detonation nanodiamond structure obtained during the sample characterization. The proposed technique can be used in studies of nanoscaled samples with paramagnetic impurities.

References

1. T. Staudacher, et al. Nuclear Magnetic Resonance Spectroscopy on a (5-Nanometer)3 Sample Volume. – Science, 2013, 339, 561
2. Kuzmin V. et al. Angstrom-scale probing of paramagnetic centers location in nanodiamonds by ^{3}He NMR at low temperatures. – Phys. Chem. Chem. Phys., 2018, 20, 1476
3. Alakshin et al. The home-built pulse nuclear magnetic resonance spectrometer with digital quadrature detection for ^{3}He research at low temperatures. – Magn. Reson. Solids, 2013 **15**, 13104
4. O. A. Shenderova, – Detonation nanodiamonds: science and applications, Pan Stanford Publishing, Singapore, 2014

NMR relaxation of fractal macromolecules

Maxim Dolgushev[1] and Denis A. Markelov[2]

[1]Sorbonne Université, CNRS, Laboratoire de Physique Théorique de la Matière Condensée, LPTMC, 4 place Jussieu, F-75005 Paris, France.
[2]St. Petersburg State University, 7/9 Universitetskaya nab., St. Petersburg, 199034, Russia
E-mail: dolgushev@lptmc.jussieu.fr
https://www.lptmc.jussieu.fr/users/dolgushev/

This contribution deals with the local orientational mobility of hyperbranched macromolecules, which have fractal architecture. This property is investigated with the focus on the NMR relaxation by means of the spectral density $J(\omega)$. The macromolecules are modeled in the framework of semiflexible treelike polymers [1] in the form of Vicsek fractals [2]. As for dendrimers [3-7], also for fractal macromolecules the semiflexibility plays a crucial role for the NMR relaxation [8]. By looking on the segments having different location in the Vicsek fractal, we find that the function $\omega J(\omega)$ has a single maximum for the fully flexible structures; its position is independent of the location of the labeled segments. For the segments of a semiflexible Vicsek fractals, the function $\omega J(\omega)$ is very broad and its broadness is directly related to the location of the segments in the macromolecule. This feature reflects the overall relaxation of the branch that is originated by the labeled segment and the overall relaxation of subbranches that build this branch. Thus, the inner segments display a broader shape of the function $\omega J(\omega)$. This behavior differs from that of the dendrimers, where one observes rather narrow peaks of $\omega J(\omega)$ [3]. Also, for very large fractal macromolecules the most inner segments do not feel their remoteness from the periphery anymore and the effect of broadening gets saturated.

References

1. M. Dolgushev, A. Blumen, *J. Chem. Phys.* **131**, 044905 (2009).
2. F. Fürstenberg, M. Dolgushev, A. Blumen, *J. Chem. Phys.* **138**, 034904 (2013).
3. D.A. Markelov, M. Dolgushev, Yu.Ya. Gotlib, A. Blumen, *J. Chem. Phys.* **140**, 244904 (2014).
4. D.A. Markelov, S.G. Falkovich, I.M. Neelov, M.Y. Ilyash, V.V. Matveev, E. Lähderanta, P. Ingman, A.A. Darinskii, *Phys. Chem. Chem. Phys.* **17**, 3214 (2015).
5. D.A. Markelov, A.N. Shishkin, V.V. Matveev, A.V. Penkova, E. Lähderanta, V.I. Chizhik, *Macromolecules* **49**, 9247 (2016).
6. O.V. Shavykin, I.M. Neelov, A.A. Darinskii, *Phys. Chem. Chem. Phys.* **18**, 24307 (2016).
7. D.A. Markelov, M. Dolgushev, E. Lähderanta, *Annu Rep. NMR Spectrosc.* **91**, 1-66 (2017).
8. D.A. Markelov, F. Fürstenberg, M. Dolgushev, submitted.

Fast technique for crystallinity estimation of solids by the transverse magnetization and double quantum relaxation

Leonid Grunin[1,2]

[1]*Resonance Systems GmbH. Seestrasse 28, D-73230, Kirchheim u. Teck, Germany*
[2]*Volga State University of Technology, Lenin sq. 3, Yoshkar-Ola, Russia*
E-mail: mobilenmr@hotmail.com
http://www.nmr-design.com

Knowing structural organization of polymers remains one of the most demanding issue for the last 40 years and its importance is still growing because of the necessity of new materials introduction to our life. Most of polymeric stuff possess so called semicrystalline structure that means they have *more* (crystalline) and *less* (amorphous) ordered volumes. There is a variety of methods to estimate their populations based on X-Ray diffraction, Infra-Red Spectroscopy, analyzing of solubility in chemically aggressive liquids and many others. One very attractive approach is based on the Time-Domain NMR relaxation. It potentially shows far better measurements convenience and accuracy comparing to enumerated above.

At the first glance the simplest way would conclude in calculation of the Free Induction Decay (FID) fast relaxing component contribution to the overall transverse relaxation signal. This component for ordered crystallites nearly always has an oscillating "beat" of Pake doublet nature and its shape is known to be fitted with models like

$$a_s(t) = A_s \exp\left(-\tfrac{1}{2} a_s^2 t^2\right) \cdot \cos \tfrac{1}{2} bt \quad \text{or} \quad a_s(t) = A_s \exp\left(-\tfrac{1}{2} a_s^2 t^2\right) \cdot \sin(bt) / (bt) \tag{1}$$

while the amorphous part normally relaxes as the monotonic Gaussian $a_m(t) = A_m \exp\left(-\tfrac{1}{2} a_m^2 t^2\right)$

Here indexes *s* and *m* denote "short" and "long" solid FID signals. The crystallinity ξ value can be calculated straightforward as

$$\xi \propto \frac{A_s}{A_s + A_m} \tag{2}$$

Unfortunately, in fact the quality of fitting of the mentioned "beat" by functions (1) is not always stably acceptable for precise crystallinity measurements in industrial applications. Moreover, for some polymers the NMR relaxation parameters *a* and *b* in (1) are temperature depended. Due to this the approach (2) cannot be considered as really robust.

In presented talk we make the effort to eliminate temperature effect on the measured crystallinity. We also suggest the smooth way of fitting by processing both the time- and frequency-domain data.

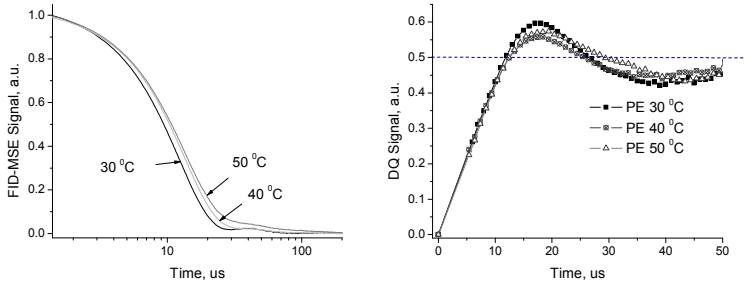

Figure 1. FIDs and QD Build-up curves for PE samples at different temperatures

The idea behind this compensation originates from temperature independence of the initial growth of the normalized double quantum (DQ) build-up curve (refer to *Figure 1*). While the dipolar residual parameter D_{res} which defines the NMR lineshape and FID signal is the function of both polymer chains structure and dynamics, the behavior of the DQ curve until it firstly reaches its asymptotic value 0.5 is determined by only structure and nearly not depends on temperature. On the other hand, the build-up DQ experiment turns like much more time consuming than just one Magic Sandwich Echo (MSE)-FID acquisition, hence it is not competitive to be applied for routine measurements.

In the proposed technique we first acquire the normalized DQ curve and use it to calculate the static limit of dipolar interactions D_{eff} and then the second moment M_{2eff} for a given class of samples (i.e. polyethylene, celluloses etc). The values of M_{2eff} are constant and can be stored in the database of the measuring instrument.

For compensating of sample dynamics influence it is necessary to get the temperature dependence of dynamic base order parameter $S_b(T)$ for each class of materials. This procedure concludes in obtaining the MSE-FIDs at different temperatures, fitting them with functions (1) in both time- and frequency domains, estimating of the residual second moment M_{2res},

$$M_{2res} = \frac{A_s}{A_s + A_m} M_{2s} + \frac{A_m}{A_s + A_m} M_{2m}, \tag{3}$$

and following calculation of the $S_b(T)$

$$S_b(T) = \sqrt{\frac{M_{2res}}{M_{2eff}}} \tag{4}$$

The fast stage of routine measurements will be hence just the FID-MSE acquisition, deriving M_{2res} as the fitted value and backward estimation of the temperature independent M_{2eff}.

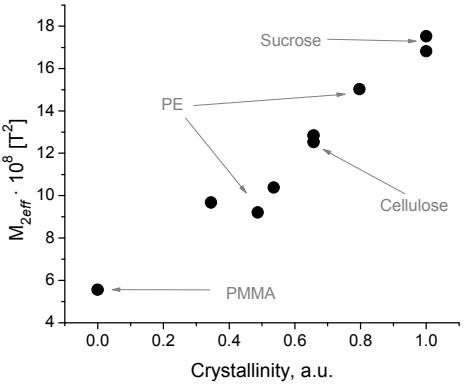

Figure 2. The second moment plot versus Crystallinity for different classes of samples

In Figure 2 we demonstrate the versatility of the offered approach to get the crystallinity content by the TD-NMR for really various range of materials.

All measurements were performed by the Spin Track NMR Analyzer with 10 mm tube od and the duration of 90^0 pulse equal to 1.6 microseconds. Pulse sequences of FID-MSE and DQ-Buildup were supplied by the vendor.

Analysis of NMR spectra of ionic liquid EAN with the addition of inorganic salts

Alexandr V. Ievlev[1], Vladimir V. Matveev[1], Mikhail A. Vovk[2]

[1]Faculty of Physic, department of nuclear-physics research methods, Saint-Petersburg State University, Russia
[2]Center for Magnetic Resonance of Research Park of St. Petersburg State University
E-mail: a.ievlev@spbu.ru

Introduction

Recently, a class of substances called ionic liquids has been intensively studied. Interest in such objects arose first due to the extensive field of application, and secondly due to the interesting physical-chemical properties. To date there are a lot of ILs applications known as "green chemistry", new chemical reactions including cellulose transformation, the uptake of carbon dioxide, for novel electrochemical devices. Among these multiple applications of ionic liquids is design of electrolytes for supercapacitors, ion batteries, fuel cells etc. The purpose of this paper was to compare the NMR spectra of a well-known ionic liquid EAN with the addition of various inorganic salts.

Results and discussion

Figure 1 shows the comparative NMR spectra, the rulers of the samples under study, at room temperature. We studied both the pure ionic liquid and its mixtures with inorganic metal salts, namely nitrates of aluminum, calcium, magnesium, and lithium. The spectra can be easy divided into two groups with different properties. The first group includes $LiNO_3$ and $Ca(NO_3)_2$ salt solutions. These spectra as well as dried pure EAN (Figure 2) contain an addition weaker line at ca. 4.8 ppm, which can be assigned to residual water in each dried solution and/or in the not absolutely dried NMR tube. This line shows a significant intensity in the "as prepared" samples, and practically diminishes in the samples after vacuum drying procedure. And these NMR data are completely correlated with the result of the "Fisher" test.

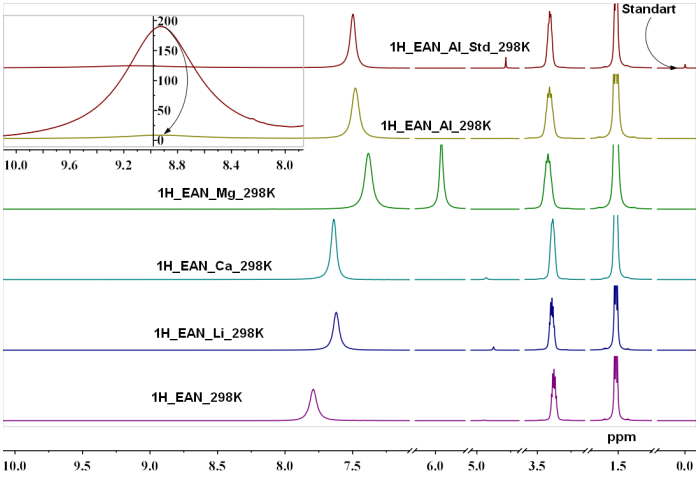

Figure 1. ^1H NMR spectra of EAN solutions of $M(NO_3)_n$; $M^{n+}=Li^+$, Ca^{2+}, Mg^{2+}, Al^{3+}

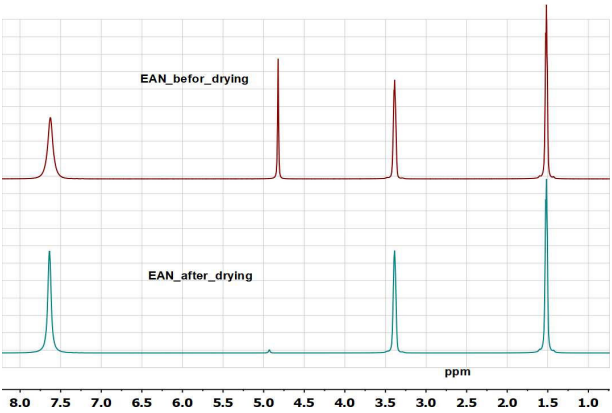

Figure 2. ^{1}H NMR spectra of EAN before and after vacuum drying procedure. Left to right: NH_3-, CH_2-, and CH_3-groups

Otherwise, ^{1}H NMR spectra of EAN solutions of $Al(NO_3)_3$ and $Mg(NO_3)_2$ salts contain a clear observed additional line in weaker field (i.e. with larger δ) as compared to the line of water impurity. The lines dispose in a substantially weaker field as compared to water in pure water, in pure EAN or in aqueous solutions of lithium and calcium nitrates. Since the lines corresponding to EAN solvent remain in both spectra, and the ratio of their integrals is maintained, it is evident that the additional line appeared as a result of the addition of aluminum and magnesium salts to EAN. Therefore it is reasonable to assume that this line belongs to water which is contained in the salt crystalline hydrates namely, in $Al(NO_3)_3 \cdot 9H_2O$ and $Mg(NO_3)_2 \cdot 6H_2O$. As evident from the spectra this water cannot be removed by the drying procedure. The reason of it may be connected to entrance of a part of water molecules into the primary solvation shell of the Al^{3+} and Mg^{2+} metal cations. This effect is consistent with the well-known fact that some of water molecules in aqueous solutions of some inorganic salts are associated with (bonded to) metal cations, i.e. are located in the cation primary solvation shell and differ in the properties from water in the solvent volume.

Conclusion

The NMR spectra reveal obviously that in the studied solutions Mg^{2+} and Al^{3+} cations continue to hold water molecules in their first solvation shell even after vacuum-drying procedure. This solvated water is not detected by conventional Karl Fisher test which finds the solutions as practically dry. It is possible to assume that this solvated water will not prevent to use the solutions as electrolytes for electrochemical devices [1].

Acknowledgements

The work was partly supported by RFBR, grant № 17-03-00057. The NMR measurements have been carried out partially in Center for Magnetic Resonance of Research Park of St. Petersburg State University and partially in the Instrumental Centre of University of Santiago de Compostela.

References

1. Vladimir V. Matveev, Alexandr V. Ievlev, Mikhail A. Vovk, Silivia Bouzón-Capelo, Oscar Cabeza, Elena López -Lago, Julio R. Rodriguez, Luis M. Varela, and Erkki Lähderanta “NMR investigation of inorganic salt solutions in EAN ionic liquid”, to be submitted.

EPR spectra simulation from MD data using Redfield theory and direct propagation method

Sergei A. Izmailov[1], *Sevastyan O. Rabdano*[1], *Ivan S. Podkorytov*[1], *Nikolai R. Skrynnikov*[1,2]

[1]*Laboratory of Biomolecular NMR, SPbSU, 199034, 7/9 Universitetskaya nab., St. Petersburg*
[2]*Department of Chemistry, Purdue University, 47907, 560, Oval Drive,*
West Lafayette IN, USA
E-mail: sergei.a.izmailov@gmail.com
http://bio-nmr.spbu.ru

In general, investigation of a spin system evolution with a stochastic Hamiltonian requires knowledge of dynamical statistics to obtain observables. Usually those statistics are not known, and their characteristics are a subject of speculation. The differences in those dynamic parameters are crucial. For example, they allow us to discriminate between different protein environments by means of the EPR spectroscopy using nitroxyl spin labels. In particular, we can assess the mobility of the different elements of secondary structure and probe the constraining effect of the side chains at the surface of the protein. Nowadays molecular dynamics simulations are able to provide atomic resolution information about molecular motions at time scales up to several microseconds in a reasonable amount of computational time. This allows us to obtain the desired statistics from MD simulations and thus successfully simulate the EPR spectra.

In this report two general approaches to generate EPR spectra are described. First method is a robust propagation of density matrix via the Liouville equation using time-dependent spatial coordinates from the MD simulations [1]. Second approach is based on the Redfield theory, formulated in the operator basis [2]. Both methods are applicable to an arbitrary spin system.

We have found that the two methods produce identical results for MTSL-labeled small protein GB1, freely tumbling in solution (collaboration with the group of S. Saxena, University of Pittsburgh). This opens the path for analyzing the characteristic features of the EPR spectra in terms of the powerful Redfield formalism, e.g. by analyzing the cross-correlation effects [3].

Acknowledgements

This work is supported by RSF grant 15-14-20038 and benefited from the use of the Computing Center at the SPbSU Research Park.

References

1. Kuprusevicius, Egidijus, Gaye White, and Vasily S. Oganesyan. *Faraday discussions* 148 (2011): 283-298.
2. Canet, Daniel. Progress in Nuclear Magnetic *Resonance Spectroscopy* 21.3 (1989): 237-291.
3. Brutscher, Bernhard. Concepts in Magnetic Resonance Part A 12.4 (2000): 207-229.

How to Optimize NMR Approach for Structure Elucidation of Small Molecules on Bruker Spectrometers

Dr. Vadim V. Kachala, NMR spectroscopy specialist

Bruker Ltd., Pyatnitskaya st. 50/2 b.1, 119017 Moscow, Russian Federation
vadim.kachala@bruker.com

2D NMR spectroscopy is approved and very informative method for structure determination of many classes of organic molecules. During last 25 years many methods were improved, as spectrometer vendors followed growing requirements of modern 2D NMR. Thus, new design of NMR probes, including Z-gradient coils, automated tuning and matching, high fidelity digital RF electronics solutions, software packages for automation, acquisition and analysis proposed new standards. Since that 2D methods have became very popular and turned from some sophisticated "state of art NMR", "secret knowledge NMR" to everyday, routine usage. Now it's hard to find a modern spectrometer where an operator couldn't find a pack of standard 1D and 2D pulse programs and parameter settings, in order to start using them "from a box". At the same time, the number of experiments used is typically limited by well known correlations, like COSY, NOESY, TOCSY, HSQC and HMBC.

In this presentation I would like to discover efficient approaches to practical application of modern NMR methods for structure elucidation tasks, including optimization of well-known methods, as well as usage of non-typical methods for optimal solution of structural problems. Some methods, as computer-assisted structure elucidation approach, based on Bruker's CMC-SE software will be reviewed.

Skin-Effect Compensated Optimal Control Pulses for Excitation in a Conductive Medium

Boris Kharkov[1], Leonard Strouk[2], Alexej Jerschow[2]

[1]Laboratory of Biomolecular NMR, St. Petersburg State University, St. Petersburg, 199034, Russia.
[2]Department of Chemistry, New York University, 100 Washington Sq. East, New York, NY 10003 USA
E-mail: kharkov@nyu.edu

Introduction

In contrast to conventional NMR in non-conductive materials, spectroscopy of samples containing metals, e.g. batteries, is complicated by systematic distortions that affect both the applied radio-frequency (rf) fields and registered spin response. These distortions originate from eddy currents that are induced in metal upon rf irradiation, the phenomenon is typically referred as "skin effect" [1]. In this work, we describe an optimal control theory based approach to design rf pulses for excitation in conductive samples such as bulk metals.

Application of optimal control theory (OCT) [2] to searching new NMR excitation techniques allows to tailor pulse shapes to suit best to the particular problem in study. In previous works, OCT was primarily used for adjusting NMR experiments to specifics of a spin system and nuclear interactions in it, while in this work, we use OCT to address the skin effect problem. Thus, the project aims to study the possibility of using the OCT numerical simulations to find novel rf excitation profiles, characterized by improved performance comparing to conventional methods.

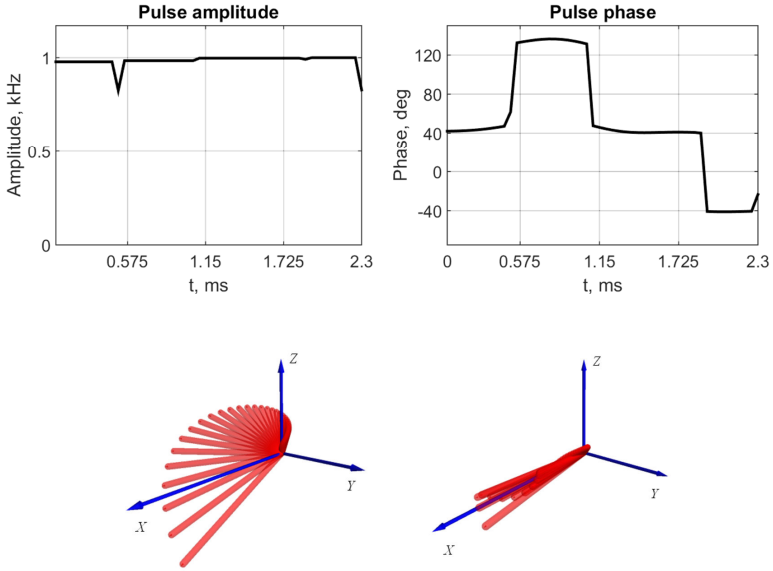

Figure 1. OCT designed pulse shape. Bottom: comparison of magnetization distribution in metal after a rectangular 120° pulse (maximum signal, left) and OCT pulse (right)

Figure 1 shows the optimal control designed pulse profile and the comparison of magnetization distribution in a metal sample after a rectangular 120˚ pulse and the OCT pulse. It can be seen that OCT pulse leads to higher magnetization coherence among different layers in the sample that leads to 75% higher signal intensity. The refocusing and selective metal excitation pulse design strategies will be discussed as well.

References

1. M. Mehring, D. Kotzur, O. Kanert, Phys. Stat. Sol. (b), 1972, 53, K25.
2. N. Khaneja et al., J. Magn. Reson., 2005, 172, 296.

NMR relaxometer for the estimation of the spin-spin proton relaxation time of the living tissue

Denis D. Kosenkov[1,2], Yuriy I. Neronov[1,2], Aleksey N. Zolotov[1,2], Nikolay N. Seregin[1]

[1]Mendeleyev Institute for metrology, St. Petersburg, Moskovsky pr. 19, Russia
[2]Saint Petersburg National Research University of Information Technologies, Mechanics and Optics, St. Petersburg, Kronverkskiy pr. 49, Russia
E-mail: wdenkosw@gmail.com, yineronov@mail.ru, alexzolotov2014@gmail.com

Introduction

Earlier, in work [1-4] the use of a desktop permanent magnet B = 0.128 T as of the basis for a mini-NMR tomograph was reported. This device allows one to accumulate the image from the living tissues of the index finger or the thumb by placing the participant's hand in the registration area between the polar magnets. Figure 1 shows three images of the index finger section that were obtained from echo NMR signals located at intervals of TE = 8, TE = 40 and TE = 60 ms from the first 90-degree excitation impulse.

The interval between the exciting pulses was set to TR = 900 ms. As you can see, different tissues have different spin-spin proton relaxation times. In particular, the tissues adjacent to the skin cover no longer contribute to the echo signal during the 60 ms interval. However, the bone marrow tissue continues to radiate a sufficiently intense NMR signal.

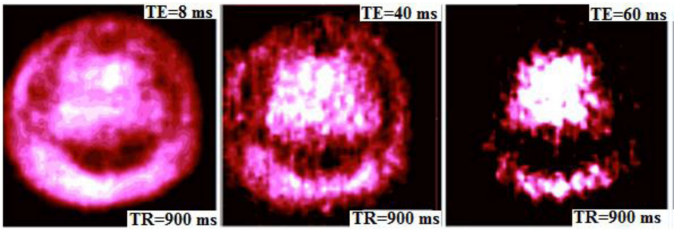

Figure 1. Images of the section of the index finger obtained at different time intervals between 90-degree and 180-degree pulses

Description of relaxation time registration methodology

Biological tissue is a quite intricate molecular system. Spin relaxation times, which may be measured by relaxational NMR approaches, could be used as parameters, that characterize the concentration of paramagnetic centers and mirror the condition of living tissue.

In this paper authors used the base of this device in order to determine spin-spin relaxation time more exactly. The radio-electronic part was replaced with the newer one, where modern microelectronic integrated circuit was used. To process the resonance frequencies, the AD9958 chip was used, which synthesizes reference frequencies for recording NMR signals from both protons and deuterons. Signals from deuterons were recorded from an additional sample and used to stabilize the phase conditions of the proton resonance.

Having estimated the span of T2 data, it was stated, that the most stabile results could be acquired with the application of Hans approach and consecutive extension of the interval between 90- and 180-degree impulses by 2 ms. The time interval between 90-degrees impulses was set to 3 s.

The corresponding cycle contains 40 NMR echo-signals, which by Fourier transformation were transformed into a spectrum. Amplitudes of the signals were saved for further analysis.

After the end of the cycle (2 minutes) the amplitudes are shown on the screen (red vertical lines) alongside with the calculated values (black vertical lines), which are acquired using the least square method (Fig. 2), which allows the operator maintain the performance of the device and the process of obtaining the data.

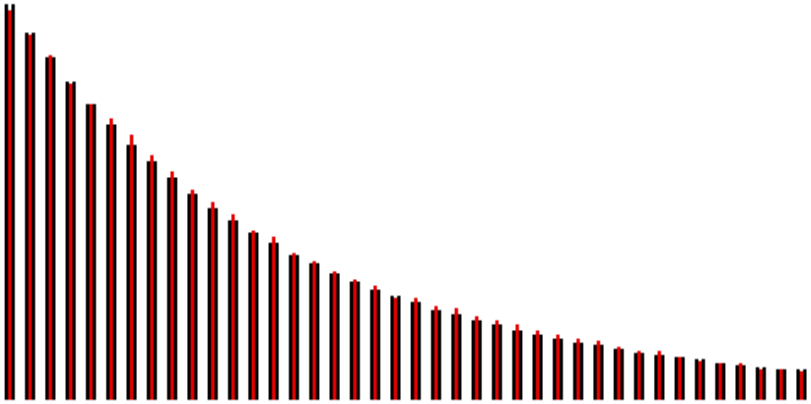

Figure 2. Sequence of 40 NMR echo-signal amplitudes (calculated and experimental values). The first echo signal was registered at time interval TE = 16 ms and the last one at TE = 172 ms

Evaluation of the error of registration

Fig. 3 shows the results of testing the device in the mode described above. The error for a single measurement as a rule was 1%, which was determined from the value of the root-mean-square spread of the discrepancy between the experimental and calculated amplitudes dA / A. It follows from 35 results (Figure 3) that the typical spread for T2 with sequentially recorded data (t = 20 ± 1 oC) is also at the level of 1%.

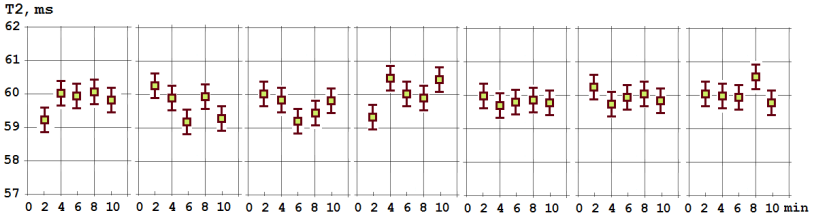

Figure 3. Evaluation of the stability of the instrument and the error of registration T2 ≈ 60 ms was performed for an ampoule with a water solution with the addition of a "Magnevist" preparation containing paramagnetic gadolinium atoms used in contrast MRT diagnostics

For living tissues, if only one exponent is used to describe the data, the root-mean-square deviations dA /A of the amplitudes of the experimental data from the calculated ones are at the level: RMS ≈ 5.3%. In the case of using two exponentials, the root-mean-square deviations for dA /A decrease to: RMS ≈ 1%.

The expression A (t) = Ao [w × exp (– t / T2a) + (1-w) × exp (– t / T2b)] was used.

Moreover, only two parameters T2a and T2b were determined with allowance for the normalization (Ao = 100%) and using the value w = 0.617 for the weight parameter, which was

determined experimentally for this method. The constancy of w is due to the fact: that the same structures of living tissue were in the registration zone for different participants in the experiment. Using this technique, the authors searched for the influence of external factors on the relaxation times.

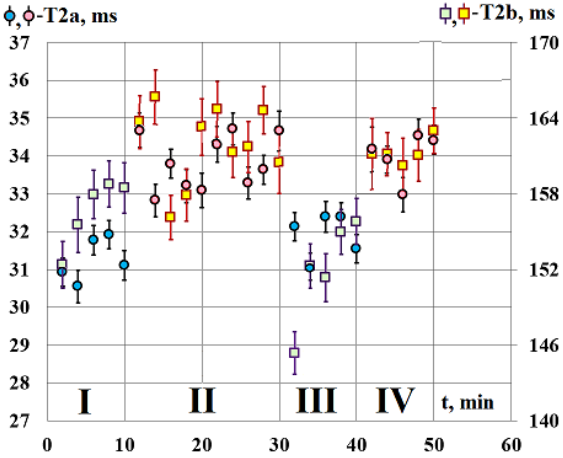

Figure 4. Changes in parameters T2a and T2b depending on the time of registration and the state of metabolic activity of the tissues of the participant in the experiment

The spin-spin time of proton relaxation of distilled water is approximately T2 ≈ 500 ms and depends on the degree of water purification (in particular, T2 depends on the concentration of dissolved oxygen). In living tissues, it is reduced by more than an order of magnitude. The most typical for students are data: T2a ≈ 31 ms, T2b ≈ 150 ms. However, individual deviations can sometimes reach ≈ 24% for T2a and ≈ 13% for T2b.

As an example, in Fig. 4 shows the changes in these parameters for one of the participants in the experiment within 10 minutes after their arrival from the street to the laboratory (data zones I and III) and further: an increase in these parameters (zones II and IV) in the subsequent time of his stay in the laboratory, which is typical for the condition of a typical office worker.

References

1. V. K. Ivanov, Y. I. Neronov, V. A. Ivanov. Mini-NMR-tomograph of measurement technologies and computer tomography chairs SPBGU ITMO P. (in Russian). – *Scientific and technical bulletin of the St. Petersburg State Institute of Precision Mechanics and Optics (Technical University) (in Russian)*, №3, 201 (2001)
2. Y. I. Neronov, V. K. Ivanov. Mini-tomograph development for educational and scientific research goals (in Russian). – *Scientific instrument making (in Russian)*, T.16, №16, 105-112 (2006)
3. Y. I. Neronov. NMR-tomograph controlling module (in Russian) – *News of higher educational institutions. Instrument making (in Russian)*, T. 51, № 10, 47-51 (2008)
4. Y. I. Neronov, A. N. Seregin. Mini-MRI scanner and some possibilities for its use for studying living tissues – *Measurement techniques,* T. 54, № 1, 103-107 (2011)

Dehydration/rehydration processes in sodium- and copper-exchanged mordenites studied by TGA and NMR

Ekaterina Krylova[1], Marina Shelyapina[1], Hubert Harańczyk[2], Vitalii Petranovskii[3]

[1]Saint-Petersburg State University, St. Petersburg, Russia
[2]M. Smoluchowski Institute of Physics, Jagiellonian University, Kraków, Poland
[3] CNyN, National Autonomous University of Mexico, Ensenada, Mexico
E-mail: krylovaea2803@mail.ru

Cooper-exchanged zeolites are composite materials, which are more widely used to removal of nitrogen oxides from exhaust gases (de-NO_x catalysts) [1,2]. These materials have unique properties, which are influenced by a valence state of copper ions, their location, coordination in the zeolite lattice and by copper content [3]. Besides, there is another important factor: water, which easily enters into zeolite channels. It is well known, that water molecules are promoters in many physic and chemical processes in porous materials. From this perspective, study of dehydration/rehydration processes of zeolites as well as determination of water molecule localization is highly required. In this contribution, we report on the results of the study of dehydration/rehydration process in sodium and copper-exchange mordenitesdone by thermogravimetric analysis (TGA) and ^{1}H nuclear magnetic resonance (NMR).

The samples CuNaMorM*X* (where *X* = 1, 2, 3 and 6 is the number of ion-exchangeprocedures) were synthetized from Na-mordenites (NaMor) supplied by Zeolist Int. (productCBV10A) with Si/Al atomic ratio equal to 6.5. The ion-exchange procedure was done byusing the microwave assisted method. For more details see [4]. To increase the coppercontent, the exchange procedure was repeated several times up to six copper-exchangeprocedures.

To determine the water content,activation energy of water desorption and how dehydration process isaffected by the type of the extra-framework cation TGA profileswere recordedin the temperature range 40-700°C at the heating rate of 2, 10 and 20°C/min in argon stream at the rate of 50 ml/minusing a Netzsch STA 449 F1 Jupiter analyzer.Proton NMR spectra for dehydrated and gradually rehydrated samples were recorded on Bruker Avance III spectrometer(Bruker Biospin)at 300MHz.

Results of TGA studies show several stages of thermal degradation associated with desorption of water, which was confirmed by mass-spectroscopy analysis. For Na-MOR, weight loss occurs in two steps, Fig.1. Step-I can be attributed to the loss of physisorbed water located on the outer surface and ‘free’ water in the main mordenite channel. Step-II could be associated with the release of water molecules located in the vicinity of cations. For CuNa-MOR-M6 weight loss takes place in four steps. Step-I once again can be attributed to the release of the physisorbed water and ‘free’ water from the main channel; however, Step-II, which is shifted toward lower temperature as compared to Na-MOR, corresponds to the loss of water molecules that are surrounding Cu^{2+} cations. Step-III and Step-IV we associate with the release of hydroxyl groups or decay of complex cations.

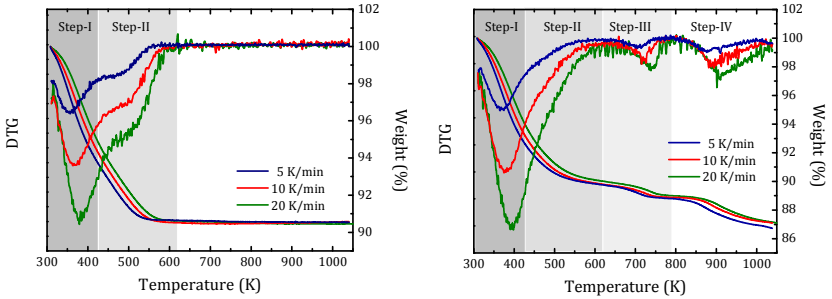

Figure 1. TG and DTG profiles for the Na-MOR (a) anf CuNa-MOR-M6 (b) samples at differentheating rates

A detailed analysis of rehydration processes was done by proton NMR spectroscopy. The obtained results allowus to distinguish different types of water (L1 and L2 lines in Fig. 2 (*a*)) with different mobility. Since neither the L1 line position nor its linewidth do not depend on the hydration level, whereas its intensity rapidly increases with hydration level $\Delta m/m_0$ increasing, see Fig. 2 (b), one attributes this line to the 'free' water molecules present in the main mordenite channel. As it is seen from Fig. 2 (b), the ratio of the integral intensities of L1 and L2 lines versus the hydration level for the Na-MOR sample can be perfectly fitted by the linear function. It means that upon hydration water molecules directly enter the main channel.

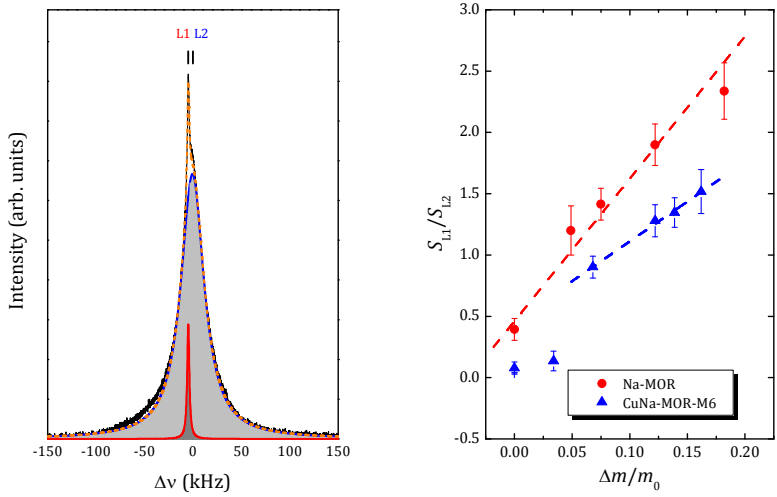

Figure 2. (a) - deconvolution of the ^{1}H NMR spectrum for the annealed CuNa-MOR-M6 sample; (b) -the ratio of the integral intensities (L1 to L2) for Na-MOR and CuNa-MOR-M6 versus hydration level; the dashed lines correspond to the linear fits

It is to be noted that Na^+ exhibits lower enthalpy of hydration as compared to Cu^{2+}, it means that if in Na-MOR water molecules formed the hydration shell of Na^+ (by entering into the small channel) the dependence S_{L1}/S_{L2} in Fig.2(*b*) should be similar to that one in Cu-Na-MOR-M6, that is not the case. For the CuNa-MOR-M6 sample, the linear dependence is observed only at $\Delta m/m_0 > 0.05$. It means that at the beginning of the hydration process the water molecules first complete the hydration shell of Cu^{2+} and only after this step fill the main channel, Fig. 3. This conclusion is consistent with the kinetic study of dehydration done by TGA.

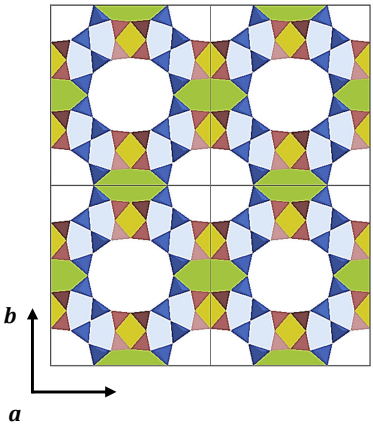

Figure 3. The 2x2x1 mordenite cell, a view along the [001] direction

Acknowledgements

The TGA studies were done at the Thermogravimetric and Calorimetric Research Centreof the Research Park of SPSU. The authors thank the bilateral mobility program of student and staff exchange between St Petersburg and Jagiellonian Universities for the support of the stays of E.A.K. and M.G.S. at Jagiellonian University. The 1H-NMR spectra were recorded with the equipment purchased thanks to the financial support of the European Regional Development Fund in the framework of the Polish Innovation Economy Operational Program (contract no. POIG.02.01.00-12-023/08).

References

1. D. Berthomieu, G. Delahay // Catal. Rev. Sci. Eng., 48, 269–313 (2006)
2. Chen Y. // Prog. Chem., 26, 248–258 (2014)
3. P. Vanelderen et al. // Coord. Chem., 257, 483–494 (2013)
4. Y.M. Zhukov, et al. // Microp. Mesopor. Mat., 224, 415–419 (2016)

Topological structure and mobility of polymer chains in branched poly(meth)acrylates studied by NMR

Tatiana P. Kulagina[1], *Svetlana V. Kurmaz*[1], *Grigorii E. Karnaukh*[1], *Oleg M. Vyaselev*[2]

[1]*Institute of Problems of Chemical Physics RAS, Semenov prospect, Chernogolovka, Moscow region, 142432, Russia*
[2]*Institute of Solid State Physics RAS, Academician Ossipyan St.,2. Chernogolovka, 142432, Moscow region, Russia*
E-mail: tan@icp.ac.ru

Introduction

Application of our theory of free induction decay (FID) and stimulated echo in polymer networks [1, 2] to branched polymers are represented. The methods of determination of correlation function of molecular motion of polymer chains from NMR experiments directly (free induction decay (FID) and stimulated echo) are developed on the base of the theory. The modeling of FID and stimulated echo in branched poly(meth)acrylates (PMMA) and comparison with experiments are carried out.

Behavior of branched Poly(meth)acrylates and samples

Branched and highly branched polymers synthesized in one step using controlled radical copolymerization of mono- and multifunctional monomers are polydispersed macromolecular irregular structures, the degree of branching in which does not exceed 50% [3]. The topological structure of branched macromolecules is characterized by a high concentration of terminal chains in the peripheral layers and branching knots. This structure determines such unusual properties of branched polymers as high solubility in various organic media, low characteristic viscosity [η] compared to that of linear polymers with close MW, low sensitivity of the reduced viscosity to a change in the polymer concentration in solution, thermodynamic compatibility with polymers of another chemical nature, and high sorption capability along with the ability to transport low_molecular weight substances.

One of the efficient methods for studying the structure, molecular mobility, and intermolecular interaction in polymer systems is the NMR method [3, 4]. The method is applied for study branched poly(meth)acrylates (PMMA) with different molecular mass and different parts of brancher ethylene glycol dimethacrylate (EGDM): 1decanethiol (DT), which restricts polymer chain growth 100:15:15 (B6), 100:8:8 (B4), 100:8:7 (B13), 100:8:6 (B14), 100:8:5 (B15) The introduction of DT into the system restricts the growth of polymer chains and prevents the formation of macrogel. Branched poly(methyl methacrylates) (PMMA) containing terminal chains and branching knots are amor_phous powders.

The aim of this work is to develop the theory of stimulated echo in multi-spin systems and its application to obtain quantitative information about structure and dynamics in branched polymers out the observed signals.

Results and discussion

The theory of FID and stimulated echo without a magnetic field gradient

The method for the determination of the fraction of the effective polymer network and terminal chains from the FID amplitude was proposed on the basis of the earlier developed pulse NMR theory for linear and cross_linked polymers [2]. The resulting FID process in the samples is presented as a sum of polarization decays from the chains with free ends ($G_0(t)$) and from the chains whose ends are fixed ($G_c(t)$)

$$G(t) = (1 - p)G_0(t) + pG_c(t), \quad (1)$$

where p is the fraction of the effective network, and $G0(t)$ and $Gc(t)$ are calculated theoretically. Note that all equations are presented for dimensionless time $t = t^*\omega loc$, where ωloc is the local field.

The function $G_c(t)$ depends on the a distribution function $P(N)$ [1] between knots. Assuming that a FID signal $G(t)$ may be described in a Andersson-Weiss model:

$$G_c(t) = \exp\left[-\frac{1}{2}\left\langle\delta^2\varphi(t)\right\rangle\right] = \exp\left[-\int_0^t\left(t-t'\right)k\left(t'\right)dt'\right] \tag{2}$$

where $k(t)$ is a correlation function, that contains all information about substance:

$$k(t) = \left(-\ln G(t)\right)^{\cdot} \tag{3}$$

It was proposed a general approach for calculating the spin echo signals, produced by the stimulated echo method [2] under the influence on a spin system by sequence of three RF pulses. The stimulated echo signal was obtained and was observed at the time point $\tau_2 + 2\tau_1$, where τ_1 – the time interval between the first and second pulses, τ_2 – the time interval between the second and third pulses:

$$A_2(\tau_1,\tau_2) = \exp\left[-\frac{1}{2}\left(2\left\langle\delta^2\varphi(\tau_1)\right\rangle - \left\langle\delta^2\varphi(\tau_2+2\tau_1)\right\rangle + 2\left\langle\delta^2\varphi(\tau_2+\tau_1)\right\rangle - \left\langle\delta^2\varphi(\tau_2)\right\rangle\right)\right] \tag{4}$$

It was proved, that at $\tau_1 << \tau_2$,

$$A_2(\tau_1,\tau_2) = G^2(\tau_1)\exp\left[k(\tau_2+\tau_1)\tau_1^2\right] \tag{5}$$

According (5) the correlation function takes the form:

$$k(\tau_2+\tau_1) = \frac{1}{\tau_1^2}\ln\frac{A_2(\tau_1,\tau_2)}{G^2(\tau_1)} \tag{6}$$

The correlation function of molecular motions in branched polymers

In this work a possibility of obtaining of a correlation function directly from NMR experiments is represented. On the base of previously developed theory of free induction decay (FID) and stimulated echo there are two methods of the definition of $k(t)$ are proposed.

In the work calculations of the FID and of the stimulated echo $A_2(\tau_1,\tau_2)$ were made and a view of the correlation function was defined at various average length of chains N_0 between nodes of polymer and for different distribution function of chains length.

A comparison analysis of the experimental and calculated data showed that an effective network was formed in sample B6 (Fig. 1). This effective network has the following parameters: exponential function $P(N)$ of chain distribution over lengths between the knots, average chain length $Nc_0 = 17$, length of terminal chains $N_0 = 49$, network fraction 0.45, developed segmental motion, and correlation time $\tau_c = 10^{-3}$ s. The SE amplitude of echo A_2 was calculated for sample B6 at the above indicated parameters in the high temperature case by Eq. (4) with the exponential function of chain distribution over lengths $P(N)$.

The correlation functions calculated using the data for the FID by Eq. (3) and A_2 by Eq. (6) are presented in Fig. 2. The coincidence of these functions is observed, which confirms that the SE theory is applicable for the determination of correlation functions in branched polymers.

The experimental FID signals and line shapes at different temperature were obtained for all samples. The experimental data in the high-temperature case at 150 °C are presented above. The central parts of line shapes almost coincide for all samples, indicating the formation of the same effective network, as it follows from the synthesis conditions of the samples. Minor

differences associated with the influence of free ends of the polymer chains due to an insufficiently high temperature are observed on the line shape wings.

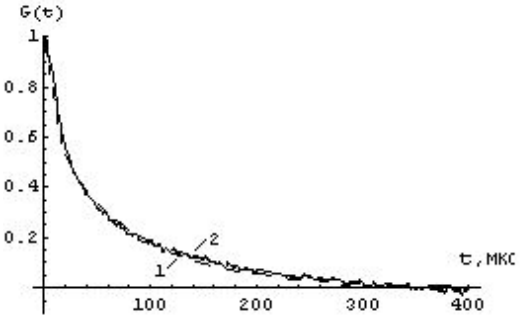

Figure 1. Comparison of the experimental (1) and theoretical (2) FIDs of the samples B6

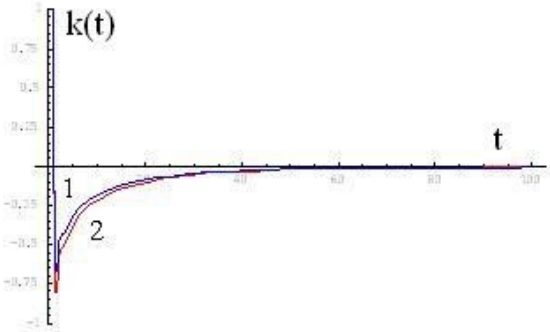

Figure 2. Comparison of the correlation functions calculated using the data for FID (1) and A_2 (2) of sample B6

So, the theories of free induction decay and stimulated echo without magnetic field gradient proposed in the work make it possible to determine the correlation function molecular motion numerically directly from experiments.

References

1. T.P. Kulagina, G.E. Karnaukh, A.N. Kuzina, and L.P. Smirnov. - *Russian Journal of Phys. Chem. B*, **7**, 170-176 (2013).
2. T.P. Kulagina, V.A. Varakina and A.N. Kuzina, *Doklady Phys. Chem. Part 2* - **444**, 79-82. (2012).
3. T.P. Kulagina, S.V. Kurmaz, V.P. Grachev, V.P Tarasov, *Russian Chemical Bulletin.* – **60**, 1500-1504 *(2011)*.
4. T. P. Kulagina, G. E. Karnaukh, S. V. Kurmaz, and O. M. Vyaselev. - *Russian Chemical Bulletin.* - **65**, 2494-2499 *(2016).*

Isolation and Characterization of Bioactive Secondary Metabolites from the Deep Sea Derived Fungi *Penicillium* sp. SCSIO.XWFO1254

Kaliaperumal Kumaravel, Salendra Limbadri, Yonghong Liu

Key laboratory of Marine Natural Product Chemistry, South China Sea Institute of Oceanology, Chinese Academy of Sciences, Guangzhou, China - 510301
E-mail: kumarbio06@gmail.com

Introduction

Deep Sea Derived fungi an extremophile seems to produce structurally diverse secondary metabolites which has immense biomedical importance in terms of anticancer, antiviral and antimicrobial etc., In the past decades exploring the deep sea environment for its microbial resource and its derived metabolites attracts the natural product chemists which tends to the culture condition of such extremophiles in lab environment. In the present study a deep sea derived fungi of *Penicillium* sp SCSIO.XWFO1254 from 2000 metre depth of Indian Ocean region was isolated. The fungi were fermented under lab environment and its secondary metabolite isolation was effected through HPLC and structural characterization through NMR and biological screening through High throughput screening method was done.

Methods

Deep sea soil sediment was subjected for serial dilution and its microbial load were plated on Malto bact (MB) agar supplemented with sea salt. Single colony of microbes from the plates were then screened and subjected for mass fermentation using solid rice medium for 60 days. After 60 days of culture the fermented fungal culture were extracted using organic systems of Acetone/Ethyl Acetate. The crude fungal extract were then prepared for Medium pressure chromatography (MPLC) using silica gel (300 – 400 Mesh size) to get sub fractions, followed by LH-20 (Sephadex) and then by semi-preparative Reversed phase HPLC (RP-HPLC)(C-18) to obtain the pure compounds. The purified compounds were then subjected for NMR spectral studies for structural characterization and finally its biological screening was assessed in terms of anticancer, antiviral, anti-tuberculosis and antimicrobial.

Results

Nearly 7 diverse classes of secondary metabolites of Quinone, alkaloid and terpenoids were isolated from the *Penicillium* sp SCSIO.XWFO1254. Compound **1** and compound **6** exhibited significant biological activity in terms of anticancer and antiviral activity.

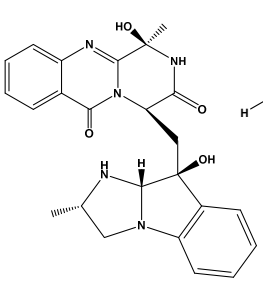

Compound-1

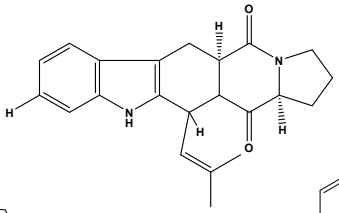

Compound-2

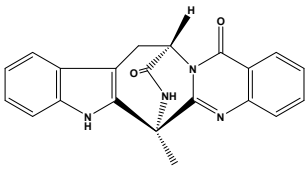

Compound-3

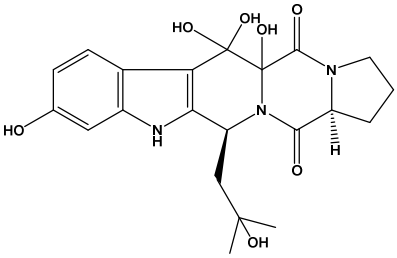

Compound-4

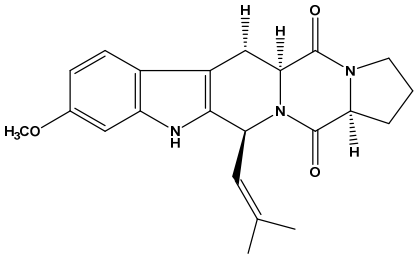

Compound-5

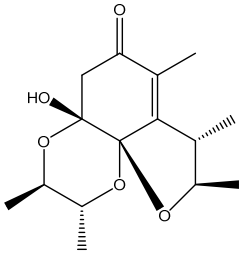

Compound-6

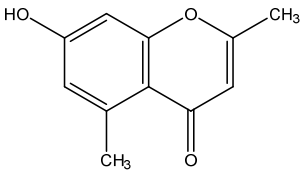

Compound-7

Acknowledgements

This work was supported by grants from the Strategic Priority Research Program of the Chinese Academy of Sciences (XDA11030403), the National Natural Science Foundation of China (41376162, 41476135, and 41406187).

References

1. *Chen S*, *Wang J*, *Lin X*, *Zhao B*, *Wei X*, *Li G*, Kaliaperumal Kumaravel, *Liao S*, *Yang B*, *Zhou X*, *Liu J*, *Xu S*, *Liu Y*, *Organic Letters*, 5;18(15):3650-3 (2016).
2. *Chen S*, *Wang J*, *Lin X*, , *Wei X*, *Li G*, Kaliaperumal Kumaravel, *Liu Y. Fitoterapia, 117:71-78 (2017).*

Multiexponential distribution of ^{14}N NQR relaxation times in tetrazole derivatives

Sultonazar Mamadazizov, Anna Neniukhina, Galina S. Kupriyanova

Institute of physics and mathematics, Immanuel Kant Baltic Federal University,
E-mail: sultonazar.mamadazizov@mail.ru

Introduction

In recent years, considerable interest has been shown in the study of tetrazole derivatives, which attract attention as highly nitrogenous compounds for use as a component of rocket fuels and blended explosives. Tetrazole derivatives are used as inhibitors of corrosion in copper and aluminum and as a convenient starting material for the synthesis of other tetrazole derivatives. Moreover, tetrazole rings are increasingly being used as isosteric substitutes for various functional groups, which are used for creation of novel biologically active substances. Important issues for the creation of biological substances are the identification of undesirable polymorphic forms, the establishment of ways to form hydrogen bonds. These problems can be solved by NQR methods, since the NQR spectral parameters are sensitive to the local environment of ^{14}N nuclei, and the relaxation times are sensitive to lattice vibrations, to the influence of molecular dynamics. 5 aminotetrazole has been studied previously by various methods [1, 2]. It was found that the space group 5-aminotetrazole monohydrate is P21 / c and there are four molecular in a unit cell Z = 4. Because of the crystal symmetry, each nucleus of the tetrazole molecule has one set of frequencies [2]. The theoretical analysis of the relaxation of a nucleus with spin 1 showed that the relaxation is described by a biexponential function. However, in earlier studies it was found that the relaxation of nitrogen is exponential [2]. In this paper, the spin-spin and the spin-lattice relaxation of 14N in 5 ATZH were studied using inverse Laplace transform in order to obtain more detailed information on the dynamics of nuclei

Results and Discussion

^{14}N NQR frequencies and the relaxation times in 5-aminotetrazole monohydrate (5ATZH) were measured by ^{14}N NQR method with the use of the pulse NMR-NQR spectrometer Tecmag Apollo with TNMR software. The Carr-Purcell-Meiboom-Gill (CPMG) sequence was used for T_2 measurements and inversion-recovery, saturation- recovery and Csaki-Bene sequences were used for T_1 measurements. The distribution of the spin-lattice relaxation times for all ^{14}N nuclei at frequencies 3.7, 3.61, 3.33, 3.14 and 2.74 MHz was obtained by using the inverse Laplace transform. Laplace transform result for 3.14 MHz is shown in Fig. 1. Three peaks in the distribution are observed at 60 ms, 405 ms and 2200 ms. It should be noted that the peak width is proportional to the number of resonant nuclei. From this it can be concluded that most of the nuclei relax in the region of 2200 ms. Unfortunately, as can be seen from Fig. 1 the two-exponential decay of the magnetization expected for a quadrupole nucleus with spin = 1 could not be observed using the inverse Laplace transform. However, we should note the interesting fact of the appearance of several peaks in the distribution of spin-lattice relaxation times. This pattern is also observed for other measured frequencies. One of the reasons for the appearance of the fast components can be the process of polarization transfer between nuclei having the same frequencies, but differing in the direction of the principal axes of the electric field gradient tensors. On the other hand, it can be caused by the presence of various polymorphic structures.

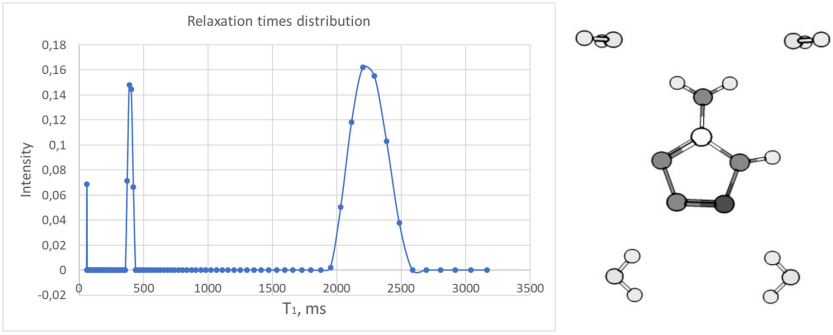

a) *b)*

Figure 1. The distribution of relaxation times on frequency 3.143 MHz (a) in molecule of 5 aminotetrazole monohydrate (b) at room temperature

Acknowledgements

The authors thank the Russian Foundation for Basic Research (project # 16-32-50224) for the support of the stay of S.M. at Saint Petersburg State University.

References

1. M. H. Palmer, D. Stephenson, and A. S. Smith, "14N quadrupole coupling tensor in solid pyrazole, 1H-1,2,4-triazole, and 1H-tetrazole theory and experiment," *Chem. Phys.*, vol. 97, pp. 103–111, 1985.
2. J. Pirnat *et al.*, "14N NQR in the tetrazole family," *Chem. Phys.*, vol. 364, no. 1–3, pp. 98–104, 2009.
3. S. Vega. Theory of T1 relaxation measurements in pure nuclear quadrupole resonance for spin I=1. J. Chem.Phys. V.61, N3, 1974
4. N.Ya. Sinyavsky, I.G. Mershiev and G.S. Kupriyanova. The study of polymorphic states of paradichlorobenzene by means of nuclear quadupole resonance. Solid state Magnetic Resonance. 2016 Jule *http://dx.doi.org/10.1016/j.ssnmr.2016.07.002*

Complete assignment in ^{1}H NMR spectra and conformational analysis of some modified triterpenoids in solution

Sergei A. Marchenko, Alla D. Zorina, Stanislav I. Selivanov

Institute of Chemistry, State University of Saint-Petersburg, University prospect 26, 198504, Saint-Petersburg, Russia
E-mails: nmr.group.spbu@gmaill.com; znvolk@mail.ru; platinist@yandex.ru

Introduction

Modified triterpenoid analogues are characterized by a wide range of pharmacologic action and are promising scaffolds for designing new pharmaceuticals. For example, compounds of dammarane and oleonane types exhibit antiphlogistic, antitumor, antiviral, and other kinds of activity [1, 2]. The introduction in the structure of natural triterpenoids of nitrogen heterocyclic fragments makes it possible to improve the pharmacologic profile of these compounds and also to reduce their side effects.

Application of NMR spectroscopy in structural and conformational analysis of natural products is mostly based on measurement and correct interpretation of spin-spin coupling constants (J) and through-space interactions between magnetic nuclei in the molecules under investigation. Relationship between vicinal scalar constant ^3J and dihedral angle θ [3] and very strong dependence of nuclear Overhauser effect (NOE) on internuclear distance r: $\eta_{(NOE)} \sim r^{-6}$ [4] are well-known and widely used in practice in combination with different *C*omputer-*A*ssisted *S*tructure *E*lucidation (CASE) algorithms [5].

The main problem of triterpenoid NMR study is very complicated for interpretation aliphatic range of proton spectra where about twenty or more overlapped multiplete signals are usually situated. In addition, the rather large molecular weight of these compounds (about 450 – 600) leads to an increase in the correlation time of the diffusion motion τ_c compared to, for example, steroid estrogens and androgens [6]. If the dipole-dipole relaxation mechanism dominates, this may lead to the decrease in the longitudinal relaxation time T_1 and to the increase the value of $\omega_o\tau_c$. In the last case it may lead to the inability to use the calibration method for estimating internuclear distances by measuring the NOE.

NMR ^{1}H spectra of model triterpenoids **1** and **2** (Fig. 1) were studied by different correlation methods (COSY-DQF, NOESY, HOESY, J-COSY, HSQC, COLOC) and by using T_1-relaxation data to determine opportunities and limitations of these methods for elucidation of the absolute configuration of compounds under investigation.

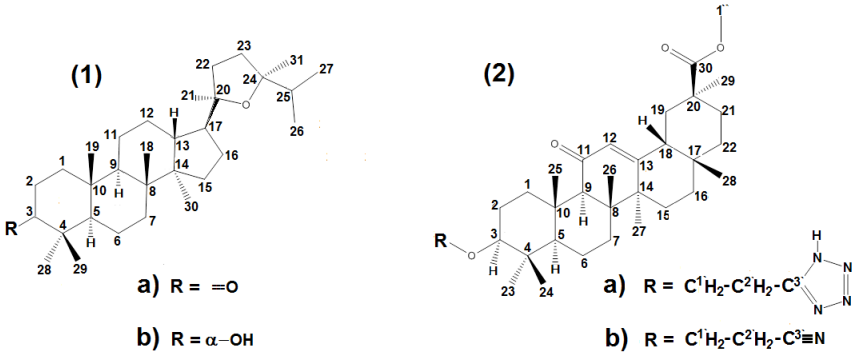

*Figure 1. Structures of triterpenoids **1** and **2**. Numbering of atoms is shown by figures*

Identification of proton signals

Complete signal assignments in aliphatic range 0.7 – 2.2 ppm of ^{1}H spectra of compounds **1** and **2** were produced on base cross-peak network in phase-sensitive COSY-DQF spectra and stereochemical assignments (α- or β-orientation) were fully validated by analysis of NOESY spectra. Moreover, some selective decoupling experiments ^{1}H{^{1}H} were used to prove long-range scalar interactions between protons which are in "W"-configuration.

Signal assignments in NMR ^{1}H spectrum of compound **2a** at 300 MHz on base NOE data from phase-sensitive NOESY spectrum, which was recorded at mixing time 0.2 s, are presented in Fig. 2. Spatial interactions of the proton H^{12} (5.69 ppm.) with protons $H^{18\beta}$ (2.08 ppm) and $H^{19\beta}$ (1.9 ppm) and methyl group 26 (1.11 ppm) on the β-face of the molecule and with proton $H^{9\alpha}$ (2.33 ppm) on its α-face are clearly visible in this 2D spectrum. The integral intensities of corresponding cross-peaks even at a qualitative level are in good agreement with the calculated values of the interproton distances in the preferred conformation of the triterpenoid **2a** (Fig. 2).

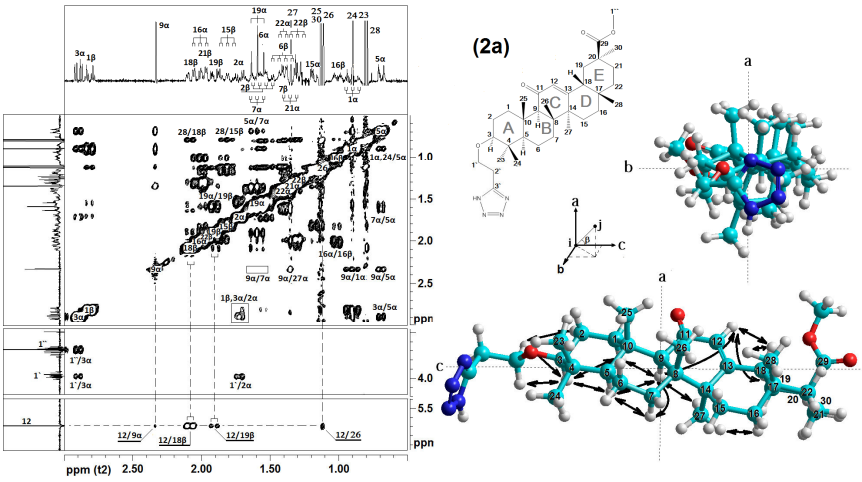

*Figure 2. NOESY spectrum (τ_m = 0.2 s) and most preferred conformation of triterpenoid **2a** on which through-space dipole-dipole interactions are shown by double arrows*

For example, intensity of the cross-peaks 12/18β and 12/9α are *related to each other as18:1* while the corresponding calculated distances are 2.27 and 3.9 Å. All the axial protons on the α-face of the rings A and B ($H^{1\alpha}$, $H^{5\alpha}$, $H^{7\alpha}$ and $H^{3\alpha}$) were detected because of their spatial interaction with the proton $H^{9\alpha}$ and with each other. Simultaneously, the spatial orientation of methyl groups 27 and 28 is easily determined due to their intensive through-space interactions with protons $H^{9\alpha}$ and $H^{18\beta}$, respectively. The latter confirms the cis-conjunction of rings D and E.

Experimental evidence of spatial structure

Vicinal constant $^3J_{H\text{-}H}$ application

About twenty scalar constants $^3J_{H\text{-}H}$ between vicinal protons in rings A, B, D and E of compound 2a were determined with high accuracy (±0.1 Hz) and compared with their values calculated on base empiric Karplus-type relationship of Altona *et al* [7]. Good agreement

between the experimental and calculated data sets of $^3J_{H\text{-}H}$ gives us the important evidence of most preferred conformation of compound 2a (Fig. 2).

Interproton distance $r_{H\text{-}H}$ application

Fourteen through-space interactions in NOESY spectrum of compound 2a were choose to estimate corresponding interproton distances $r_{H\text{-}H}$ by calibrate method [4, 6]. Distance 1.76 Å between germinal protons $H^{19\alpha}$ and $H^{19\beta}$ was used as reference value to calculate all unknown proton-proton distances r_{ij} on base cross-relaxation rates σ_{ij} determined from experimental dependence of S_{ij}/S_{ii} on mixing time τ_m where S_{ij} and S_{ii} are volume-integral intensities of cross- and diagonal peaks, respectively, in NOESY spectra.

In case of isotropic diffusion motion approach eight experimental data points are overestimated compared with calculated values (see closed circles on Fig. 3-1) and only six data points (open circles) are situated within ±5% of the error (dash lines). This discrepancy was eliminated by introducing a correction associated with the axially symmetric structure of the compound 2a (see projections of 2a relative to the main axes on Fig. 2). The correction for the diffusion anisotropy was determined using the Woessner relationship [8] and the result of its account is location of almost all points in the limits of 5% error (Fig. 3-2).

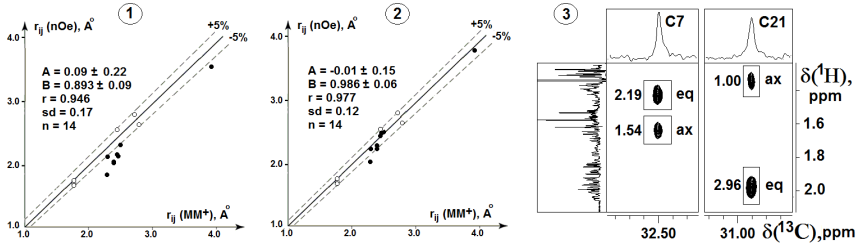

*Figure 3. 1 and 2 – Correlations between experimental (nOe)and calculated (MM^+) interproton distances r_{ij} in **2a** under assumption of isotropic and anisotropic diffusion motion, respectively. Parameters of linear correlation Y = **A** + **B**X, **r** (Pearson's correlation coefficient) and **sd** (rmsd, in Hz) for **n** (number of data points) are presented. 3 – Fragments of HOESY spectrum (τ_m = 0.2 s) of compound **2a** (integral intensities are given by figures)*

It should be noted that the diffusion anisotropy parameter $D_\parallel/D_\perp$ was determined experimentally (Fig. 3-3) by measuring the ratio of the heteronuclear Overhauser effects (HOE) from the axial and equatorial protons in the methylene group $C^{21}H_2$. The ratio of these HOEs is equal almost to 1:3. It corresponds to the anisotropy parameter 12 ± 2 which exceeds its calculated value obtained from moments of inertia around the main axes almost twice.

Acknowledgments

Spectral investigations were performed in the Resource Centers "Magnetic Resonance Research Centre" and "Chemical Analysis and Materials Research Centre" of the Saint-Petersburg State University. The study was carried out under the financial support of the Russian Science Foundation (grant no. 17-13-01124).

References

1. D. Schmitz, J. Zapp, R. Bernhardt, *FEBS J.*, 2012, vol. 279, p. 1663–1674.
2. J. Song, H. Ko, E.J. Sohn *et al*, *Bioorg. Med. Chem. Letters* 2014. v. 24, p. 1188–1191.
3. L.B. Krivdin, R.N. Contreras, *Ann. Reports on NMR Spect-py*, 2007. vol. 61. p. 133–245.

4. D. Neuhaus, M.P. Williamson, *"The Nuclear Overhauser Effect in Structural and Conformational Analysis"* (2nd ed.), Wiley-VCH, New York, 2000. 619 P.
5. M. Elyashberg, A.J. Williams, K. Blinov, *Nat. Prod. Rep*. 2010. vol. 27(9). p. 1296–1328.
6. S.I. Selivanov, A.G. Shavva, *Russian. J. Bioorg. Chem*. 2002, vol. 28(3), p. 194–208.
7. C.A.G. Haasnoot, F.A.A.M. Leeuw, C. Altona, *Tetrahedron* 1980. vol. **36**(19), 2783–2792.
8. D.E. Woessner *J. Chem. Phys.* 1962. vol. 36(1), p. 1–4.

An inductively-coupled volumetric resonator based on wire metamaterials for local sensitivity enhancement on a 3 T MRI system

Anna Mikhailovskaya[1], Alena Shchelokova[1], Dmitry Dobrykh[1], Ivan V. Sushkov[2], Irina Melchakova[1], Alexey Slobozhanyuk[1,3] and Andrew Webb[4]

[1]Department of Nanophotonics and Metamaterials, ITMO University, Saint Petersburg, Russia
[2]Department of Radiology, Vreden Russian Institute of Traumatology and Orthopedics, St. Petersburg, Russia
[3]Nonlinear Physics Center, Research School of Physics and Engineering, Australian National University, Canberra, Australia
[4]C.J. Gorter Center for High Field MRI, Department of Radiology, Leiden University Medical Center, Leiden, The Netherlands
E-mail: a.mikhailovskaya@metalab.ifmo.ru

Introduction

Standard volumetric and surface radiofrequency (RF) coils for magnetic resonance imaging (MRI) are usually constructed from metallic conductors with appropriate tuning and matching circuits [1]. Alternatively, one can replace conventional conductors with high permittivity materials [2]. Recently it has been shown that resonators based on high permittivity dielectrics can be used for local and global RF shimming and local signal-to-noise ratio (SNR) enhancement for ultra-high frequency magnetic resonance imaging and microscopy [3, 4, 5]. However, it is challenging to design such resonators for clinical field strengths (e.g., 1.5–3 T) because of the relatively large geometric dimensions of structures realized with moderate permittivity. On the other hand, metamaterials and metasurfaces with artificially designed electromagnetic properties are good candidates for local sensitivity enhancement [6] via inductive coupling to the body coil. In this study, we propose and characterize a new design of a compact annular meta-resonator based on the combination of wire metamaterials structure and high permittivity dielectric material. The current approach reduces the required outer diameter of a similar dielectric resonator substantially thus making possible to design compact structures for 3 T. When used in an inductively coupled wireless mode, the sensitivity of the meta-resonator was measured to be slightly higher than that of the dielectric resonator.

Electromagnetic simulations

A cylindrical dielectric resonator supports a large number of electromagnetic modes, the frequencies of which depend upon the particular geometry and relative permittivity of the material used [7]. For MRI purposes, we are interested in circularly polarized hybrid electromagnetic modes (HEM_{11}) [3]. The proposed meta-resonator supports the eigenmode profile which is similar to the HEM_{11} mode of the dielectric one at the desired frequency. To evaluate the appropriate designs of annular water-based dielectric resonator and meta-resonator we performed electromagnetic simulations using a commercial software package (CST Microwave Studio 2017). Fig. 1 shows a schematic view of the geometries of a conventional annular dielectric resonator used for comparative experiments and new meta-resonator, respectively. The inner diameter d=100 mm and length h=232 mm were equal for both structures, while the outer diameters were varied in order to tune the HEM_{11} mode of the resonators at 123.3 MHz [Fig. 1 (c)]. As a result, it was obtained that the dielectric resonator has an external diameter of D_{DR}=322 mm, and a meta-resonator D_{MR}=214 mm that is in 37% smaller. At the same time for both cases, the magnetic field is localized in the area of interest (central part of the resonators) and highly homogeneous, while the electric field is concentrated

outside this area [Fig. 1(d)]. The permittivity of distilled water used in both resonators is 78 with a conductivity of 0.006 S/m. The wire length l_w=182 mm was chosen to be approximately half of the wavelength at the operational frequency of 3 T MRI. The wires were placed in such way that the spacing between them was 4 mm and the distance from the air annulus was 10 mm.

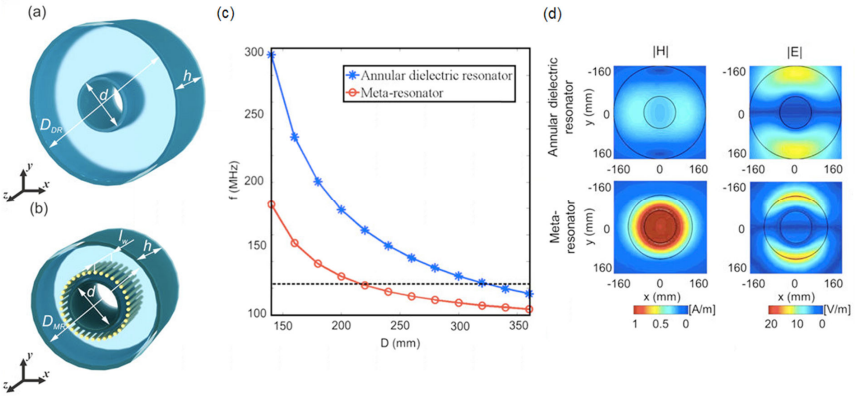

Figure 1. Schematic view of the geometries of the annular dielectric resonator (a) and meta-resonator (b) with the following dimensions: d=100 mm, h=232 mm, D_{DR}=322 mm, D_{MR}=214 mm, l_w=182 mm. (c) Numerically calculated resonance frequency of the HEM_{11} eigenmode as a function of the outer diameter (D) for an annular dielectric resonator (blue curve) and meta-resonator (red curve), dashed black curve indicates the Larmor frequency at 3 T. (d) 2D maps of the magnetic and electric fields for annular dielectric resonator (top panel) and meta-resonator (bottom panel)

Phantom imaging

All MRI experiments were performed on a 3 T Siemens Magnetom Verio whole-body clinical system at the Russian Scientific Research Institute of Traumatology and Orthopedics named after R.R. Vreden. Fig. 2 shows coronal gradient echo images of a courgette, which was used as a test object. Images were acquired using a gradient echo sequence: field of view 300 × 300 mm^2, acquisition matrix 512 × 512, slice thickness 5 mm, repetition time 573 ms, echo time 12 ms. The birdcage body coil, which is embedded in the bore of the scanner was used for RF transmission and signal detection. Due to inductive coupling to the birdcage coil, both resonators concentrate the flux of the latter to produce a stronger field. As a result, both resonators significantly increase the SNR in comparison with the birdcage body coil used alone. A factor of 6.3 was achieved with the annular dielectric resonator and a factor of 7.3 with the meta-resonator. The RF power level was calibrated in each case to obtain the maximum signal, corresponding to Ernst angle excitation. Due to the fact that both resonators also improve transmit field, the input voltage amplitude was reduced by a factor of 12.5 for the annular dielectric resonator and 17 for the meta-resonator in comparison with standard examination with the birdcage coil alone. It means that specific absorption rate level delivered to the patient can be decreased while maintaining optimum image quality.

Conclusions

We have proposed and experimentally investigate in 3 T scanner a new design of annular resonator based on the combination of a wire metamaterial and high permittivity dielectric.

While the performance of the annular dielectric and meta-resonators are almost identical the geometrical dimensions differ significantly, which is crucially important for practical applications.

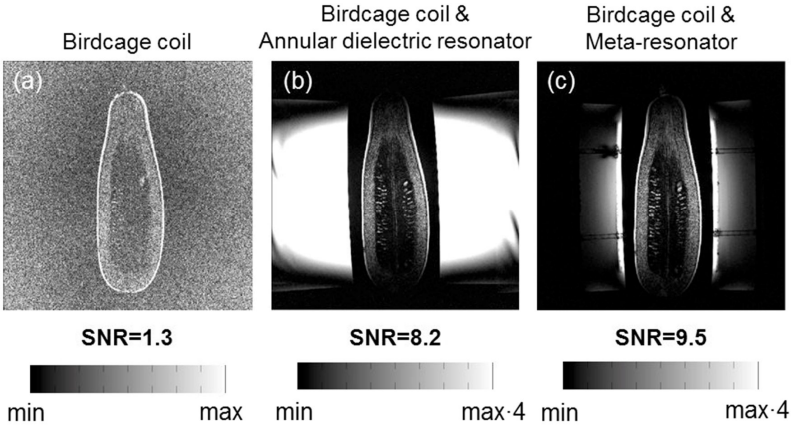

Figure 2. MR images of a courgette obtained (a) with the birdcage coil only, (b) with the birdcage coil and annular dielectric resonator, (c) with the birdcage coil and meta-resonator, (d) with a 4-channel local receive coil wrapped around the courgette

Acknowledgements

This research was supported by by the Government of the Russian Federation (Grant No. 074-U01). The authors are grateful to Dr. M. Zubkov and to Mr. E. Kretov for assistance with measurements and to Dr. C. A. T. van den Berg, Dr. A. J. Raaijmakers, Prof. P. A. Belov for useful discussions at the preliminary stage of the project.

References

1. J. Vaughan and J. Griffiths, “RF Coils for MRI”, New York: Wiley (2012).
2. H. Wen, F. A. Jaffer, T. J. Denison, S. Duewell, A. S. Chesnick and R. S. Balaban, “The evaluation of dielectric resonators containing H2O or D2O as RF coils for high-field MR imaging and spectroscopy”, *J. Magn. Reson. B,* 110, 117-123 (1996).
3. S. A. Aussenhofer and A. G. Webb, “Design and Evaluation of a Detunable Water-Based Quadrature HEM_{11} Mode Dielectric Resonator as a New Type of Volume Coil for High field MRI”, *Magn. Reson. Med*, 68, 1325-1331 (2012).
4. S. A. Aussenhofer and A. G. Webb, “High-permittivity solid ceramic resonators for high-field human MRI,” *NMR Biomed*., 26, 1555 (2013).
5. J. J. Bluemink, A. J. E. Raaijmakers, W. Koning, A. Andreychenko, D. S. Rivera, P. R. Luijten, D. W. J. Klomp and C. A. T. van den Berg, “Dielectric wave-guides for ultrahigh field magnetic resonance imaging”, *Magn. Reson. Med.,* 76, 1314–1324 (2016).
6. A. P. Slobozhanyuk, A. N. Poddubny, A. J. E. Raaijmakers, C. A. T. van den Berg, A. V. Kozachenko, I. A. Dubrovina, I. V. Melchakova, Y. S. Kivshar, P. A. Belov, “Enhancement of Magnetic Resonance Imaging with Metasurfaces”, *Adv. Mater.,* 28, 1832–1838 (2016).
7. D. Kajfez and P. Gullion, “Dielectric Resonators”, Atlanta, GA: Noble Publishing Cooperation, 574 (1998).

Low field ^{14}N nuclear magnetic resonance detection of liquid substances

G. V. Mozzhukhin[1], G. S. Kupriyanova[2], S. Mamadazizov[2], A. Maraşlı[1], B. Z. Rameev[1,3]

[1]Gebze Technical University, 41400 Gebze/Kocaeli, Turkey; mgeorge@yandex.ru
[2]Baltic Federal University by Immanuel Kant, 236041 Kaliningrad, Russian Federation
[3]E. Zavoisky Kazan Physical-Technical Institute, 420029 Kazan, Russian Federation

Nuclear Magnetic Resonance (NMR), which is a well-known powerful analytical tool in physics, chemistry and material science, is prospective technique for detection of liquid explosives [1-3]. In the most cases a low-or moderate- field (<1 T) ^{1}H NMR device to measure time-domain (relaxation) properties is proposed for scanning liquid substances at security checkpoints. Unfortunately, classical NMR sequences provide acceptable measurement times only for the case of the spin-spin relaxation (T_2), while measurement of other parameters that could be probed by time-domain NMR require too long times. In this study, we review the possibilities to discriminate a number of nitrogen-based energetic/flammable/ toxic liquids by use of ^{14}N NMR technique. Fortunately, the most benign liquids including water, drinks and other liquids frequently met in luggage are characterized by zero or small nitrogen content. We compare the ^{14}N NMR relaxation parameters of a number of nitrogen liquids and discuss the prospects of this technique for application in detection of very broad class of dangerous liquids as well as substances banned for public transportation.

Tecmag Apollo NMR console, 500 W *Tomco* power amplifier, home-made permanent magnet system with a magnetic field of 0.575 T and a home-made RF probe with a resonance frequency of about 1.770 MHz were used in the ^{14}N NMR experiments. Three groups of nitrogenous liquids were studied: nitrates, nitrites and some toxic substances (e.g. dimethyl-formamide/acetamide). The Carr-Purcell-Meiboom-Gill (CPMG) sequence was used for the T_2 measurements, while inversion-recovery and Csaki-Bene sequences [4] were used for T_1 measurements. The field gradient of our magnetic system was obtained from ^{1}H NMR experiments to be G=3Gs/cm. Our calculations revealed that contribution of magnetic field inhomogeneity in ^{14}N NMR is much smaller comparing to ^{1}H NMR because much smaller gyromagnetic ratio of ^{14}N nitrogen nuclei.

In this work, we studied three groups of materials: explosive and flammable liquids including NO_2 group, liquids with NO_3 group as well as the toxic substances with single atom of ^{14}N. In our case, most toxic and explosive liquids had small values of T_1 and T_2 allowing their easy discrimination from the relatively safe materials containing NO_3 group. The identification of liquids was carried out by measurements of T_1 and T_2 and NMR frequency of ^{14}N. ^{14}N nuclei have much shorter relaxation parameters with respect of protons that allows measuring these illicit substances in very small time. A contributions of quadrupole mechanism and fast movements of small-sized molecules in the short relaxation observed are discussed. Thus, we demonstrated that ^{14}N NMR is a prospective method for the detection of nitrogen-based illicit liquids.

The work was supported by NATO Science for Peace and Security Programme (NATO SPS grant No. 985005 [G5005]) and TUBITAK grant under the Programme 2221 for Visiting Scientist (G. S. Kupriyanova). Authors also acknowledge a partial support by East Marmara Development Agency (MARKA, project No. TR42/16/ÜRETİM/0013) and by Research Fund of Gebze Technical University (grants Nos. BAP 2015-A-19 and BAP 2017-A-105-44).

References

1. D. T. Burns, R. J Lewis, Analysis and characterisation of nitroglycerine based explosives by proton magnetic resonance spectrometry, Analytica Chimica Acta 300 (1995) 221-225
2. L. J. Burnett, Liquid explosives detection, SPIE Vol. 2092 Substance Detection Systems (1993) 208-216.
3. S. Kumar, W.C. McMichael, Y.-W. Kim, A.G. Sheldon, E. E. Magnuson, L. Ficke, T. K. Chhoa, C. R. Moeller, G. A. Barrall, L. J. Burnett, P.V. Czipott, J. S. Pence, D. C. Skvoretz, Screening sealed bottles for liquid explosives, Proceedings of SPIE Vol. 2934 (1997)126-137.
4. A.Csaki, G.Bene, Use method de mesure de T1 par echos de spin, Comp. Rend, 251 (1960) 228-229.

Influence of the charged peptide dendrigrafts topology on the large-scale properties and their internal structure

B. M. Okrugin[1], D. A. Markelov[1], I. M. Neelov[2]

[1]St. Petersburg State University, 7/9 Universitetskaya nab., St. Petersburg, 199034 Russia
[2]St. Petersburg National Research University of Information Technologies, Mechanics and Optics (ITMO University), Kronverkskiy pr. 49, St. Petersburg, 197101 Russia
E-mail: borisokrugin@gmail.com
http://www.silikoflask.com

Nowadays the hyper branched macromolecules, also called dendrimers, are often find their application in medicine [1, 2]. The main feature of the dendrimers is that the number of terminal groups increases faster than volume and this make them attractive for the further functionalization through the terminal groups on the periphery.

Classical dendrimers, described in literature, possess the regularity of branching, that is the number of branches, emerging from each branching point and the spacers length. This type of model was proposed by de Gennes and Hervet [3]. They assumed that all of the terminal groups are localized at the same distance from the dendrimer core. According to their theory the dendrimer volume fraction is an increasing function of the distance from the dendrimer core till the periphery. However, many experiments [4] and computer simulations [5, 6] proves the uniform of the radial dendrimer density distribution. These experimental and theoretical predictions are nowadays harmonized with the existing theory.

Nevertheless, not only regular hyper branched molecules can be synthesized. The more complex dendritic structures become more and more common in researches. Our research deals with the dendritic structures, where distinctive feature is the asymmetry of branching and linear core. They called poly-L-lysine (PLL) dendrimers. The Lysine structure is represented on the figure 1 a). As you can see the lysine structure calls for the asymmetry of branching. When the lysine represents the spacer then the connection goes from the NH_2 head atom to the OH tail atom. If it is the branching point than it splits the growth direction from the head atom (NH_2) to two tail atoms (NH_2 and OH). The schematic representation of the lysine structure you may find on the figure 2b. The core of the lysine dendrigrafts are built from the 8 lysine residue (figure 2). It's easy to notice that lysine core has 8 points from which the branches can grow.

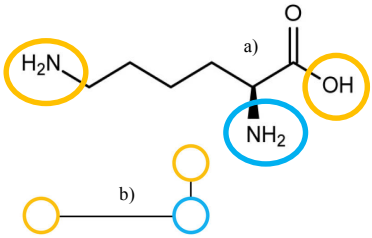

Figure 1. a) The Lysine structure. In blue we mark the head atom. In Yellow the tail atoms. b) Schematic representation of the lysine structure

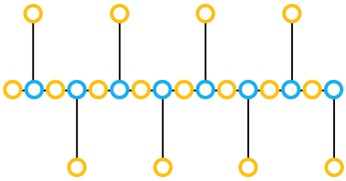

Figure 2. Schematic representation of the dendrimers core made from 8 lysine residues

Using the GROMACS package for molecular dynamic simulations we've studied six branches which were made from the lysine residues with different degree of branching. We established that in spite the same dendrigrafts molar weights the gyration radiuses are differ,

depending on the degree of branching. Orientational autocorrelation functions (P1 and P2) were considered for different segments. The effect of the macromolecular topology on the local orientation mobility of the segment were studied. In particular, for all types of dendrigrafts, it was established that that the mobility of the terminal groups is higher than for the inner groups. This conclusion is consistent with the results of studies of classical dendrimers [8]. Additionally, we considered spectral density, J, for the ^{1}H vector, manifested in NMR, for the inner pairs and in terminal groups that can be extracted from experimental data in future.

References

1. G.M. Dykes, Dendrimers: A review of their appeal and applications, J. Chem. Technol. Biotechnol. 76 (2001) 903–918.
2. P.J. Gittins, L.J. Twyman, Dendrimers and supramolecular chemistry, Supramol. Chem. 15 (2003) 5–23.
3. P.G. de Gennes, H. Hervet, Statistics of « starburst » polymers, J. Phys. Lettres. 44 (1983) 351–360.
4. M. Ballauff, C.N. Likos, Dendrimers in solution: Insight from theory and simulation, Angew. Chemie - Int. Ed. 43 (2004) 2998–3020.
5. M.L. Mansfield, L.I. Klushin, Monte Carlo Studies of Dendrimer Macromolecules, Macromolecules. 26 (1993) 4262–4268.
6. D. Boris, M. Rubinstein, A self-consistent mean field model of a starburst dendrimer: Dense core vs dense shell, Macromolecules. 29 (1996) 7251–7260.
7. J.S. Kłos, J.U. Sommer, Properties of dendrimers with flexible spacer-chains: A monte carlo study, Macromolecules. 42 (2009) 4878–4886.
8. D.A. Markelov, M. Dolgushev, E. Lahderanta, NMR Relaxation in Dendrimers, Annual Reports on NMR Spectroscopy. 91 (2017) 1-66.

NMR signal enhancement in hydrogenation reactions with parahydrogen

Ekaterina V. Pokochueva[1,2], *Dudari B. Burueva*[1,2], *Kirill V. Kovtunov*[1,2], *Igor V. Koptyug*[1,2]

[1]*International Tomography Center, 3A Institutskaya St., 630090, Novosibirsk, Russia*
[2]*Novosibirsk State University, 2 Pirogova St., Novosibirsk, Russia*
E-mail: pokochueva@tomo.nsc.ru

Introduction

Nuclear magnetic resonance spectroscopy is a highly informative method for studying chemical structures and properties of various compounds. However, one of its major disadvantage is low nuclear spin polarization, which leads to low signal sensitivity. In order to overcome this problem, several methods of hyperpolarization were developed - including parahydrogen-induced polarization (PHIP). PHIP is based on the conversion of correlated spin order of para-hydrogen (p-H_2) – a spin isomer of hydrogen with total nuclear spin I=0 – into polarization of a target molecule via catalytic hydrogenation. For a successful observation of PHIP effects in NMR spectra of hydrogenation products, two atoms from the same p-H_2 molecule should be added to the same product molecule – in other words, hydrogenation process should occur via pairwise addition of the hydrogen atoms [1]. A promising type of catalysts for the production of PHIP effects are supported metal catalysts, but the percentage of the pairwise addition on such catalysts is usually low, therefore, there is a necessity in systematic studies of the catalysts in hydrogenation reactions in terms of PHIP effects observation.

Liquid-phase hydrogenation

In order to study PHIP effects in liquid-phase experiments, we performed hydrogenation of different phenylalkynes (phenylacetylene, 1-phenyl-1-propyne and 3-phenyl-1-propyne) with parahydrogen over different metal catalysts supported on TiO_2 (Rh/TiO_2, Pd/TiO_2, Ir/TiO_2, Pt/TiO_2). It was found that all catalysts show different catalytic activity and selectivity that can be affected by both the nature of active metal and percentage of metal loading (Fig. 1).

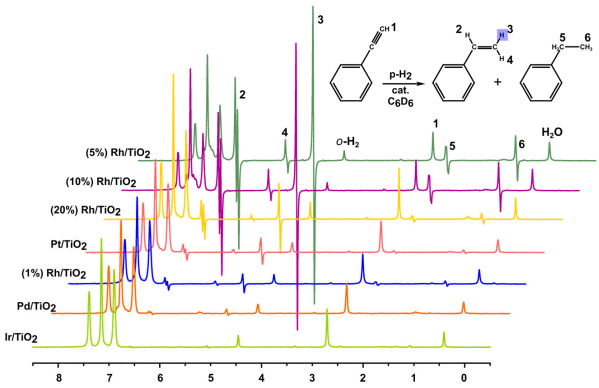

Figure 1. Reaction scheme of phenylacetylene hydrogenation and ^{1}H NMR spectra acquired during hydrogenation of phenylacetylene with parahydrogen over different catalysts

It was demonstrated that the most selective catalyst is Pd/TiO_2 – however, for the production of hyperpolarized product Rh/TiO_2 with 5% metal loading was shown to be best for the all substrates under investigation. Also this catalyst provided the highest conversion rate.

Use of Ir/TiO_2 was found to be inappropriate, because the catalyst shows almost zero activity and doesn't sustain pairwise addition. In the study of liquid-phase hydrogenation reactions kinetics it was shown that reaction order with respect to hydrogen is nearly the same for pairwise and non-pairwise addition – this fact, apparently, indicates the similar nature of catalytically active sites for pairwise and non-pairwise addition routes.

Gas-phase hydrogenation

Although many catalysts of different nature were tested in various gas-phase hydrogenation reactions with parahydrogen, there is still no understanding of how the catalyst preparation method can affect on its selectivity towards pairwise addition. In order to find the influence of preparation method we tested a series of Rh/TiO_2 catalysts in 1,3-butadiene hydrogenation. The optimal catalyst for PHIP effects observation was found – it provides signal enhancement of ca. 200 fold, corresponding to 6% polarization (Fig. 2). Such values are the highest for Rh/TiO_2 catalysts reported to date.

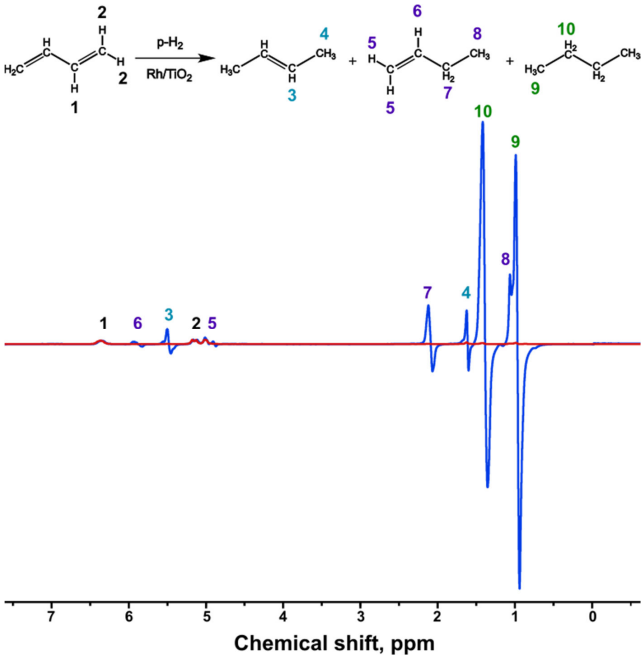

Figure 2. Reaction scheme of 1,3-butadiene hydrogenation and ^1H NMR spectra acquired in hydrogenation of 1,3-butadiene with parahydrogen (blue line) and normal hydrogen (red line) over Rh/TiO_2

Acknowledgements

This work is supported by Russian Foundation for Basic Research (grant No. 16-03-00407 A and No. 17-54-33037 OHKO_a).

References

1. K. V. Kovtunov *et al.* – *Top. Curr. Chem.*, 338, 123-180 (2013).

Fast Field cycling as a tool for studying molecular dynamics in solids

Alexei F. Privalov, Benjamin Kresse, Manuel Becher, Michael Vogel, Franz Fujara

Institut für Festkörperphysik, TU Darmstadt, Hochschulstr 6. 64289 Darmstadt Germany
E-mail: alexei.privalov@physik.tu-darmstadt.de

Fast Field Cycling (FFC) NMR has become attractive in science and technology due to its capability to gain unique information on microscopic dynamics in a large variety of materials. FFC allows studying field-dependent and thereby frequency-dependent spin phenomena like spin-lattice relaxation (SLR) or polarization transfer in NMR-NQR experiments. In practice, a periodically cycled magnetic field is apllied, which is different for evolution and detection periods with the advantage of having the same detection field for all cycles [1]. Specific features of the FFC equipment and various experimental techniques are discussed. FFC studies of dynamical properties over a broad frequency and temperature range of various systems, in particular in superionic conductors [2], polymers [3] and nano-sized materials [4] are presented.

References

1. F. Fujara, D. Kruk, A.F. Privalov, "Solid State Field-Cycling NMR relaxometry: Instrumental Improvements and New Applications". *Progress in Nuclear Magnetic Resonance Spectroscopy*. **82**, 39–69, 2014.
2. M. Graf, B. Kresse, A. F. Privalov, M. Vogel. Combining ^{7}Li NMR field-cycling relaxometry and stimulated-echo experiments: A powerful approach to lithium ion dynamics in solid-state electrolytes. *Solid State Nuclear Magnetic Resonance*. **51–52**, 25–30, 2013.
3. M. Hofmann, B. Kresse, A. F. Privalov, L. Heymann, L. Willner, N. Aksel, N. Fatkullin, F. Fujara, and E. A. Rössler, Segmental Mean Square Displacement: Field-Cycling ^{1}H Relaxometry vs Neutron Scattering. *Macromolecules*. **49**, 7945–7951, 2016.
4. L.B. Gulina, M. Schäfer, A.F. Privalov, V.P. Tolstoy, I. V. Murin, M. Vogel, Synthesis and NMR investigation of 2D nanocrystals of the LaF_3 doped by SrF_2. *Journal of Fluorine Chemistry*. **188**, 185–190, 2016.

Dynamic modes in spin-labeled protein revealed by MD simulations: experimental and computed EPR spectra

Sevastyan O. Rabdano[1], Sergei A. Izmailov[1], Ivan S. Podkorytov[1], Timothy F. Cunningham[2], Cristopher Jaroniec[3], Sunil Saxena[2], Nikolai R. Skrynnikov[1,4]

[1]Laboratory of Biomolecular NMR, SPbSU, 199034, 7/9 Universitetskaya nab., St. Petersburg
[2]Department of Chemistry, University of Pittsburgh, Pittsburgh, PA 15260, USA
[3]Department of Chemistry & Biochemistry, Ohio State University, Columbus, OH 43210, USA
[4]Department of Chemistry, Purdue University, 47907, 560, Oval Drive, West Lafayette IN, USA
E-mail: sevastyan@rabdano.ru
http://bio-nmr.spbu.ru

The EPR spectroscopy of proteins spin-labeled with nitroxyl-containing MTSL tag provides a plethora of information on protein structure and dynamics. The continuous-wave EPR spectra of protein samples report on molecular motions that take place on timescales ranging from ps to μs. The sidechain flexibility and overall tumbling contribute to the total dynamics. In particular, local dynamics depends on the positioning of MTSL on the protein surface, reflecting variations in backbone dynamics and steric constraints arising from proximal side chains. Here we present the simulated EPR spectra for three proteins: (*i*) B1 domain of immunoglobulin G binding protein (6 kDa) spin-labeled at 5 different sites; (*ii*) nucleosome in compact (crystal MD simulation, 827 kDa) and extended (solution MD simulation, 200 kDa) states labeled at N-termini of H3 or H4 histones; and (*iii*) the cytochrome bo3 labeled at two different sites. In order to sample the relevant conformational space, the respective MD trajectories have been recorded with lengths from 1 to 5 μs. The position of MTSL label in these simulations varies from fully flexible intrinsically disordered region to rather rigid β-sheet. The overall tumbling regimes are also sampled, as indicated by a wide range of correlation times found in the three protein samples. Additionally, the effect of water model was studied for common models SPC/E, TIP3P, TIP4P-EW.

The simulated EPR spectra are compared with the experimental data for systems (*i*) and (*iii*). The influence of overall tumbling and MTSL-bearing sidechain dihedrals jumps ($\chi_{1\text{-}5}$) on the lineshape of spectra is discussed.

Acknowledgements

This work is supported by the Russian Science Foundation (grant #15-14-20038).

Magnetic phase separation and its temperature evolution in porous carbon-based doped by Au and Co nanomaterials

V. A. Ryzhov[1], A. V. Lashkul[2], V. V. Matveev[3], P. L. Molkanov[1], A. I. Kurbakov[1,3], I. A. Kiselev[1], K. G. Lisunov[4], D. Galimov[5], E. Lähderanta[2]

[1]B. P. Konstantinov Petersburg Nuclear Physics Institute, NRC ''Kurchatov Institute", Russia
[2]Department of Mathematics and Physics, Lappeenranta University of Technology, Finland
[3]Saint-Petersburg State University, Russia
[4]Institute of Applied Physics ASM, Republic of Moldova
[5]South Ural State University, Russia
E-mail: ryzhov_va@pnpi.nrcki.ru

Introduction

Nowadays, it is evident that carbon-based nanomaterials represent a novel class of ferromagnetic (FM) matter, which does not contain basically any FM metal components [1]. Such materials attract considerable attention due to a high-temperature FM behavior (with the Curie temperature T_C above room temperature) observed in various carbon structures, accompanied with the magnetic hysteresis and the remanent magnetization [1, 2]. The listed features make these materials quite attractive for applications both in technique (spintronics, light magnets) and in biology as well as in medicine, the latter being connected with low toxicity due to vanishing concentration of metallic elements [1, 2]. A possible role of magnetic impu-rities in origination of FM ordering of carbon-based materials is under question till now [1, 2]. To clarify this question comparative investigations of glassy carbon-based nanomaterials doped by nonmagnetic (for example Ag, Au etc.) and magnetic (for example Co, Ni, Fe etc.) metal ions were carried out in this work.

Experimental results

The porous glassy carbon samples doped with 0.004 mass% of Au (S-Au) and with 0.117 mass% of Co (S-Co), which have been prepared and studied earlier in [3, 4], were investigated. Preparation details have been described in Ref. [3]. The atomic force microscopy investigations of the samples doped with Ag, Au and Co provided evidences for the presence of carbon nanoparticles with a broad size distribution given by the average, $R_{av} \sim 60$ nm, and the maximum, $R_{max} \sim 110$ nm, particle radii in all the above listed above [3].

Magnetic properties of the both samples were studied in measurements of: (i) magnetization in ZFC and FC regimes with a SQUID magnetometer: (ii) the second harmonic of magnetization of the longitudinal nonlinear response (NLR-M_2) in the parallel *dc* and *ac* magnetic fields, $H(t) = H + h\cdot\sin\omega t$ ($h \approx 14.3$ Oe and $f = \omega/2\pi \approx 15.7$ MHz) under the condition of $M_2 \propto h^2$ [5]; (iii) electron magnetic resonance spectra with registration of off-diagonal component of the magnetic susceptibility tensor, $M_y(\omega) = \chi_{yx}(\omega)h_x(\omega)$. The latter was provided by using a cylindrical two-mode balanced cavity with TE_{111} type of the electromag-netic oscillations and deep frequency-independent uncoupling between excitation and detection modes accompanied by high spectrometer sensitivity [6].

The magnetization study as well as measurements of the nonlinear longitudinal response to a weak ac field and electron magnetic resonance give evidences for a presence of magnetic nanoparticles (MNPs) embedded in paramagnetic/ferromagnetic matrix of S-Au/S-Co samples respectively, both samples being in magnetically phase-separated state at temperatures above 300 K. Paramagnetic centers located in matrix outside the MNPs were observed in the S-Au composite by EMR. According to NLR-M_2 results they reveal exchange interactions providing matrix ferromagnetic (FM) ordering below $T_C \approx 210$ K in Au-doped sample and well above 350 K in Co-doped one. For the former, NLR-M_2 data suggest

a percolation character of the matrix long-range FM order, which is mainly caused by a porous amorphous sample structure. Amorphous structure was found earlier by neutron diffraction [7]. Temperature dependence of the magnetization in the Au-doped sample evidences presence of antiferromagnetic (AF) interactions of MNPs with surrounding matrix centers. At magnetic ordering below T_C these interactions promote origination of ‘‘domains” involving matrix fragment and surrounding MNPs with near opposite orientation of their moments that decreases the magnetostatic energy. On further cooling, the domains exhibit AF ordering below $T_{cr} \sim 140$ K < T_C, resulting in formation of a peculiar ‘‘ferrimagnet”. The porous amorphous structure leads to absence of translational and other symmetry features through the samples that allows canted ordering of magnetic moments in domains and in whole sample providing ‘‘canted ferrimagnetism”. At low temperatures $T_{tr} \sim 3$ K, ‘‘order-order” transition, evidencing the non-Heisenberg character of this magnetic material, occurs from ordering like ‘‘canted ferrimagnet” to FM alignment, which is stimulated by external magnetic field. The data for Co-doped sample imply the similar evolution of magnetic state but at higher temperatures above 350 K. This state exhibits more homogeneous arrangement of the FM nanoparticles and the FM matrix. In S-Co order-order transition occurs at higher $T_{tr} \sim 10–15$ K as well and followed by formation of long-range FM ordering found earlier by neutron diffraction. Doping of carbon-based nanomaterials by magnetic metals provides advantages for their possible practical applications as Co-doped sample with higher T_C (>350 K) and larger remanent magnetization evidences.

References

1. T. Makarova, F. Palacio (Eds.), Carbon-Based Magnetism, Elsiver, North-Holland, 2006.
2. Y. Kopelevich, P. Esquinazi, J. Low Temp. Phys. 146, 629 (2007).
3. E. Lähderanta, A.V. Lashkul et al. J. Nanosci. Nanotech. **12,** 9156 (2012).
4. E. Lähderanta, V.A. Ryzhov, A.V. Lashkul et al. JMMM **383**, 78 (2015).
5. V.A. Ryzhov, I.I. Larionov, and V.N. Fomichev. Zh. Tekh. Fiz .**66,** 183 (1996) [*Sov. Phys. Tech. Phys.* **41,** 620 (1996)].
6. V.A. Ryzhov, E.I. Zavatskii et al. Zh. Tekh. Fiz. **65,** 133 (1995) [*Tech. Phys.* **40,** 71 (1995)].
7. E. Lähderanta, V.A. Ryzhov et al. JMMM **383**, 78 (2015).

In vitro and *in vivo* applications of ^{1}H-NMR spectroscopy in the biological field

Corentin Schepkens[1,2], Jean-Marie Colet[1]

[1]Laboratory of Human Biology & Toxicology, University of Mons, Belgium
[2]Laboratory of Lipid Metabolism and Cancer, KU Leuven, Belgium
E-mail: corentin.schepkens@umons.ac.be

Introduction

The Omics family is referred to several biological fields in science such as genomics, proteomics and metabolomics. The main goal of Omics sciences is to study a pool of biological molecules to retrieve pertinent (functional and dynamic) and global information on a specific biological event. Metabonomics is an arm of the metabolomics field, in which the metabolites study is used to understand biological perturbation (as for example in cancer) or genetic manipulation on a complex system [1], and transpose these observations for a biological interpretation.^{1}H-NMR is a great analytical tool in the metabonomics field, it allows fast acquisition, the simultaneous detection of dozen of metabolites in one sample, and also the ability of a semi-quantification. Combined to multivariate data analysis tools, it allows a rapid discrimination among study observations. In this abstract, the application of ^{1}H-NMR approach on *in vivo* and *in vitro* studies handled in our laboratory will be described.

Classic pattern in a metabonomic study

The classic pattern of a metabonomic study using a ^{1}H-NMR based approach is illustrated below (Fig. 1). The 1st step is to get the samples, from a human or animal study (tissue, urine and plasma) or from an *in vitro* study based on cell culture (cells and culture media). The 2nd step is to prepare the samples for NMR acquisition using phosphate buffer and the reference TSP. The generated spectra can be processed through the MestRenova software, for phase and baseline corrections. The software is also able to cut the spectra in small subregions of 0.04 ppm-length, called descriptors. NMR-spectra are about 10ppm long, which gives a total of 250 descriptors for one spectrum. The binning tool calculates the area under the curve for each descriptor to get numerical data. The 3rd step is to process the data into the SIMCA-P+ multivariate data analysis software that is able to identify a subset of descriptors from a larger set and correlate them as discriminant in groups separation. The metabolites corresponding to those discriminant descriptors are then identified in the 4th step using the Chenomx software and the Human metabolome database. Finally, identified metabolites are considered for biological interpretation.

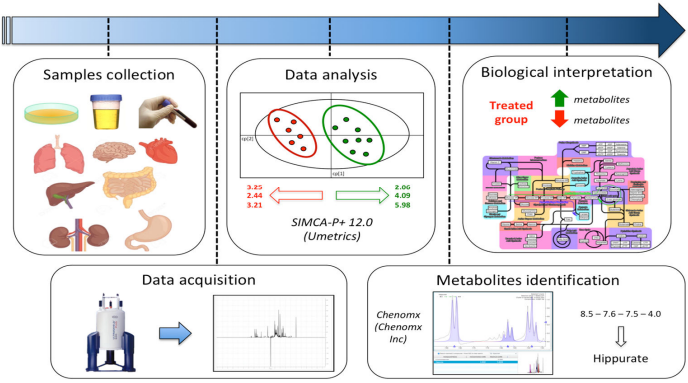

Figure 1. Classic pattern of aNMR based approach

In vitro application of ^{1}H-NMR spectroscopy:
impact of glutamine deprivation on human melanoma cancer cells metabolism

The following pilot study was realized on 451-Lu human cells grown in DMEM high glucose, supplemented with pyruvate or glutamine, 10% FBS and antibiotics. Two groups were considered in this study, one control group in which the cells were grown in classic medium (Glutamine: + / Pyruvate: -) named **GLUT** group, and one experimental group called **PYR** group in which cells were grown in a different medium (Glutamine: - / Pyruvate: +). For in vitro study, the samples need to be collected using a specific protocol that allows the metabolites extraction without enzymatic disturbances. To make it short, cells are removed from the flasks using cold methanol to quench the metabolism. Then a chemical extraction using methanol, water and chloroform is performed to separate the aqueous metabolites from the macromolecules (lipids, proteins, DNA) that can interfere in the NMR signal.

Figure 2 focuses on one spectral area of the spectra in details (from 3.00 to 4.30 ppm), where the metabolic changes are clearly seen. The PYR cells present higher level of glucose than the control cells, highlighting a perturbation in the glycolytic pathway. This perturbation is confirmed by the decreased of lactate production, the end product of the glycolytic pathway, a decrease in myo-inosotol level also produce through the glycolytic pathway, and finally a perturbation of the Creatine/Phosphocreatine ratio reflecting a perturbation in the ATP production in those cells. Glutaminolysis is highly used by the cancer cells for *de novo* lipogenesis process, in order to produce free fatty acids (FFA) from citrate. The PYR cells can no longer use this process due to the glutamine deprivation, and it appears that these cells use an overactivation of the choline metabolism, with an increase in Phophocholine (PCho) and Glycerophosphocholine (GPC) to resynthesize FFA from other pathways.

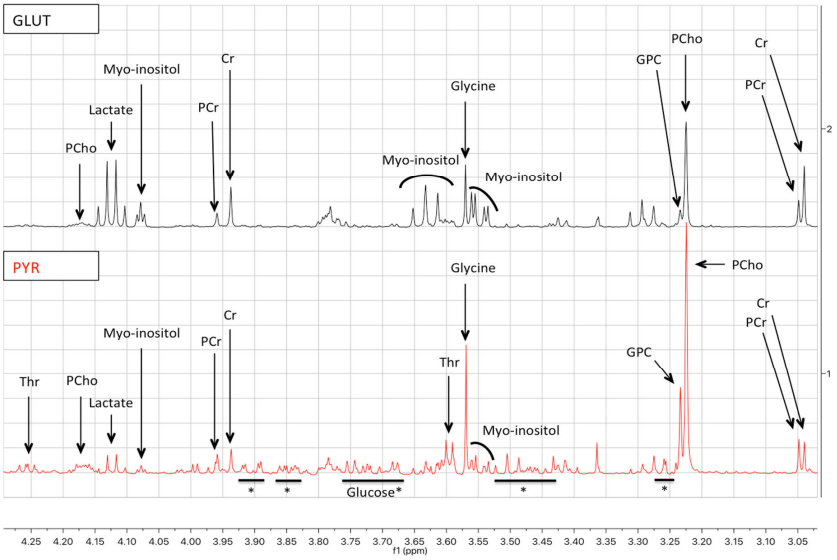

Figure 2. Magnified area of the spectra from 3.0 to 4.3 ppm of the intracellular compartment of 451-Lu cells grown in a medium supplemented with glutamine (GLUT) or pyruvate (PYR)

In vivo application of ^{1}H-NMR spectroscopy:

prenatal testosterone exposure induces metabolic perturbations in male rats at puberty

This study is based on an animal model using Sprague-Dawley rats. In this experimental work, pregnant rats were exposed to either a low or a high dose of testosterone at a late stage during pregnancy. Male rats born during the study were allowed to grow up to a pubertal state, then a 24-hour fraction of urine was collected before necropsia. The urine samples were analyzed using our NMR-based approach, which provided strong results on the metabolic disturbances of androgen prenatal exposure. In this study, a high number of samples were analyzed and a model using the SIMCA-P+ was calculated. The model is illustrated on Fig. 3 below, with the Scores Plot on the bottom gathering all the samples from the three groups and the Loadings Plot on the top displaying all the discriminating metabolites. The increases in taurine and allantoin levels are indicative of enhanced antioxidant mechanisms in response to the oxidative stress caused in those rats. The decreases in succinate, citrate and α-ketoglutaric acid levels (intermediates of Krebs cycle) and the glycosuria are indicative of carbohydrate metabolism disorder in Testo 1 and 3mg rats.

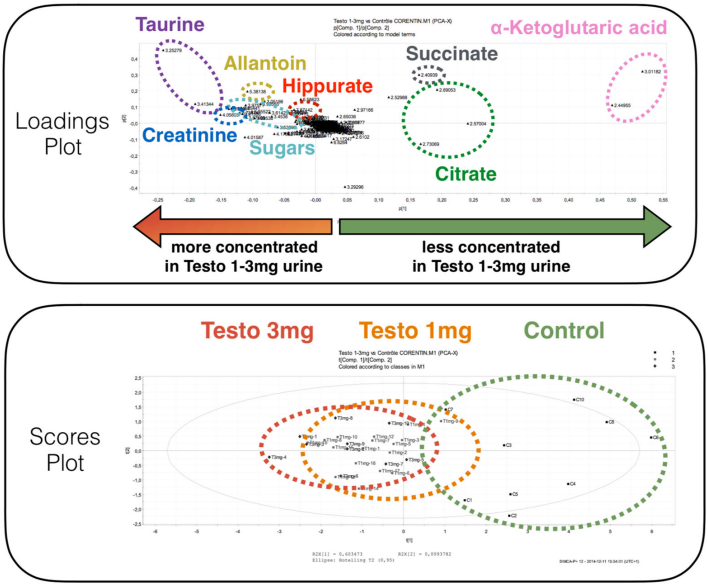

Figure 3. Scores Plot and Loadings Plot showing the metabolic disturbances in rats prenatally exposed to testosterone

Acknowledgements

We sincerely thank the General, Organic, and Biomedical Chemistry laboratory (University of Mons) for the technical service related to the ^{1}H-NMR spectrometer use.

References

1. Nicholson J. and Lindon J., System biology: Metabonomics (**2008**) Nature 455, 1054-1056

Ferromagnetic resonance study of FeRh thin films near the antiferromagnetic-ferromagnetic phase transition

Anna Semisalova[1,2], Sven Stienen[1], Craig W. Barton[3], Roman Boettger[1], Rantej Bali[1], Thomas Thomson[3], Michael Farle[4], Jürgen Fassbender[1], Kay Potzger[1], Jürgen Lindner[1]

[1]*Helmholtz-Zentrum Dresden – Rossendorf, Institute of Ion Beam Physics and Materials Research, Dresden, Germany*
[2]*Lomonosov Moscow State University, Faculty of Physics, Moscow, Russia*
[3]*University of Manchester, School of Computer Science, Manchester, UK*
[4]*University of Duisburg-Essen, Faculty of Physics and CeNIDE, Duisburg, Germany*
E-mail: a.semisalova@hzdr.de
https://www.hzdr.de/db/Cms?pOid=48745&pNid=107

Introduction

The nearly equiatomic FeRh alloy with the chemically ordered B2 crystal structure demonstrates an unusual phase transition from antiferromagnetic to ferromagnetic (FM) order at ~370 K. This first-order phase transition can be driven not only by temperature [1,2], but also by an external magnetic field, induced strain or spin polarized current [3,4]. Moreover, the chemical disordering, i.e. the structural transformation from B2 to A2 state (for example, caused by ion irradiation [5,6]) leads to the controllable shift of the phase transition temperature as well as an increase of the low-temperature ferromagnetic signal. Ferromagnetic resonance (FMR) technique can be used as a powerful tool for investigation of magnetic structure and anisotropy across such phase transition in FeRh.

Ferromagnetic resonance in FeRh

Temperature-dependent FMR

Here, we present the results on temperature dependent ferromagnetic resonance in FeRh thin films. The films of 40 nm thickness were deposited on single crystal MgO(001) substrates using magnetron sputtering from a nominally $Fe_{50}Rh_{50}$ alloy target at 600°C and post-annealed at 750°C. The temperature dependence of the FMR absorption line across the phase transition allows to analyze the development of FeRh magnetization, resonance field and linewidth with temperature (Fig. 1). FMR spectra taken at temperatures below the phase transition reflect the complex magnetic structure of the films revealing the contribution of a FM interfacial layer with cubic anisotropy. The angular dependence of the resonance field shows the coupling of the magnetic moment of this FM layer with the antiferromagnetic FeRh film. Our findings allow to characterize the interfacial layer which is ferromagnetic at temperatures below phase transition, where the main part of the FeRh film is antiferromagnetic. This ferromagnetic layer can play a crucial role in the performance of ultrathin FeRh films.

Effect of ion irradiation

Also, we discuss the effect of chemical disorder induced with 20 keV Ne^+ ions irradiation on magnetic properties. Angular dependence of FMR spectra reveals the formation of a magnetic phase with an out-of-plane magnetization easy axis after ion irradiation with low fluence (5×10^{12} ions/cm^2). The possible origin of this ferromagnetic phase will be discussed.

Acknowledgements

The support of Ion Beam Center (HZDR) is acknowledged. We thank Dr. S. Zhou (HZDR) for help with maintaining the experimental setups.

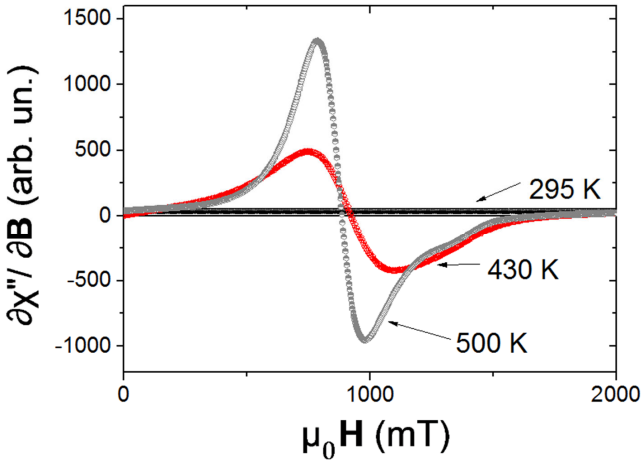

Figure 1. Ferromagnetic resonance spectra of FeRh thin film at different temperatures

References

1. E. Mancini, F. Pressacco, M. Haertinger et al. – *J. Phys. D: Appl. Phys.*, **46**, 245302 (2013).
2. A. Heidarian, S. Stienen, A. Semisalova et al. – *Phys. Stat. Solidi (b),* **254**, 1700145 (2017).
3. R.O. Cherifi, V. Ivanovskaya, L.C. Phillips et al. – *Nat. Mater.*, **13**, 345-351 (2014).
4. I. Suzuki, T. Naito, M. Itoh et al. – *Appl. Phys. Lett.*, **107**, 082408 (2015).
5. A. Heidarian, R. Bali, J. Grenzer et al. – *Nucl. Instr. Meth. Phys. Res. Sect. B,* **358**, 251-254 (2015).
6. S.P. Bennett, A. Herklotz, C.D. Cress et al. – *Mater. Res. Lett.*, **6**, 106-112 (2018).
7. S. Fisher, B. I. Yachtman. – *Vacuum State Comm.*, **7**, 1234-1237 (2003).

Problem books on NMR spectroscopy (review)

N. M. Sergeyev

Department of Chemistry Moscow State University
E-mail: sergeyev2010@yandex.ru

The solution of individual problems and, moreover, the compilation of reasonable problems with parallel discussion of the solutions of these problems, taking into account the accuracy and uniqueness of the solution, originality and speed of implementation of this decision is an essential part of each science [1]. We analyzed the known collections of problems in NMR spectroscopy (in particular, such books as R. Silverstein et al [2], R Macomber [3], P. Atkins et al [4]). Recommendations are given for problem solving and the methods of preparation of original problems. The advantages and disadvantages of individual books are analyzed. It is noted that many textbooks problems are formulated with an excess of conditions. Some typical situations are considered in solving certain problems are considered. An analysis of an example of an invalid problem is given

References

1. G. Pólya How to Solve It, Mathematics and Plausible Reasoning Princeton University Press 2004 (there is a translation into Russian)
2. R. Silverstein et al "Spectrometric Identification of Organic Compounds" Wiley 2005, (Russian translation available)
3. R. Macomber, A Complete introduction to Modern NMR Spectroscopy Wiley 1998
4. P. Atkins and G. de Paula, Physical Chemistry, 10th edition 2014, Oxford University Press

Determination of the Structure of Hyperbranched Polyester BOLTORN and its Derivatives with *L*-lactide and Methyl Ether of Polyethylene Glycol Using NMR-spectroscopy methods

V. A. Shpotya[1], *A. M. Perepukhov*[1], *A. V. Maksimychev*[1], *V. I. Gomzyak*[2], *S. N. Chvalun*[2]

[1]*Moscow Institute of Physics and Technology*
[2]*Moscow Technological University (M. V. Lomonosov Institute of Fine Chemical Technologies)*
E-mail: shpotya.valeriya@yandex.ru

Introduction

The synthesis and study of proprieties of macromolecules with complex architecture (such as polymer brushes, star-shaped etc.) have attracted increasing interest with different research groups during recent years. The dendrimers and their less regular analogues – hyperbranched polymers are of particular interest because of the large number of peripheral functional groups in their structure. Such groups can be modified to adapt base macromolecule for a specific scientific and technological problem. Due to the possibility of varying physical and chemical proprieties, such molecules can be used as universal transport platform for different substances. In particular, they can be used as nanoconteiners for targeted delivery of drugs.

In this work the properties of hyperbranched polyester based on 2,2-bis(methylol)propionic acid (commercial name BOLTORN) and its derivatives with *L*-lactide and methyl ether of polyethylene glycol (polylactid groups) are studied by NMR-spectroscopy methods. The number of polylactid chains and their length determine the chemical and physical properties of the final molecule. The aim of this work was to determine the number of polylactid chains and their length in the BOLTORN derivatives. This task required for determination of the number of active centers in the molecule BOLTORN.

Estimating the number of active centers

The number of active centers in the molecule BOLTORN, which are the potential places for polylactid chains attachment, is given by the structure of molecule and it can be estimated using NMR-methods. The molecule BOLTORN consists of the core and repeat units, which can be divided in 3 types: terminal units (T), linear units (L) and dendrite units (D). The active centers are hydroxyl groups, which are located in terminal and linear units. The chemical shifts of three types of units differ in ^{1}H-NMR spectrum. Figure 1 shows the full ^{1}H-NMR spectrum of molecule BOLTORN and a part of spectrum corresponding to the protons of CH_3-groups. In this paper, we determine the correspondence of different types of units with signals in the ^{1}H-NMR spectrum of molecule BOLTORN using the methods of one-dimensional and two-dimensional NMR-spectroscopy (^{1}H-NMR, ^{13}C-NMR, TOCSY, HMBC, HSQC). In earlier published articles devoted to the study of structure of molecule BOLTORN with NMR - methods, there were differences in corresponding, which were resolved by using two-dimensional methods [1, 2].

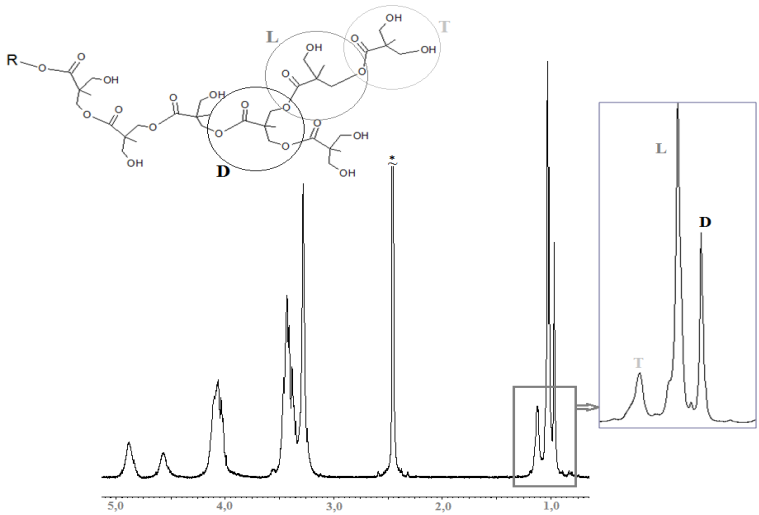

Figure 1. Different types of units of molecule BOLTORN and its ^{1}H-NMR spectrum

The characteristics of signals in the NMR spectrum of molecule BOLTORN, such as their position, integrals and corresponding groups in the structure of BOLTORN, are collected in Table 1. The last column of Table 1contains integrals calculated under the assumption that the first three signals correspond to terminal, linear and dendrite units respectively and their integrals are correct. Assuming this data we can estimate the degree of branching (DB) that defines by the formula (1). In our case DB ≈ 0.5.

$$DB = \frac{D+T}{D+L+T}. \quad (1)$$

Table 1. The position, integrals and corresponding groups of the signals in ^{1}H-NMR spectrum of molecule BOLTORN

№	Position, ppm	Corresponding group	Integral	Calculated integral
1	0.91...0.99	CH_3-(T)	45.94	-
2	0.99...1.08	CH_3-(L)	78.46	-
3	1.08...1.23	CH_3-(D)	24.34	-
4	3.33...3.53	CH_2-OH	115.06	113.56
5	3.95...4.21	CH_2-OR	89.36	84.76
6	4.48...4.68	OH-(T)	19.92	30.62
7	4.77...4.99	OH-(L)	25.38	26.15

Estimating the number of polylactid groups

The spectrum of the derivative of BOLTORN and polylactid contains separated signals of different units of the polylactid chain (terminal units and internal units) and merged signals of molecule BOLTORN (without division into D-L-T types). In the ^{13}C-NMR spectrum, the

signal of quaternary carbon of BOLTORN corresponds to dendrite type (Figure 2). This led us to argument that all active centers (hydroxyl groups) react completely with polylactid chains. Hence we can estimate the number of polylactid chains (it is equal to the number of active centers of BOLTORN) and their length. The discrepancy between the integrals of signals of BOLTORN and terminal units of polylactid chains can be explained by the presence of free-floating aggregates of polylactid groups in the mixture. This is confirmed by DOSY experiment.

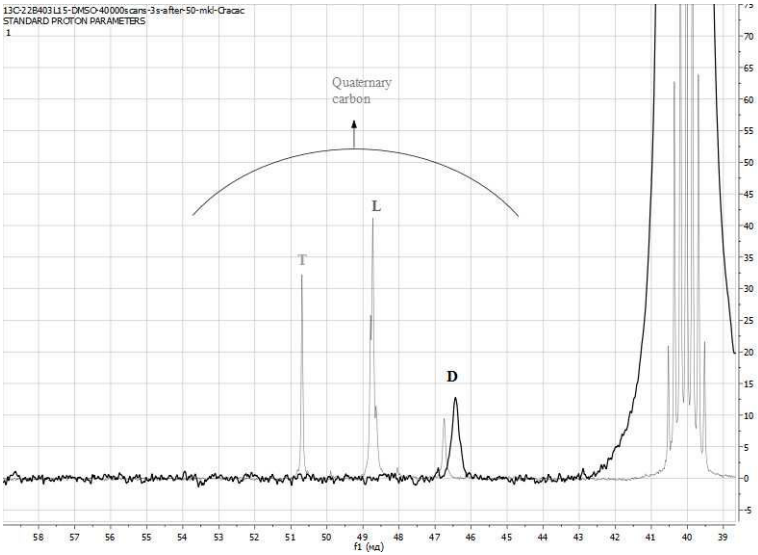

Figure 2. The part of ^{13}C-NMR spectrum of the derivative of BOLTORN and polylactid that corresponds to quaternary carbons (light grey line – the part of pure BOLTORN spectrum)

Conclusion

In this work, we estimated the number of polylactid chains and their length for derivatives of the molecule BOLTORN. We derived the correspondence of signals in ^{1}H-NMR spectrum of molecule BOLTORN with the protons from different groups of BOLTORN. According to the obtained data, we calculated the degree of branching (DB), which amount to 0.5.

References

1. F.Kh. Karataeva, M.V. Rezepova, M.P. Kutyreva, G.A. Kutyrev, N.A. Ulakhovich, Structure of Hyper-Branched Polyester Polyol BOLTORN H2O–COOH. NMR Data // *Jhurnal Obshchei Khimii.* 2010. V. 80. No. 9. pp. 1513–1517
2. Ema Zagar, Majda Zigon, Stepan Podzimek, Characterization of commercial aliphatic hyperbranched polyesters // *Polymer* 47. 2006. pp 166–175

EPR study of electron-acceptor sites during dehydrochlorination of 1-chlorobutane over metal oxides

Ekaterina I. Shuvarakova[1,2], Alexander F. Bedilo[1,2], Vladimir V. Chesnokov[1]

[1]Boreskov Institute of Catalysis SB RAS, Novosibirsk 630090, Russia
[2]Novosibirsk Institute of Technology, Kosygin Russian State University, Novosibirsk 630099,
E-mail: katerina.shuv@gmail.com

Introduction

One of the most intriguing properties of many heterogeneous acid catalysts is their ability to generate spontaneously organic radical cations upon adsorption of aromatic electron donors [1]. ZSM-5 zeolites and sulfated zirconia materials possessing exceptionally strong electron-acceptor sites capable of ionizing compounds with very high ionization potentials, such as benzene (IP = 9.2 eV).[2] The existence of weaker electron-acceptor sites with electron affinities ~ 7 eV in large quantities on the surface of many conventional oxides is no less remarkable. Electron-acceptor sites of different strength can be characterized using aromatic probes with different ionization potentials [2, 3].

It was shown earlier that the catalytic activity of nanocrystalline MgO during dehydrochlorination of 1-chlorobutane substantially increases with time due to the MgO conversion to $MgCl_2$ [4]. This increase coupled with a surface area decrease indicates that more active sites are formed on the surface during this reaction. Recently we reported that weak electron-acceptor sites formed due to the MgO halogenation might be responsible for solid-state reaction between nanocrystalline MgO and CF_2Cl_2 [5, 6]. In this study, we investigated weak electron-acceptor sites formed during dehydrochlorination of 1-chlorobutane on the surface of catalysts based on γ-Al_2O_3 and ZrO_2 using perylene as spin probes. A good correlation between their concentrations and the catalytic activity was found.

Experimental

Samples of pure and sulfated γ-Al_2O_3 and ZrO_2 with different concentrations of doped sulfates were studied in catalytic dehydrochlorination of 1-chlorobutane. The samples were placed in an EPR sample tube, activated in an argon flow for 1 h at the reaction temperature, and subjected to reaction with 1-chlorobutane. 1-Chlorobutane conversion to a mixture of butenes was monitored by gas chromatography. After the reaction was carried out for the desired time, the sample was quickly cooled down to room temperature and filled with a 2×10^{-2} M solution of perylene in toluene. The concentration of electron-acceptor sites was determined by integration of the EPR spectra registered immediately after the spin probe adsorption and after additional heating at 80°C for 18 hours.

Results and discussion

Samples of pure and sulfated γ-Al_2O_3 and ZrO_2 are characterized by substantial concentrations of electron-acceptor sites depending on the concentration of doped sulfates. Dependence of 1-chlorobutane conversion over pure and sulfated γ-Al_2O_3 on the time on stream is shown in Figure 1 (A). The catalytic activity of pure Al_2O_3 increased during the first 20 min on stream due to the surface chlorination that is known to increase the concentration of electron-acceptor sites. EPR spectra obtained immediately after perylene adsorption after reaction for desired time are also shown in Figure 1 (B).

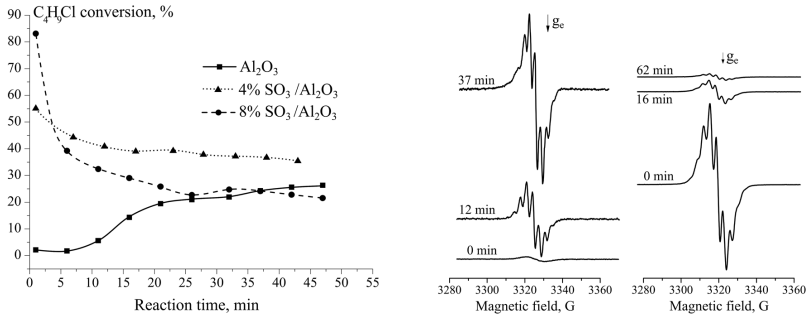

A *B*

Figure 1. 1-Chlorobutane conversion vs. time on stream for 1-chlorobutane dehydrochlorination over sulfated alumina at 220°C:
(A) and EPR spectra obtained immediately after perylene adsorption,
(B) after reaction with 1-chlorobutane over γ-Al_2O_3 (left) and 8%SO_3/ γ-Al_2O_3 (right)

Activity of sulfated samples was higher initially, and it is in good agreement with higher concentration of electron-acceptor sites. Their activity gradually decreased during the reaction reaching values similar to those close on γ-Al_2O_3. Overall, a good correlation was observed between the catalytic activity in dehydrochlorination of 1-chlorobutane and the concentration of weak electron-acceptor sites.

Similar results were obtained for pure and sulfated zirconia. The catalytic activity of pure ZrO_2 increased during first 20 min reaching 20% conversion as seen in Figure 2 (A). The concentration of weak electron-acceptor sites measured immediately after reaction also increased. Sulfated samples showed much higher catalytic activity initially and 1-chlorobutane conversion gradually decreased as did the intensity of EPR spectra (Figure 2 (B)).

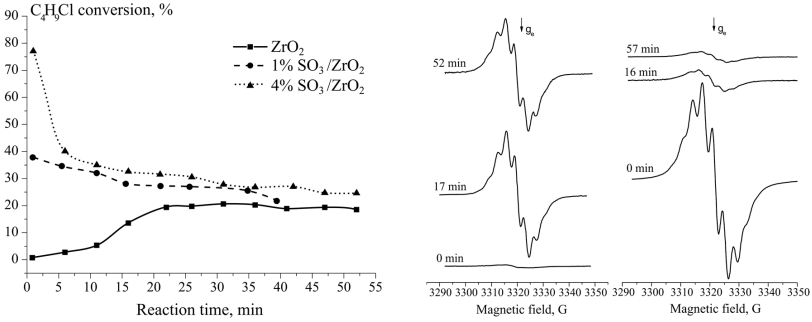

A *B*

Figure 2. 1-Chlorobutane conversion vs. time on stream for 1-chlorobutane dehydrochlorination over sulfated zirconia at 220°C:
(A) and EPR spectra obtained immediately after perylene adsorption,
(B) after reaction with 1-chlorobutane over ZrO_2 (left) and 4%SO_3/ ZrO_2 (right)

Conclusions

Concentrations of electron-acceptor sites were measured during a catalytic dehydrochlorination of 1-chlorobutane over pure and sulfated γ-Al_2O_3 and ZrO_2. It is shown that the concentration of weak elector-acceptor sites correlates with the catalytic activity. The obtained results indicate that weak electron-acceptor sites tested using perylene may be the active sites accounting for 1-chlorobutane dehydrochlorination in the active state of the catalysts. It seems to be very important to study possible correlations between the concentrations of electron-acceptor sites and catalytic activity of various catalytic reactions taking place on surface acid sites to elucidate the possible role of electron-acceptor sites in these reactions.

References

1. H. Garcia and H.D. Roth, *Chem. Rev.* **2002**, *102*, 3947-4007.
2. A.F. Bedilo, A.M. Volodin, *Kinet. Catal.* **2009**, *50,* 314-324.
3. A.F. Bedilo, E.I. Shuvarakova, A.A. Rybinskaya, D.A. Medvedev, *J. Phys. Chem. C* **2014**, *118*, 15779-15794.
4. I.V. Mishakov, A.F. Bedilo, R.M. Richards, V.V. Chesnokov, A.M. Volodin, V.I. Zaikovskii, R.A. Buyanov, K.J. Klabunde, *J. Catal.* **2002**, *206*, 40-48.
5. A.F. Bedilo, E.I. Shuvarakova, A.M. Volodin, E.V. Ilyina, I.V. Mishakov, A.A. Vedyagin, V.V. Chesnokov, D.S. Heroux, K.J. Klabunde, *J. Phys. Chem. C* **2014**, *118*, 13715-13725.
6. A.A. Vedyagin, A.F. Bedilo, I.V. Mishakov, E.I. Shuvarakova, *J. Serb. Chem. Soc.* **2017**, 82, 523–538.

Evaluation the delayed contrast enhancement as a tool for the differential diagnostics between brain metastases and neurotoxoplasmosis

P. I. Simeshchenko[1,2], A. A. Drozdov[1,2], V. M. Cheremisin[1,2], I. I. Kamyshanskaya[1,2], A. A. Yakovlev[1,3], V. B. Musatov[1,3], I. P. Fedunyak[3], V. B. Danilov[1]

[1]St. Petersburg State University, Faculty of Medicine, St. Petersburg, Russia
[2]Mariinsky Hospital, St. Petersburg, Russia
[3]Clinical Infectious Hospital No.30 named after S.P. Botkin, St. Petersburg, Russia
E-mail: simeshchenko@gmail.com; a_a_drozdov@mail.ru

Introduction

The problem of differential diagnosis in the syndrome of multiple brain lesions with mass effect and the ring-type contrast enhancement with MRI or CT is important for any hospital that provides emergency medical care. The most common diagnostic dilemma that requires prompt solution is the differentiation between the neoplastic and infectious processes due to the principal differences in management and the dependence of the outcomes of treatment on the early start.

Among the neoplastic processes with multiple brain lesions, special attention should be provided to metastatic lesions as the most common form in this group. In turn, among the infectious processes, special attention should be paid to neurotoxoplasmosis because of the high similarity of radiological signs with the metastatic lesions. These include the zone of ring-shaped accumulation of a contrast with uneven width, the variability in the visualization of the central part of the focuses on T1 and T2 weighted images (WI), the absence of MR-signs of restricted diffusion or the presence of such changes only in part of the focus, as well as the presence of perifocal edema and mass effect.

The wide distribution of magnetic resonance and computer tomographs, the simplicity and reproducibility of the delayed contrast method, the high rate of HIV infection, on the one hand, the complexity, limited distribution and invasiveness of the method of stereotactic biopsy, on the other, determine the need for the attentive study of the delayed contrast method in the differential diagnostics between toxoplasmosis and metastatic brain lesions.

Purpose of the study

Refinement of the radiological semiotics of neurotoxoplasmosis and similar forms of the metastatic lesion, evaluation of the diagnostic potential of the delayed contrast method in the differential diagnosis between these conditions, determination of the optimal time interval between the administration of contrast medium and delayed scanning.

Materials and methods

For the study, we selected patients who had multiple brain lesions with a mass effect and a ring-shaped type of contrast agent enhancement based on computed or magnetic resonance tomography imaging. For the study we collected data about the localization and histological type of metastatic diseases, clarified the HIV status of the patients, CD4+ cell level, concomitant states and analyzed the past medical records. The etiology of multifocal brain lesions was confirmed by histological methods (stereotactic biopsy, autopsy) or by the response to drug therapy.

In summary, the study group comprised 38 patients aged 26 to 76 years, 18 of them were men and 20 women who received treatment at Mariinsky Hospital or St. Petersburg State Clinical Hospital "Clinical Infectious Diseases Hospital named by S.P. Botkina" from 2014 to 2018. For every patient, the magnetic resonance imaging was performed at the St. Petersburg Mariinsky Hospital (Siemens Magnetom Avanto 1.5T) with the administration of the half-

molar gadolinium-containing contrast medium (Magnetist or Omniscan) at the concentration of 0.2 ml/kg. The MRI program included T2 FLAIR in axial projection (TE = 8000, TR = 98, TI = 2370), T1 Turbo Spin Echo (TSE), weighted images in 3 projections (TR = 493, TE = 9.7), DWI (b = 50, 500, 1000) with the construction of the ADC, T2* WI in the axial projection.

After native MR imaging, a gadolinium-containing half-molar contrast medium was administered and early post-contrast T1-WI were achieved in 3 projections, T2-WI in 3 projections (TR = 4880, TE = 93), T1 GRE (TR = 544, TE = 4,76, Flip angle = 70). Delayed post-contrast T1 TSE images were achieved in the axial projection at 15, 30 and 45 minutes after the administration of contrast agent. Four patients have interrupted the study before performing a scan 45 minutes after the administration of the contrast agent and were excluded from the sample.

A total of 153 foci were evaluated, with mass effect and the ring-shaped contrast enhancement. At the first stage, the neuroradiologist performed a subjective assessment of the presence or the absence of contrast agent accumulation in the central part of each focus on delayed images. To objectify the data for each focus, a ratio of the signal intensity from the center of the focus to the contralateral, unchanged zone on T1-WI before and after the contrast agent administration were calculated. The region-of-interest (ROI) was of a circular shape, the diameter was defined as half the diameter of the central zone of the focus (that did not accumulate the contrast agent).

The calculated relations have been analyzed and compared with neuroradiologists subjective assessment. The higher value of the indicator for late post-contrast images in comparison with early post-contrast images reflected the accumulation of contrast medium in the central part of the focus.

The presence of statistically significant differences between the groups was determined by the exact Fisher test then the sensitivity and specificity of the MR sign of the accumulation of contrast medium in the center of the focus as the criterion for differential diagnosis between toxoplasmosis and metastatic lesion were determined.

Results and discussion

Of 38 patients, the toxoplasmosis group included 21, a group of metastatic lesions included 17 patients. The average age of patients in the toxoplasmosis group was 39.5 ± 8.4 years, in metastatic lesions group 56.7 ± 12.3 years. A total of 153 focal brain lesions with mass effect and the ring-shaped accumulating of the contrast agent were analyzed. Among them, 63 foci were due to toxoplasmosis and 89 were metastatic lesions.

Among 17 patients with metastatic disease, 6 had breast cancer, 4 had lung cancer, 2 had pancreatic cancer, 2 had melanoma, 1 had ovarian cancer, 1 had kidney cancer, and 1 patient was with metastatic lesions of unidentified cancer. All patients with neurotoxoplasmosis were HIV-positive, the average level of CD4 lymphocytes among them was 134 cells/μl.

Out of 153 foci, central accumulation of contrast agent in a delayed phase was recognized in 83 cases. Among all cases, the sign was present in 30 minutes after contrast administration. Subjective assessment of the radiologist about the accumulation of contrast medium in the central part of the focus coincided with the growth of the ROI ratio by at least 19% in 30 minutes. Out of 89 metastatic foci, 81 accumulated a contrast agent in the delayed period, while out of 63 foci of toxoplasmosis, the accumulation of contrast agent by the central part of the focus was detected only in 2 cases.

An example of a focus accumulating contrast in the delayed phase is shown in Fig. 1; a focus without the accumulation of contrast in delayed phase is shown at Fig.2.

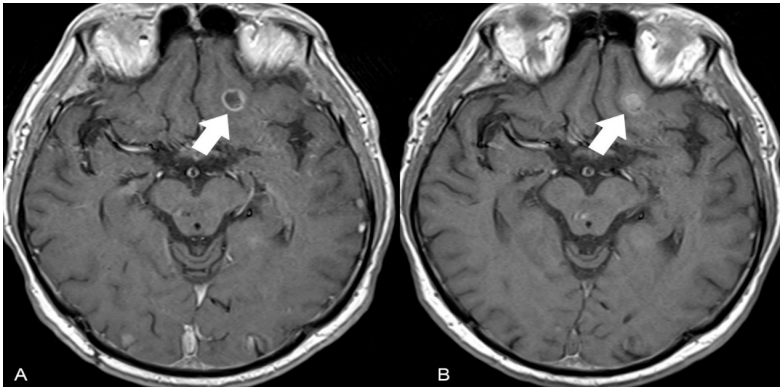

Figure 1. MRI of patient Yu, 1955, with metastases of the lung cancer. Postcontrast T1-WI in the axial projection. The arrow indicates an additional pathological structure with ring-shaped contrast enhancement in early phase (A), after 15 minutes it accumulates contrast agent in the centrally (B)

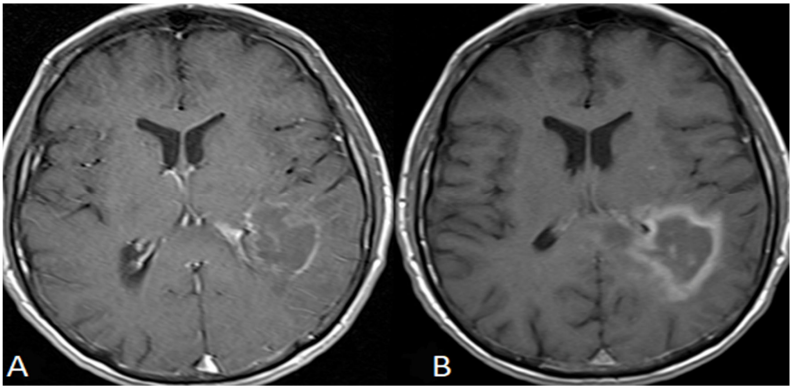

Figure 2. MRI of the patient A. 1977, neurotoxoplasmosis. T1-WI images in the axial projection, A - were obtained immediately after the administration of contrast agent, B - 45 minutes after the administration of contrast agent. In the left parieto-temporal region, the pathological structure with the accumulation of contrast along the annular type, without signs of accumulation in the central zone

The presence of central contrast enhancement at the delayed images significantly increases the probability of metastatic nature of the lesions. The exact Fisher test confirmed the presence of statistically significant differences between the two study groups ($p < 0.05$). Calculated sensitivity of the method was 88%, specificity 95%.

Thus, the application of the delayed contrast method in the MRI study allows differential diagnosis of neurotoxoplasmosis and brain metastases in an emergency hospital.

References

1. Trofimova T.N., "The defeat of the brain in HIV-infected patients. Clinical-laboratory and radiological comparisons., "Medical academic journal, v. 15, pp. 31-38, 2015.
2. Kornienko V.N., Diagnostic Neuroradiology, Moscow: Moscow, 2009.
3. Kathleen R. F., "Imaging of brain metastases," *Surgical Neurology International,* no. 4, pp. 209-219, May 2013.
4. Tse V, "Brain Metastasis Differential Diagnoses," 23 May 2017. [Online]. Available: https://emedicine.staging.medscape.com/article/1157902-differential. [Accessed 10 Jan 2018].
5. Chinn R.J., "Toxoplasmosis and primary central nervous system lymphoma in HIV infection: diagnosis with MR spectroscopy.," *Radiology,* vol. 197(3), pp. 649-54, Dec 1995.

In situ NMR/MRI of Hyperpolarized Molecules

Alexandra Svyatova[1,2], Nikita Chukanov[1,2], Oleg Salnikov[1,2],
Kirill Kovtunov[1,2], Igor Koptyug[1,2]

[1]Novosibirsk State University, Pirogova Street 2, 630090, Novosibirsk, Russia,
[2]International Tomography Center, Institutskaya Street 3A, 630090, Novosibirsk, Russia
E-mail: alexandra.svyatova@tomo.nsc.ru

Introduction

The main disadvantage of nuclear magnetic resonance (NMR) is the low sensitivity because of a small difference between the spin levels populations at the thermal equilibrium. Hyperpolarization methods can significantly changed population of spin levels and, as a result, NMR signal intensity can be increased by several orders of magnitude. Among the hyperpolarized techniques the methods based on parahydrogen (p-H_2) use are under the interest.

Signal Amplification By Reversible Exchange (SABRE)

Parahydrogen can be successfully used for the NMR signal enhancement in two major approaches: Parahydrogen-Induced Polarization (PHIP) [1] and Signal Amplification By Reversible Exchange (SABRE) [2]. PHIP based on the hydrogenation reaction with the step of pairwise hydrogen addition to unsaturated bond of substrate. The principle of the second technique is reversible exchange of p-H_2 and ligands over metallic Ir center of Ir metal complex. This exchanging process generates high levels of nuclear spin polarization of an appropriate ligand. The SABRE process can be realized at both high magnetic field (HF-SABRE) [3] and low magnetic field (conventional SABRE) [4]. In HF-SABRE experiments the hyperpolarization is directly formed and detected in high magnetic field of NMR spectrometer. This fact opens up opportunity to do *in situ* MRI/NMR experiments that is highly important in the case of hyperpolarized contrast agents.

SABRE experiments are simple to use, because it needs only the system to bubble p-H_2 through the solution of SABRE catalyst and substrate. HF-SABRE does not require sample shuttling from low field to the spectrometer like in conventional SABRE approaches.

Molecules

Despite the benefits of ^{1}H atoms, such as a high gyromagnetic ratio and natural abundance of magnetic isotope (98.985%), it has some disadvantages. The short lifetimes of hyperpolarized molecules and background signal in the experiments with living tissues, limit an amount of possible application of SABRE. To solve this problem, polarization transfer from protons to other nuclei (^{13}C, ^{15}N, ^{19}F, etc.) can be realized that, without doubt, expand the limits of possible biomolecules, which potentially can be used as contrast agents in MRI. In this work 3-fluoropyridine (3-Fpy), imidazole-$^{15}N_2$ and nicotinamide-^{15}N were investigated by SABRE and HF-SABRE approaches.

^{15}N-labeled molecules are under the interests because they have long relaxation times T_1 and nitrogen is widely presented in many biomolecules. Although not all molecules which are ideal for SABRE are also biologically relevant, in this work we presented the study of two biomolecules: imidazole-$^{15}N_2$ and nicotinamide-^{15}N, which can be used in the metabolic processes imaging. For the first time 2D magnetic resonance imaging (MRI) was done for these directly hyperpolarized via HF-SABRE molecules.

NMR studies of signal enhancement using ^{15}N-labeled molecules are widely spread, but the synthesis of such molecules is expensive. An alternative for this nucleus is ^{19}F. Natural abundance of ^{19}F is 100%. It provides the difference only 17% comparing to hydrogen signal intensity. Here ^{15}N-3-Fpy and ^{14}N-3-Fpy were tested.

SABRE of 3-Fpy

^{1}H NMR SABRE experiments with ^{15}N-3-fluoropyridine and ^{14}N-3-fluoropyridine were done at high magnetic field, which was equal to 9.4 T. Parahydrogen was bubbled through the solutions of ^{15}N-3-Fpy or ^{14}N-3-Fpy (100 mM) and SABRE catalyst [Ir(IMes)(COD)Cl] (5 mM) in CD_3OD. Hydrogen pressure was 70 psi, flow rate of parahydrogen delivery was 60 sccm, p-H_2 enrichment was 81-86%. The spectra were acquired immediately after bubbling in the fringe field of the 9.4 T NMR spectrometer (Figure 1).

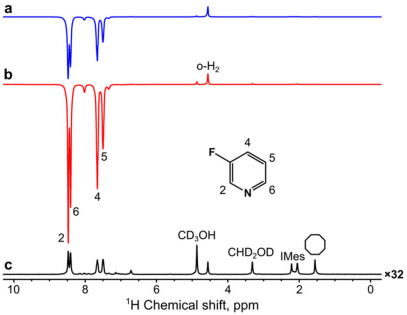

Figure 1. (a) ^{1}H SABRE spectrum of the solution with ^{15}N-3-FPy. (b) ^{1}H SABRE spectrum of the solution with ^{14}N-3-FPy. (c) Thermal ^{1}H spectrum of the solution after relaxation of polarization multiplied by a factor of 32

For comparison, the thermal spectrum is presented, which was acquired after polarization relaxation. The resulted enhancement factors were equal to 105 and 199 for ^{15}N-3-Fpy and ^{14}N-3-Fpy respectively. It corresponds to the amount of ^{1}H polarization: 0.339% in case of ^{15}N-3-FPy and 0.643% in case of ^{14}N-3-FPy.

In SABRE experiments with pyridine, spontaneous polarization transfer from hydrogen atoms to nitrogen is existed 5]. The results of HF- SABRE experiments with ^{15}N-3-FPy and [Ir(IMes)(COD)Cl] in CD_3OD showed that polarization transfer decreases with the presence of fluorine atoms in 3 times that can be explained by the fast relaxation of the molecules with fluorine (Figure 2).

Therefore, the enhancement factors in the experiments with 3-Fpy were insufficiently high for its MRI visualization.

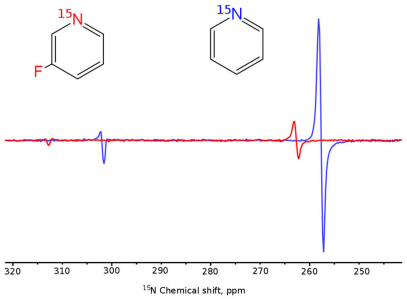

Figure 2. ^{15}N HF-SABRE NMR spectra acquired after bubbling of parahydrogen through the solution with ^{15}N-3-FPy (red) ^{15}N-Py (blue) and [Ir(IMes)(COD)Cl] catalyst in CD_3OD at 7.2 T

MRI of HF-SABRE hyperpolarized imidazole-$^{15}N_2$ and nicotinamide-^{15}N

In HF-SABRE experiments with solutions of imidazole-$^{15}N_2$ or nicotinamid-^{15}N (100 mM) and [Ir(IMes)(COD)Cl] catalyst (10 mM) in methanol-d_4 the gas mixture was 90%-enriched by parahydrogen and was bubbled through the solutions. Magnetic field was equal to 9.4 T. The resulted enhancement factors were equal to 120 and 100 for of imidazole-$^{15}N_2$ and nicotinamid-^{15}N respectively.

For MRI experiments Fast Low Angle SHot (FLASH) pulse sequence was used. It is standard pulse sequence on the Bruker's MRI scanners which allows to do MRI experiments antiphase peaks shapes. (Figure 3).

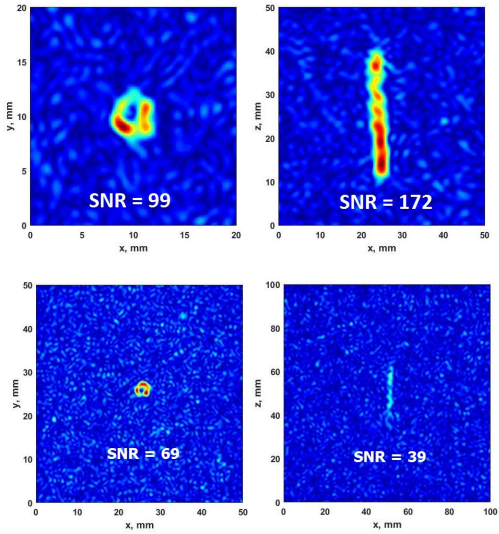

Figure 3. ^{15}N MRI of hyperpolarized imidazole-$^{15}N_2$ (top) and nicotinamide-^{15}N (bottom) using HF SABRE technique and FLASH pulse sequence (TE = 6 ms, number of acquisitions = 32). Parahydrogen was bubbled continuously through the solutions. Low signal at the center of the left images corresponds to the presence of capillary

Conclusion

SABRE and HF-SABRE approaches allow to increase intensity of NMR signal significantly. The presence of fluorine decreases amount of transferred polarization from hydrogen to nitrogen atoms in the experiments with 3-FPy. ^{15}N MRI of in situ hyperpolarized biomolecules was demonstrated with good spatial resolution.

Acknowledgements

This work was supported by grants from RFBR #(17-54-33037 OHKO_a, 16-03-00407-a).

References

1. C. R. Bowers, D. P. Weitekampю - *J. Am. Chem. Soc.*, 109, 5541–5542 (1987).
2. R. W. Adams, J. a Aguilar, K. D. Atkinson, M. J. Cowley, P. I. P. Elliott, S. B. Duckett, G. G. R. Green, I. G. Khazal, J. López-Serrano, D. C. Williamson. - *Science*, 323, 1708–1711 (2009).

3. D. A. Barskiy, K. V. Kovtunov, I. V. Koptyug, P. He, K. A Groome, Q. A. Best, F. Shi, B. M. Goodson, R. V. Shchepin, A. M. Coffey, K.W.Waddell, E. Y. Chekmenev. - *J. Am. Chem. Soc.,* 136, 3322–3325 (2014).
4. K. V Kovtunov, L. M. Kovtunova, M. E. Gemeinhardt, A. V Bukhtiyarov, J. Gesiorski, V. I. Bukhtiyarov, E. Y. Chekmenev, I. V Koptyug, B. Goodson. - *Angew. Chemie Int. Ed.,* 56, 10433 –10437 (2017).
5. K. D. Atkinson, M. J. Cowley, P. I. P Elliott, S. B. Duckett, G. G. R. Green, J. López-Serrano, A. C. Whitwood. - *J. Am. Chem. Soc.,* 131, 13362-13368 (2009).

^{7}Li diffusion in solid electrolytes as studied by NMR spectroscopy

Tatiana Zinkevich[1,2], Sylvio Indris[1], Helmut Ehrenberg[1]

[1]Institute for Advanced Materials – Energy Storage Systems, Karlsruhe Institute of Technology, Karlsruhe, Germany
[2]Electrochemical Energy Storage, Helmholtz-Institute Ulm, Germany
E-mail: tatiana.zinkevich@kit.edu

Introduction

All-solid-state batteries have recently attracted much attention due to the fact that, in contrast to dangerous and flammable liquid electrolytes, solid conducting materials can offer an increased stability and safety. In addition, such batteries might possess a higher energy density. All these features make them promising candidates for large-scale battery production.

One of the key challenges is the development of solid electrolytes, which could compete with liquid materials in terms of ionic conductivity. High conductivity is of great significance for the performance of a battery. Impedance spectroscopy is one direct way to measure conductivity, but sometimes obtaining reliable results with this method is somewhat difficult due to grain boundary and electrode contributions.

Another option is to use solid-state NMR spectroscopy, which provides several techniques to characterize Li-ion dynamics. Among these are the following:

– temperature-dependent relaxation time studies, which are sensitive to ns-μs mobility;

– the analysis of the heating-induced line narrowing appearing in static NMR spectra;

– self-diffusion coefficient measurements with magnetic field gradients, which are sensitive to the translational motions at distances of several μm.

The combination of these techniques provides a complete picture of ion mobility in Li-containing electrolytes.

In the current work we discuss the applicability of the above mentioned methods for the characterization of ion conducting properties of promising solid electrolytes.

Line narrowing effect

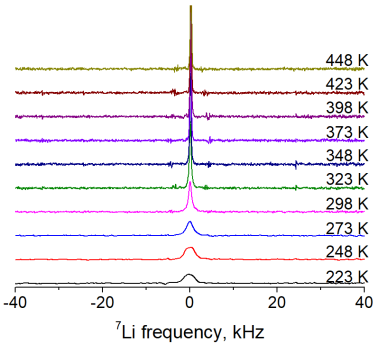

Figure 1. ^{7}Li NMR spectra at different temperatures for Li_6PS_5I.

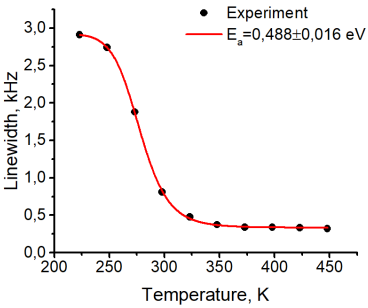

Figure 2. The linewidth of the central ^{7}Li signal as a function of temperature with fitting [1]

^{7}Li is a quadrupolar nucleus with a rather low quadrupolar coupling constant. Thus, its spectrum consists of the central signal and quadrupolar satellites on both sites of the central

line. Being influenced by the dipolar interaction, the central transition undergoes a motional narrowing effect in response to heating as can be seen from Figure 1 and 2.

Applying one of different possible approaches, e.g. the fitting procedure by Hendrickson-Bray [1] the activation energy of the motion can be roughly estimated.

$T_1/T_{1\rho}$ relaxation time measurements

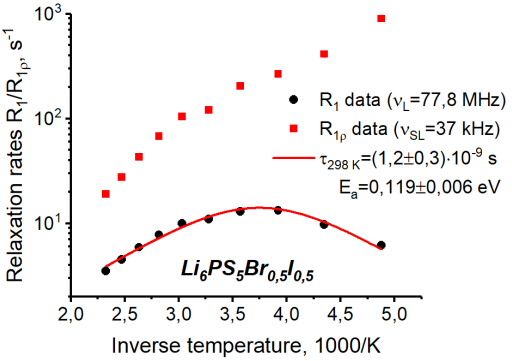

Figure 3. Relaxation rates as a function of temperature in $Li_6PS_5Br_{0,5}I_{0,5}$

Relaxation rates $R_1/R_{1\rho}$ are sensitive to motions occurring at the frequencies close to the Larmor frequency (ω_L) of the nucleus or to the frequency of the spin-lock field (ω_{SL}) as indicated by the equation:

$$R_1/R_{1\rho} = \frac{1}{T_1/T_{1\rho}} \sim \frac{\tau_C}{1+(\omega_{L/SL}\tau_C)^2}$$

where τ_C is the correlation time of the motion, which in the simplest case changes with temperature according to the Arrhenius low:

$$\tau_C = \tau_0 exp\left(\frac{E_a}{k_B T}\right)$$

where E_a is the activation energy of the process, T denotes temperature, and k_B the Boltzmann constant.

Therefore, by measuring the temperature dependence of the relaxation time, one can obtain the correlation time of the motion and its activation energy. An example of $R_1/R_{1\rho}$ temperature dependencies with fitting results is given in Figure 3.

Experimental data show the existence of the single motional process in the ns to µs timescale with an activation energy of 0.12 eV. The correlation time and the activation energy themselves do not provide useful information about the electrolyte's performance. One can convert these parameters into the diffusion coefficient D and the conductivity value σ by combining with X-ray diffraction data and applying the following equations:

$$D = \frac{l^2}{2d} K_{exchange}$$

$$\sigma = \frac{DNq^2}{k_B T}$$

where l is the average Li^+ jump length (l=2.46 Å), d is the dimensionality of motion, $K_{exchange}=1/\tau_C$, $N = n/V$ is the Li-ion density defined as the number of lithium ions per unit cell volume, q is the charge of the charge carriers, k_B denotes the Boltzmann constant and T the

temperature. For $Li_6PS_5Br_{0.5}I_{0.5}$, which is presented in Figure 3, the calculated parameters are D=2.8·10^{-12} m^2/s and σ=4.8 mS/cm.

Self-diffusion coefficient measurements

Pulsed-field gradient diffusion measurements have already proven to be a useful method to determine the speed of the translational motion in liquids. In solid samples the diffusion is generally much slower, and high gradients are required to track such movements. Moreover, the issues with short relaxation times may pose a problem when measuring the diffusion experiments.

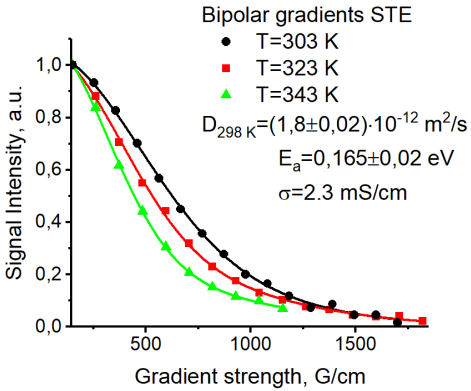

Figure 4. The results of the diffusion experiments carried out at different temperatures for $Li_{10}SnP_2S_{12}$

A stimulated-echo pulse sequence with bipolar gradients can help to overcome these difficulties and provides reliable results. Figure 4 demonstrates diffusion curves measured at different temperatures along with the fitting according to the standard Stejskal-Tanner equation.

As expected the diffusion process becomes faster with increasing temperature. Assuming an Arrhenius behavior, one can extract the activation energy of the motion.

The ionic conductivity was estimated from the Nernst-Einstein equation to be 2.3 mS/cm at room temperature, which is in a good agreement with earlier measurements by impedance spectroscopy.

The aim of the current work is to show how NMR spectroscopy can be used in characterization of the ion mobility in solid electrolytes. We optimized the set of the experiments in order to obtain a comprehensive and reliable dynamical picture. Other important details of these techniques will be given in the frame of my report.

References

1. Hendrickson J. R., Bray P. J. A phenomenological equation for NMR motional narrowing in solids. *J. Mag. Res.* 1969 9 (**3**), 341-357 (1973).

An estimate of the change in the spin-spin relaxation time of protons of living tissue upon its cooling

Aleksey N. Zolotov[1,2], Yuriy I. Neronov[1,2], Denis D. Kosenkov[1,2]

[1]Mendeleyev Institute for metrology, St. Petersburg, Moskovsky pr. 19, Russia
[2]Saint Petersburg National Research University of Information Technologies, Mechanics and Optics, St. Petersburg, Kronverkskiy pr. 49, Russia
E-mail: alexzolotov2014@gmail.com, wdenkosw@gmail.com, yineronov@mail.ru.

Introduction

The task of medical care is to detect such initial pathological abnormalities in the human body, which may turn into significant violations of functioning of living tissues. In this regard, the development of such a public diagnostic devices is required, which will allow to form a digital portrait of physiological state of a person for the timely identification of irreversible changes.

Modern NMR tomogramphs with superconducting magnets are expensive devices. They allow one to clearly visualize the relative positioning of organs of a living organism. Contrast difference between neighboring organs is ensured, first of all, by the fact that different cellular structures of living tissues are characterized by spin relaxation times of T1 and T2,

In works [1-2] it was found that if the error in estimating T1 and T2 of living tissue is reduced to 1%, then these parameters themselves can have diagnostic value. The times of spin-spin relaxation are very sensitive to the average statistical concentration of paramagnetic centers, which, in particular, include: active forms of oxygen; enzymes of biochemical reactions having unpaired electron; various free radicals, metal atoms possessing paramagnetic properties, such as copper atoms, etc.

In this paper, we continue to investigate the diagnostic capabilities of a small tabletop device: pulsed NMR installation with a permanent magnet with a field of 0.13 T.

The device consumes less than 30 watts, has a compact design and can be controlled from a laptop.

Some results of the influence of external conditions on T2a and T2b

In this paper, the authors evaluated the effect of physical stress on the hand of the participant in the experiment before recording T2a and T2b. It turned out that, as a rule, the moderate physical load is almost not reflected in the average results, but there was a greater dispersion of the data. It was assumed that the parameters T2a and T2b may depend on the variation of the oxygen content in the air. To test this assumption, an experiment was performed, in which the participant inhaled an oxygen-enriched mixture (90% oxygen and 10% nitrogen). However, the parameters T2a and T2b did not show any significant deviations. Further, the influence of the increased content of negative ions in the air (the effect of the Chizhevsky lamp) was verified. For several hours of conducting the experiment, the method of recording T2a, T2b used by us did not reveal any appreciable abnormalities.

A significant decrease in the parameters T2a, T2b (by ≈10%) was recorded on cooling. For this, the participant of the experiment put the palm into the water with snow for 1 minute (Fig. 1, left part). With a similar cooling of the ampoule with vegetable oil (Figure 1, right side) the parameters T2a and T2b decreased by 35% and by 16%. We can see that for vegetable oil there is a different dependence for T2a and T2b when the temperature regime is restored. These parameters belong to different groups of protons.

By such a comparison (Fig. 1), one can evaluate the resistance of living tissue to the effects of cold.

A similar decrease in T2a and T2b (by 13 and 8%, respectively) was detected earlier in work [1] as a deviation from the norm due to fourfold application of a typical blood pressure measuring device in the sequential determination of the arterial pressure of the participant's hand. At the same time, it remains unclear, whether the use of a tonometer slows down metabolic processes or a decrease in T2a and T2b is the consequence of slagging of cellular structures due to the restriction of blood supply.

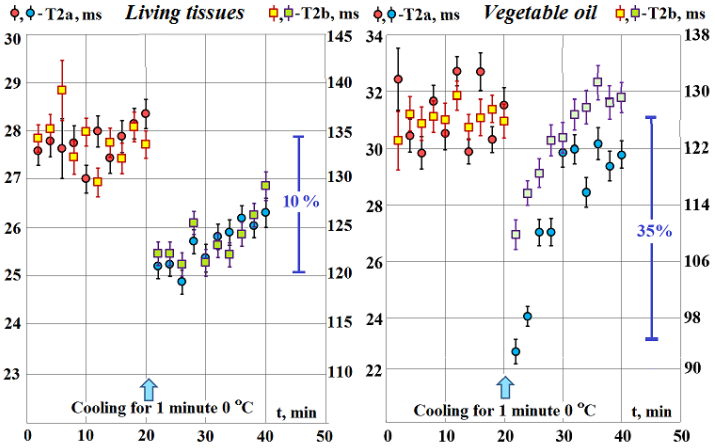

Figure 1. Comparison of T2a and T2b data for living tissues and ampoules with vegetable oil, recorded at room temperature (t = 20 °C) and after cooling (1 minute at 0 °C)

We noticed that the cooling is manifested in different ways on the data of T2a and T2b for different participants in the experiment. In Fig. 2 shows the results for T2a and T2b, which show a wide spread of data. These data can indicate that in this case, the manifestation of periodic oscillations for T2a is possible.

The metabolism in living tissues often occurs in an autooscillatory mode. Self-oscillatory regimes of chemical reactions underlie such important processes as cardiac contractions, respiration, diurnal activity rhythms, etc. In such regimes, the concentrations of certain metabolites change periodically.

Moreover, if a periodic change in metabolites is associated with a change in the average concentration of paramagnetic centers, periodic changes in the spin-spin proton relaxation times should be observed.

However, in general, preliminary experiments conducted by us show that for a healthy participant in the experiment, the T2a, T2b data characterize a certain level of metabolic activity of living tissues, which has a sufficiently high resistance to external conditions.

The data obtained are already sufficient to state: a more thoroughly made equipment of such a relaxometer can provide more accurate results, which can be very effective for diagnosis of the state of living tissues.

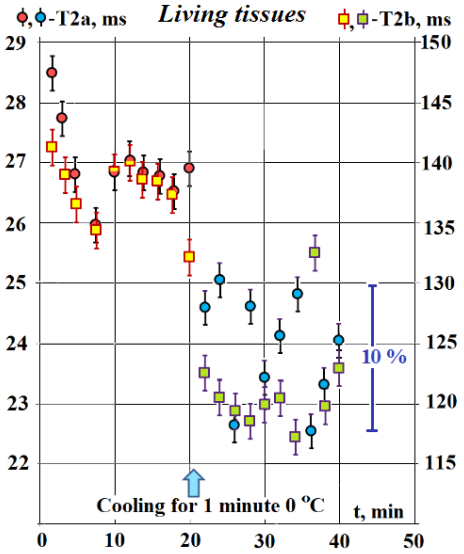

Figure 2. Results of the determination of the parameters T2a and T2b for one of the participants in the experiment. The data for the average office worker status and the data after cooling his palm for 1 minute at 0 ° C are presented. After cooling, the results for T2a show a dependence characteristic of periodic cycles

References

1. Y. I. Neronov, A. N. Seregin. Mini-MRI scanner and some possibilities for its use for studying living tissues – *Measurement techniques,* T. 54, № 1, 103-107 (2011)
2. D. D. Kosenkov, Y. I. Neronov, A. N. Zolotov, N.N. Seregin. NMR relaxometer for the estimation of the spin-spin proton relaxation time of the living tissue – *International Youth School-Conference; Magnetic Resonance and Its Applications, April 1–6 (2018); Saint-Petersburg, Russia; Book of abstracts Spinus-2018.*

Global Spectrum Deconvolution and its applications in NMR spectroscopy

Vadim Zorin[1], Felipe Seoane[1], Mike Bernstein[1], Stanislav Sykora[2], Carlos Cobas[1]

[1]Mestrelab Research, Santiago de Compostela, Spain
[2]Extra Byte, Castano Primo (Mi), Italy
E-mail: vadim@mestrelab.com
http://www.mestrelab.com

Mnova is a multivendor software suite designed for processing and analysis of NMR and LC/GC/MS data. Its multiplatform and plugin-based architecture provides high level of automation, expendability and easy-of-use.

Global Spectrum Deconvolution (**GSD**) is a technique for an automatic peak analysis of NMR spectra [1]. GSD analyses frequency-domain NMR spectra and produces a highly accurate list of NMR peaks with refined peak parameters including position, amplitude, linewidth and shape. GSD has been at the core of Mnova data analysis for many years, and has proved to be highly reliable and fast. It is widely used in Mnova as a preparation step for many advanced analysis routines.

Several well-established applications of GSD for NMR analysis will be discussed including NMR peak autoclassification, multiplet analysis, automatic assignments, automatic structure verification.

Recently we proposed a new technique of "quantitative GSD": **qGSD**. It is based on careful analysis of the residuals after GSD processing, and correcting GSD lineshapes in a way which minimizes the residuals. We will show that for well-resolved spectral lines qGSD can offer quantitation precision which is significantly improved over conventional GSD, and approaches or meets the precision of the classical sum integration. At the same time, the technique also provides a good quality quantitative analysis of the lines within overlapped regions.

References

1. Schoenberger, T.; Menges, S.; Bernstein, M. A.; Pérez, M.; Seoane, F.; Sýkora, S.; Cobas - *C. Anal. Chem.* 88 (7), 3836–3843 (2016).

Poster Session

Influence of polysaccharide shell on magnetic resonance relaxation and colloidal stability of SPIONs nanosuspension

Angelina A. Agureeva[1], Inessa A. Fagradyan[1], Pavel P. Shirinkin[2], Svetlana A. Zubkova[2], Aleksandra A. Efimova[3], Yaroslav Yu. Marchenko[4]

[1]Faculty of Chemical and Biotechnology, St. State Institute of Technology (Technical University), Russian Federation
[2]Faculty of Electronics, St. Petersburg Electrotechnical University "LETI", Russian Federation
[3]Faculty of Physics, St. Petersburg State University, Russian Federation
[4]Laboratory of Medical Nanotechnology, Federal State Unitary Enterprise "State Research Institute of Highly Pure Biopreparations", Russian Federation
E-mail: agurangelina@mail.ru

Introduction

Superparamagnetic Iron Oxide Nanoparticles (SPIONs) are widely used for biomedical applications. It is necessary, that SPIONs are compatible with tissues of the body and have the ability to conjugate bioligands for targeted delivery. For this aim nanoparticles of Fe_3O_4 are coated with a biocompatible polysacharide polymers.

In this work, the magnetic nanoparticles (MNPs) were synthesized as magnetite nanocrystals. The obtained MNPs were covered with three organic polymers: chitosan, dextran and carboxydextran. Their stability at the magnetic field was investigated and possibility to use as a contrast agent was estimated.

Methods and results

The MNPs were synthesized with chemical co-precipitation method and were coated with chitosan (100 kDa, Sigma), dextran (9-11 kDa, Serva) and carboxydextran (10-20 kDa, Sigma). The iron oxide suspensions were treated by ultrasound at 22 kHz [1].

To assess the aggregate stability of the suspensions at magnetic field, the spin-spin relaxation times T_2 were continuously monitored at various times. The relaxation times were measured with Bruker spectrometer CXP-300 at frequency 300 MHz in the cylindrical ampoule (diameter 5 mm) at room temperature. Polymer coated SPIONs had high colloidal stability at concentration 0.02 mM[Fe]/l (Fig.1).

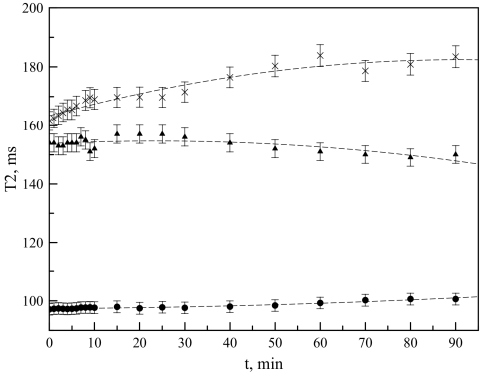

Figure 1. The dependence of relaxation time T_2 on the exibition time in a homogeneous magnetic field of spectrometer (circle - dextran, cross - carboxydextran, triangle – chitosan)

At such concentration optimal conditions of solution for switching assay are fulfilled [2]. Moreover, the experiments at concentrations 0.2, 2 mM[Fe]/l had proved that the resulting nanosuspensions were stable at homogeneous magnetic field.

During the aggregation, there is a change in T_2 (decrease) and in the case of precipitating of the large aggregates from the detection zone, the relaxation time T_2 tends to the one of the solvent (Fig.2).

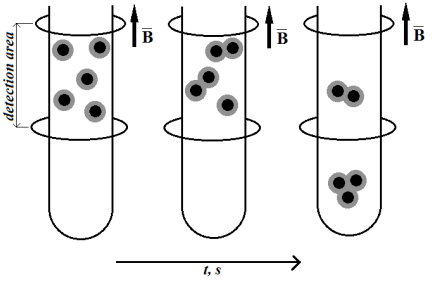

Figure 2. The schematic view of MNPs clusters formation

The coefficients of magnetic relaxivity were estimated from concentration dependences of relaxation times T_1,T_2, T_2^* and calculated by the formula:

$$R_i = r_i \cdot C + A,$$

where $R_i = 1/T_i$ (for T_1, T_2, T_2^*) [s^{-1}], r_i - the coefficients of magnetic relaxivity [l/(mM·s)], C – concentration of ferrum in solution [mM/l], A – const.

The results are shown in the Table 1. The dependences of the magnetic relaxation rate of protons R_2 and R_2^* on the concentration of iron in the solution for all samples are presented in the Fig. 3.

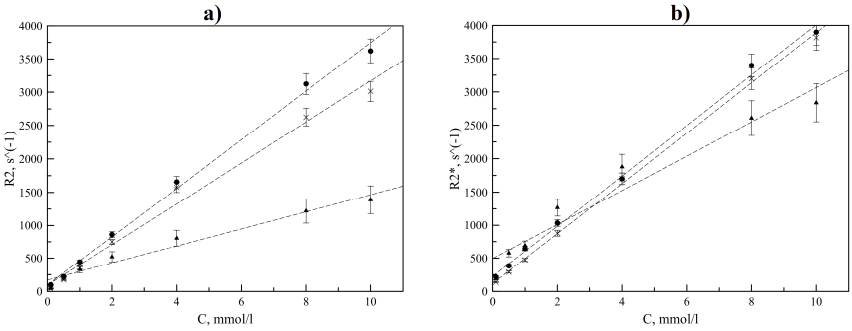

Figure 3. The dependences of the magnetic relaxation rate of protons R_2 (a) and R_2^* (b) on the iron concentration in solution
(circle - dextran, cross - carboxydextran, triangle – chitosan)

For measuring relaxation times were used the standard impulse sequences (one-pulse sequences, inversion recovery and CPMG). The magnetic precession decays were recorded at different exposure times in magnetic field 7.1 T of spectrometer.

Table 1. Relaxivity

Shell	r_1, l/(mM·s)	r_2, l/(mM·s)	r_2^*, l/(mM·s)
Chitosan	0.7	130	257
Dextran	1.2	365	378
Carboxydextran	0.7	308	377

Conclusion

The obtained samples of polymer coated SPIONs had the properties of negative contrast agents and can be used in MRI studies as biomarkers added to the MNPs suspension in switching assay technique.

Acknowledgements

We are grateful for help in experimental work to L. Y. Yakovleva, I. N. Voevodina and B. P. Nikolaev.

References

1. B. P. Nikolaev, L. Y. Yakovleva, Ya. Y. Marchenko. Superparamagnetic iron oxide nanoparticles conjugated with epidermal growth factor (SPION–EGF) for targeting brain tumors// International Journal of Nanomedicine. – 9, 273-287 (2014).
2. Parr M. et al. Switching assay as a novel approach for specific antigen-antibody interaction analysis using magnetic nanoparticles //Journal of Physics: Conference Series. – IOP Publishing, 2016. – Т. 741. – №. 1. – С. 012062.

Structure-dissolution relationships in Co(II)-containing phosphate glasses

Dahiana Avila[1], Delia Brauer[1]

Otto Schott Institute of Materials Research, Friedrich Schiller University, Fraunhoferstr. 6, 07743 Jena, Germany
E-mail: dahiana.avila@uni-jena.de
http://www.brauergroup.uni-jena.de/

Introduction

The homogeneity of the doping of a paramagnetic species into a diamagnetic host can be assessed through quantitative NMR according to a model function[1] that correlates the molar fraction of the paramagnetic dopant x_{para} with the respective fraction of target "visible" nuclei $f_{visible}$ as follows:

$$f_{visible} = exp[-k_1 \cdot x_{para}^{k_2}] \quad (1)$$

where the constants k_1 and k_2 are fitting parameters and $f_{visible}$ is defined by

$$f_{visible} = \frac{A_{doped}/n_{doped}}{A_{non-doped}/n_{non-doped}} \quad (2)$$

where A and n are the peak area and the number of moles of the respective doped and non-doped samples. This is nothing else than the relative area normalized by using the non-doped sample as reference. The model assumes that the target nuclei inside the wipe-out radius r_0 will not contribute to the NMR signal due to the broadening and shift caused by paramagnetic effects. Thus, A_{doped} corresponds to the area under the peak that remains at the same position as the non-doped sample. In case of uniform distribution of the paramagnetic dopant in the system, the decay of the NMR signal should follow Eq. 1 and at certain concentration, $f_{visible}$ should vanish completely meaning that all target nuclei are under the influence of paramagnetic centers.

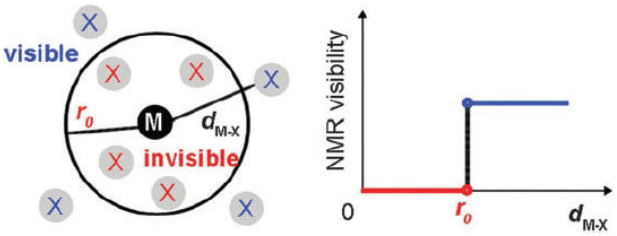

Figure 1. Scheme of the influence sphere model, where M is the paramagnetic ion and X the NMR active nuclei[1]

Co(II)-containing phosphate glasses

Phosphate glasses have the potential to be used as controlled release materials in medicine, e.g. for bone and wound healing, as their solubility can be tailored over a wide range by varying their composition. Cobalt ions have recently attracted interest as they promote blood vessel formation (angiogenesis) and show some antibacterial efficacy. Upon implantation, the cobalt-containing glasses would degrade at a certain rate, thereby releasing cobalt ions into the

body. The great advantage of ions locally released from an implant (rather than from e.g. orally administered medication) is that they are released exactly at the location where they are needed which results in an optimized therapeutic effect and minimized side effects.

In the present work, structural analysis by P-31 MAS NMR of a glass system before and after aqueous immersion was combined with dissolution kinetics in Tris buffer (0.025M, pH 7.4) through time-dependent P-31 NMR, pH and ICP-OES measurements, in an attempt to better our understanding of how glass composition, structure and dissolution behavior are interconnected for the system $45P_2O_5$-(30-*x*)CaO-$25Na_2O$-*x*CoO (*x*: 0.5 to 5 mol%).

Results

Homogeneity of doping

According to P-31 MAS NMR, all glasses were composed of pyrophosphate Q^1 and metaphosphate Q^2 species with chains from 8 to 9 phosphate groups in length. Moreover, MAS NMR was also used to assess the doping homogeneity of Co^{2+} into the phosphate glass via a novel method based on NMR[1], which correlates paramagnet effects on the NMR spectra with random distribution of paramagnet species into the diamagnetic glass (Fig. 2).

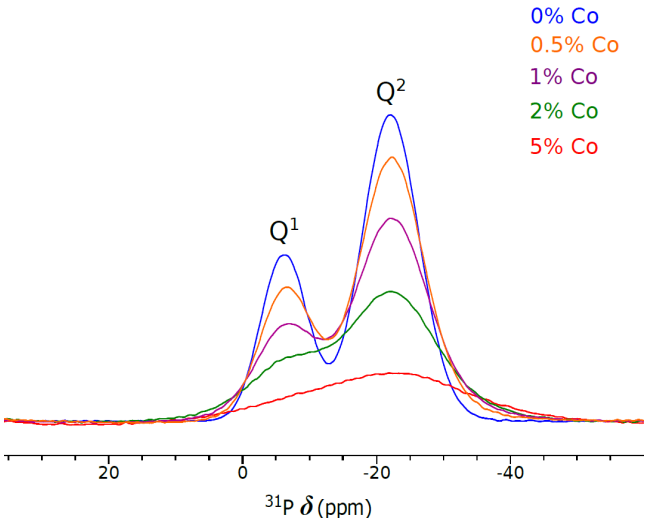

Figure 2. Stack plot of ^{31}P MAS NMR spectra of the phosphate glass system at 12.5 kHz

Complexes between Co^{2+} and phosphate fragments in solution

Dissolution experiments showed congruent dissolution with the rate of degradation decreasing with increasing CoO content. They also evidenced the average result of two competing reactions, thus ion exchange and hydrolysis of polyphosphates, being the CoO content proportional to relative more acidic pH values at early time periods. This was consistent with P-31 solution NMR findings, which through paramagnet effects indicated that the presence of CoO trapped in complexes (Fig. 3), led to hydrolytic degradation of long-chain phosphates into trimetaphosphate.

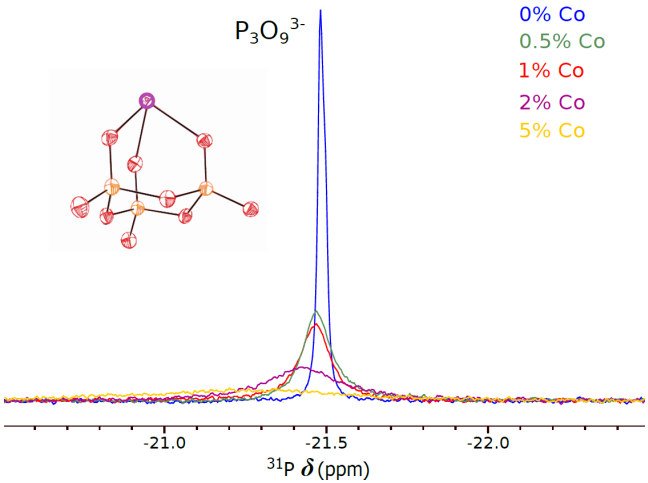

Figure 3. Stack plot of ^{31}P NMR spectra of $P_3O_9^{3-}$ after 7 days of glass immersion in Tris

Glass after aqueous immersion

According to P-31 MAS NMR, the precipitates obtained after 14 days of glass immersion in Tris buffer solution (0.025M) were composed mainly by amorphous orthophosphate Q^1 with minor amounts of Q^0 and Q^2 species, the later decreased with increasing CoO content.

Acknowledgements

I would like to thank Nuttawan Sawangboon[1] and Wolfram Hartramph[1] for producing the glass system and carrying out the dissolution experiments.

References

1. Li, W.; Celinski, V. R.; Weber, J.; Kunkel, N.; Kohlmann, H.; Schmedt auf der Günne, J. Homogeneity of Doping with Paramagnetic Ions by NMR. *Phys. Chem. Chem. Phys.* **2016**.

Molecular dynamics simulations of alkylammonium nitrate ionic liquids. The effect of nitrate-anion model parameters

Vsevolod V. Beshanov, Andrei V. Egorov

Faculty of Physics, Saint Petersburg State University, Russia
E-mail: serevarno@mail.ru

Introduction

Alkylammonium nitrate ionic liquids (ILs) have been extensively studied in the recent years for both fundamental and technological reasons. Nevertheless, several important aspects of the ions solvation and transport still remain unclear. ILs can be effectively modeled via molecular dynamics (MD) simulations, capable to provide molecular-level description of any liquid system. However, MD simulations are based on man-made potentials describing the interactions between the molecules and the key part of any modeling is the choice of models employed. The present study is focused on the performance of nitrate-anion models proposed for aqueous nitrate solutions to describe alkylammonium nitrate ILs.

Simulation details and results

Three alkylammonium nitrate ILs: ethyl-, propyl-, and butylammonium nitrate, were considered. In each case, a system of 300 nitrate and 300 alkylammonium ions in cubic cell with periodic boundary conditions was simulated in the *NPT* ensemble at 298 K and atmospheric pressure using the *MDynaMix* package [1]. The alkylammonium cations were modeled using the potentials described in Refs. [2-4]. Model nitrate anion was treated as a 4-site planar structure with a central nitrogen atom and three oxygen atoms at a distance of 1.22 Å with all O-N-O angles of 120° [5]. Intermolecular interactions were described as the sum of Coulomb and Lennard-Jones (6-12) potentials. Three different potential parameters sets, taken from Refs. [6-8], were considered.

The effect of nitrate-anion model parameters on the structural and dynamical properties of alkylammonium nitrate ILs we studied in details. A special attention was given to the peculiarities of nitrate-anion local solvation.

Acknowledgements

This work was supported by the Russian Foundation for Basic Research (grant 17-03-00057a).

References

1. A. P. Lyubartsev, A. Laaksonen. − *Comp. Phys. Comm.*, **128**, 565-589 (2000).
2. T. Mendez-Morales, J. Carrete, O. Cabeza, et al. – *J. Phys. Chem. B*, **118**, 761-770 (2014).
3. V. Gomez-Gonzalez, B. Docampo-Alvarez, O. Cabeza, et al. – *J. Chem. Phys.*, **143**, 124507 (2015).
4. T. Mendez-Morales, J. Carrete, J. R. Rodriguez, et al. − *Phys. Chem. Chem. Phys.*, **17**, 5298-5307 (2015).
5. C. Ebner, R. Sansone, S. Hengrasmee, M. Probst. − *Int. J. Quant. Chem.*, **75**, 805-814 (1999).
6. T. Megyes, S. Balint. − *J. Phys. Chem. B*, **113**, 4054-4064 (2009).
7. Y. Umebayashi, W.-L. Chung, T. Mitsugi, et al. – *J. Comput. Chem. Jpn.*, **7**, 125-134 (2008).
8. A. Laaksonen, H. Kovach. – *Can. J. Chem.*, **72**, 2278-2285 (1994).

55 Years of EPR laboratory at St.-Petersburg Electrotechnical University "LETI"

Yu. V. Bogachev, M. N. Knyazev, A. V. Nikitina

Department of Physics, Saint-Petersburg Electrotechnical University "LETI",
5, prof. Popov st., Saint-Petersburg, 197376, Russia
E-mail: Yu.Bogachev@mail.ru

The laboratory of electron paramagnetic resonance (EPR) at the Department of Physics of the St.-Petersburg Electrotechnical Institute "LETI" appeared in 1962 as the result of reorganization of the previously existing radiotechnical laboratory.

The main directions of scientific work of the EPR laboratory in 60-ies was:

- spin resonance and its application to the study of properties of substances and materials,
- scientific equipment developing and producing.

The tasks that were solved in the EPR applications area, were mostly oriented on studying of radiation defects in technically important materials – single crystals of oxides and radio ceramics. The role of defects in the processes of aging and polarization of dielectric materials was clarified. Defects that occur in transparent dielectrics were investigated under the influence of laser irradiation, including irradiation with a giant pulse with an energy of 0.3 J. A theory of electron autoemission in oxides was developed. Also the EPR study of the nature of color centers in quartz minerals and quartz products had an important value for geophysics and radio electronics.

EPR spectrometers working at 10^{10} and 10^{8} Hz frequencies were developed.

X-band EPR spectrometer (Fig.1) with HF-modulation had a sensitivity of 10^{11} spin / G and resolution of few mG.

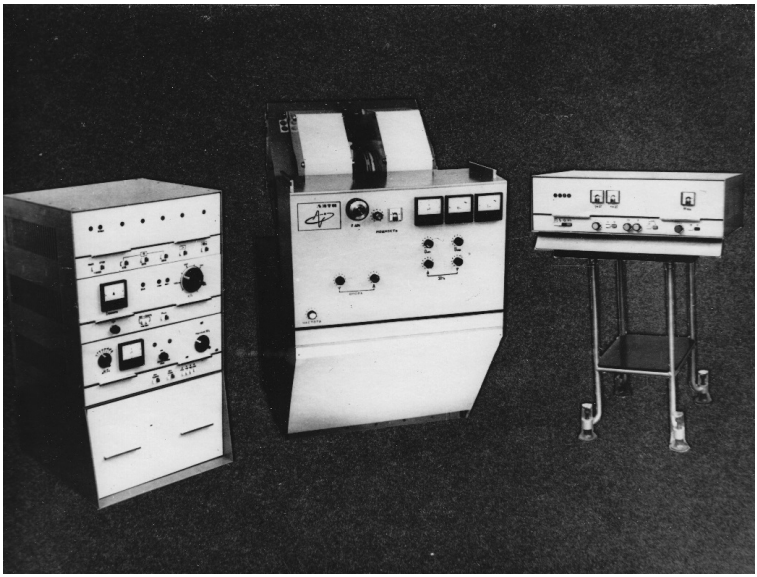

Figure 1. X-band EPR spectrometer "LETI" in 60-ies

Induction method for registration of EPR signals with the use of the balanced resonator excited by two mutually orthogonal modes was developed. This method made possible to observe resonance in rotating fields, determine the sign of the spin transitions, and study the behavior of the spin system under the action of fields of two different frequencies.

A helium cryostat for EPR studies up to 4 K was created.

The low-field EPR spectrometer operated in 10 – 100 MHz frequencies band, was developed and used primarily for studies of substances with large dielectric losses at high frequencies.

Further development of the EPR laboratory in LETI has been associated with the development of compact module EPR equipment, which can be characterized by good performance at compact size, low weight and minimized costs. This equipment can be used in research, in analytical applications and for educational process. This device with open architecture could be useful for example for mobile laboratories carrying out technological control, medical diagnostics analysis and ecological monitoring.

We developed a new compact EPR equipment [1], [2]. The original EPR instrumentation (Fig. 2) consist of electromagnet, EPR cavity (TE 102 type), EPR microwave unit, EPR signal control and recording unit and power supply unit. Maximum EPR ampoule diameter (11 mm) in the microwave cavity of EPR spectrometer allow to use the finger dewar for the nitrogen temperature measurements. We have also developed compact digital temperature control unit for 100~400 K range.

Figure 2. Compact EPR equipment

Specifications of compact EPR equipment are presented in Table 1.

Table 1 Specifications of compact ESR equipment

Parameter	**Value**
ESR sensitivity	$2x10^{10}$ spin/(10^{-4} T)
ESR operating frequency	9.0~9.6 GHz
Maximum microwave power	0.15 W
Induction of magnetic field	0.05~0.7 T
Maximum ESR ampoule diameter	11 mm

Together with the researchers from various scientific centers of Russia and other countries, specialized compact EPR equipment has been successfully tested for solving the following problems [3-5]:

- investigation of the behavior of paramagnetic ions of transition metals (Mn^{2+}, Fe^{3+}, Cu^{2+}, Cr^{3+}) in aqueous and aqueous-acid matrices in liquid and frozen states;
- determination of photo-oxidizable impurities (metals with variable valence V^{2+}, Cr^{2+},Fe^{2+} and others, aromatic compounds – benzene, hydro-xenon, oil products) in water solutions;
- determination of isotopic composition, deuterium concentration in natural waters;
- evaluation of traces of non-paramagnetic metals of different groups (Ag, Pb, Cd, Hg, Pb and others) in solutions by the extraction radiospectroscopy analysis;
- monitoring of spin-labeled waters pumped into oil wells to increase the oil output;
- determination of vanadium (IV) and free radicals contents in oil and oil products;
- control of quantum haemotherapeutics methods such as ultraviolet and laser blood irradiation and millimeter wave irradiation of nonthermal action;
- determination of membrane states and the peculiarities of thrombocyte lipid peroxidation by spin-labeling method for patients with unstable stenocardia;
- investigation of the antioxidant system of blood protection at different forms of stresses (immobilized, infectional, operational);
- control over the antioxidant applications in case of different infections;
- detection of nitric oxide (NO) radicals in animal cells and tissues, specifically in cardio-vascular and central nervous system, alimentary canal, immune and reproductive system;
- study of new spin labels, probes and traps (imidazoline and imidazolidine nitroxides) in molecular biology and medicine (as spin pH-sensitive probes for measurement of local pH-values inside various cells and tissues, as a contrast enhancers in NMR-Tomography);
- ecologic monitoring of spin-labeled sewage;
- evaluation of retrospective doses of radiation in EPR-biodosimetry using the measure of EPR signal of dental enamel;
- separation of magnetically anisotropic and isotropic spin interactions by the orientationally modulated EPR method in solids.

Technical features and possibilities of our compact EPR equipment have been tested in the international intercomparison trial on “self-calibrated” EPR dosimeters [5]. Experimental data obtained not only on our instrumentation (model EPR-10-Mini) but also on EPR spectrometers of other manufactures at the same measurement conditions give evidence of high performance of our compact EPR spectrometer.

One of the significant applications of our compact EPR spectrometer is it’s usage in the synthetic rubber industry for the EPR control in the technological process of isoprene polymerization catalyst preparation [3].

The obtained dependencies between the variation of EPR spectra parameters and the component ratios, the temperature and the catalyst preparation time, permitted to develop and implement the automated system of the EPR control in the technological process of the isoprene polymerization catalyst producing. The described system has been realized under continuous dynamic operating technological conditions in the synthetic rubber industry, it is based on compact ESR analyzers equipped with a specialized microprocessor system developed in EPR laboratory “LETI”.

Automated EPR analyzers are successfully used from 1979 at six large factories producing synthetic rubber (polyisoprene) in Russia.

References

1. Bogachev Yu.V., Drapkin V.Z., Knyazev M.N., Chernenko Yu.S. Compact problem-oriented EPR equipment. (Rus.). [J]. Izvestia SPbSETU "LETI", Russia, 2009, 7: 12-22.
2. http://www.resonance-m.com
3. Bogachev Yu.V., Drapkin V.Z., Knyazev M.N., Kuzmina N.N., Chernenko Yu.S. EPR and ENDOR investigations of isoprene polymerization catalysts. The EPR application in synthetic rubber industry. (Rus.). [J]. Izvestia SPbSETU "LETI", Russia, 2009, 3: 9-14.
4. Bogachev Yu.V., Drapkin V.Z., Knyazev M.N., Mamikin A.I., Serdyuk A.S., Frolov V.V., Chernenko Yu.S.. Magnetic resonance. Basics and applications (Rus.). [M]. Saint-Petersburg, SPbSETU "LETI", Russia, 2009: 1 - 240.
5. Gancheva V., Yordanov N. D., Callens F., Vanhaelevyn G., Raffi J., Onori S., Malinen E., Sagstuen E., Fabisiak S., Peimel-Stuglik Z. International intercomparison trial on "self-calibrated" dosimeters. [J]. Radiat. Phys. Chem., 2008, 77: 357 – 364.

Investigation of MRI contrast efficiency and aggregation stability of magnetic nanoparticles by NMR-relaxometry

Yu. V. Bogachev[1], A. A. Kostina[1], A. V. Nikitina[1], V. A. Sabitova[1], Ya. Yu. Marchenko[2], B. P. Nikolaev[2]

[1]Department of Physics, Saint-Petersburg Electrotechnical University "LETI", 5, prof. Popov st., Saint-Petersburg, 197376, Russia,
[2]State Research Institute of Highly Pure Biopreparations, 7, Pudojskaia st., 197110, Saint-Petersburg, Russia
E-mail: nastya_nikitina1996@mail.ru

Introduction

At present, multifunctional magnetic nanoparticles (MNPs) are finding increasing applications in medicine for theranostics [1-3]. For this purpose, they must have certain magnetic characteristics, to be stable (have a low aggregation capacity), biocompatible, nontoxic, flexible and have a high magnetic resonance (MR) relaxation efficiency.

The aim of this work is the analysis and summarizing our experimental results of MR studies of composite MNPs to determine their aggregation stability and relaxation efficiency in aqueous solutions.

Experimental methods

NMR measurements in a magnetic field of 7.1 T were performed on the NMR spectrometer CXP-300 (Bruker, Germany) for the resonant frequency of protons of 300 MHz. All measurements were carried out at room temperature in standard glass ampoules 5 mm in diameter without rotation.

NMR measurements in a magnetic field of 0.33 T were performed on the NMR relaxometer (Spin Track, Russia) for the resonant frequency of protons of 14 MHz. To measure the time of spin-lattice relaxation T_1 pulse sequence "inversion-recovery" was used 180°-τ-90°(90° pulse of 2.6 μs; the duration of the 180° pulse of 5.2 μs). To measure the time of the spin-spin relaxation T_2 pulse sequence used is the Carr-Purcell-Meiboom-Gill (CPMG) (90° pulse of 2.6 μs; the duration of the 180° pulse of 5.2 μs).

NMR measurements of T_1 and T_2 relaxation times were carried out for the following samples of magnetic nanoparticles:

1) superparamagnetic iron oxide nanoparticles in model media: in distilled water, in 2% agar-agar gel, in an aqueous solution of albumin (50 g / l);
2) magnetic nanoparticles based on iron oxide in the shell of dextran conjugated with some proteins (EGF – Epidermal Growth Factor and HSP70 - Heat Shock Protein);
3) standard sample of MNPs fluid MAG-DX 4104 (Chemicell, Germany).

Results and discussion

Graphs of longitudinal $R1$ and transverse $R2$, $R2^*$ nuclear magnetic relaxation rates of water protons on the concentration of magnetic nanoparticles (C) obtained in accordance with the experimental results of the NMR relaxation measurements presented in Fig. 1 (a, b), and 2 (a). For most samples studied graphic dependences $R_i(C)$ are linear and are described by the functions $R_i = r_i \cdot C + R_{0i}$, where C is the concentration of MNPs, R_{0i} is the constant determined by the relaxation rate of water protons in the absence of MNPs, r_i is the relaxation efficiency. For such samples the relaxation efficiency is defined as the tangent of the slope of the straight line $R_i(C)$ and has a constant value r_{si}. The dependence of $r_{s2}(C)$ for some investigated samples is given in Fig. 2 (b).

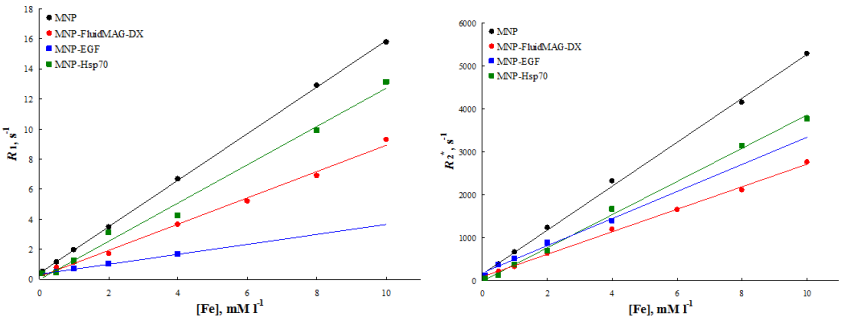

Figure. 1. The dependence of the longitudinal R_1(a) and the transverse R_2^* relaxation rate on the concentration of magnetic nanoparticles in a 7,1 T magnetic field

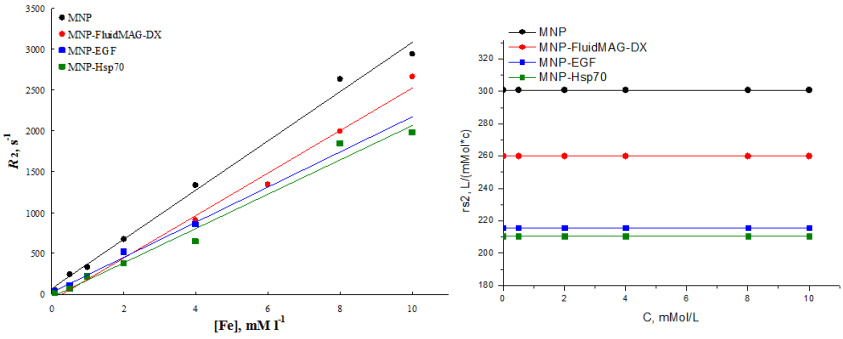

Figure. 2. The dependence of the transverse relaxation rate R2 (a) and the static relaxation efficiency r_{s2} (b) on the concentration of magnetic nanoparticles in 7,1 T magnetic field

The values of static relaxation efficiency for some investigated samples are shown in Table 1.

Table 1. Static relaxation efficiency

Sample	MNP	MNP-FluidMAG-DX	MNP-EGF	MNP-Hsp70
r_{s1}, L/(mMol*c)	1.55	0.87	0.33	1.27
r_{s2}, L/(mMol*c)	301	260	216	211

Higher values of the static relaxation efficiency correspond to a stronger negative MRI contrast abilities of this agent.

For some samples of MNPs the concentration dependence of the transverse relaxation rate of water protons R_2 (C) is non-linear (fig. 3, a). The analysis of this dependence shows a decrease in the relaxation efficiency with increasing MNPs concentration. The observed phenomenon was attributed to instability of these MNPs in aqueous solution and their ability to form clusters or aggregates when the MNPs concentration in the solution increases. This effect of MNPs aggregation was observed visually for these samples and increased with

increasing residence time of the sample in the magnetic field of the NMR relaxometer. Similar results were obtained earlier in the NMR relaxation study of protons in aqueous solutions of iron oxide MNPs with Si-C shell [4].

The aggregation of the nanoparticles affects the outer-sphere proton relaxation processes and as well as the diffusion of protons in the vicinity of magnetic centers, resulting in lower relaxation rates as compared to single magnetic nanoparticles.

In the case of nonlinear dependence R_2 (C) to determine the aggregation ability of the magnetic nanoparticles, rational to introduce the concept of dynamic relaxation efficiency, which can be found as the first derivative of a function at a given point of the curve R_2 (C), i.e. $r_{d2} = \frac{\partial R_2}{\partial C}$. The dependence of the dynamic relaxation efficiency of the concentration is non-linear (fig. 3, b) and allows to evaluate the aggregation stability of these magnetic nanoparticles.

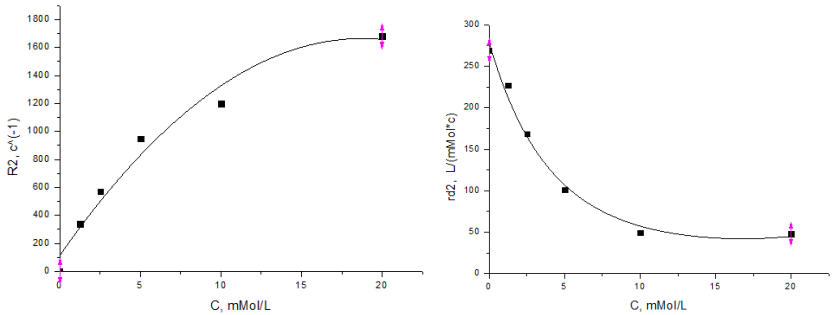

a) *b)*

Figure 3. The dependence of the transverse relaxation rate R2 (a) and the dynamic relaxation efficiency r_{d2} (b) on the concentration of magnetic nanoparticles in 0,33 T magnetic field

In this case we see that for small values of the concentration of MNPs the relaxation efficiency is much higher than for large concentrations.

Acknowledgements

Part of this work was supported by Ministry of Education and Science of the Russian Federation (project 3.6522.2017).

References

1. Jinhao Gao, Hongwey Gu, Bing Hu. Multifunctional Magnetic Nanoparticles: Design. Synthesis, and Biomedical Applications. // Accounts of chemical research, 2009, vol.42, No.8, pp.1097-1107.
2. Shao H., C Min, Issadore D., Min C., Liong M., Chung J., Weissleder R., Lee H. Magnetic Nanoparticles and microNMR for Diagnostic Applications. // Theranostics. – 2012. - Vol. 2(1). – P.55-65.
3. R. Thomas, In-Kyu Park, Yong Yeon Jeong. Magnetic Iron Oxide Nanoparticles for Multimodal Imaging and Therapy of Cancer. // Int.J.Mol.Sci. 2013, vol.14, pp.15910-15930.
4. Yu.V. Bogachev, Ju.S. Chernenko, K.G. Gareev, I.E. Kononova, L.B. Matyushkin, V.A. Moshnikov. S.S. Nalimova, Appl. Magn. Reson., 45, 329 (2014).

Fe/Ag bimetallic system supported on mordenites: EPR, NMR and Mössbauer study

Dmitrii Bogdanov[1], Perla Sánchez-Lopez[2], Jacek Gurgul[3], Kazimierz Łątka[4], Anna Shmyreva[1,5], Marina Shelyapina[1], Vitalii Petranovskii[2]

[1]Saint Petersburg State University, 7/9 Universitetskaya nab., St. Petersburg, Russia 199034
[2]CNyN, Universidad Nacional Autónoma de México, Ensenada 22860, Baja California, México
[3]Jerzy Haber Institute of Catalysis and Surface Chemistry, Polish Academy of Sciences, Niezapominajek 8, PL-30239 Krakow, Poland
[4]Institute of Physics, Jagiellonian University, Łojasiewicza 11, 30-348 Kraków, Poland
[5]Charles University, Ovocný trh 5, Prague 1, 116 36, Czech Republic
E-mail: d.bogdanov@spbu.ru

Fe/Ag bimetallic systems supported on zeolites have been the subject of intensive study [1-5]. Fe-Ag interaction affects catalytic [3], ferromagnetic [4], electronic [5] and many other properties of the host material. In some cases, the introduction of Fe leads to the ordering of Ag species in the zeolite matrix, which is highly important for the design of composite materials. In this contribution, we report on the result of our comprehensive study of the state of iron in monometallic and Fe/Ag bimetallic systems supported on mordenite.

Samples were prepared from sodium mordenite with a SiO_2/Al_2O_3 molar ratio of 13, supplied by Zeolist International. Silver and iron cations were introduced into the zeolite by ion exchange from aqueous solutions of $AgNO_3$ and $FeSO_4$. One of the purposes of this work was to characterize the created iron-containing species and to study how the component deposition order during the ion exchange processes (Fe after Ag or Ag after Fe) and/or reaction temperature (20 and 60 ^oC) affects the properties of the obtained materials.

In addition to the general characterization of the samples done by X-ray diffraction analysis, scanning electron microscopy, X-ray photoemission spectroscopy, thermal analysis, we used various spectroscopic methods sensitive to paramagnetic and ferro-/ferrimagnetic states of iron: electronic paramagnetic resonance (EPR), ^{57}Fe nuclear magnetic resonance (NMR) and ^{57}Fe Mössbauer spectroscopy.

All the methods used indicate that the iron ions in the studied mordenite samples are in the 3+ state. The Fe^{3+} ions are mainly in tetrahedral coordination and belong to three different species: Fe ions, which have entered into mordenite matrix substituting Al^{3+}; magnetically ordered species; free Fe^{3+} ions coordinated by water molecules. However, the distribution between these fractions strongly depends on the method of preparation.

Acknowledgements

The structural, elemental and EPR analyses were carried out at the Research Park of Saint Petersburg State University: Centre for X-ray Diffraction Studies, Interdisciplinary Resource Centre for Nanotechnology, Centre for Physical Methods of Surface Investigation, and Centre for Magnetic Resonance. This work was partially supported by DGAPA-UNAM IN107817 Grant.

References

1. S.G. Aspromonte, M.D. Mizrahi, F.A. Schneeberger, J.M. Ramallo López, A.V. Boix. J. Phys. Chem. C 117 (2013) 25433–25442.
2. Y. Ono, T. Baba. Phys. Chem. Chem. Phys. 17 (2015) 15637-15654.
3. D. Li, G. Yang, P. Li, J. Wang, P. Zhang. Catal. Today 277 (2016) 257–265.
4. R. Das, M. Gupta, S.K. Srivastava. J. Magn. Magn. Mat. 433 (2017) 162–168.
5. K. Ciesielski, G. Chajewski, M. Samsel–Czekala, A. Hackemer, A.P. Pikul, D. Kaczorowski. Solid State Commun. 257 (2017) 32–35.

Cuban MR Project

C. Cabal[1,2], A. Fernandez[1], M. Lores[1], E. Gonzalez[2], A. Bordelois[2], JC. Garcia[2], H. Sánchez[2]

[1]Medical Biophysics Center, University of Oriente,
[2]Faculty of Physics, Havana University, Cuba.
carlos.cabal@fisica.uh.cu

Introduction

Cuban´s experiences concerning to the calculation, design, construction and validation Magnetic Resonance (MR) technology are presented. Cuban MR Technology includes MR relaxometer, Magnetometers and MR imaging (MRI) whole body machines. The MR relaxometers and MRI systems were development in ending of the 80 ties and introduced in several Cuban's hospitals where were working during more than 15 years.

Cuban´s experiences concerning to quantitative MR associated with molecular, preclinical and clinical studies of significant diseases and the drug development are presented.

MR "in vitro" and "in vivo" studies of Sickle Cell disease (SCD) [1-4], the Diabetic Foot Ulcer (DFU) [5], the Brain Tumor Response (BTR) [6] and the Pharmacokinetics of Magnetic Nano Particles (MNP) [7], as example are presented. Furthermore, MR contributions to diagnostic and selection of therapeutic pathways are discuses.

MRI Cuban Machine

The Cuban´s MRI machine general view is presented in the figure 1. In this work is discussed the possibilities and restriction of the principal blocks and the improving and characterization process of these machines.

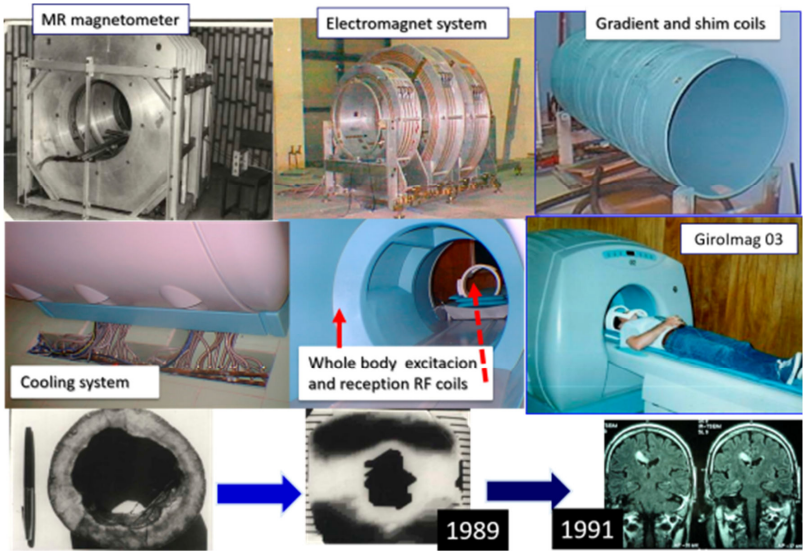

Figure 1

MR Relaxation and Electron Spin Resonances studies of SCD

SCD was the first molecular disease described. Due to the polymerization of hemoglobin S (HbS), the erythrocyte is deformed, the permeability and elasticity of the

membrane change, hemolysis is caused and rheology is modified, leading to painful vaso-occlusive crises [1, 4].

^{1}H T1 and T2 were determinate with the Cuban relaxometer at 4MHz using IR, Hahn and CPMG pulse sequences at 36 ºC and with an error <5%. The measurements were performer during 8 h of the spontaneous deoxygenation of blood sample of more than 80 patients [2, 3].

Typical T1 and T2 temporal behaviors in HbA and HbS samples are shown in fig 2A [2, 3]. The kinetic of deoxyHbS polymerization are characterized by 3 stages: initial (I), nucleation (II) and termination (III) (1-4). The initial phase is delimited by the Delay time (t_D) (9). After the t_D, an autocatalytic formation of polymers takes place (II). Once nucleation concludes, ^{1}H relaxation tend to stabilize (III). The different MR behavior in HbA and HbS solutions could be associated with the molecular mobility or the Hb magnetism variations (oxyHb: diamagnetic and deoxyHbS: paramagnetic) and the appearance of micro in homogeneities at the end of the polymerization process [2, 3].

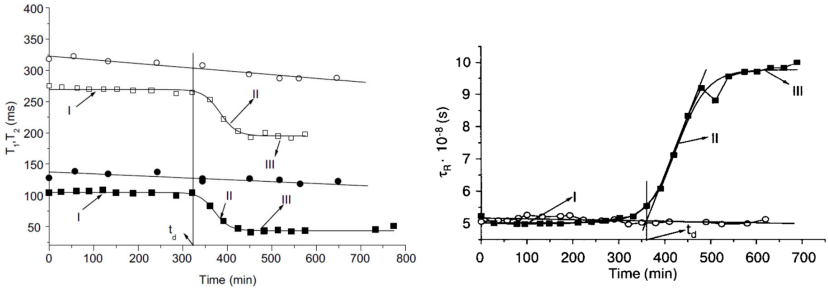

A *B*

Figure 2

From the T1, T2 and T1/T2 ratio values, in the regions I-III, can be concluded that $\tau_C \approx 4x10^{-8}s$. A more precise quantitative evaluation of τ_C variation was done by ESR. Figure 2B shows the temporal behavior of τ_R determinate by ESR [3]. It's a good agreement between the ^{1}H MR relaxation and ESR by the spin labeling method data.

The existing strong correlation between the MR parameters (T1, T2,τ_R , η_μ) with the t_D has been allowed to stablish a new diagnostic method for the differentiation between the Crises and Steady stages of the patients. Furthermore, this MR procedure made possible the discovery of the anti-sickling action of the Vanillin as a therapeutic drug [1-4].

MRI/MRS Quantitative Evaluation of Brain Tumor Response (BTR) and DFU response under treatment

MR quantitative information for the evaluation of the BTR and DFU during treatment has been firstly reported [5, 6]. The purpose of this investigation was to set up the methodologies necessary for the study of two complexes pathological scenario. All MRI and MRS were performed with a 1.5 T Symphony Master Class system (Siemens).

Specifics MRI pulse sequences (FSE, IR, STIR, FLAIR, DWI), with and without Contrast agents (CA), was optimized in order to obtain reproducible quantitative data, during the healing process [5, 6].

DFU response

A special device was created to be placed in the head RF coil in order to guarantee the reproducibility of the feet positioning. It was demonstrated that the RF coil parameters (Q and

B1 homogeneity) don't change. The device provides two affixed sets of external markers connected with internal anatomic markers as a foot position reference [5].

DFU lesion sizes (Area and volume), Edema volume, as well as Apparent Diffusion Coefficient (ADC), and metabolites changes, were determined by MRI/MRS during a clinical trial phase IV. Regardless of ADC complex dependence on tissue characteristics, if the measurements are performed under identical conditions (foot position, pulse sequence, slice orientation, etc.) we could hypothesize that ADC relative values changes, are connected to the tissue texture differences in the lesion. [5].

BTR

Fourteen pediatric patients were evaluated on MRI/MRS for >2 years [6]. "In vivo" T1, T2, and ADC maps, in the lesion and its surrounding was determinate in order to have a assessment of the relative changes of the Spectral Density function of MR relaxation process in the tumor region. This evaluation was done with and without the standard CA [6]. It was possible to define three different tumor volume related to different molecular mobility's. Furthermore, spectral amplitude ratios of NAA, Cho and Cr metabolites peaks has been determinates in the lesion and healthy areas located in the contra-lateral hemisphere.

The present MRI/MRS results are in perfect agreement with the clinical evaluation confirming the MR possibilities when a standardized robust protocol is used [6].

MNP. Pharmacokinetics (PK) by MR relaxation and MRI

MRI is a complementary technique to follow PK of MNP [7]. By successive MRI we studied the evolution of contrast in the liver and measured the absorption, residence time and excretion of MNP-PEG-$(NH_2)_2$ during a one month in Winstar rats. MNP solutions Relaxivities was determinate "in vitro" and "in vivo" by MR relaxation and MRI [7].

The best RF coils for the study of rats in 1,5T MRI clinical machine was selected calculating the SNR, CNR and NUI of phantom of two different RF coils: the Head and Flexible coil; being the flexible one better in in more than 25 %.

The measured intensities I_i were normalized to the background I_0 and the ratio $(I_i-I_0)/I_0$ was calculated as a time function after MNP injection (See figure 3). Two different areas of the liver was evaluated (red and blue lines) and one muscle area (pink line), taken as a control. The graphics have three regions. The first one with is associated with the entrance of the MNP in the liver: absorption period. The second can be attributed to the liver stationary state: residence. Finally the last region is connected to the excretion. The MNP PK parameters are reported [7].

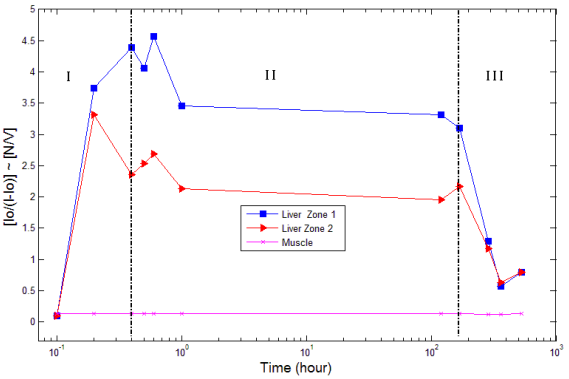

Figure 3

Acknowledgements

Authors express gratitude to Lora Hospital, and to the Medical-Surgical-Research Center, Cuba. Likewise thanks patients and coworkers related to these studies.

References

1. A. Fernández, C. Cabal, J. Losada, E. Alvarez, et al, *Hemoglobin*, **29**, pp.181-187 (2005).
2. M. Lores, C. Cabal. *Appl Magn Resonan*.; **28**, 1, pp. 1 – 6 (2005).
3. M. Lores, C. Cabal, O.R Nascimento, A.M Gennaro. *Appl Magn Resonan*, **30**, pp. 121- 128. (2006).
4. A. Fernandez; C. Cabal; M. Lores; J. Losada; et al, *Hemoglobin*, **33**, pp. 206 – 213 (2009).
5. C. Cabal, E. González, J. Berlanga, D. Darias, et al, *J. of Radiology Research and Practice*, Article ID 783980, DOI: 10.5171/2014.783980 (2014).
6. E. González; C. Cabal; G. Sáurez; A. Lage; et al, *Pediatrics International*, **56**, pp. 43-46, doi: 10.1111/ped.12212 (2014).
7. A. Ruiz, Y. Hernández, C. Cabal, E. González, et al, *Nanoscale*; 5(23):11400-8. doi: 10.1039/c3nr01412f. Epub 2013 Jul 5. (2013).

Cross-polarization dynamics in the spinning glycine powder

Laurynas Dagys, Vytautas Balevičius

Institute of Chemical Physics, Vilnius University,
Sauletekio av. 3, Vilnius LT-10222, Lithuania.
E-mail: dagys.laurynas@gmail.com

Introduction

Nuclear Magnetic Resonance (NMR) is progressively marching into the field of crystallography. Thus it gets more important to achieve the best techniques possible for determining structural properties of various functional materials. Often these materials have complex structure. Hence, it has become difficult to investigate structure even with such techniques as X-ray diffraction or Neutron diffraction. Cross-polarization (CP) is an NMR experiment which involves using two different nuclei species like hydrogen, carbon etc with a spin number of ½. CP is a magnetization transfer from one species to another through dipolar coupling. This means that kinetics of such transfer is dependent on the internal solid-state structure. Therefore it opens the new possibilities to investigate complex systems like powder, confined, meso- and nano-structured materials [1, 2]. For these purposes, the glycine powder as a model system was picked two show advantages of using this NMR technique.

Experimental setup

NMR measurements were carried out on Bruker AVANCE III HD spectrometer operating at resonance frequencies of 400 and 100 MHz for ^{1}H and ^{13}C respectively. MAS measurements for ^{1}H→^{13}C CP were performed at 7 kHz spinning rate. The glycine powder was tightly packed into 80 µl zirconia rotor for the best possible spinning stability. A rectangular variable contact time pulse shape was used in CP-MAS experiments in order to fulfill one of the Hartmann-Hahn matching conditions. The RF fields were 100 kHz and 93 kHz for ^{13}C and ^{1}H, respectively. The CP kinetics were obtained by changing contact pulse from 20 µs to 10 ms with a step of 10 µs and repetition delay of 2 s. NMR spectra were processing using Topspin 3.2 software. The kinetic curves of ~1000 points were analyzed using *Microcal Origin 9* and *Mathcad 15* packages.

Results and analysis

The CP kinetics observed in powdered glycine sample exhibit different kinetics for the different carbon peaks (Fig. 1). This illustrates that even in the same molecule different atoms can have different structural properties according to the proton surroundings.

There are two distinct models that explain CP mechanism in a "thermodynamical" point of view (Fig. 2). They represent how populations of the states (polarization) in the separate spin sub-systems can interchange to another. It is described by relaxation constants and coupling constant. For amorphous materials with no order classical model (1st equation) has to be used. In crystalline or/and more ordered matter isolated spin pairs can emerge resulting in oscillations during the initial signal build-up. Therefore non-classical model (2nd equation) is applied where oscillation are described by function g(t).

$$I(t) = \frac{I_0\left(\exp\left(\frac{-t}{T_{1\rho}}\right) - \exp\left(\frac{-t}{T_{IS}}\right)\right)}{1 - \frac{T_{IS}}{T_{1\rho}}},$$

$$I(t) = I_0 \left\{ \exp\left(\frac{-t}{T_{1\rho}}\right) - \exp(-1{,}5k \cdot t) \cdot g(t) + \frac{N-1}{N+2}\left[\exp\left(\frac{-t}{T_{1\rho}}\right) - \exp(-k \cdot t) \right] \right\},$$

$$g(t) \to \exp\left(\frac{-t^2}{2T_2^2}\right)$$

Time T_{IS} macroscopically describes polarization build-up in the carbon subsystem. Parameter $T_{1\rho}$ is the spin-lattice relaxation time in the rotating frame, k_1 and k_2 are rate constants which describe the decay of the oscillations and b is the dipolar spitting. If one has such sample where crystallites have random size spin pairs, previous equation has to be averaged over all distances. In that case function g(t) can be rewritten to Gauss function.

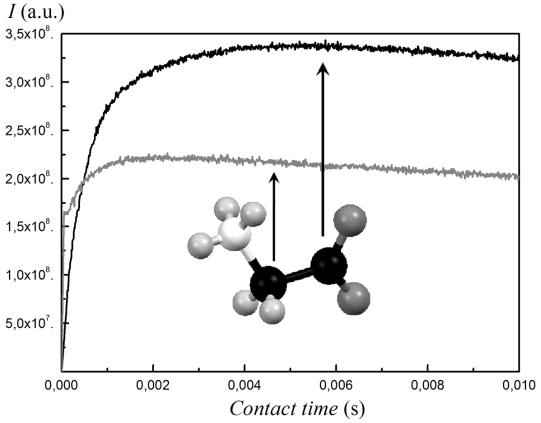

Figure 1. ^{1}H-^{13}C CP-MAS kinetics in powdered glycine sample for n=1 Hartmann-Hahn condition. Sample was spun at 7 kHz MAS rate in room temperature. Different curves associated with polarization transfer to different carbon nuclei. Molecule is drawn in zwitterionic state

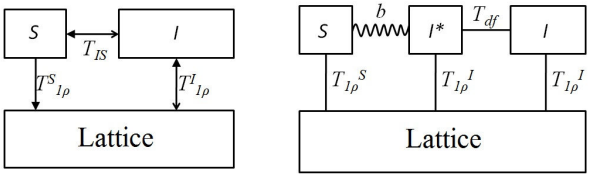

Figure 2. Classical (on the left) and Non-Classical (on the right) models of the NMR cross-polarization. S and I indices represent separate spin sub-systems (hydrogen, carbon-13), b is dipolar coupling constant, T_{df} is spin diffusion time, $T_{1\rho}$ is longitudinal relaxation time in the rotating frame

It is seen from the first figure, that no intense oscillations can be found, and hence it could be due to amorphous sample. In order to prove that one must compare parameters obtained by fitting with previously described models. These parameters are shown in the following table.

Table 1. Parameters of the curve fitting using previously given equations

Peak	Classical model					
	I_0 (a.u.)	$T_{1\rho}$ (s)	T_{IS}(s)	R^2		
-COOH	3.3E8	∞	5.6E-4	0.987		
-CH_2-	2.3E8	0.083	1.2E-4	0.528		
	Non-Classical model					
	I_0 (a.u.)	$T_{1\rho}$ (s)	T_2 (s)	T_2 (1/s)	N	R^2
-COOH	1.7E8	∞	5.2E-4	1617	2.2E29	0.992
-CH_2-	1.4E8	0.083	3.6E-6	3095	4	0.969

The R-squared clearly represent agreement with the specific model. Carbon in the carboxyl group can make up randomly distributed spin pairs with the hydrogen in such way that both models describe CP kinetics well. However, methylene group has chemically attached hydrogen, and thus composes higher order in the spin-pair distribution.

Conclusion

$^{1}H \rightarrow ^{13}C$ Cross-polarization (CP) kinetics upon Magic Angle Spinning (MAS) in glycine powder was studied in the present work. Even in this simple molecule, two distinct ^{13}C signals yield different CP kinetics (Fig. 2). Acquired curves were analyzed using well refined spin coupling models [2]. It was deduced, that these differences occur because of the distinctive neighboring proton properties in the nano-scales. This is confirmed by convergence between classical and non-classical models for the carboxyl group kinetics and by parameters of a non-linear fitting for the methylene group curve. It is seen that carbon lacking direct protons form less ordered network with the surrounding protons also creating diverging number of non-equivalent spin couples. In the other hand, methylene carbon forms ordered network but powder is to some extent amorphous. This conclusion can be done analyzing the convergence of the two models.

Acknowledgements

We would like to acknowledge Center of Spectroscopic Characterization of Materials and Electronic/Molecular Processes (Scientific infrastructure „SPECTROVERSUM“) at Lithuanian National Center for Physical Sciences and Technology for the use of spectroscopic equipment. We thank Professor Maria Gdaniec for the help collecting and analyzing crystallographic data.

References

1. V. Klimavičius, L. Dagys, V. Chizhik, V. Balevičius – *Appl. Magn Reson.,* **48**, 7 (2017).
2. L. Dagys, V. Klimavičius, B. Balevičius – *J. Chem. Phys.,* **145**, 114202 (2016).

The application of the metabonomic approach to predict drug-induced liver injury: The case of acetaminophen and its non-toxic isomer

Deborah De Luca, Jean-Marie Colet

Laboratory of Human Biology & Toxicology, University of Mons, Belgium
E-mail: deborah.deluca@umons.ac.be

Study summary

Drug-induced liver injury (DILI) is a serious issue for the pharmaceutical industry, and is still a major cause of drug attrition during development and withdrawal from the market. Nowadays, DILI are detected by conventional parameters based on late toxic events, including serum transaminases elevation. Even if these parameters are generally informative, the need remains for mechanistic and predictive biomarkers.

In this context, application of emerging "Omics" approaches could be useful. The "Omics" suffix refers to multi-parametric techniques focusing on global changes involved in disease or treatment, instead of conventional methods which evaluate one single parameter at a time. In this work, the ability of ^{1}H-NMR metabonomics to characterize DILI has been evaluated.

For that, acetaminophen (APAP, N-acetyl-p-aminophenol) and its meta-isomer (AMAP, N-acetyl-m-aminophenol) were selected as prototypical compounds. APAP is an analgesic and antipyretic drug responsible for most DILI cases in the Western Europe and the United-States. At therapeutic doses, no adverse effect was reported, while overdoses can cause dramatic hepatic damages leading to acute liver failure. In this case, APAP undergoes CYP450 bioactivation into NAPQI, an electrophile intermediate able to bind to hepatic proteins, leading to toxicity. However, its structural isomer AMAP is able to form liver protein adducts but without inducing any toxicity in mice.

Impact of APAP and AMAP exposure has been investigated by metabonomics under and in vitro conditions on HepaRG cell line. The results have shown that APAP-induced hepatotoxicity is associated with energetic pathways disruption and loss of redox homeostasis. However, in vitro results were discordant to the well-established in vivo data, revealing AMAP toxicity in HepaRG cell line. The combination of conventional cell-based assays to metabonomics profiling indicates that AMAP hepatotoxicity was due to mitochondrial energy disruption and oxidative stress.

Even if the introduction of this novel technology in the drug discovery pipeline is still premature, this study by supporting their mechanistic potential, offers new insights in drug development and more generally, in challenges encountered by the pharmaceutical industry.

Acknowledgements

This work was partially funded by UCB Pharma S.A Belgium (Braine l'Alleud).

Investigation of the *electron-rich* binuclear Pt(II) 1,10-phenanthrocyanine $[(py)_2Pt(\mu\text{-phencyanine}^-)Pt(py)_2]Cl_3$ by the ESR method. Localization of PSC in temperature accessible electron-excited radical states

Viktor N. Demidov[1], *Stanislav M. Sukharzhevsky*[2], *Lidya N. Vedeneeva*[3], *Andrey V. Zinchenko*[4], *Tatyana B. Pakhomova*[4]

[1]*Company "Pro-Brite", Russia, St. Petersburg, 192289, Sofiyskaya, 93*
[2]*Faculty of Chemistry, St. Petersburg State University, RC "MRMI", Russia, Peterhof, 198504, Universitetsky pr., 26*
[3]*Perm Nat. Inv. Polytech. University, Russia, Berezniki, 618404, Thälmann'a ul., 7*
[4]*St. Petersburg State Technological Institute, Russia, St. Petersburg, 190013, Moskovsky pr., 26*
E-mail: vndemidov@mail.ru

Introduction

ESR spectroscopy is one of the effective tools of the investigation of the paramagnetic spin center (PSC) distribution in the chemical compounds. Investigation of the high-energetic phosphorescence triplet states by ESR method was formed as the independent scientific direction for a long time [1, 2]. In the these decades, the direction connected with formation and investigation of the compounds with stoichiometric concentration of PSC (organic paramagnetic compounds [3, 4] and molecular magnetic compounds [5]) is intensively developing. The third investigation direction of the character and nature of PSC is the studying of the *chemical systems* being in the *thermodynamic equilibrium* (*quasi-equilibrium*) when the singlet forms are capable to turn into the radical or biradical states by *thermal way*, not by photochemical activation. The temperature accessible radical and biradical forms (triplet biradical, degenerate biradical or monoradical) appear, thereby [6, 7]. Such electron transitions are frequent and linked to proton transfer (indirect electron transitions [8]). Such kind of transitions (equilibrium, quasi-equilibrium and non-equilibrium) are *dually* treated: as transitions into temperature accessible electron-exited states [9, 10] and formation of new radical forms at basic electronic states (for example, phenyloxenium ion) [11]. Besides, the method developed for investigation of the thermodynamic non-equilibrium structure transitions is likely applicable in this case as well. Fact of the existence of PSC in diamagnetic simples without a photo exiting has been registered in the sample of chlorophyll under dark conditions [12]. According to the quantum chemical theory of the perturbation of molecular orbitals (PMO) one of possible photo-exited states "*adds*" to the wave function of main state of the thermic system [13]. That pulls together the consideration of strong-nonequilibrium $S_0 \rightarrow S^*$ transitions with the successive intercombinatorial conversion S* into one of the triplet states T_{high} and *thermic transitions* $S_0 \rightarrow T_{low}$ and shows actuality of the investigation problem of the *temperature accessible* radical and biradical states (including triplet states) of the chemical systems in the *thermo operated* (*thermo directed*) entropic controllable processes (since energy of these transitions can be too low, $h\nu \approx kT$).

Results and Discussion

The compounds of new structure cyanine class $[Pt_2(A)_2(\mu\text{-phencyanine})]X_3$ (A = NH_3, py, 3-, 4-pic, en, X = Cl, J, $[BF_4]$, $[BPh_4]$) got the name 1,10-phenanthrocyanines [14-16] (similar to apoquinocyanines containing quaternized *dihydro*-biquinolines [17-19]). The new 1,10-phenanthrocyanine azachromophores have the higher biological activity to pathogenic bacteria and viruses than their more simple 1,10-phenanthroline precursors[16]. It can be connected with existence of *electron-rich* ligand forms in their structure, which give *redox*-active behavior to the compounds. It is found that 1,10-phenanthrocyanines of Pd(II) and Zn(II) have a trend to complex formation with calf thymus DNA [20].

It has appeared the *electron-rich* ligands μ-1,10-phencyanine (somewhat unexpectedly) are sources of large quantity of PSC in the compound structures. These PSC give the intensive ESR signals in the solid states as well as in solutions. The binuclear glass 1,10-phenanthrocyanines of Zn(II) L_nZn^{2+}(μ-phencyanine)$Zn^{2+}L_n$ (L = phen, en, H_2O, ^-OAc) show the ESR signals with a weak anisotropy with values of g-factor 2.003-2.004 (300 K) [21]. The appearance of the ESR signals for these diamagnetic compounds have been interpreted as a result of the *thermo-induced* $S_0 \rightarrow T_{low}$ transitions into the *temperature accessible* electron-exited radical (biradical) state.

In the present work the *electron-rich* 1,10-phenanthrocyanine complex of Pt(II) $[(py)_2Pt(\mu\text{-phencyanine}^-)Pt(py)_2]Cl_3$ has been investigated by the ESR spectroscopy (298 K) in more detail. The ESR spectrum of $[(py)_2Pt(\mu\text{-phencyanine}^-)Pt(py)_2]Cl_3$ is represented on Fig. 1. The spectrum has the signals of several types with the complicated contour (hyperfine structure). There is a single anisotropic band with value ΔB_p = 63,0 Gs with intensity and g-factor values: I = 5,80 rel. un. и $g_\perp$ 2,0197, g_{II} 1,9850; $A_\perp$ 13,5–15,0 Gs, A_{II} 46 Gs on the spectrum. Series of the less intensive narrow signals adjoin the previously mentioned band. For the nearest of them ΔB_p = 7,0 Gs, I = 0,36 rel. un. Ratio of the intensities for these two signals is 16,1. We have found the similar narrow bands with $\Delta B_p \sim 5–7$ Gs for the *electron-rich* 1,10-phenanthrocyanines of Zn(II) as well [21]. According to their genesis they have been assigned to the *electron-rich* bridge 1,10-phenanthrocyanine ligand in the coordination structure of Zn^{2+}(μ-phencyanine)Zn^{2+}. The appearance of the hyperfine structure signals in the ESR spectra of the 1,10-phenanthrocyanine platinum complex apparently confirms the fact that spin-exchange interactions in biradical forms of ligand μ-phencyanine are suppressed for platinum compounds and the degree of π-conjugation of $C(sp^2)$-co-condensed 1,10-phenanthroline fragments decreases within the μ-phencyanine ligand structure.

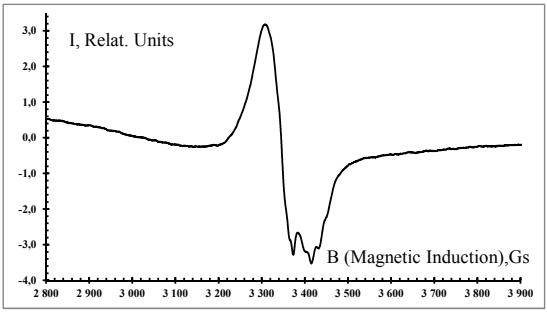

Figure 1. ESR spectrum of complex $[(py)_2Pt(\mu\text{-phencyanine}^-)Pt(py)_2]Cl_3$ in the solid state

Decreasing of the spin-exchange interactions within the structure Pt^{2+}(μ-phencyanine$^-$)Pt^{2+} is rather a result of influence of coordination centers of Pt^{2+} $5d^8$ (spin-orbital interaction) on μ-phencyanine$^-$. That must lead to dispersal of the spin density in the temperature accessible electron-exited radical states of the complex and appearance of new PSC ($Pt^{+\bullet}$ ions) in comparison with 1,10-phenanthrocyanines of Zn(II).

Conclusions

The obtained results point to the fact that the localization of PSC in the *electron-rich* 1,10-phenanthrocyanine complex $[(py)_2Pt(\mu\text{-phencyanine}^-)Pt(py)_2]Cl_3$ is too complicated and apparently assumes the existence of the different electron-rich radical states. Spin-noncompensated cation-radicals of platinum $Pt^{+\bullet}$ as well as anion-radical (or dianion biradical) forms of the bridge 1,10-phenanthrocyanine ligand (μ-phencyanine) can be among them. The

nature of the last that can be bonded (from our point of view) with the temperature accessible triplet biradical (or degenerate biradical) states as well as with anion-radical forms will be discussed in the future.

ESR Measurements

The ESR investigation of 1,10-phenanthrocyanine complex of Pt (II) in the solid state (298 K) has been carried out in the Resource Centre "Magneto-resonance methods of investigation" of the Scientific Park of St. Petersburg State University on the spectrometer ELEXSYS E580 (X-BAND).

References

1. S.P. McGlynn, T. Azumi, M. Kinoshita, Molecular Spectroscopy of the Triplet State. – Prentice Hall, Englewood Cliffs, New Jersey, 1969.
2. V.N. Parmon, A.I. Kokorin, G.M. Zhidomirov. Stable Biradicals (in Russ.). – "Nauka", Moscow, 1980.
3. E.G. Rosantsev. Organic Paramagnetics (in Russ.), ed. E.G. Rosantsev, M.D. Gol'dfeyn, V.F. Pulin. – Saratov State Univ., Saratov, 2000.
4. M.D. Gol'dfeyn, E.G. Rosantsev. *Univ. Proc. Volga Region*, No. 1 (5), 60-72 (2014).
5. E.V. Tretyakov, V.I. Ovcharenko. *Russ. Chem. Rev.*, **78** (11), 971-1012 (2009).
6. C. Wentrup, M.J. Regimbald-Krnel, D. Müller, et al. *Angew. Chem. Int. Ed*., **55** (47), 14600-14605 (2016).
7. Y. Morita, T. Aoki, K. Fukui, et al. *Angew. Chem. Int. Ed*., **41**, No. 10, 1793-1796 (2002).
8. K.K. Kalninsh, A.F. Podolsky. *J. Struct. Chem.* (in Russ.), **41**, No. 4, 701-709 (2000).
9. K.K. Kalninsh. Electron Exciting in Chemistry (in Russ.).–IMC RAS, St. Petersb., 1998.
10. K.K. Kalninsh, E.F. Panarin. Excited States in Chemistry of Polymers (in Russ.). – IPC St. Petersburg State UTD, 2007.
11. Ming-De Li, T.R. Albright, P.J. Hanway. *J. Am. Chem. Soc.*, **137** (32), 10391–10398 (2015).
12. A.F.H. Anderson, M. Calvin. – Univ. Calif. Ernest O. Lawrence Radiation Lab. Berkeley, *Bioorganic Chem. Quarterly Rep.*, 119-128 (1963).
13. R.G. Pearson. Symmetry rules for chemical reactions: orbital topology and elementary processes. –A Wiley-Interscience Publ., New York, 1976.
14. V.N. Demidov, S.A. Simanova, A.I. Savinova, et al. *Ross. Khim. Zhurn. (Zhurn. Ross. Khim. Ob. D.I. Mendeleev)* (in Russ.), **53**, No. 1, 128-134 (2009); *Russ. J. Gen. Chem.*, **79**, No. 12, 2807-2814 (2009).
15. V.N. Demidov, N.A. Kasyanenko, V.S. Antonov, et al. *Ross. Khim. Zhurn. (Zhurn. Ross. Khim. Ob. D.I. Mendeleev)* (in Russ.), **54**, No. 6, 120-135 (2010); *Russ. J. Gen. Chem.*, **82**, No. 3, 602-620 (2012).
16. V.N. Demidov. – Diss. D. Chem. Sci. (in Russ.), St. Petersburg State Technol. Inst. (Techn. Univ.), 2010.
17. K. Afarinkia, M.-R. Ansari, C.W. Bird, et al. *Tetrahedron Lett.*, **37**, No. 27, 4801-4804 (1996).
18. F. Kröhnke, H. Dickhäuser, I. Vogt. *Justus Liebigs Ann. Chem.*, **644**, No. 1, 93-108 (1961).
19. E. Calzavara. *Science Ind. Phot.*, **10**, 193 (1939).
20. S.V. Paston, V.M. Bakulev, V.N. Demidov, et al. *News St. Petersburg State Univ.* (in Russ.), Ser. 4, Phys., Chem., **2 (60)**, No. 3, 299-304 (2015).
21. V.N. Demidov, S.M. Sukharzhevsky, S.V. Paston, et al. *News St. Petersburg State Univ.* (in Russ.), Ser.4, Phys., Chem., **4 (62)**, No. 2, 138-144 (2017).

Investigation and characterization of mixed-matrix membranes based on composite PVA – fullerenol

Maria E. Dmitrenko, Anna I. Kuzminova, Anastasia V. Penkova

Institute of Chemistry, St. Petersburg State University, 7/9 Universitetskaya nab., St. Petersburg, 199034, Russia
E-mail: m.dmitrienko@spbu.ru

Introduction

Nowadays, pervaporation is one of the promising membrane technologies that can be a good alternative method to classical separation processes of liquid mixtures (e.g. distillation or extraction). One of the key factors for the effective performance of the pervaporation (high selectivity and permeability) is the proper choice of a membrane. In this regard, the development of new polymeric membranes with improved transport properties is a very important task. It can be achieved by the modification of the polymer matrix by inorganic filler that yields in developing the mixed – matrix membranes (MMMs). It allows combining of the best properties and advantages of both polymer and inorganic structures. The mixed-matrix membranes with inorganic filler inside of a polymeric matrix offer the possibility to overcome the trade-off between the permeability and selectivity of the polymeric membranes. Among the inorganic particles fullerene takes and important place due to its unique π-electronic structure. In the present work polyvinyl alcohol (PVA) was used as the polymeric matrix for mixed matrix membranes preparation. Water soluble fullerene derivative – polyhydroxylated fullerene (fullerenol) was used as a modifier and a cross-linking agent for PVA.

The aims were to prepare and characterize the structure of mixed-matrix membranes based on polyvinyl alcohol modified by fullerenol and to test them in pervaporation dehydration of water-organic mixtures. The optimal conditions for the preparation of membranes based on the composites PVA-fullerenol were developed. Structural and physicochemical properties of the membranes were studied by various methods of investigation (spectroscopic methods (NMR, FTIR), X-ray diffraction analysis, scanning electron microscopy, thermogravimetric analysis, differential scanning calorimetry, swelling experiments and measurement of contact angles). The developed membranes were tested for dehydration of industrially important solvents (ethanol, tetrahydrofuran, acetic acid) by pervaporation to evaluate the effects of internal changes. It was shown that the transport characteristics of mixed-matrix PVA membranes were essentially improved as compared to pristine PVA-based membranes due to the changes of structure and morphology of the polymeric membranes.

Acknowledgements

This work was supported by Russian Science Foundation [grant No. 17-73-20060]. The experimental work was facilitated by equipment from Resource Centers: Research Centre for Nanotechnology, Research Centre for X-ray Diffraction, Research Centre for Physical Methods Surface Investigation, Magnetic Resonance Research Centre, Thermal Analysis and Calorimetry, Chemical Analysis and Materials Research Centre and GEOMODEL at St. Petersburg State University.

Ultra-narrow low-field nuclear spin resonance in NV centers in bulk diamond crystal

Alexander K. Dmitriev[1], *Anton K. Vershovskii*[1]

[1]*Ioffe Institute, 26 Politekhnicheskaya, St. Petersburg 194021, Russia*
E-mail: antver@mail.ioffe.ru

Introduction

The application of methods based on optically detected magnetic resonance (ODMR) to negatively charged nitrogen vacancy (NV^-, or just NV) color centers in diamond crystals has brought forth relatively simple new methods of controlling nuclear spins. These spins are considered to be excellent candidates for solid-state quantum information processing because of their very long coherence time [1, 2]. Typically, level anticrossing (LAC) [1, 2] or combined microwave (MW) and radiofrequency (RF) excitation [3] are used to address chosen spin state, and the width of observed resonances exceeds hundreds of kilohertz. To reduce the resonance width, special techniques, such as single spin excitation, should be used. Here, however, we report on ultra-narrow (~7 kHz HWHM) resonances, which can be excited and optically detected in ultra-weak (≥1 G) magnetic fields using a single RF field ~4.95 MHz.

Ground-state nuclear spin resonance

Level structure of $^3A_2$ state is defined by Hamiltonian [4, 5]

$$H = D(S_z^2 - \frac{1}{3}\vec{S}^2) + E(S_x^2 - S_y^2) + g_s\mu_B\vec{B}\cdot\vec{S} + \\ + A_\parallel S_z I_z + A_\perp(S_x I_x + S_y I_y) + PI_z^2 - g_I\mu_N\vec{B}\cdot\vec{I}, \quad (1)$$

where $\mu_B = h\cdot 13.996\cdot 10^9$ Hz/T is the Bohr magneton, $\vec{I}$ is the ^{14}N nuclear ($I = 1$), $\vec{S}$ is the electron spin of NV center ($S = 1$), $\mu_N = h\cdot 7.622\cdot 10^6$ Hz/T is the nuclear magneton, $D = 2.87$ GHz and E are axial and transverse zero-field splitting (ZFS) parameters, $g_s = 2.003$ and $g_I = 0.403$ are electron and nuclear g-factors, $A_\parallel = -2.16$ MHz and $A_\perp = -2.7$ MHz are axial and transverse hyperfine splitting parameters, $P = 4.95$ MHz is the quadrupole splitting parameter.

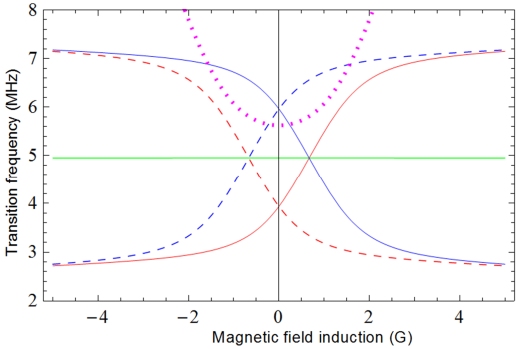

Figure 1. Calculated frequencies of nuclear transitions in diamond crystal with E = 1.8 MHz. Red lines denote |1,1>↔|1,0> and |1,0>↔|1,−1> transitions (first digit is electronic, second – nuclear spin projection), green represents |0,0>↔|0,±1>, blue represents |−1,1>↔|−1,0> and |−1,0>↔|−1,−1>. Dotted magenta line represents a spin-flip electron-nuclear transition |1,−1>↔|−1,1>

Frequencies of nuclear transitions, calculated from (1) for diamond crystal with E = 1.8 MHz, are shown in Fig. 1. All of these transitions, save for the pure nuclear $|0,0\rangle \leftrightarrow |0,\pm1\rangle$ transitions, are strongly dependent on the magnetic field, and therefore they should be broadened by an inhomogeneous magnetic field in the crystal.

It is not evident *a priori* that these resonances can observed using only RF excitation without MW: they can only appear in the ODMR spectrum under the condition that optical pumping creates a population difference between $|0,0\rangle$ and $|0,\pm1\rangle$ levels. Nevertheless, in our experiment we have recorded both nuclear $|0,0\rangle \leftrightarrow |0,\pm1\rangle$ and spin-flip electron-nuclear $|1,-1\rangle \leftrightarrow |-1,1\rangle$ transitions (Fig 2).

The experimental setup was described in [6]: a synthetic diamond of SDB1085 60/70 grade (manufactured by Element Six) with dimensions 0.1 × 0.3 × 0.3 mm was subjected to electron irradiation ($5 \cdot 10^{18}$ cm^{-2}) and subsequent annealing in Ar at 800°C over 2 hours. The crystal was used at room temperature; it was attached by optically transparent glue to the end of an optical fiber.

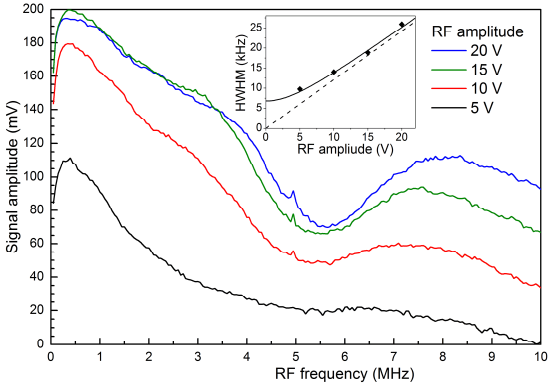

Figure 2. RF ODMR spectra at zero field recorded at different RF amplitudes; inset − signal width dependency on RF amplitude at B = 10 G

RF ODMR spectra recorded at zero magnetic field (Fig.2) exhibit a) a wide hollow centered at ~5.6 MHz and therefore, according to Fig.1, with high certainty attributed to the spin-flip electron-nuclear transition, and b) a narrow peak centered at 4.95 MHz, corresponding to the $|0,0\rangle \leftrightarrow |0,\pm1\rangle$ nuclear transition. The resonance linewidth dependency on RF amplitude was recorded at 10 G in order to maximize signal-to-noise (SNR) ratio (inset on Fig.2). Fitting shows that the linewidth (HWHM) extrapolated to zero RF amplitude is only 6.8 kHz, corresponding to transverse relaxation time $T_2^* = 23$ μs. The ODMR signal cutoff frequency $f_1 = 215$ Hz is limited by the population relaxation constant: $T_1 \geq 1/(2\pi \cdot f_1) = 740$ μs.

To check that observed resonances really correspond to the $|0,0\rangle \leftrightarrow |0,\pm1\rangle$ nuclear transition, we recorded RF ODMR spectra in magnetic fields up to 100 G (Fig.3). The very low SNR ratio in Fig 3 is due to 1) noisy environment, and 2) the low RF amplitude chosen in order to avoid broadening the resonance line. Nevertheless, it is apparent that the value of the resonance splitting corresponds to the expected value of 2·307 Hz/G; the simultaneous shift in the resonance lines is yet to be explained.

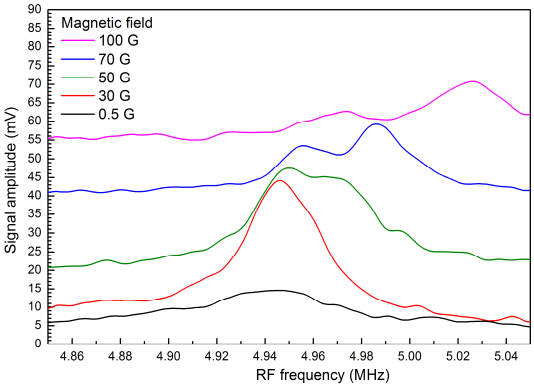

Figure 3. RF ODMR spectra recorded at different magnetic field values

Conclusion

Our experiment shows that ultra-narrow (<10 kHz) nuclear transition resonances can be observed in RF ODMR signal at room temperature in a low magnetic field without additional MW excitation; the signal-to-noise ratio of these resonances is subject to further improvement. This can be an important step to a simple and compact scheme of nuclear spin control for the task of quantum computation.

References

1. F. Jelezko et al. – *Phys. Rev. Lett*., 93, 130501 (2004).
2. V. Jacques et al. – *Phys. Rev. Lett.,* 102, 057403 (2009).
3. M.V. Gurudev Dutt et al. – *Science*, 316, 1312 (2007).
4. S. Felton et al. – *Physical Review B*, 79, 075203 (2009).
5. R. Fisher et al. – *Physical Review B*, 87, 125207 (2013).
6. A.K. Dmitriev, A.K. Vershovskii – *JOSA B*, 33, B1-B4 (2016).

Phase noise spectrum of microwave active ring oscillators based on spin-wave delay lines

A. V. Drozdovskii, A. B. Ustinov, B. A. Kalinikos

Department of Physical Electronics and Technology, St. Petersburg Electrotechnical University, St. Petersburg, 197376, Russia
E-mail: ustinov-rus@mail.ru

Introduction

One of the ways to achieve a low level of the phase noise is to use the so-called active ring oscillators based on a delay line with a large time delay. The delay lines could be realized with waves of different nature. Thus, the acoustic wave [1] – [3], optical wave [4], [5], and spin wave (SW) [6–8] delay line oscillators are known for a long time. The spin-wave oscillators based on epitaxial YIG films have several advantages. Among them are a relatively small size and a broad frequency tuning range comparable with that for the YIG sphere oscillators. Note also that the YIG-film spin-wave devices have a planar geometry and can be easily fabricated by conventional photolithography and surface mounted electronic components.

Purpose of this work is a detailed theoretical and experimental study of the phase noise spectrum for a microwave oscillator based on a YIG-film spin-wave delay line that resolves the contradiction. The theory for the first time takes into account ferromagnetic resonance linewidth of the film, which is the main factor determining the phase noise level.

Experiment

A schematic diagram of the experimental oscillator is shown in Fig. 1(a). The main part of the oscillator circuit was an experimental delay line that used a 13.6 μm thick single crystal YIG film with a narrow linewidth, a saturation magnetization of 1950 Gs, and unpinned surface spins. A value of ΔH measured for frequency of 5300 MHz was 0.55 Oe.

The propagation structure consisted of a long and narrow YIG film strip 2-mm-wide placed across two 50-μm-wide 2-mm-long microstrip line antennas (MA on Fig. 1(a)). Note that it was possible to vary a distance d between the antennas in the range of 0.5-20 mm. A static magnetic field H from electromagnet (EM) of 1150 Oe was applied parallel to the long edge of the YIG strip and the propagation path from the input antenna to the output antenna. This film-field configuration supported the propagation of surface spin waves. The experimental oscillator circuit also included a microwave amplifier (A). A variable attenuator (Att) was used to control the feedback loop gain. A 10-dB directional coupler (DC) served for taking a part of the microwave signal out of the active ring for analysis. A signal source analyser Rohde & Schwarz FSUP26 was utilized for measurements of the phase noise spectra of generated continuous wave signal.

A representative example of the experimentally obtained transmission characteristic for the SW delay line with d = 2.5 mm is given in Fig. 1(b). The arrow on graph (b) shows the frequency at which continuous wave generation was observed. This frequency was equal to 5410 MHz.

In order to study the influence of the ring time delay on the phase noise we have performed a set of measurements for different delay times. Note that the ring delay time was mainly due to the spin-wave delay time τ_{sw} because the electronic delay time in the rest of the ring was small compared to τ_{sw}. The spin-wave delay time is determined by the distance between the excitation and reception antennas as $\tau_{sw} = d/V_g(\omega)$, where $V_g(\omega)$ is a group velocity of carrier spin waves. The measurements were performed for three values of d of 1.5 mm, 10 mm, and 19 mm and, consequently, for three delay times of 25 ns, 120 ns, and 243 ns. The phase noise spectra of the microwave signals obtained for these delay times are shown in Fig. 2.

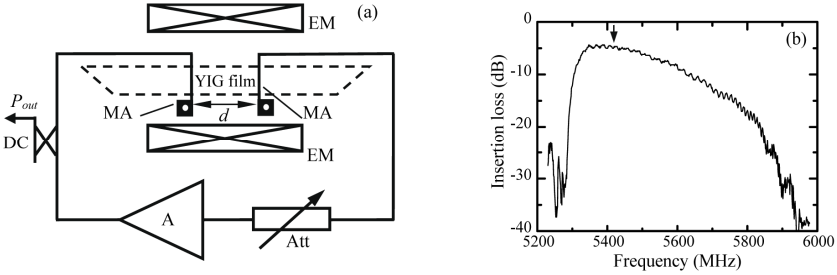

Figure 1. (a) Block diagram of the oscillator.
(b) Amplitude-frequency characteristic of the spin-wave delay line

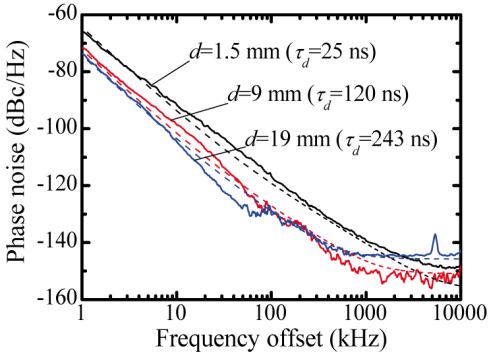

Figure 2. The theoretical (dashed lines) and experimental (solid lines) phase noise spectra of the spin-wave oscillator

A numerical simulation of the phase noise spectra was carried out for the experimental parameters of the oscillator. As is seen the theoretical and experimental noise spectra were in good agreement. Detailed analysis of the theory will be provided in the conference presentation as well as in the full paper.

Acknowledgements

The theoretical investigation was supported in part by Ministry of Education and Science of Russian Federation (Project "Goszadanie"). The fabrication and characterization of the microwave oscillator was supported in part by Russian Science Foundation (Grant# 14-12-01296-P).

References

1. J. Henaff, "Application of SAW-Oscillators to Digital Communications", *1979 Ultrasonics Symposium (IEEE)*, pp. 855-860, 1979.
2. L. Eichinger, B. Fleischmann, P. Russer, R. Weigel, "A 2 GHz surface transverse wave oscillator with low phase noise", *IEEE Trans. on Microwave Theory and Techniques*, vol.36, no 12, pp. 1677-1684, 1988.
3. J. Grajal, F. Calle, J. Pedrós, J.L. Martínez-Chacón and A. Jiménez, "AlGaN/GaN-based SAW delay-line oscillators", *Microwave and Optical Technology Letters*, vol. 50, iss. 11, pp. 2967-2970, 2008.

4. X. S. Yao, L. Maleki, “Optoelectronic oscillator for photonic systems”, *IEEE Journal of Quantum Electronics*, vol. 32, iss. 7, pp. 1141-1149, 1996.
5. J. Capmany, D. Novak, “Microwave photonics combines two worlds”, *Nature Photonics*, vol. 1, pp. 319-330, 2007.
6. P. Kabos and V.S. Stalmachov, *Magnetostatic Waves and Their Application*, Netherlands: Springer-Science+Business Media Dordrecht, 1994.
7. D. D. Stancil and A. Prabhakar, *Spin waves: Theory and applications*, New York: Springer, 2009.

Aluminum and gallium nuclei as microscopic probes for pulsed ENDOR diagnostics in garnet ceramics doped with paramagnetic ions

E. V. Edinach[1], *A. G. Badalyan*[1], *R. A. Babunts*[1], *Yu. A. Uspenskaya*[1], *N. G. Romanov*[1], *H. R. Asatryan*[1], *G. V. Mamin*[2], *S. B. Orlinskii*[2], *P. G. Baranov*[1]

[1]*Ioffe Institute, 194021 St. Petersburg, Russia*
[2]*Kazan Federal University, Institute of Physics, 420008 Kazan, Russia*
E-mail: elena.edinach@mail.ioffe.ru

Introduction

Garnet ceramics doped with transition and rare-earth ions are widely used as scintillator materials that convert high energy radiation into visible or infrared light [1]. Coherent properties of rare-earth single-spin qubits in YAG have been recently demonstrated [2]. Transition elements, in particular manganese, exert a strong influence on the emission properties of scintillator materials. An important direction for optimizing the properties of scintillators is the use of mixed garnets based on Al and Ga ions. Of special interest is information on the position of the Al and Ga in the crystal lattice of mixed garnets.

Garnets crystallize in a cubic form and are described by the formula $C_3(A,D)_5O_{12}$, where three different cation sites are indicated. C is a dodecahedral site, A and D are octahedral and a tetrahedral sites, respectively. The site C can be occupied by Y or Lu, the sites A and D are frequently occupied by Al or Ga ions. The two sites have different properties, as we show in this paper. We used electron spin echo (ESE) detected electron paramagnetic resonance (EPR), and pulsed electron-nuclear double resonance (ENDOR) techniques for diagnosing the cerium and manganese environment in garnet ceramics.

Experimental

All ceramic samples were prepared at Philips Research Eindhoven by sintering a mixture of base oxides of 4N-purity in air atmosphere. They were doped with either 0.2 mol.% Ce or 0.1 mol.% Mn. Based on X-ray diffraction patterns it was concluded that all samples consist of a single garnet phase. The W-band (94 GHz) ESE detected EPR and ENDOR spectra were measured by using the Hahn-echo decay sequence $\pi/2$ - τ - π, with $\pi/2 = 16$ ns and $\tau = 180$ ns. To measure T_2 the ESE signal amplitude was monitored by using the Hahn-echo decay sequence $\pi/2$ - τ - π, where τ was varied from 180 ns up to 2.2 μs, $\pi/2 = 16$ ns. ENDOR was measured by using Mims sequence $\pi/2$ - τ - $\pi/2$ – T - $\pi/2$ -τ - ESE, $\tau = 228$ ns, $T = 19.8$ μs, for RF pulse $T_{RF} = 18$ μs.

Results and discussion

Fig. 1 (left panel) shows W-band ESE-detected EPR signals of Mn^{2+} ions in $Y_3Al_5O_{12}$:Mn, $Y_3Ga_5O_{12}$:Mn and $Y_3Al_{1.5}Ga_{3.5}O_{12}$:Mn ceramics. The relative intensity of the lines corresponding to $M_S = 1/2 \leftrightarrow -1/2$ transitions is the largest since they have the slightest angular variation. Also marked are weak partly resolved sextets belonging to $M_S = \pm 3/2 \leftrightarrow \pm 1/2$ transitions. Fine structure components corresponding to $M_S = \pm 5/2 \leftrightarrow \pm 3/2$ transitions were not detected because of low intensity.

Fig.1 (right panel) shows ESE detected ENDOR spectra of Mn^{2+} observed in the frequency range close to the ^{27}Al, ^{69}Ga, and ^{71}Ga Larmor frequencies in $Y_3Al_5O_{12}$:Mn, $Y_3Ga_5O_{12}$:Mn, and in $Y_3Al_{1.5}Ga_{3.5}O_{12}$:Mn mixed ceramics.

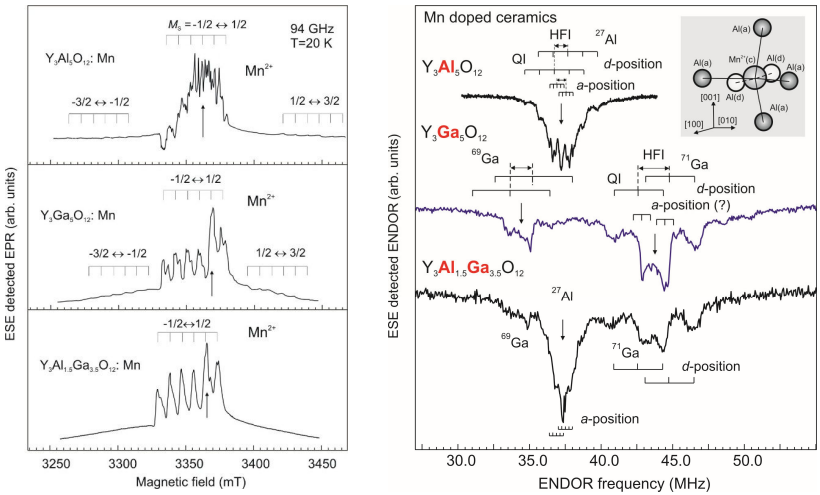

Figure 1. ESE detected EPR (left panel) and ENDOR (right panel) signals of Mn^{2+} ions in $Y_3Al_5O_{12}$:Mn, $Y_3Ga_5O_{12}$:Mn and $Y_3Al_{1.5}Ga_{3.5}O_{12}$:Mn ceramics. Arrows show the fields at which the ENDOR spectra were measured. The arrows show the Larmor frequencies for ^{27}Al, ^{69}Ga, and ^{71}Ga nuclei. The quadrupole and hyperfine interaction (QI and HFI) splittings are marked. Inset: A sketch of the nearest environment of Mn^{2+} ions with aluminum (or Ga) atoms in two positions

One can see the groups of lines arranged symmetrically with respect to the ^{27}Al, ^{69}Ga, ^{71}Ga nuclear Zeeman frequencies $\upsilon(^{27}\text{Al})$, $\upsilon(^{69}\text{Ga})$ and $\upsilon(^{71}\text{Ga})$ indicated by arrows. These groups are related to the HFI and quadrupole interaction of Mn^{2+} with the neighboring Al (Ga) nuclei in octahedral (a) and tetrahedral (d) positions.

To analyze the Mn^{2+} EPR spectra the following spin Hamiltonian has been used:

$$\hat{H} = \mu_B \vec{B} \cdot \hat{g} \cdot \hat{\vec{S}} + D\left(S_z^2 - \frac{1}{3}S(S+1)\right) + E\left(S_x^2 - S_y^2\right) + \sum_i (\hat{\vec{S}} \cdot \hat{A}_i \cdot \hat{\vec{I}}_i + \hat{\vec{I}}_i \cdot \hat{P}_i \cdot \hat{\vec{I}}_i - g_N \mu_N \vec{B} \cdot \hat{\vec{I}}_i), \quad (1)$$

where μ_B is the Bohr magneton, $\hat{\vec{S}}$ is the electron spin operator. The first term describes the Zeeman interaction and the second two terms describe the fine structure splitting (for S > 1/2). The last term describes the hyperfine, quadrupole, and nuclear Zeeman interactions with ligand ions, respectively. Here $\hat{\vec{I}}_i$ are nuclear spin operators for the i-th nucleus of Al (Ga), which are summed over the Al (Ga) nuclei that interact with the electron. Here g_N is the nuclear g-factor of the Al, Ga or Mn nucleus, and μ_N is the nuclear magneton. In order not to complicate the formula, we assume that i = 1 describes the parameters of the Mn ion.

In ENDOR spectra of $Y_3Ga_5O_{12}$:Mn and $Y_3Al_{1.5}Ga_{3.5}O_{12}$:Mn ceramics, the signals of the ^{69}Ga isotope are smaller, although it has twice the higher natural content compared to the ^{71}Ga isotope. There are at least two types of ENDOR spectra of Al, differing in magnitude of the quadrupole interaction. Calculated values of the electric field gradient as well as the gradient values measured by nuclear magnetic resonance (NMR) show that in aluminum garnets the electric field gradient in a tetrahedral (d) position of Al is several times larger than that in an octahedral (a) position [3]. We can assume that the ENDOR spectra with larger quadrupole splitting are due to the quadrupole interaction with Al ions occupying tetrahedral positions,

whereas the spectra with smaller quadrupole splitting belong to Al in octahedral position. Thus, the ENDOR data can be used for studying the Al-Ga replacement process in mixed garnets

One can see from Fig. 1 (right panel) that addition of Ga into $Y_3Al_5O_{12}$:Mn ceramics results in relatively smaller ENDOR signals corresponding to the tetrahedral positions of Al as compared to the octahedral positions. In mixed ceramics $Y_3Al_{1.5}Ga_{3.5}O_{12}$:Mn, the relative amplitude of the ENDOR lines for Ga in tetrahedral positions as compared to octahedral positions is larger than for the $Y_3Ga_5O_{12}$:Mn ceramics. Thus, we can conclude that Ga replaces Al starting from tetrahedral positions. This agrees with the results of Ref. 4 where ENDOR of Ce doped aluminum and aluminum-gallium garnets was studied. The quadrupole splitting, caused by ^{27}Al nuclei surrounding the Mn^{2+} ion, is P ≈ 0.85 MHz, and the electric field gradient $V_{zz}(Al) = 3.125\times1021$ V/m^2. We assume that this splitting is due to aluminum occupying a tetrahedral position with a larger electric field gradient. The HF interaction for this position is A(d) = 0.75 MHz. The smaller splitting between the neighboring lines P ≈ 0.18 MHz seems to be the quadrupole splitting for aluminum occupying an octahedral position (a) with the electric field gradient $V_{zz}(Al) \approx 6.5\times1020$ V/m2. The HF interaction value for a-positions is A(a) = 0.65 MHz. There are several possible configurations of the Mn^{2+} ion nearest environment, so in the experiment we observe an average picture. The HF interaction with Al neighbors is suggested to be transferred through the oxygen ligands that surround manganese and aluminum.

The isotropic ^{69}Ga central-atom HF interaction constant for 4s-electron is 12210 MHz (15515 MHz for 71Ga), more than three times larger compared to that for ^{27}Al. A similar relationship was observed for the hyperfine interaction constants with Al and Ga, which indicates that the spin density of the Mn^{2+} unpaired electrons near Al and Ga is approximately the same.

Summary

In conclusion, EPR and ENDOR techniques were applied to measure hyperfine and quadrupole interactions for Mn^{2+} in garnet based scintillator ceramics for assessment of the unpaired electron spatial distribution and definition of the electric field gradient at Al and Ga sites. First results were obtained on the quadrupole interaction for Al and Ga nuclei in garnet ceramics, and octahedral and tetrahedral Al and Ga positions were separated. The electric field gradients on Al and Ga were shown to be close in magnitude for both positions (*d* and *a*). The electric field gradient on aluminum nuclei near the Mn^{2+} ion possessing an excess negative charge in the garnet lattice was shown to be approximately 2.5 times larger than that on Al nuclei near the Ce^{3+} ion having a neutral charge in the lattice.

Acknowledgements

This work has been supported by the Ministry of Education and Science of Russia under agreements #14.604.21.0200, RFMEFI60417X0200.

References

1. H. Ogino, A. Yoshikawa, M. Nikl, J.A. Mares, J. Shimoyama, K. Kishio, J. Cryst. Growth **311**, 908 (2009).
2. P. Siyushev, K. Xia, R. Reuter, M. Jamali, N. Zhao, N. Yang, C. Duan, N. Kukharchyk, A. D. Wieck, R. Kolesov, J. Wrachtrup, Nature Communications **5**, 3895 (2014).
3. V. H. Schmidt, E. D. Jones, Phys. Rev. B 1, 1978 (1970).
4. A. G. Badalyan, G. V. Mamin, Yu. A. Uspenskaya, E. V. Edinach, H. R. Asatryan, N. G. Romanov, S. B. Orlinskii, P. G. Baranov, V. M. Khanin, H. Wieczorek, and C. Ronda, Phys. Status Solidi B 254, 1600631 (2017).

MRI study of the influence of superparamagnetic iron oxide nanoparticles (SPIONs) entrapped in cellulose microbeads on the relaxation properties of water in agarose matrix

Aleksandra A. Efimova[1], Yaroslav Yu. Marchenko[2], Peter I. Zaitsev[2], Angelina A. Agureeva[3], Inessa A. Fagradyan[3], Pavel P. Shirinkin[4], Svetlana A. Zubkova[4]

[1]Faculty of Physics, St. Petersburg State University, Russian Federation
[2]Laboratory of Medical Nanotechnology, "State Research Institute of Highly Pure Biopreparations", Russian Federation
[3]Faculty of Chemical and Biotechnology, St. State Technological Institute (technical University), Russian Federation
[4]Faculty of Electronics, St. Petersburg Electrotechnical University "LETI", Russian Federation
E-mail: sashaefimova15@yandex.ru
Scientific supervisor: Asoc. Prof. Dr. P. M. Tolstoy, Department of Physical Organic Chemistry Institute of Chemistry, Saint-Petersburg State University

Introduction

The method of magnetic resonance imaging (MRI) has found wide application in the field of medical diagnostics and monitoring, as well as for studying various characteristics of biological tissues. The prevalence of the method is due to the fact that the MR images show soft body tissues with different contrast, depending on the organs observed. The possibility of such studies is due to an intensive signal of protons of water, which is an integral part of living organisms. For effective diagnostics, paramagnetic substances are often used as contrast agents, providing significant enhancement of relaxation contrast. Therefore, research and development of such materials is of particular interest.

In this work, as a contrast agent we propose to use superparamagnetic iron oxide nanoparticles (SPIONs) entrapped in cellulose microbeads (CM) with or without a protective polymeric layer of chitosan. Cellulose is widely applied as biocompatible material in affinity chromatography and in cell separation technology. The cellulose can be converted into porous beads (spherocells) with high specific internal surface. Porous spherocells can uptake large amount of magnetite and have higher relaxivity than usual aqueous suspensions of SPIONs. CM/SPION system potentially may serve as a model contrast agent for MRI study of large eukaryotic cells such as macrophages and mesenchymal stem cells [1].

The goal of this work is to study the contrast enhancement by biocompatible mesoporous cellulose microspheres loaded by SPIONs (CM/SPION) by investigating the proton relaxation characteristic of water in agarose matrix.

Methods

Cellulose microbeads with high porous surface/volume ratio were formed by emulsification condensation of cellulose solution in oil. Particle's morphology is a tortuous network of large and very small pores. Gel-like structure with large pores (100–1000 nm) ensures an efficient water diffusion and exchange of external solvent with adsorbed water in cellulose body. This allows for co-precipitation reaction of iron oxide in cellulose.

The superparamagnetic iron oxide nanoparticles were prepared by co-precipitation of iron salts Fe^{2+}/Fe^{3+} in alkaline media at 80 °C. The precipitation was performed in mesoporous cellulose previously impregnated with iron salts and subsequent dropwise addition of NH_4OH under nitrogen gaseous atmosphere with vigorous stirring suspension.

The phantom samples were prepared in a 10 mm glass tube containing five 10 mm layers of various composition in agarose. Further, only the following five layers were

considered: agarose (1), spherocells (2), SPIONs entrapped in CM (3), SPIONs entrapped in CM with chitosan (67.5 μmol/L) (4) and SPIONs entrapped in CM with chitosan (6.75 μmol/L) (5).

MR images were collected using Bruker Avance III 400 WB spectrometer. The following pulse sequences were used: 1-TriPilot – for presetting the geometry of the tested slices; FLASH, RARE-T1 and TurboRARE-T2 – for obtaining contrast images of selected layers; RARE-T1+T2-map – for the subsequent analysis and determination of the relaxation characteristics.

Results

Figure 1 shows the sequence of five layers obtained with FLASH method.

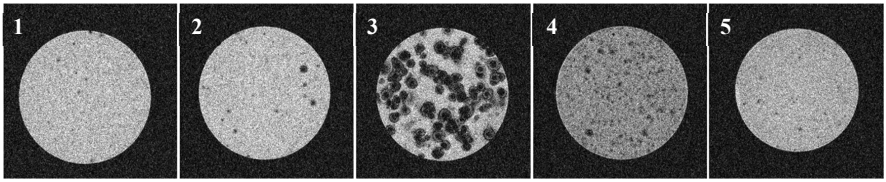

Figure 1. FLASH-images of five considered layers
(slice thickness is 0.5 mm, the size of each image is 12x12 mm)

On the images obtained with the RARE-T1+T2-map sequence in each layer in an arbitrarily chosen 1.2x1.2 mm area containing the investigated nanoparticles, the mean relaxation times T_1 and T_2 were calculated. The values obtained are presented in *Table 1*.

Table 1. Relaxation time constants T_1 and T_2 for investigated layers.

	Layer 1	Layer 2	Layer 3	Layer 4	Layer 5
T_1, ms	2450 ± 30	2855±79	2700±50	2376±23	2276±120
T_2, ms	51 ± 1	35±3	20±4	17±5	30±2

Microspheres loaded by SPIONs induce large perturbations of the magnetic field inside the globules and around them [2]. These magnetic perturbations manifest as black image voids shown in *Figure 1* (layer 3). The magnetized sphere behaves as a single magnetic dipole, whose filed drops as an inverse cube of the distance to the observed nucleus. The size of the nanoparticles estimated from the MRI in FLASH regime is comparable with the size estimated from the optical microscopy, shown in *Figure 2*. The results evidence that it is feasible to use cellulose microspheres for the study of biological cells labelled by SPIONs.

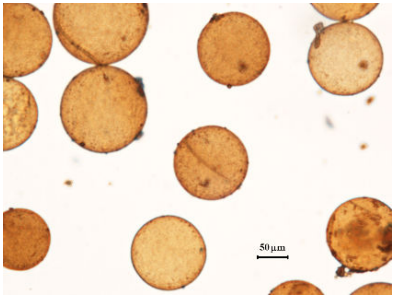

Figure 2. Light microscopy of cellulose microbeads loaded with SPIONs

Conclusions

- Biocompatible magnetic cellulose microspheres were produced by chemical deposition of iron oxide nanoclusters inside pores as model contrast agents for MRI diagnostics of magnetically labeled cells.
- Magnetic microbeads provide strong shortage of transverse relaxation times T_2 of water protons due to specific particle structure, high content of magnetic nanoclusters of magnetite, static-dephasing regime relaxation and intense water interchange in perturbed magnetic field around iron oxide nanocrystals.
- The study of phantom samples of gels loaded by microbeads by MR imaging demonstrates the contrast efficiency of magnetic cellulose microbeads as negative contrast agent.

Acknowledgments

We are grateful to B.P. Nikolaev, L.Y. Yakovleva, I.N. Voevodina for preparation of magnetic dispersions, cellulose microspheres and useful discussions, A.S. Mazur for help in conducting the MRI experiments.

References

1. C.V. Bowen, X. Zhang, G. Saab, P.J. Gareau, B.K. Rutt, *Magn. Reson. Med.*, **2002**, *48*, 52–61
2. R.J.S. Brown, *Phys. Rev.*, **1961**, *121*, 1379–1382

Mutual influence of low-frequency and microwave resonances in quantum magnetometers system with laser pumping of alkali atoms

Sergey V. Ermak, Eduard A. Sagitov, Vladimir V. Semenov

Dept. of Quantum electronics, Peter the Great St. Petersburg Polytechnic University, Saint-Petersburg, 195251, Russia
E-mail: e-sagitov@mail.ru

We have studied the mutual influence of low-frequency and microwave resonances in quantum magnetometers system with laser pumping ^{87}Rb vapor at the D_2 line of the head doublet. One of the magnetometers was based on a low-frequency spin generator principle, while the second one was built as passive microwave spectrometer with a resonance frequency lock loop. The paper analyzes the frequency shifts in the low-frequency and microwave channels of the tandem of magnetometers associated with the simultaneous action of the resonant radio fields on the alkali metal atoms and manifested in the frequency shifts of the spin generator for fixed changes in the amplitude of the microwave field. The physical nature of such frequency shifts is associated with the coherence circulation between the magnetic sublevels of the alkali atoms "dressed" by the spin oscillator low-frequency field. Absolute value of this shift strongly depends on the magneto-dipole transition number and reaches its maximum at 0-0 microwave transition, which is commonly used in the atomic frequency standards. The mutual influence of low-frequency and the microwave channels in magnetometers tandem was checked during the experiment in two modes: a) measurements of the frequency shift of the spin generator $\delta\nu_{SG}$ at the fixed detuning of the microwave frequency $\delta\nu_{UHF}$; b) measurements of the frequency shift for the microwave resonance $\Delta\nu_{UHF}$ at the fixed detuning of the spin generator frequency $\Delta\nu_{SG}$ due to the change of the phase shift in the feedback circuit. The experiment showed a big difference in the magnetometers tandem low-frequency and microwave channels interaction for operation modes "a" and "b": so for example, when the same artificial deviations $\delta\nu_{UHF}$ and $\Delta\nu_{SG}$ in magnetic field of 0.01 Oe $\delta\nu_{SG}$ respect to $\Delta\nu_{UHF}$ was the order of magnitude of 10^2.

Synthesis of sulfonated phthalocyanine complexes having triazole and naphthyl fragments

Anna A. Filippova[1], Mikhail I. Razumov[1], Serafima A. Znoyko[2], Artur S. Vashurin[2]

[1]Faculty of Fundamental and Applied Chemistry, Ivanovo State University of Chemistry and Technology, Russian Federation
[2]Ivanovo State University of Chemistry and Technology, Russian Federation
E-mail: anna.filippova96@gmail.com
http://www.isuct.ru

Introduction

Imparting solubility in various media to phthalocyanine macrocycles conduces their application in medicine [1], catalysis [2], electronics [3]. Introducing certain substituents into peripheral positions of a phthalocyanine makes it amphiphilic. Solubility in most of organic solvents may be reached by insertion of hydrophobic fragments of, for example, aliphatic or aromatic nature. Carboxy- or sulfo-groups placed on a periphery of the macrocycle impart solubility in water medium. Sulfonic groups are the most prospective ones due to increasing solubility' range depending on pH value. However, sulfonation enhances aggregation of a macrocycle in solution [4].

The work reports synthesis of bifunctionally-substituted derivatives of cobalt phthalocyanine having peripheral substituents of amphiphilic nature.

Experimental

NMR spectra of the solutions were recorded by means of NMR spectrometer Bruker AVANCE-500 (Germany) at operating frequency 500 MHz (^{1}H) at the temperature of 298.2 K. Chemical shifts were measured with reference to the internal standard – tetramethylsilane. The accuracy of measurements was ± 0.005 ppm.

Results

At first, compounds **I** and **II** were synthesized by melting cobalt(II) chloride with 4-(1-benzotriazolyl)-5-(1-naphthoxy)phthalonitrile and 4-(1-benzotriazolyl)-5-(2-naphthoxy) phthalonitrile, respectively. Corresponding sulfo-acids **III** and **IV** were obtained after (scheme 1).

Structural characterization of obtained compounds, being next step of the work, was performed by ^{1}H NMR-spectroscopy. Deuterated water D_2O and deuterated dimethylsulfoxide DDMSO were used as solvents. Presence of paramagnetic metal center (Co(II)) does not significantly affect ^{1}H NMR spectrum because of metal shielding by bulky peripheral substituents.

^{1}H NMR spectrum of **III** (500 MHz, DMSO (*d6*)): δ (ppm) 7.45 (Ar-5H), 7.94 (Ar-4H), 8.07 (Ar-6H), 8.29 (Ar-3H) – triazole group, 7.64 (Ar-8H), 7.73 (Ar-7H), 7.85 (Ar-11H), 8.18 (Ar-10H), 8.53 (Ar-9H), 8.85 (Ar-12H)– naphthoxy-group, 8.97 (SO_3H).

^{1}H NMR spectrum of **IV** (500 MHz, DMSO (*d6*)): δ (ppm) 7.48(Ar-5H), 7.75 (Ar-4H), 7.94 (Ar-6,7H), 8.14 (Ar-3H) – triazole group, 8.33 (Ar-2H) – macrocycle, 8.72 (Ar-8,9,11H) – naphthoxy-group, 8.83, 8.81 (SO_3H).

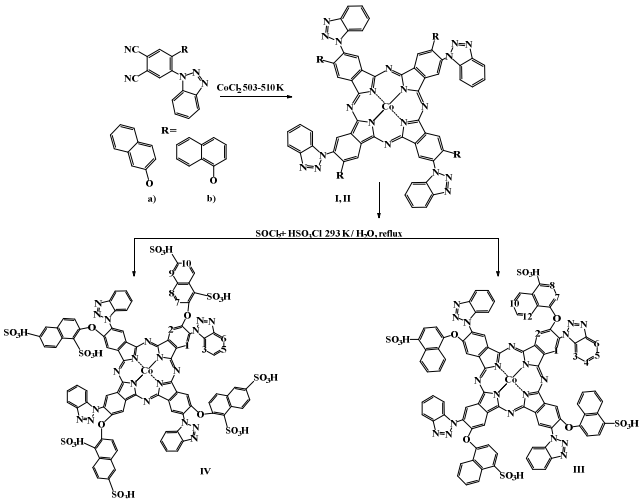

*Scheme 1. Synthesis of phthalocyanines **III** and **IV***

Chemical shift relative to standard sulfo-group protons' positions was found in NMR-spectrum of phthalocyanine **III** in DDMSO. This fact indicates the macrocycle to exist as molecular form. Signals of the same protons in D_2O are not shifted suggesting **III** to be ionized form. Most of the proton signals in D_2O for **III** are shifted into strong field region compared to signals of those ones in DDMSO. This is caused by association phenomenon occurred in a solution [5]. Associates in this case are formed due to overlapping π-electronic systems of phthalocyanine molecules.

Compound **IV** in D_2O has to be noted to exist in ionized state proved by absence of sulfo-group protons' signal in ^1H NMR spectrum.

Conclusion

Cobalt phthalocyaninates having triazole and sulfonaphthyl fragments on the periphery were obtained. Molecular or ionized state of the molecule was shown by means of NMR-spectroscopy to depend on the solvent's nature.

Acknowledgements

The work is supported by a grant from the President of the Russian Federation (grant number MK-161.2017.3).

References

1. W. Yu, M. Ye *et.al.* – *Nanomedicine*, doi:10.1016/j.nano.2018.02.005 (2018)
2. A. B. Sorokin. – *Chem. Rev.*, **113**, 8152–8191 (2013)
3. N. Silva, S. Calderon et.al. – *J. Electrochem. Soc.,* doi:10.1016/j.jelechem.2017.12.068 (2018)
4. T. Nyokong. – *Coord. Chem. Rev.*, **251**, 1707–1722 (2007)
5. S. M. Marcuccio, P. I. Svirskaya *et.al.* – *Can. J. Chem.,* **63**, 3057–3069 (1985)

Dynamic structure of noradrenalin according to NMR data and quantum mechanical calculations

Tatyana A. Ganina, Vyacheslav A. Chertkov

Lomonosov Moscow State University, Moscow, Russia
E-mail: tanushkin663@mail.ru

Introduction

The present work was aimed at quantifying the dynamic structure of noradrenalin and its protonated form according to NMR data and quantum mechanical calculations [1, 2]. Conformational dynamics in noradrenalin proceeds due to extremely fast processes of internal rotation around simple bonds C_1-C_2 and $C_{4'}$-C_1 (Fig. 1).

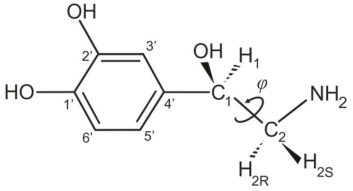

Figure 1. Structure and atom numbering of noradrenalin

Methods

The dynamic structure of noradrenalin and its protonated form in D_2O, CD_3OD and DMSO-D_6 solutions have been studied with the goal of obtaining accurate information to simulate molecular mechanisms of their action in living systems. The potential energy surface for internal rotation about the single C_1-C_2 bond has been constructed in terms of the Møller–Plesset second-order perturbation theory using *aug-cc-pvtz* basis set (Fig. 2).

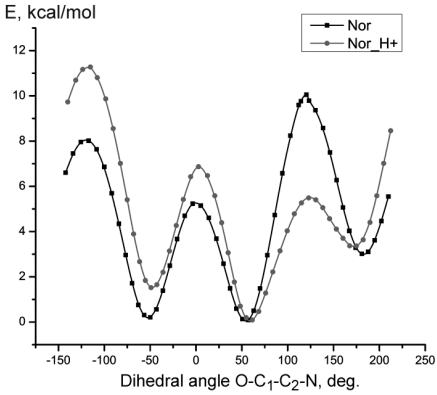

Figure 2. Potential energy surfaces of noradrenalin and its protonated form

The relative contributions of the conformers have been estimated by solving the vibrational problem according to the large-amplitude vibration model. Based on a set of high resolution of 1D and 2D experiments, complete spectral assignment of all peaks have been performed (including the signals of the diastereomeric protons H_{2S} and H_{2R}). This allows us to get the presentable set of NMR parameters good enough for succeed conformational analysis.

The conformational dependences of the most characteristic coupling constants for noradrenalin and its protonated form have been calculated at the FPT DFT B3LYP/6-311++G(2df,2p) level of theory.

Results

The most stable conformers of noradrenalin and its protonated form have **g+** and **g–** configuration (Fig. 3). The protonation of noradrenalin causes additional stabilization of **g+** form, which is obviously due to strong dipole-dipole interaction of polar groups of this conformer. In reasonable accordance with the data for adrenaline [3], our data shows the contribution of the form **t** with the transoid orientation of oxygen and nitrogen atoms does not exceed 1% for all solvents involved in this study.

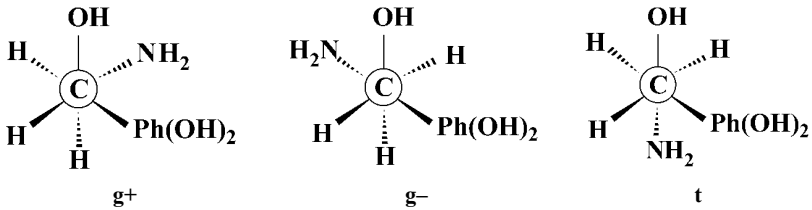

Figure 3. The principal conformers of noradrenalin

Acknowledgement

Authors express gratitude to Dr. D.N. Laikov for the valuable discussion.

References

1. T.A. Ganina, V.A. Chertkov – *Russ. J. Org. Chem*., **52**, 489-498 (2016).
2. T.A. Ganina, D.A. Cheshkov, V.A. Chertkov – *Russ. J. Org. Chem*., **53**, 12-23 (2017).
3. P. Carcabal, L.C. Snoek, T. Van Mourik – *Mol. Phys.*, **103**, 1633–1639 (2005).

Inhomogeneous magnetic state in mechanochemically synthesized nanopowder sample of $CuFeS_2$ according to $^{63,65}Cu$ NMR spectrum in the local field

Stanislav O. Garkavyi[1], Ekaterina V. Shmidt[1], Stanislav V. Shmidt[1], Vadim L. Matukhin[1], Nikolay K. Andreev[1], Erika Dutkova[2]

[1]Kazan State Power Engineering University, Kazan, 420066, Russia
[2]Institute of Geotechnics, Slovak Academy of Sciences, Košice, Slovakia
E-mail: ololoiev77@mail.ru

Introduction

Recently, semiconductor nanocrystals of chalcopyrite $CuFeS_2$ have attracted special attention as materials for possible application in energy technologies of direct energy conversion. The possibility of tuning the value of the band gap in a wide range caused an interest in nanocrystalline chalcopyrite for its use in solar cells. It was found that $CuFeS_2$ nanoparticles have a larger band gap (1.2 eV) than bulk chalcopyrite (0.6 eV), and this feature depends on the size and shape of the particles [1,2]. In addition, when studying the thermoelectric properties of nanosized chalcopyrite, a great decrease in the thermal conductivity and a significant increase of the power factor were found in comparison with the bulk sample [2]. Thereby, special attention is now devoted to the development of new methods for the preparation of chalcopyrite nanocrystals. In this paper, we present the results of a study of a nanopowder sample of chalcopyrite $CuFeS_2$ prepared by mechanochemical synthesis by the $^{63.65}Cu$ NMR method in a local field.

NMR spectrum of $^{63.65}Cu$ in a local field

The $^{63,65}Cu$ NMR spectrum in a local field were registered at T=77 K for the nanopowder sample of $CuFeS_2$ using the Tecmag-Redstone multipulse NMR/NQR spectrometer. For comparison, the $^{63,65}Cu$ NMR spectra in a local field were measured also for the sample of natural mineral $CuFeS_2$ (from the deposit Talnakh). The nanopowder samples under study containing particles of 30 nm dimensions was made using mechanochemistry method. The method used is described in detail elsewhere [3]. The resonance line measurements were performed by the NMR spin-echo method with synchronous detector using the step-by-step frequency swiping and signal accumulation. The first and second pulse duration were equal to 6 and 12 microsecond, correspondently. The intervals between pulses were chosen to be 55 microseconds, and the repetition time 150 ms. The signal was accumulated 3000 times at each step of signal recording, the signal sampling time 5 microseconds.

The $^{63,65}Cu$ NMR spectrum in a local field for the nanopowder sample of $CuFeS_2$ (Fig. 1a) represents itself two wide lines with maxima at the frequencies corresponding to central NMR transitions (1/2 <-> -1/2) of two isotopes of $^{63,65}Cu$ NMR. Satellite lines, represented for the natural $CuFeS_2$ in Fig. 1 (b), were not observed in the case of mechanochemically synthesized $CuFeS_2$ (Fig. 1a). The nuclear Hamiltonian is described by

$$H=-\gamma_N\hbar\mathbf{I}\mathbf{B}_{int} + h\nu_Q/6[3I_Z^2-I^2].$$

The first term of the Hamiltonian represents the Zeeman interaction between the nuclear magnetic moment $\boldsymbol{\mu}=\gamma_N\hbar\mathbf{I}$ and the internal (local) field $\mathbf{B}_{int}$, where γ_N is the nuclear gyromagnetic ratio and $\mathbf{I}$ is the nuclear spin. The second term in the Hamiltonian represents the nuclear quadrupole interaction between the electric field gradients (EFG) and the nuclear quadrupole moment Q. Here, ν_Q is the nuclear quadrupole frequency, defined by $\nu_Q=3eQV_{ZZ}/2I(2I-1)h$. The nuclear spins of ^{63}Cu and ^{65}Cu are equal to I = 3/2. Usually, for the antiferromagnetic state of this mineral six resonance lines are observed: three resonance line for each isotope. These three lines include the central line (ν_{CL}) corresponding to the transition

(1/2 <-> -1/2) in internal field, and two satellite lines (ν_{SL}) for the transitions (3/2 <-> 1/2) and transitions (-3/2 <-> -1/2) due to interactions of a quadrupole moment of a Cu nuclear with EFG at the positions of Cu nuclei [4]. The magnitude B_{int} of the internal field may roughly be evaluated from the frequency of the central transition ($\nu_{CL}=\gamma B_{int}$), neglecting the second order effect of the quadrupole interaction. Using the values ν_{CL}=19.81 MHz (21.24 MHz) and γ = 11.285 MHz/T (12.089 MHz/T) for ^{63}Cu (^{65}Cu), we obtain B_{int} =1.76 T (1.76 T) as an approximate value. The observed difference of the spectral line form of the nanopowder sample of $CuFeS_2$ of that of ^{63,65}Cu NMR of a semiconductor sample of natural $CuFeS_2$ allows us to suggest that the magnetic structure of the nanopowder sample is more complex and associated with its defective structure.

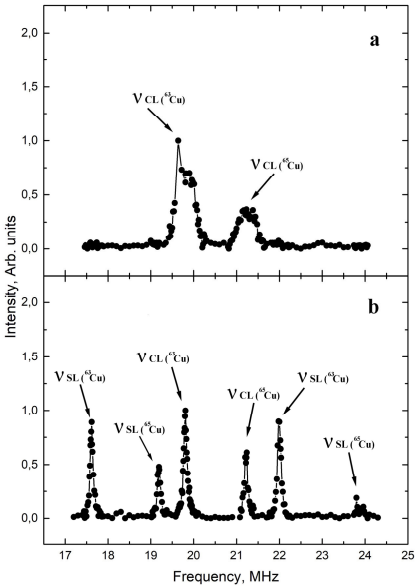

Figure 1. NMR spectrum of ^{63,65}Cu in a local field at 77K in $CuFeS_2$ samples, a - mechanochemically synthesized nanopowder sample, b - natural mineral sample

It was found in that nanopowder sample of mechanochemically synthesized $CuFeS_2$ has the heterogeneous state: simultaneously in a powder paramagnetic and ferromagnetic states coexist in a antiferromagnetic matrix. The experimentally observed NMR spectrum of ^{63,65}Cu is probably due to antiferromagnetic ordered areas of $CuFeS_2$. The satellite lines cannot be observed due to the defectiveness of a nanopowder under study that leads to the high spread of local electric and magnetic fields, large width of resonance lines with low amplitudes.

References

1. Wang Y.-H.A., Bao N., Gupta A. - Solid State Sci., Vol. 12, № 3. P. **387–390**(2010).
2. Liang D. Ma R., Jiao S., Pang G., Feng S. – Nanoscale, Vol. 4, № 20. P. **6265–6268** (2012).
3. Balaz P., Balaz M., Achimovicova M., Bujnakova Z., and Dutkova E.,- J. Mater. Sci. 52: **11851-11890** (2017).
4. Gavrilenko A.N., Pogoreltsev A.I., Matukhin V.L., Korzun B.V., Schmidt E.V., Sevastianov I.G. J. Low Temp. Phys. Vol. 175, № 5-6. P. **618–626** (2016).

Self-diffusion weighed MR imaging in low magnetic field

Svetlana V. Ievleva, Konstantin V. Tyutyukin, Viacheslav V. Frolov, Artem A. Voloshin

Faculty of Physics, Saint-Petersburg State University, Russia
E-mail: ievlevasvetlanka@mail.ru

Introduction

In the report a receiving of magnetic resonance diffusion weighed imaging (DWI) in a very low magnetic field. The special attention is paid to the receiving DWI of objects with short relaxation T_2 using three-pulse sequence. Experiments of this kind have been carried out first.

DWI in low field

The most apparatus for medical magnetic resonance imaging (MRI) uses a magnetic field several Tesla. That is connected with financial expenses and doesn't put to use MRI certain persons. The last decade an interest in low field MRI increases a few, but there are little DWI experiments. The first work was executed in the Earth field [1]. A difficulty of low field experiment consists not only of bad sensitivity but also of emergence of concomitant gradients [2] that distort image. In the presented study an intermediate field 7 mT has been used: 3 orders of magnitude less than standard high field (3 T) and 2 orders of magnitude more than Earth field (0.05 T). In this case a field is yet very low, but the concomitant gradients don't influence.

Three-pulse sequence technique

Common technique to realize DWI is Hahn echo. This technique has been used to get a low field DWI as it reported in [3]. In real objects, for example, as biological tissue, a difficulty due to a short relaxation time T_2 and slow diffusion arises. In such conditions the echo decays before molecules change its position noticeably. The difficulty increases in conditions of low field because as a rule T_2 shrinks with frequency reduction. Nevertheless in many cases T_1 remains rather long, and in such situation three-pulse sequence technique lets to register self-diffusion because the transversal magnetization doesn't decays during a spacing τ_2 between 2th and 3th pulses (see Fig. 1). For the reception of NMR signal so-called reflected echo is used.

The experiment was carried out with a home-build NMR mini-imager in field 7 mT. The imager admits samples up to 5 cm in diameter and in height and has no cooling system. For a control of generation of radiofrequency pulses, switching-on of gradient pulses and data acquisition interface National Instrument has been used. The special control computer program in “LabVIEW” has been created, and appropriate phantoms was made.

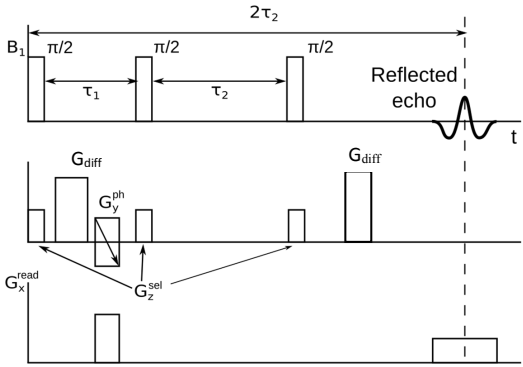

Figure 1. Diagram of pulse sequence for getting of DWI.
G_z^{sel} - slice selecting gradient, G_x^{read}, G_y^{ph} are frequency and phase encoding gradients, G_{diff} is diffusion gradient

References

1. A. Mohoricˇ, J. Stepisˇnik, M. Kos, G. Planinsˇic. Self-Diffusion Imaging by Spin Echo in Earth's Magnetic Field - *Journal of Magnetic Resonance* **136,** 22–26 (1999)
2. Chizhik V., Frolov V., Kupriyanov P., Tyutyukin K. Reduction of effect of concomitant gradients in low magnetic field MRI via optimization of gradient magnetic system - *Appl. Magn. Res.* **48,** 687-698 (2017)
3. Ievleva S.V., Luzhetckaia N.V., Tyutyukin K.V., Frolov V.V. Diffusion-weighted magnetic resonance imaging in an ultra-low magnetic field - *Appl. Magn. Res.* **48,** 699-706 (2017)
4. Chizhik V.I. Nuclear Magnetic Relaxation - Saint-Petersburg: Ed. SPBU (2004)

Synthesis of phthalodinitriles having bifunctionally-substituted fragments

Anastasia A. Kerner[1], Anna A. Filippova[1], Tatiyana V. Tikhomirova[2], Serafima A. Znoyko[2], Viktor V. Aleksandriiskii[2], Artur S. Vashurin[2]

[1]Faculty of Fundamental and Applied Chemistry, Ivanovo State University of Chemistry and Technology, Russian Federation
[2]Ivanovo State University of Chemistry and Technology, Russian Federation
E-mail: arenrek@gmail.com
http://www.isuct.ru

Introduction

Substituted phthalodinitriles are used for synthesizing macroheterocyclic compounds - phthalocyanines. Phthalocyanine macrocycles exhibit unique properties conducing application of them in fields of nonlinear optics [1], photonics [2], medicine [3]. There are a lot of ways of obtaining such compounds [4], though the most prospective one is synthesis starting from dinitriles. Directed functionalization of phthalodinitriles provides obtaining phthalocyanine molecules of desired properties [5].

Phthalodinitriles 4-(2-*tert*-butyl-4,5-dicyanophenylsulfonyl)benzene (**II**) and 4-(2-*tert*-butyl-4,5- dicyanophenylsulfonyl)benzoic acid (**III**) are synthesized and characterized by means of NMR spectroscopy resulting from current work.

Experimental

NMR-spectra of the solutions were recorded by means of NMR spectrometer Bruker AVANCE-500 (Germany) at operating frequency 500 MHz (^{1}H) at the temperature of 298.2 K. Chemical shifts were measured with reference to the internal standard – tetramethylsilane. The accuracy of measurements was ± 0.005 ppm.

Results

At first, disubstituted phthalodinitriles **II** and **III** were obtained by nucleophilic substitution of NO_2-group in refluxing DMF in presence of trimethylamine upon addition of thiophenol and 4-mercaptobenzoic acid, correspondingly (Fig. 1).

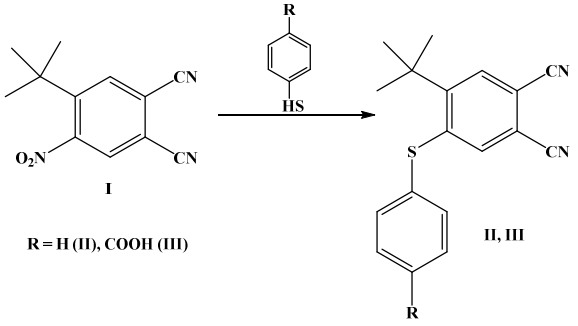

Figure 1. Synthetic route for phthalodinitriles II and III

Next step was confirmation of the structure of compounds **II** and **III** by ^{1}H and two-dimensional HMBC ^{13}C-^{1}H NMR-spectroscopy using $CDCl_3$ as a solvent (Fig. 2). According to ^{1}H NMR-spectra chemical shift of tert-butyl group (relative to standard being tetramethylsilane) was 1.56 and 1.60 ppm, respectively. Difference in chemical shift of t-Bu-

group for obtained compounds is small indicating no effect caused by replacing a proton with a carboxyl group. Signals of phenylsulfonyl group are registered in weak field – 7.33 and 8.15 ppm, correspondingly.

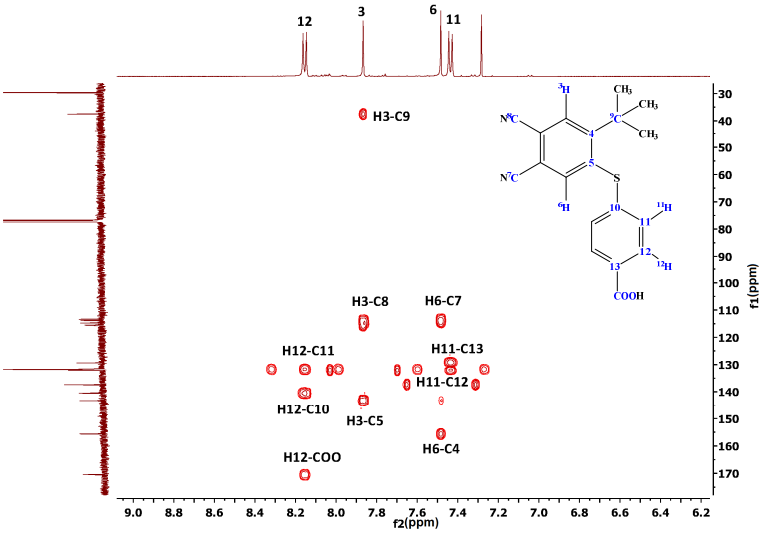

Figure 2. Two-dimensional spectrum HMBC ^{13}C-^{1}H of III

Heteronuclear two-dimensional NMR-spectroscopy ^{1}H–^{13}C HMBC was applied in order to additionally support signals' correlation and structure of obtained compounds. The method allows detection of correlating protons and carbon atoms. In this way, crossing signals of different C-H interactions were obtained.

Conclusion

Novel bifunctionally-substituted phthalodinitriles were synthesized. Structure of the compounds was confirmed by means of NMR-spectroscopy.

Acknowledgements

The work is supported by the Russian Science Foundation (project 17-73-20017).

References

1. M. Calvete, D. Dini. – *J. Photochem. Photobiol., C,* 35, 56-73 (2018)
2. E. Jiang, C. He *et.al.* – *Opt. Mater.,* 64, 193-202 (2017)
3. H. Akcay, R. Bayrak. – *Spectrochim. Acta, Part A,* 114, 531-540 (2013)
4. V. Nemykin. – *Rev. Acc.,* 2010, 136-208 (2010)
5. A. Vashurin, V. Maizlish *et.al.*– *J. Mol. Struct.,* 1160, 440-446 (2018)

The possibility of nuclear quadrupole resonance for distinguishing paracetamol different manufacturers and different forms (parties) from the same manufacturer of the spectral characteristics

Rustem R. Khusnutdinov[1], Irek R. Mukhamedshin[2]

[1]Institute of Electric Power Engineering and Electronics, Kazan State Power Engineering University, Kazan, Russia
[2]Institute of Physics, Kazan Federal University, Kazan, Russia
E-mail: khrr@yandex.ru

Introduction

There is a serious problem of counterfeit (counterfeit) medicines now. In different countries, the percentage of detected counterfeit medicines varies, including because government agencies that control the quality of medicines do not have sufficient laboratory facilities to conduct examinations. For example, in Russia there are only 12 monitoring and analytical laboratories subordinate to the Federal Service for Surveillance in Health Care (Roszdravnadzor) and these laboratories are subject to a check of less than one percent of the LP. According to various sources, the percentage of counterfeit in Russia ranges from 3-4% to 10-15% for some drug groups. In the world, it is estimated that counterfeit medicines represent approximately 10% for a total of 51.6 million pounds sterling [1, 2].

Paracetamol (PCM; IUPAC name: N-(4-hydroxyphenyl) ethanamide, C8H9NO2 or acetaminophen) is a widely used analgesic and antipyretic. It is produced under more than 80 trademarks (Panadol, Tylenol, Lekadol, Plicet, Daleron, Lupocet, etc.) in the form of tablets, capsules, powders and liquid suspensions. Cases of pronounced abuse of counterfeit paracetamol, among other medicines, have been reported in some less-developed countries in the last years [3, 4].

Paracetamol – (acetaminophen) antipyretic and analgesic medicine is one of the most popular drugs in the world. It is produced under more than 50 trademarks in various forms - tablets, capsules, powders, candles, syrups, etc. The great popularity led to the fact that paracetamol, despite the relatively inexpensive price, counterfeited often enough.

Nuclear quadrupole resonance (NQR) spectroscopy is a "fresh" method for detecting counterfeit medicines in a non-destructive way. Besides that it is possible to determine the authenticity of a medicine by comparing its spectrum with a reference ("fingerprint"), the NQR technique makes it possible to distinguish between drugs that contain the same active ingredient produced by different manufacturers (under different trademarks), as well as various batches and a series of medicines of one manufacturer.

NQR of paracetamol

Figure 1 shows the structure of the paracetamol molecule and the fragment of the spectrum. The frequencies of the NQR transitions, relaxation times, and line width parameters are given in Table 1.

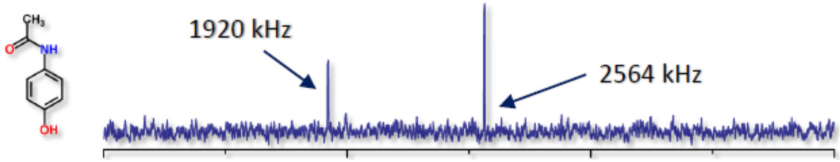

Figure 1. Molecule structure and NQR spectra of paracetamol

Table 1. The frequencies of the NQR transitions, relaxation times, and line width parameters for monoclinic form of paracetamol

NQR frequencies, ν, (MHz)	Δν, linewidth (Hz)	T_1, (s)
2,564	1,400	11
1,921	1,800	5
643		

Experimental

Measurements were performed on a spectrometer Apollo Tecmag. NQR experiments were carried out on *Apollo Tecmag* NQR/NMR console (0.1-100 MHz) with two-channel transmitter and one-channel receiver modules. Two *Tomco BT-00500-Beta* power amplifiers with output power of up to 500 W have been used. The detector unit includes transcoupler, a quarter wave lines π- filter 1,5-3.6 MHz bandwidth, a low-noise single-channel preamplifier Miteq and signal sensor. Using the sensor circuit shown in Fig. 2, where an optimally calculated [5] rectangular solenoid is used as the coil (L), it is possible to distinguish between different manufacturers according to the NQR spectrum.

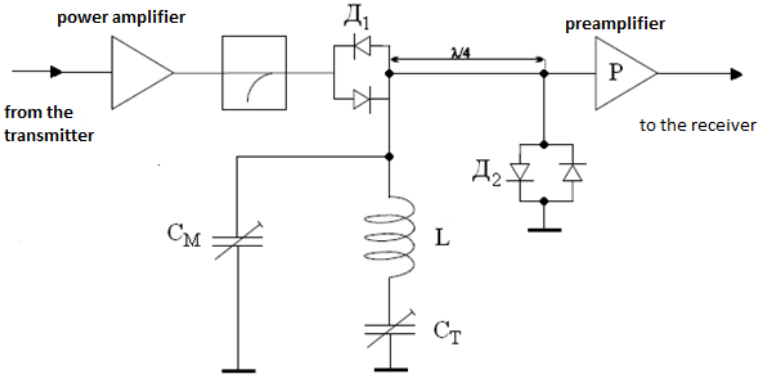

Figure 2. Switching scheme of the NQR signal sensor with the transmitter output and the preamplifier input. Here S_M is an alternating capacitor for matching the circuit, C_T is a variable capacitor for tuning the circuit at the resonant frequency, D_1 and D_2 cross-diodes

The results of the measurements show that, although the resonant frequency is the same for all the measured samples, the line width differs for different manufacturers. For different forms of the same manufacturer, a clear difference in the NQR spectrum for tablets and capsules was also obtained. According to [6] the broadening is the result of a narrow distribution in size of the tensor components of the electric field gradient 14N, mechanical stress caused by compression of tablets at the factory. The broadening differs at different frequencies. On the average, the broadening increases with increasing compaction pressure. The lines of paracetamol spectrum in powders, with a lower pressing pressure, give a narrower width line parameter.

References

1. Martino, R., Malet-Martino, M., Gilard, V., and Balayssac, S. Counterfeit drugs: analytical techniques for their identification. –*Analytical and Bioanalytical Chemistry,* 398(1), 77-92 (2010).
2. Gallagher, J. (2015). *http://www.bbc.co.uk/news/health-33183330*. (accessed January 26, 2018).
3. A.I. Wertheimer, J. Norris. – *Res. Social Admin. Pharm*., 5, 4–16 (2009).
4. Millions of counterfeit drugs seized in the EU, *http://topnews.in/millions-counterfeit-drugs-seized-eu-299089*.
5. Barras J., Katsura S., Sato-Akaba H., Itozaki H., Kyriakidou G., Rowe M. D., Althoefer K. A., and Smith J. A. S., Variable-pitch rectangular crosssection radiofrequency coils for the nitrogen-14 nuclear quadrupole resonance investigation of sealed medicines packets. – *Analytical Chemistry,* 84(21):8970- 8972 (2012).
6. Luznik J., Pirnat J., Jazbinsek V., Lavric Z., Srcic S., and Trontelj Z., The influence of pressure in paracetamol tablet compaction on 14N nuclear quadrupole resonance signal. – *Applied Magnetic Resonance,* 44(6), 735-743 (2013).

Analysis of correlation functions by method of molecular dynamics

Naira R. Khusnutdinova, Aidar R. Yulmetov

Institute of Physics, Kazan Federal University, Kazan, Russia
E-mail: nai.khus@yandex.ru

Introduction

The relations between the experimentally measured nuclear Overhauser effect (NOE) cross-relaxation rates and the spectral density makes it possible to use NMR to study of dynamic behavior of biomolecules. So, the correlation function, related with spectral density contains the most detailed information on molecular dynamics, which can be extracted using experimental methods – such as NMR spectroscopy. To get more detailed information we need computer modelling of molecular dynamics. We started with computer model and got correlation function, which could be compared with experiment.

Theory

In order to study the effect of internal dynamics on the accuracy of NMR structures, we generated correlation functions from a molecular dynamics trajectory. The theory relating relaxation rates accessible by NOE experiments to correlation functions describing molecular motions has been reviewed in publications [1, 2]. The main quantity derived in 2D NOE experiments is the cross-relaxation rate σ_{ij} describing the rate at which magnetization is transferred between spins i and j via dipolar coupling:

$$\sigma_{ij} = \frac{\pi}{5}\gamma^4\hbar^2[6J_{ij}(2\omega) - J_{ij}(0)] \quad (1)$$

where ω – Larmor frequency, γ – gyromagnetic ratio of protons. J_{ij} – spectral densities, which characterize the modulation of dipolar coupling between nuclei with time.

The spectral density is the Fourier transform of the correlation function of the dipole-dipole interaction [3].

$$J_{ij}(\omega) = 2\int_0^\infty C_{ij}(t)\cos(\omega t)\,dt \quad (2)$$

By means of the addition theorem for spherical harmonics, the expression for the correlation function for the vector between protons i and j can be written as:

$$C(t) = \frac{1}{5}\langle\frac{P_2(\hat{\mu}_{L,ij}(t)\hat{\mu}_{L,ij}(0))}{r_{ij}^3(t)r_{ij}^3(0)}\rangle \quad (3)$$

where $\hat{\mu}_{L,ij}$ − unit vector in the direction of the inter-proton vector, $r_{ij}(0)$ – the distance of the two protons, P_2 – second Legendre polynomial.

The same correlation function may be evaluated as a time average.

$$\tilde{C}(t_n) = \frac{1}{5}\frac{1}{M-n}\sum_{m=1}^{M-n}\frac{P_2\left(\hat{\mu}_{L,ij}(t_m)\hat{\mu}_{L,ij}(t_{m+n})\right)}{r_{ij}^3(t_m)r_{ij}^3(t_{m+n})} \quad (3)$$

Computer modelling

Studied molecule was modeled with GROMACs [4] package (fig. 1). Glycyl-glycyl-histadine (GGH) – molecules structure was relaxed through an energy minimization, then placed in water. There were made equilibration conducted in two phases – NVT, NPT (constant

Number of particles, Volume (or Pressure) and Temperature). Then were collected trajectories of nuclei of this molecule in water.

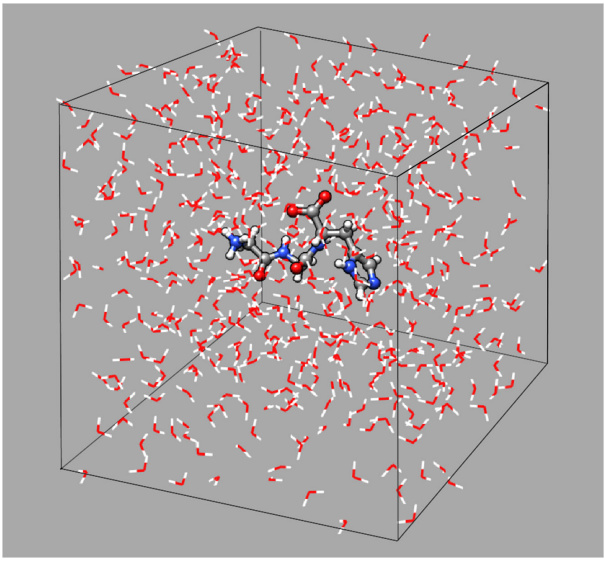

Figure 1. GGH-molecule in water

From obtained trajectories were calculated the distances of pairs of protons, basing on which it is possible to get correlation functions according (4).

With MatLab package was made code based on GROMACs trajectories data.

Example of such correlation function for 5, 6th protons is given below (fig. 2):

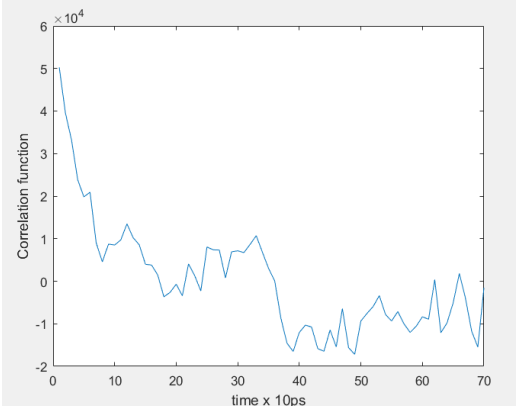

Figure 2. Correlation function

With these correlation functions it is possible to calculate spectral densities and theoretical values of cross-relaxation rates, which may be compared with experimental ones.

References

1. D. M. LeMaster, L. E. Kay, A.T. Brunger, J.H. Prestegard. Protein dynamics and distance determinations by NOE measurement. – *FEBS Letters.*, 236, 71-76 (1988).
2. C. B. Post. Internal motional averaging and three-dimensional structure determination by nuclear magnetic resonance. – *J. Mol. Biol.,* 224, 1087-1101 (1992).
3. T. R. Schneider, A.T. Brunger, M. Nilges. Influence of Internal Dynamics on Accuracy of Protein NMR Structures: Derivation of Realistic Model Distance Data from a Long Molecular Dynamics Trajectory. – *JMB*., 285, 727-740 (1999).
4. Berendsen, et al. GROMACS: A message-passing parallel molecular dynamics implementation. – *Comp. Phys. Comm.,* 91, 43-56 (1995).

Development of new polarizing agents for Dynamic Nuclear Polarization

Vytautas Klimavicius

Eduard-Zintl-Institute for Inorganic and Physical Chemistry,
Darmstadt University of Technology, Alarich-Weiss 8, Darmstadt, Germany
E-mail: vytautas.klimavicius@chemie.tu-darmstadt.de

Abstract

Solid-state Nuclear Magnetic Resonance spectroscopy (NMR) within last decades has developed into powerful tool to investigate technologically important innovative materials, as well as bio-solids. These include the investigation of intermolecular interactions at the interfaces of nanomaterials, as for example nano-particles, zeolites, metal-organic-frameworks (MOFs) or supported catalysts on carrier materials such as mesoporous silicates or other oxides [1]. Nevertheless, a major drawback in the application of solid-state NMR techniques is the inherent low sensitivity. The reasoning is the small energy differences of the nuclear spin-levels, which result in small population differences in thermal equilibrium, in other words, polarization. DNP is the most powerful and promising hyperpolarization technique due to much larger applicability for different systems of interest [2]. These days the main challenge DNP face is tailoring the technique to the systems of interest. It is performed by introducing radicals as polarizing agents (PA) to the system and there are several ways to proceed.

In present report new advancements in synthesis of novel PA and their application to DNP will be presented. A set of novel trityl-nitroxide biradicals were synthesized and their DNP performance was tested which showed similar enhancement factors as for conventional PA and DNP matrixes. Moreover, it was shown that high enhancement is achieved in studying catalytically active systems. It was shown that non-destructive matrixes and novel biradicals as PA are suitable for studying quadrupolar nuclei in complex catalytically active systems.

References

1. Gutmann, T.; Buntkowsky, G. In *Modern Magnetic Resonance*; Webb, G. A., Ed.; Springer International Publishing: Cham, 2017.
2. Lilly Thankamony, A. S.; Wittmann, J. J.; Kaushik, M.; Corzilius, B. *Progress in Nuclear Magnetic Resonance Spectroscopy* **2017**, *102-103*, 120-195

Collective dynamics in various antiferroelectric liquid crystal mesophases probed by NMR relaxometry

M. Knapkiewicz, M. Bielejewski, A. Rachocki

Institute of Molecular Physics Polish Academy of Sciences, M. Smoluchowskiego 17, 60-179 Poznan, Poland

After the discovery of polymer-stabilized liquid crystals, followed by a spectacular number of their applications, scientists from all over the world have started experiments with polymer stabilization of various liquid crystal phases. A continuation of this interesting trend has led to widening of the temperature range of the SmC*-alpha phase. This liquid crystal phase is characterised by very fast response time (of the order of microseconds), therefore in our opinion the polymer stabilization of this phase can soon become of great scientists' interest.

In our work we have concentrated on the effect of polymer network on the physical properties of the SmC*-alpha phase. Especially, the molecular dynamics of liquid crystal molecules was the aim of our study. The proposed research fits squarely into the current trend of searching for new composite materials for modern technology.

The first effort was focused on the characterization of the base liquid crystal materials. The molecular dynamics of different liquid crystal phases detected in the neat liquid crystal we would like to describe on the basis of the fast-field cycling ^{1}H NMR relaxometry experiments. The example of the data obtained from this method, the so-called relaxation profiles, are presented in the figure below.

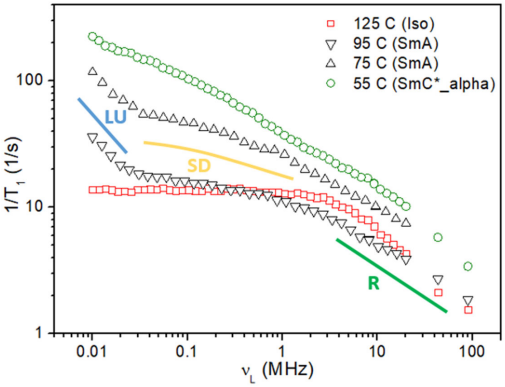

Figure 1. Proton spin-lattice relaxation times in D16 liquid crystal measured as a function of magnetic field strength (expressed in frequency units) at selected temperatures: overall molecular reorientational motion (R), self-diffusion (SD), layer undulations (LU)

The analysis of the experimental data will allow for calculation of physical quantities as structural factors, correlation times, diffusion coefficients, and cut-off frequencies. Thanks to the knowledge on these quantities the character and the time scale of dynamical processes occurring in the given mesophases will be gained.

Acknowledgments

The authors acknowledge support from ITC Conference Grant in the frames of COST ACTION CA15209 – European Network on NMR Relaxometry.

Quantum-mechanical calculations of hydrogen-bonded complexes of phosphine oxide H_3PO with various proton donors

Mikhail Kostin[1], Peter Tolstoy[2]

[1]Faculty of Physics, Saint-Petersburg State University
[2]Institute of Chemistry, Saint-Petersburg State University
E-mail: kostin-micha@mail.ru

The ^{31}P nucleus is of particular interest in the study of hydrogen-bound complexes by NMR methods. The reasons for this is that the phosphorus atom is often located close to proton-donor and proton-acceptor oxygen atoms, has a wide range of chemical shifts and exhibits 100% natural abundance and a high gyromagnetic ratio.

Correlations between the change of the proton chemical shift change upon complexation and the hydrogen bond geometry [1] or the energy [2] are often used for the spectral diagnostics of intermolecular complexes. Similar information on ^{31}P NMR spectra is scarce in the literature [3, 4].

In this work we focus on the study of model complexes (Fig. 1) formed by phosphinoxide H_3PO with hydrogen halides (a), nitrogen-containing heterocyclic compounds (b), alkenes (c), phenols (d), amines (e), carboxylic acids (f), alkanes (g), CH-acids of types HCN (h) and $CHCl_3$ (i) in the gas phase. The goal is to assess the possibility of using ^{31}P chemical shift as a marker for predicting the geometry and energy of hydrogen bonds.

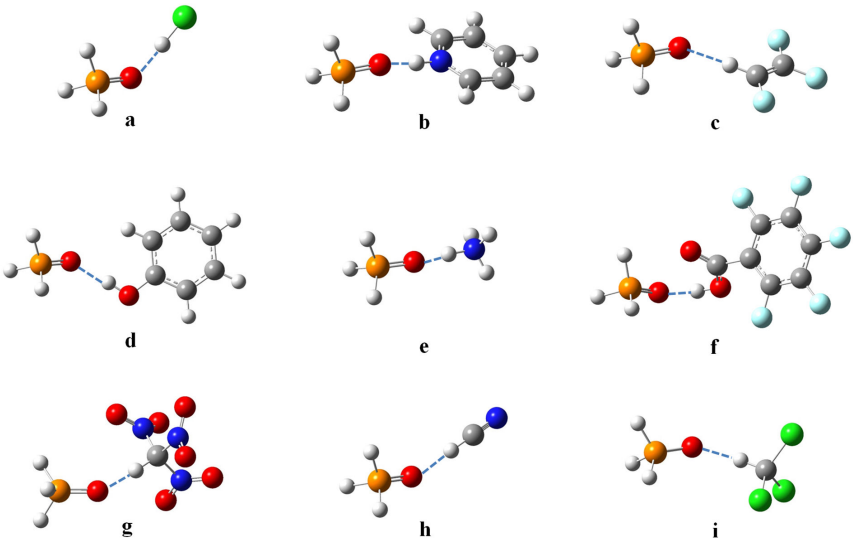

Figure 1. Complexes of phosphinoxide H_3PO with proton donor

Acknowledgements

This work was supported by RSF grant 18-13-00050.

References

1. H.-H. Limbach, P.M. Tolstoy, N. Perez-Hernandez, J. Guo, I.G. Shenderovich, G.S. Denisov, "OHO Hydrogen Bond Geometries and NMR Chemical Shifts: From Equilibrium Structures to Geometric H/D Isotope Effects with Applications for Water, Protonated Water and Compressed Ice", *Israel J. Chem.*, **2009**, *49*, 199-216.
2. G.S. Denisov, S.F. Bureiko, S.Y. Kucherov, P.M. Tolstoy, «Correlation Relationships between the Energy and Spectroscopic Parameters of Complexes with F···HF Hydrogen Bond», Dokl. *Phys. Chem.*, **2017**, *475(1)*, 115-118.
3. V.V. Mulloyarova, I.S. Giba, M.A. Kostin, G.S. Denisov, I.G. Shenderovich, P.M. Tolstoy, "Cyclic Trimers of Phosphinic Acids in Polar Aprotic Solvent: Symmetry, Chirality and H/D Isotope Effects on NMR Chemical Shifts", *Phys. Chem. Chem. Phys.*, **2018**, *20*, 4901-4910.
4. E.Yu. Tupikina, M. Bodensteiner, P.M. Tolstoy, G.S. Denisov, I.G. Shenderovich, "P=O Moiety as an Ambidextrous Hydrogen Bond Acceptor", *J. Phys. Chem.C*, **2018**, *122(3)*, 1711-1720.

^{1}H and ^{15}N NMR study of tautomerism in lyotropic chromonic liquid crystals

Kristina Kristinaitytė[1], Arūnas Maršalka[1], Laurynas Dagys[1], Nomeda Rima Valevičienė[2] and Vytautas Balevicius[1]

[1]Institute of Chemical Physics, Faculty of Physics, Vilnius University, Sauletekio 9-3, LT-10222 Vilnius, Lithuania
[2]Faculty of Medicine, Vilnius University, Santariskiu 2, LT-08661 Vilnius, Lithuania
E-mail: vytautas.balevicius@ff.vu.lt

Lyotropic chromonic liquid crystals (LCLCs) are a novel and important but relatively poorly studied class of soft matter. These materials have attracted considerable attention first of all in areas of electrooptics and inovative biomaterials [1]. The combination of self-assembling, ease of alignment, sensitivity to changing conditions and additives, coupled with their optical and electro-optical properties, makes these systems unique and valuable creating micropatterned materials and constructing various sophisticated components and devices, including polarizers, optical compensators, light-harvesting equipment. The fact that LCLCs are water-based, suggests and promises a future role in biosensing for medical diagnostics.

One of the most well-known LCLC material is 6-hydroxy-5-[(4-sulfophenyl)azo]-2-naphthalenesulfonic acid, also known as Sunset Yellow FCF (SSY) or Edicol. The purpose of the present work was to study the temperature and composition effects on the tautomerism dynamics in SSY aqueous solutions applying ^{1}H and ^{15}N NMR spectroscopy.

The DFT calculations predict that the dominant for SSY should be the hydrazone tautomeric form. The same conclusion concerning tautomeric forms was deduced using ^{13}C NMR [2]. However, some experimentally observed ^{13}C chemical shifts get into the range between the calculated values in azo- and hydrazone tautomers. The DFT predicted very huge difference of chemical shifts of nitrogens in those tautomeric forms – up to 260 ppm (!) and therefore ^{15}N NMR experiments look to be very promising. We decided to check this more precisely. The long-range ^{1}H–^{15}N correlation, widely known as HMBC experiment, was applied for this purpose. The observed chemical shift $\delta(^{15}\mathrm{N}) = -178$ ppm nicely correlates with the DFT calculated one at – 191.5 ppm for N–H nitrogen in hydrazone tautomer of SSY, whereas this peak in azo tautomer should be observed at +58.4 ppm. This means that ^{15}N NMR data confirm the dominance of hidrazone form of SSY at present conditions (0.7 M of SSY in water at 293 K).

References

1. J. Lydon, Chromonic review, *J. Mater. Chem*. 2010, **20**, 10071–10099.
2. D. J. Edwards, J. W. Jones, O. Lozman, A. P. Ormerod, M. Sintyureva, and G. J. T. Tiddy, Chromonic Liquid Crystal Formation by Edicol Sunset Yellow, *J. Phys. Chem. B* 2008, **112**, 14628−14636.

Neutralization of fluctuations in resonance conditions during registration of NMR spectra in the Earth's magnetic field

Pavel Kupriyanov, Vladimir Chizhik

St. Petersburg State University, Russia
E-mail: p.kupriyanov@spbu.ru

Introduction

NMR-spectra in weak fields are not split due to chemical shifts and they would seem uninformative for analysis of substances. Nevertheless, NMR in the Earth magnetic field allows ones to register the record resolution of spectra which are split due to heteronuclear interactions (*J*-coupling). Thus, the NMR in Earth magnetic field provides an opportunity to measure *J*-coupling constant with the highest accuracy. The proton spectrum has a symmetrical structure and a distance between lines determines the degree of spin interactions. As examples, several *J*-coupling NMR-spectra which were obtained with the home-built equipment [1] are represented.

There are some actual nuclear isotopes which interact with protons in liquid compounds (it is impossible to detect NMR in the Earth magnetic field in solids). The main such isotopes are presented in Table 1.

Table 1. The actual isotopes which interact with protons and form the indirect spin-spin J-coupling observed on in the Earth field NMR-spectra.

Nucleus	Abundance	Spin
^{19}F	100	1/2
^{29}Si	4.7	1/2
^{31}P	100	1/2
^{13}C	1.1	1/2

In the case of fluorine-containing liquids parameters of NMR-device allow us to register signals from both protons and fluorines. For example specter 2,2,2-trifluoroethanol (fig. 1).

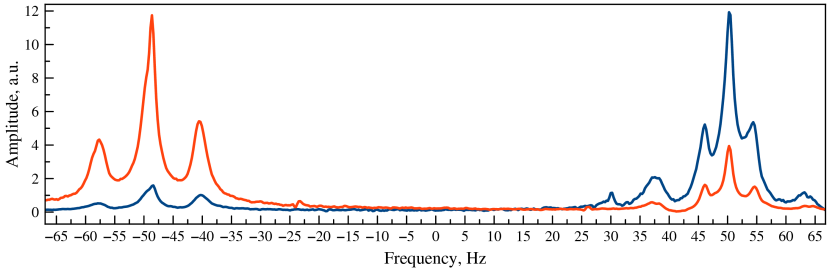

Figure 1. The spectra of 2,2,2-trifluoroethanol. The sensor of the NMR-spectrometer is tuned to the fluorine frequency (red) or to the proton frequency (blue)

Problems in the case of small natural abundance of interacting nuclei

It is very important to analyze organic liquids but the isotope ^{13}C has natural abundance of 1.1 % and satellites in proton spectra are very weak. In this case it would be effective the signal accumulation. Unfortunately, the Earth magnetic field is not stable enough, especially in

laboratory conditions. To neutralize the fluctuations of the Earth magnetic field we developed and patented the method of the stabilization of resonance conditions [2].

The principle is based on two-sensors scheme [3]. The first sensor contains an investigated sample. A sample in the second sensor is a proton liquid which possesses a single intensive line in the NMR-spectrum. The signal from the second sensor carries an information about the NMR-frequency variation with the Earth-field fluctuations. This signal is used as a reference signal when detecting a signal from the sample investigated. It allow the averaging NMR-signal as long as needed even in the most unfavorable conditions. The scheme of the device based on the method is presented in Fig. 2. The main difference from the work [3] consists in the method of forming the reference signal [2]. More details about the device construction one can find in [1, 2].

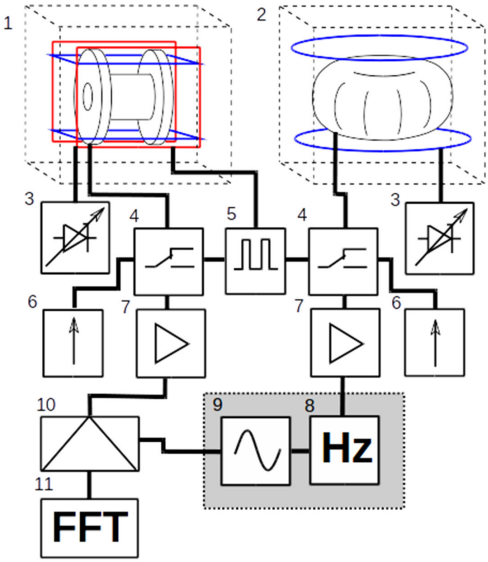

Figure 2. The device scheme for NMR-frequency stabilization: sensor for an investigated sample (1), reference sensor (2), shimm systems (3), commutation blocks (4), microcontroller (5), pre-polarization power supply (6), preamplifier (7), frequency counter (8), sine generator (9), quadrature detector (10), spectrum visualizer (11)

References

1. P. A. Kupriyanov, K. A. Dmitriev, A. V. Chizhik. On some improvements of nuclear magnetic resonance in the earth's magnetic field registration. Vestnik SPSU, T. 3. № 1. pp. 59-69. 2016.
2. V. I. Chizhik, P. A. Kupriyanov. Equipment for stabilizing the frequency of nuclear magnetic resonance in the Earth's magnetic field. Patent of Russian Federation № 175974. Bull. № 36. 2017.
3. A. Mohoric, G. Planinsic, M. Kos, A. Duh, J. Stepisnik. Magnetic Resonance Imaging System Based on Earth magnetic field". Instrumentation Science and Technology, Vol. 32, No. 6, pp. 655-667, 2004.

^{71}Ga, ^{77}Se, ^{115}In MAS NMR study of $TlGaSe_2$ and $TlInSe_2$ powder

G. S. Kupriyanova[1], I. Mershiev[1], G. V. Mozzhukhin[2], Esra Okumuş[2], and MirHasan Yu. Seyidov[2,3]

[1]Immanuel Kant Baltic Federal University, A. Nevsky St. 14, 236041, Kaliningrad, Russia
[2]Gebze Technical University, 41400 Gebze/Kocaeli, Turkey
[3]Institute of Physics Azerbaijan National Academy of Sciences, AZ - 1143 Baku, Azerbaijan

Introduction

Layer-chain crystals of the $TlMeX_2$ type are intensively studied by various methods because of their unusual properties and the relatively high positive Seebeck coefficient. The ternary chalcogenide $TlGaSe_2$ and $TlInSe_2$ are low-dimensional semiconductors, which exhibits photoconductive properties, negative differential resistance in the current-voltage characteristic, the memory effect and optical second harmotic generation [1]. The sequences of phase transitions in $TlGaSe_2$ and $TlInSe_2$ are found with the formation of modulated structures [2]. It was shown that the transformation from the high temperature paraelectric phase to the low temperature ferroelectric phase occurs via an incommensurate phase that exists in the temperature range from Tc = 107.5 to Ti = 118 K. Based on the dielectric measurements, the third phase transition around 100-103 K revealed a phase transition, which is accompanied by the formation of a ferroelectric state in $TlGaSe_2$. The phase transitions were found at high temperatures 200-215 K и 240-250 K [1-3]. However, there is no consensus on the existence of high-temperature phase transitions.

Experimental results

In the present paper we report on ^{71}Ga, ^{77}Se and ^{115} In MAS NMR studies of $TlGaSe_2$ and $TlInSe_2$ powders. The main aim of the paper is to investigate the presence of phase transitions at relatively high temperatures from -60 to 370 K. The ^{71}Ga, ^{77}Se and ^{115} In static NMR spectra and the spectra for sample rotation about the magic angle (MAS) were obtained using the Hahn echo (π / 2-τ -π) pulse sequence. The duration of the π / 2 pulses are 2.7 μs and 2.5 μs for ^{71}Ga and ^{77}Se and ^{115} In. Temperature dependences of ^{71}Ga, ^{77}Se NMR spectra and ^{71}Ga spin-lattice relaxation times T1 were measured using a NMR Varian 400 spectrometer, with superconducting magnet (B0 = 9.35 T) in the temperature range 200-330 K. The NMR MAS spectra and T1 were investigated at different rotational speeds of the sample to reveal a quadrupole interaction contribution to the linewidth and its varies with temperature. The spin-lattice relaxation times T1 were measured by means of the inversion-recovery sequence at different rotational speeds of the sample. The sequence pulses were synchronized with the rotation speed of the sample.

There was a splitting of the central component of the spectrum at a rotational speed of 5 kHz for ^{71}Ga NMR line. Both components of the ^{71}Ga NMR line spectrum have experienced contraction by lowering the temperature to 210 K. The linewidth of the central component had a minimum value at a speed of the sample 16 kHz and two satellites appeared. When the temperature decreases to 210 K, the signals of satellites were manifested in an antiphase (Fig. 1). Modeling of the ^{71}Ga and ^{115} In NMR MAS line shapes were carried out in order to identify contributions from quadrupole interaction in the presence of other types of interactions, such as anisotropy of chemical shift, indirect spin-spin Ga-Tl or In –Se interaction and dipole-dipole interaction. Since quadrupole interactions are weakened for the observed lines for powder samples due to the random distribution of crystallites, only the first order of splitting and the second order of the shift of the central component were considered. It was taken into account that if the rotation speed of the sample in MAS experiment exceeds the shift of the second order, the tensor components of the quadrupole Hamiltonian can be transformed to the

coordinate system associated with the natural axes of the gap tensor. The changes caused by the rotation of the sample were interpreted in terms of the quadrupole Hamiltonian and quadrupolar contributions were extracted.

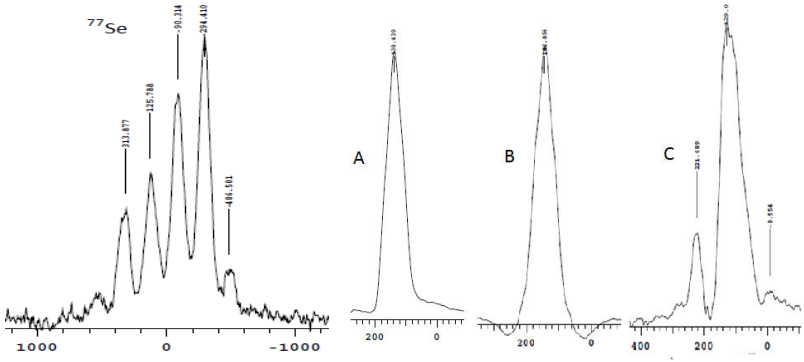

Figure 1. ^{77}Se and ^{71}Ga NMR spectra A) The static spectra were obtained using the Hahn echo ($\pi/2-\tau-\pi$) pulse sequence at 10 kHz, B) The MAS spectra with rotation of sample at 10kHz at T=65K, C) with rotation of sample at 5kHz

Acknowledgements

TUBITAK grant under the Programme 2221 for Visiting Scientist (G. S. Kupriyanova). Authors also acknowledge a partial support by East Marmara Development Agency (MARKA, project No. TR42/16/ÜRETİM/0013) and by Research Fund of Gebze Technical University (grants Nos. BAP 2015-A-19 and BAP 2017-A-105-44).

References

1. A. M. Panich, S. Kashida. Single-crystal NMR for the layered semiconductor TlGaSe2/ Journal of Physics Condensed Matter · September 2008 395211 (8pp) (doi:10.1088/0953-8984/20/39/395211)
2. Volkov A A, Goncharov Yu G, Kozlov G V, Lebedev S P, Prokhorov A M, Aliev R A and Allahverdiev K P 1983 *JETP Lett.* **37** 615
3. Abutalybov G I, Larionkina L S and Ragimova N A 1989 *Sov. Phys.—Solid State* **31** 312

Novel mixed-matrix membrane based on composite PVA – carboxyfullerene: preparation and characterization

Anna I. Kuzminova, Maria E. Dmitrenko, Anastasia V. Penkova, Sergey S. Ermakov

Institute of Chemistry, St. Petersburg State University, 7/9 Universitetskaya nab., St. Petersburg, 199034, Russia
E-mail: ai.kuzminova@mail.ru

Introduction

Currently membrane methods are alternative processes to traditional separation methods due to good characteristics. Pervaporation is a well-known membrane separation process, which is attractive and widely used in different industrial fields as an alternative process to distillation or liquid-liquid extraction. The potential of this process is especially suitable for the dehydration of different mixtures. The rapid development of membrane processes, in particular pervaporation, requires the essential improvement of the transport properties of polymer membranes that can be achieved by one of the promising and effective methods - the modification of the polymer matrix by inorganic filler to develop the mixed-matrix membranes (MMMs). MMMs combine advantages of both an inorganic and organic components and they offer the possibility to overcome the trade-off between the permeability and selectivity of the polymeric membranes. Among inorganic particles, fullerene takes an important place, since this nanoparticle retains its unique π-electronic structure inside of the polymer matrix. In the present research polyvinyl alcohol (PVA) was used as the polymeric network and combined with a water soluble fullerene derivative - carboxyfullerene used as a modifier and cross-linking agent for PVA.

The aims were to develop novel mixed-matrix membranes based on polyvinyl alcohol and its composites with carboxyfullerene and to study the correlation of structure peculiarity with transport properties for pervaporation dehydration. The structural properties of the developed composites were studied by nuclear magnetic resonance, X-ray diffraction analysis, scanning electron microscopy, sorption experiments and measurement of contact angles. Thermal properties and stability were investigated by thermogravimetric analysis and differential scanning calorimetry. The transport properties of developed membranes were tested for dehydration of industrially important solvent ethanol in a wide range of concentrations (4.4 - 90 wt.% water in the feed) by pervaporation at different temperatures. It has been shown that the addition of carbon particles to PVA matrix leads to the significant change and the improvement of membrane properties due to the changes in the structure and morphology.

Acknowledgements

This work was supported by Russian Foundation for Basic Research [grant No. 17-58-04067]. The experimental work was facilitated by equipment from Resource Centers: Research Centre for Nanotechnology, Research Centre for X-ray Diffraction, Research Centre for Physical Methods Surface Investigation, Magnetic Resonance Research Centre, Thermal Analysis and Calorimetry, Chemical Analysis and Materials Research Centre and GEOMODEL at St. Petersburg State University.

Investigation of neodymium doped YVO_4 by EPR method

Rodion F. Likerov[1], Valeriy F. Tarasov[2], Rushana M. Eremina[1,2], Ivan V. Yatsyk[1,2], Tatyana P. Gavrilova[1,2], Alexey V. Shestakov[2], Konstantin B. Konov[2], Yury D. Zavartsev[1,3], Sergey A. Kutovoi[1,3], Vladimir A. Shustov[2]

[1]Institute of Physics, Kazan (Volga Region) Federal University, Kazan, 420008 Russia
[2]Zavoisky Physical-Technical Institute (KPhTI) of the Kazan Scientific Center of the Russian Academy of Sciences, Kazan, 420029 Russia
[3]Prokhorov General Physics Institute, Russian Academy of Sciences, Moscow, 119991 Russia
E-mail: rodionlikerov@gmail.com

Introduction

At present paramagnetic centers formed by impurity rare-earth ions in crystals are considered as a promising material for quantum memory devices, for example YVO_4: Nd^{3+} [1, 2]. Electron paramagnetic resonance (EPR) is a convenient method to study paramagnetic centers. It is necessary to obtain values of g-tensor, A-tensor of hyperfine structure and crystal field parameters. Also, it is important to know relaxation times (spin-lattice and spin-spin) [3].

Neodymium doped YVO_4 crystals were grown by the Czochralski method in Ir crucibles in the 99 vol.% Ar + 1 vol.% O_2 atmosphere. The purity of primary components, i.e., V_2O_5 and Nd_2O_3 was no worse than 99.75%. We studied two YVO_4 monocrystals doped with 0.005 at. % $^{143}Nd^{3+}$ and 0.005 at. % $^{145}Nd^{3+}$. The first crystal contains only the ^{143}Nd isotope (sample I), the second crystal (sample II) contains only the ^{145}Nd isotope.

EPR experiments

Neodymium is a rare-earth element with seven stable isotopes: two odd isotopes Nd-143 and Nd-145, five even isotopes Nd-142, Nd-144, Nd-146, Nd-148, Nd-150. It is possible to observe hyperfine interactions only with odd isotopes, because of non-zero nuclear magnetic moment I=7/2. Neodymium ion Nd^{3+} electron configuration is $4f^3$, its main ground state is $^4I_{9/2}$. Since full magnetic moment J=9/2, neodymium ions are described by Kramers theorem, which states, that eigenstate are at least doubly degenerate, all calculations are done in approximation of effective spin, S_{eff} =1/2. Hamiltonian, which contains g-tensor and A-tensor is shown below:

$$\mathrm{H} = (\mathbf{S} * \mathbf{A} * \mathbf{I}) + \beta(\mathbf{H} * \mathbf{g} * \mathbf{S_{eff}}) \quad (1)$$

We observe 8 lines (2I+1) of hyperfine structure on EPR spectra of ^{143}Nd and ^{145}Nd. If sample putted into rotating magnetic field then the result will be angular dependence of resonance magnetic field. Angular dependencies of resonance magnetic field, rotated in (ac)- and (ab) planes of the monocrystal YVO_4:$^{143}Nd^{3+}$ was obtained on X-band EPR spectrometer Bruker EMX+ at T = 15K. The angular dependence is shown at figure 1 for (ac) plane.

Circles are presenting experimental data of resonance magnetic field, and solid lines are the fitting, calculated in EasySpin application [5]. The values of g-tensor and A-tensor were obtained for both sample I and sample II and are presented in Table 1.

Temperature dependences of spin-lattice and spin-spin relaxation times were measured for both samples. Theoretical calculation of spin-lattice relaxation times was obtained with following formula [6]:

$$T_1^{-1} = AT + BT^9 + Cexp\left(-\frac{\Delta}{kT}\right) \quad (2)$$

Parameters of fitting are following: A = 0.254 $c^{-1}K^{-1}$, B = $2.03 \cdot 10^{-6}$ $c^{-1}K^{-9}$, C = $1.9118 \cdot 10^{11}$ c^{-1}, Δ = 163.5 K.

Temperature dependences of spin-lattice and spin-spin relaxation times are presented at figure 2 and 3 respectively.

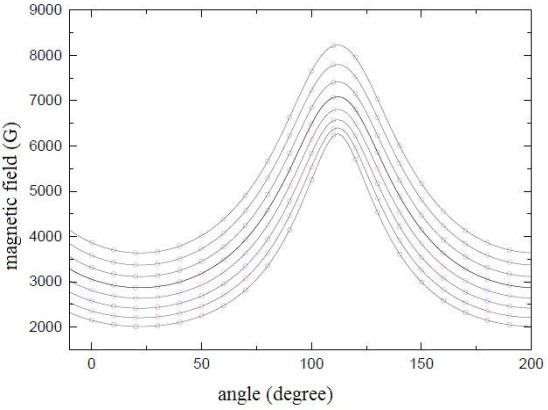

Figure 1. Angular dependence of resonance field, rotated in (ac), of the monocrystal YVO_4:$^{143}Nd^{3+}$ at T = 15K

Table 1. g-tensor and A-tensor for Nd-ions in YVO_4

	Our calculations		Guillot – Noel [4]	
	Nd-143 (sample I)	Nd-145 (sample II)	Nd-143	Nd-145
gt	2.358	2.3403	2.361±0.004	
gz	0.915	0.9136	0.915±0.003	
At	764.8 MHz	473.1516 MHz	$256.9*10^{-4}$ cm^{-1} = 770.7 MHz	$159.3*10^{-4}$ cm^{-1} =477.9 MHz
Az	358.1 MHz	186.444 MHz	$112.1*10^{-4}$ cm^{-1} =336.3 MHz	$70*10^{-4}$ cm^{-1} = 210 MHz

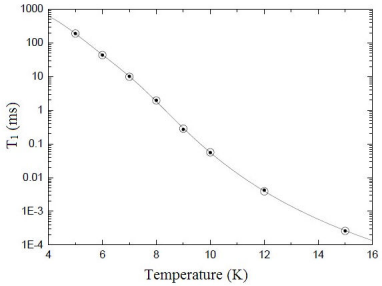

Figure 2. Temperature dependences of spin-lattice relaxation times of odd neodymium isotopes in YVO_4 monocrystals

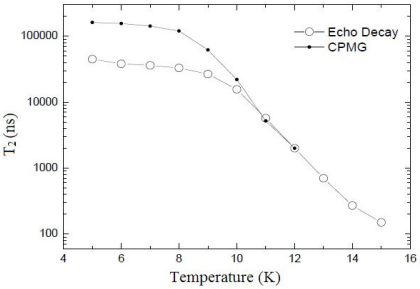

Figure 3. Temperature dependences of spin-spin relaxation times for $^{143}Nd^{3+}$ ion in YVO_4 monocrystal, obtained with ($\pi/2 - \pi$) sequence (empty circles) and with CPMG sequence (dots)

Acknowledgements

This work was supported by the Russian Science Foundation (project no. 16-12-00041).

References

1. C. W. Thiel, Thomas Böttger, R.L. Cone, J. Lumin. **131**, 353 (2011).
2. C.W. Thiel, Y Sun, R M Macfarlane, Thomas Böttger, R. L. Cone, J. Phys. B: At. Mol. Opt. Phys. **45**, 124013 (2012).
3. Y. Sun, C.W. Thiel, R.L. Cone, R.W. Equall, R.L. Hutcheson, J. Lumin. **98**, 281 (2002).
4. O Guillot-Noel, A. Kahn-Harari, B. Viana, D. Vivien, E. Antic-Fidancev, P. Porcher, J. Phys. Condens. Matter **10** 6491–6503 (1998).
5. R. M. Eremina, V. F. Tarasov, K. B. Konov, T. P. Gavrilova, A. V. Shestakov, V. A. Shustov, S. A. Kutovoi, Yu. D. Zavartsev, Appl Magn Reson **49:53–60** (2018)
6. R. Beach, M. D. Shinn, L. Davis, R.W. Solarz, W. F. Krupke, IEEEJ. Quantum Electron. **26**, 1405 (1990)

Calculation of the magnetic shielding tensor on ^{125}Te and ^{207}Pb nuclei in PbTe

Irina Lushpinskaya, Marina Shelyapina

Saint Petersburg State University, Department of Nuclear-Physics Research Methods
E-mail: irinapavlovna94@mail.ru

Lead telluride is a semiconductor with a narrow slit long used for thermoelectric applications [1]. Among the many ways to interrogate the state of semiconductors such as PbTe, nuclear magnetic resonance (NMR) of both nuclei has been extremely valuable in assessing the electronic state. For example, the Knight shift, which probes the interaction of nuclear spins with conduction band carriers (electrons or holes), provided a direct measure of carrier concentration. This readout can be performed even on samples that are not amenable to transport studies. Such readouts could, in principle, aid in the development of novel materials which cannot be produced as high quality thin films or single crystals. This potentially important technological application is currently hampered, however, by inability to separate Knight shift from chemical shift. From this perspective a correct calculation of chemical shift is highly required. Here we report on the results of our calculations of chemical shift on ^{125}Te and ^{207}Pb nuclei focusing on correct consideration of spin-orbital coupling (SOC), that could be important for heavy nuclei.

The band structure and chemical shift calculations in PbTe were done using the full-potential linearized augmented plane wave (FLAPW) method as implemented in WIEN2K package. Calculations were carried out using the generalized gradient approximation (GGA) with the exchange and correlation potential of Purdue-Berck-Ernzerhof (PBE), which is the standard GGA potential for solids. A cutoff $R_{MT}K_{max}$=7.0 for the plane-wave vector was used. Here, K_{max} is the plane-wave cutoff, and R_{MT} is the muffin-tin radius, which is taken as 2.5 bohr for all atoms. SOC was treated as a second variational procedure with scalar relativistic orbitals as a basis where states up to 8 Ry above the Fermi level were included in the basis expansion. In all calculations, self-consistency was achieved with a tolerance in the total energy of 0.1 mRy. For both ground state and NMR calculations a total number of 21×21×21 k-points was used.

PbTe crystallizes into a face centered cubic structure that with the space group Fm-3m (# 225). The unit cell is shown in Fig. 1. To optimize the crystal geometry the total energy of the unit cell was calculated as a function of the unit cell, the result is shown in Fig. 2. The lines correspond to the fitting within the Birch-Murnaghan equation of state. The optimized lattice parameter value is given in Table 1 for the both cases, with and without SOC. The calculations slightly overestimate the lattice parameter compared with experiment, 6.462 Å [2]. Accounting for SOC decreases the total energy but does not affect much the optimized lattice parameter value.

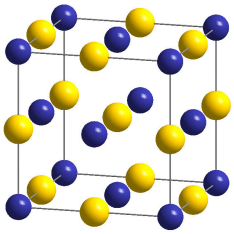

Figure 1. Unit cell of PbTe (Pb and Te atoms are marked in yellow and blue, respectively)

Using the obtained lattice parameter value, the magnetic shielding tensor σ on both ^{125}Te and ^{207}Pb nuclei was calculated. In cubic crystal $\sigma_{xx} = \sigma_{yy} = \sigma_{zz} = \sigma_{iso}$. The σ_{iso} value is listed in Table 1. As one can see from Table 1 accounting for SOC does not affect much σ_{iso} for both nuclei only slightly decreasing its value. Further, for ^{125}Te the calculated absolute chemical

shift was compared with experiment. It should be noted that in experiment one determines not the absolute but the relative chemical shift:

$$\delta_{iso}^{X} = \sigma_{iso}^{ref} - \sigma_{iso}^{X}$$

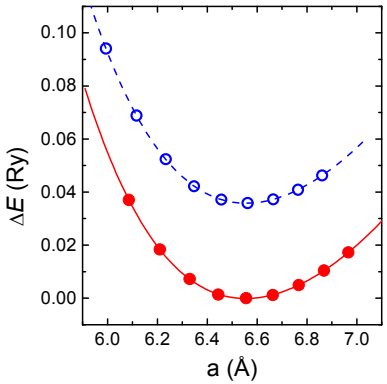

Figure 2. The total energy of the PbTe versus the lattice parameter. Open and solid symbols correspond to the calculation without and with taking into account spin-orbital coupling, respectively. The energy is given relative to the minimal value, obtained within SOC calculations.

Table 1. Lattice parameter and absolute for ^{207}Pb and ^{125}Te and relative for ^{125}Te chemical shift values in PbTe calculated without and with considering SOC.

Parameter	Without SOC	With SOC
a (Å)	6.5556	6.5540
σ_{iso} ^{207}Pb (ppm)	4772	4725
σ_{iso} ^{125}Te (ppm)	3886	3832
δ_{iso} ^{125}Te (ppm) *	-498	-445

*relatively to the absolute experimental shift in $TeMe_2$ [3]

For ^{125}Te NMR frequency is normally calibrated using the unified scale Ξ relative to a dimethyl telluride solution $TeMe_2$. The absolute σ_{iso} value for $TeMe_2$ is equal to 3388 ppm as determined in Ref. [3]. The relative chemical shift for ^{125}Te is given in Table 1 and can be used for correct separation chemical and Knight shift in experiment [4].

Acknowledgements

All calculations were carried out at the Computing Center of the Research Park of Saint Petersburg State University.

References

1. LaLonde, A. D.; Pei, Y.; Wang, H.; Snyder, G. J. Mater. Today 14 (2011) 526.
2. R. Dalven, Infrared Phys. 9 (1949) 141.
3. Y. Ruiz-Morales, G. Schreckenbach, T. Ziegler. *J. Phys. Chem. A* 101 (1997) 4121.
4. R.E. Taylor, F. Alkan, D. Koumoulis, M.P. Lake, D. King, C. Dybowski, L.S. Bouchard. J. Phys. Chem. A, 117 (2013) 8959.

Metabonomic study of the hypothyroidic effect of Sunitinib, a tyrosine kinase receptor inhibitor, in the rat

Dorian Maroil, Virginie Delsinne, Vanessa Tagliatti

Human Biology and Toxicology, faculty of medicine and pharmacy, UMONS, Belgium
E-mail: dorian.maroil@umons.ac.be
https://web.umons.ac.be/fr/

Introduction

Renal cell carcinoma is one of the most common and deadly cancer. This cancer suffers of an extremely poor prognosis due to its low survival rate in the long term and the incidence of metastasis. To date, there is no successful treatment although a multi-targeted receptor tyrosine kinase inhibitor, Sunitinib, gives significant results thanks to a strong antiangiogenic activity blocking the tumor development. Among the known side effects, a triad (hypertension, hypothyroidism and feet/hands syndrome) is correlated to a better response in patients [1].

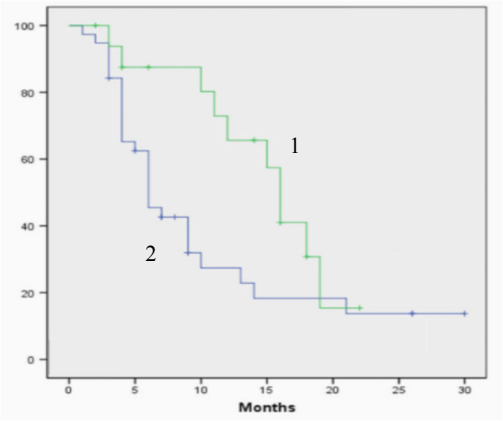

Figure 1. Survival time without tumoral progression: Hypothyroidism (1) and normothyroidism (2) patients (from [2])

It is therefore mandatory to understand the cellular mechanisms of this Sunitinib-induced hypothyroidism, not yet clarified today, in order to establish the link between treatment efficacy and such a side effect.

Metabolomic approach

In order to obtain an overview of the overall changes induced by Sunitinib, the use of metabonomic (Fig. 2) seems to be the best choice. Indeed, this approach allows to establish the complete metabolic profiles of an individual from his/her biofluids. These profiles are obtained from spectroscopic techniques combined to multivariate data analysis.

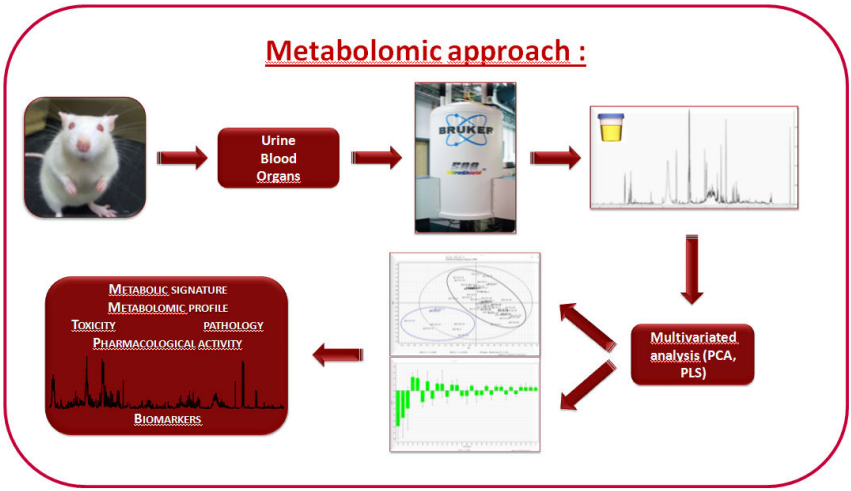

Figure 2. Metabolomic approach

Objectives

The main objectives of this work were first to establish a metabonomic urinary signature of an animal model of hypothyroidism (Fig. 3) induced by exposure to propylthiouracil (PTU) and, next, to compare this signature with the metabonomic profile of animals daily exposed to pharmacological doses of Sunitinib. Finally, this study also tried to assess the contribution of a pre-existing hypothyroidism on the effects of Sunitinib.

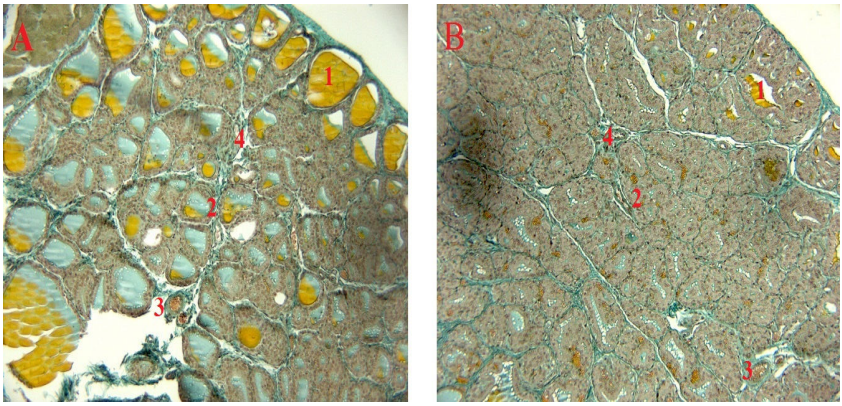

Figure 3. A: Control rat; B: Hypothyroidian model (PTU);
1: colloïd; 2: follicular cells; 3: blood vessel; 4: stroma

Results and conclusion

The metabonomic signature of PTU-induced hypothyroidism showed significant decreases in the activity of the Krebs cycle and in the urinary excretion of taurine. These changes were also observed in rats with normal thyroid function when chronically exposed to

Sunitinib demonstrating the hypothyroidian effect of this drug. Similar changes were finally recorded in animals with pre-existing hypothyroidism and exposed to Sunitinib, although at a lesser extent.

Acknowledgements

Thanks to Pr Laurent Sophie from the department of General, Organic and Biomedical Chemistry, UMONS, Belgium for her technical support.

References

1. Kollmannsberger C. *Sunitinib side effects as surrogate biomarkers of efficacy.* Can Urol Assoc J. 2016 Nov-Dec; 10(11-12Suppl7): S245-247
2. Riesenbeck L. M. and al. *Hypothyroidism correlates with a better prognosis in metastatic renal cancer patients treated with sorafenib or sunitinib.* World J Urol (2011) 29:807-813

Hydrogen/deuterium isotope effects on water molecule mobility. A molecular dynamics simulation study

Maria V. Matsidon, Andrey V. Egorov

Faculty of Physics, Saint Petersburg State University, Russia
E-mail: matchidonm@mail.ru

Introduction

Hydrogen/deuterium isotope effects are widely used in several disciplines, in particular in NMR relaxation studies. However, the interpretation of experimental data requires some assumptions which can not be made without ambiguity. In this context, computer simulations, capable to provide detailed information of all the atoms in the simulated systems should be very helpful for the understanding of isotope effects. Of course, it should be kept in mind that any classical simulation methodology is always as good as the used potential model describing the interactions between the molecules. In the present study we focus on the performance of several standard water models to describe heavy water mobility over the temperature range from −30 to 110ºC.

Simulation details and results

Simulations were carried out using the *MDynaMix* package [1]. Three different water models: three-site SPC/E [2], flexible SPC-F [3], and five-site TIP5P [4], were considered. Models for heavy water were developed by merely changing the hydrogen mass in a classical concept. In each case, a system of 256 molecules in cubic cell with periodic boundary conditions was simulated in the *NPT* ensemble at eight temperatures (243, 263, 283, 298, 303, 323, 343, and 363 K) and atmospheric pressure. At each temperature, the initial configuration for both ordinary and heavy water was the same. It was created according the following procedure: at start, the ordinary water molecules were placed in the simulation box in a regular fashion with the centers-of-mass at a cubic lattice, then, the system was relaxed in a 2 ns simulation in the NPT ensemble. Following production run for both ordinary and heavy water was 2 ns long.

Hydrogen/deuterium isotope effects on the structural and dynamical properties of water we studied in details over the temperature range from −30 to 110ºC. A special attention was given to the reorientational correlation functions for water motions.

References

1. A. P. Lyubartsev, A. Laaksonen. − *Comp. Phys. Comm.*, **128**, 565-589 (2000).
2. H. J. C. Berendsen, J. R. Grigera, T. P. Straatsma. − *J. Phys. Chem.*, **91**, 6269-6271 (1987).
3. K. Toukan, A. Rahman. − *Phys. Rev. B*, **31**, 2643-2648 (1985).
4. M. W. Mahoney, W. L. Jorgensen. − *J. Chem. Phys.*, **112**, 8910-8922 (2000).

14N NQR with Frank sequence excitation

Ivan Mershiev[1], *Bernard Blümich*[2], *Galina Kupriyanova*[1]

[1]*Institute of Physics, Mathematics and Information Technology, Immanuel Kant Baltic Federal University, Kaliningrad, Russia*
[2]*Institute of Technical and Macromolecular Chemistry, RWTH Aachen University, Aachen, D-52056, Germany*
E-mail: IMershiev@kantiana.ru

Nuclear quadrupolar resonance is a solid-state resonance spectroscopy method that allows the detection of substances that contains quadrupolar nuclei. One of the usages of this method is the detection of explosives and illicit substances, which contains the abundant 14N isotope with nuclear spin I=1. However, low frequency range, low sensitivity and high excitation power requirements limit the use of NQR spectroscopy for substance detection.

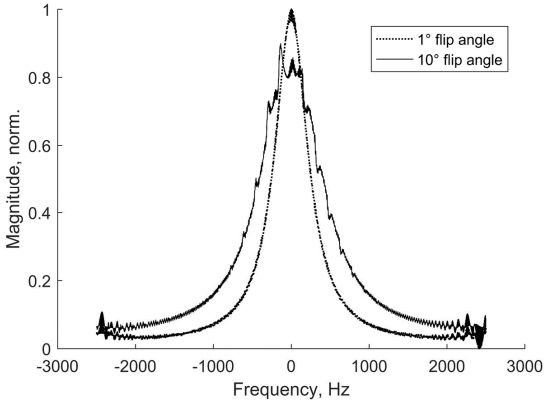

Fig. 1. Simulated NQR spectra for linear and nonlinear stochastic excitation modes

Stochastic excitation is an experimental method for NMR that allows reducing the radiofrequency excitation power up to several orders of magnitude [1]. Pseudo-random encoding allows using the coherent averaging for the FID data, which is sampled between the pulses. In this work, we propose a theoretical and experimental analysis of using the stochastic excitation in application to 14N NQR spectroscopy. As the phase modulation source, Frank sequences was used [2]. In comparison with the binary M-sequence, it has a uniform power spectrum and does not cause artifacts in the reconstructed autocorrelation spectra. Stochastic excitation in NQR may have an advantage with the use of low power and battery-powered equipment, as well as for detection of substances with long T1 relaxation times.

Acknowledgements

This work is supported by the Ministry of Education and Science of Russia and DAAD foundation (grant №1.735.2016/2.2).

References

1. R. R. Ernst, J. Magn. Reson. 3, 10 (1970)
2. B. Blümich, Q. Gong, E. Byrne, and M. Greferath, J. Magn. Reson. 199, 18 (2009).

Cyclic trimers of phosphinic acids: symmetry, chirality, proton transfer and H/D isotope effects on NMR chemical shifts

Valeriya V. Mulloyarova, Ivan S. Giba, Peter M. Tolstoy

Saint Petersburg State University, Saint Petersburg, Russia
E-mail: mylllerka20071993@gmail.com

Introduction

The phosphorus-containing acids in solutions form self-associates with strong H-bonds. In this work we have studied the self-assembly of phosphinic and phosphoric acids R_2POOH by low-temperature liquid state NMR spectroscopy in polar aprotic solution in $CDF_3/CDClF_2$. To determine the types of complexes we used the partial deuteration of samples in mobile proton sites. The investigation of proton transfer was carried out by DFT calculations (B3LYP/6-311++G(d,p)) in vacuum.

Experimental NMR spectra

In ^{1}H NMR spectrum of diphenylphosphate at the low temperature (100 K) there are two signals with different intensities (Fig.1 top). This indicates that two types of complexes with chemically non-equivalent protons and phosphorus atoms are formed in solution. After the partial H/D substitution (the degree of deuteration was 43%) the number of signals in ^{1}H spectrum is increased (Fig.1 bottom). From the number of signals the stoichiometry of self-associates could be established. NMR spectra have revealed that $(PhO)_2POOH$ forms two types of cyclic self-associates with strong H-bonds: cyclic dimers (HH and HD signals) and cyclic trimers (HHH, HHD and HDD signals). The equilibrium is shifted towards the formation of trimers.

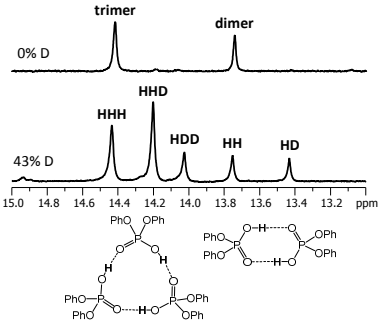

Figure 1. Low-field parts of ^{1}H NMR spectra of diphenylphosphoric acid in solution in $CDF_3/CDClF_2$ mixture at 100 K

Quantum-mechanical calculation

By quantum-mechanical calculations we have identified that the monomer of $(PhO)_2POOH$ has five stable conformers, which differ by the orientation of the –OPh group. Self-assembly of the cyclic complexes occurs by hydrogen bonding between these five conformers in various combinations. Due to the steric repulsion of the –OPh groups, not all combinations of monomers are possible (in some cases the phenyl groups would be too close to each other). Three possible dimer structures were identified. The number of possible trimers is large. It was established that the energy of H-bond in dimer less than in trimer (~11 and ~13 kcal/mol, respectively).

The dynamic of proton transfer in cyclic trimer has been studied using the model system H_2POOH. The "ring" of hydrogen bond in the optimized structure is non-planar. Due to this non-planarity there are 12 isomers (A-L, see Figure 2), which differ by the orientation of P=O and –OH groups with respect to the ring of H-bonds. All structures of isomers are equal in energy and the transition from one to another occurs by two types of wave-like motions: with proton transfer ("PT") and without proton transfer ("twist"). The energy barrier of the "twist" motion is ~2 kcal/mol and that of the "PT" motion is ~6 kcal/mol. All isomers and transitions between them are shown in Figure 2.

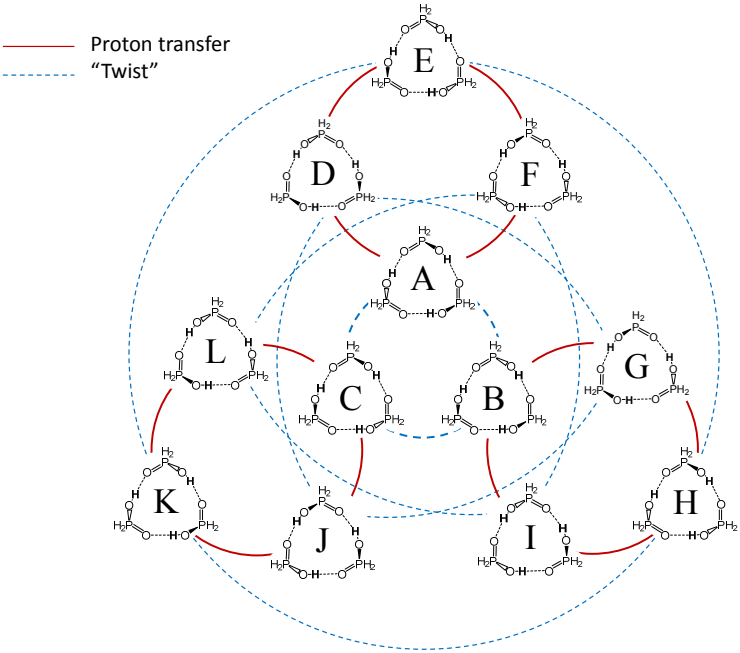

Figure 2. The complete scheme of isomers and possible transitions between them

Acknowledgements

This work has received financial support from the RFBR Grant 17-03-00590.

References

1. V. V. Mulloyarova, I. S. Giba, M. A. Kostin, G. S. Denisov, I. G. Shenderovich, P. M. Tolstoy. – *Phys. Chem. Chem. Phys.*, 20, 4901-4910 (2018).

The Dynamics of Lactaptin in solution by NMR

Sergey S. Ovcherenko[1,2], Andrey V. Shernyukov[1,2], Olga A. Chinak[3], Alexandr S. Fomin[3], Evgeniy A. Sviridov[1], Vladimir A. Richter[3], Elena G. Bagryanskaya[1]

[1]N. N. Vorozhtsov Novosibirsk Institute of Organic Chemistry of Siberian Branch of Russian Academy of Sciences
[2]Novosibirsk State University
[3]Institute of Chemical Biology and Fundamental Medicine of Siberian Branch of Russian Academy of Sciences
E-mail: ovcherenkoserjy@gmail.com

Introduction

NMR spectroscopy is a unique and powerful approach for characterizing of the overall and internal rotational motions in proteins. Nuclear spin relaxation measurement provides information on fast motions on the timescales of picosecond to nanosecond (laboratory frame nuclear spin relaxation experiments), and slow motions on the timescales of microsecond to millisecond (rotating frame nuclear spin relaxation measurements), whereas magnetization exchange spectroscopy deals with motions on the timescales of millisecond to second [1]. NMR is capable to provide us with information of the protein structure by the measuring of the parameters of spin dynamic, because the spin dynamic in structured and unstructured fragments is strongly different.

Lactaptin peptide

Lactaptin is a recombinant analogue of the proteolytic fragment of the human milk protein κ-casein, has antitumor activity and is also a membrane-active peptide capable of direct penetration into eukaryotic cells [2, 3]. Casein proteins belong to the class of proteins that do not have an ordered structure (IDP). One way to characterize IDP is to find regions in which a residual structure is present, i.e. there are some deviations from the behavior of the ideal, devoid of any structural propensity chain (*random coil*).

The analysis of the relaxation data of ^{15}N amide atoms measured by NMR enables to determine the protein back-bone chain dynamic. Also the measuring of HETNOE values which have a high sensitivity to fast local movements allow to easily identify protein regions with different local mobility.

Relaxation data

We measured T_1, T_2 and NOE parameters of ^{15}N in amide groups of the protein back-bone chain. The results are shown in Fig 1. It is clearly shown that regions of the peptide near to N- and C –terminus demonstrate increased T_1 and T_2 relaxation values in comparison with the values of the other fragments that means short correlation time of the chain ends and hence their increased local mobility. Also the HETNOE values of these fragments are negatively large that as well demonstrate their high local mobility and confirm the previous statement [4].

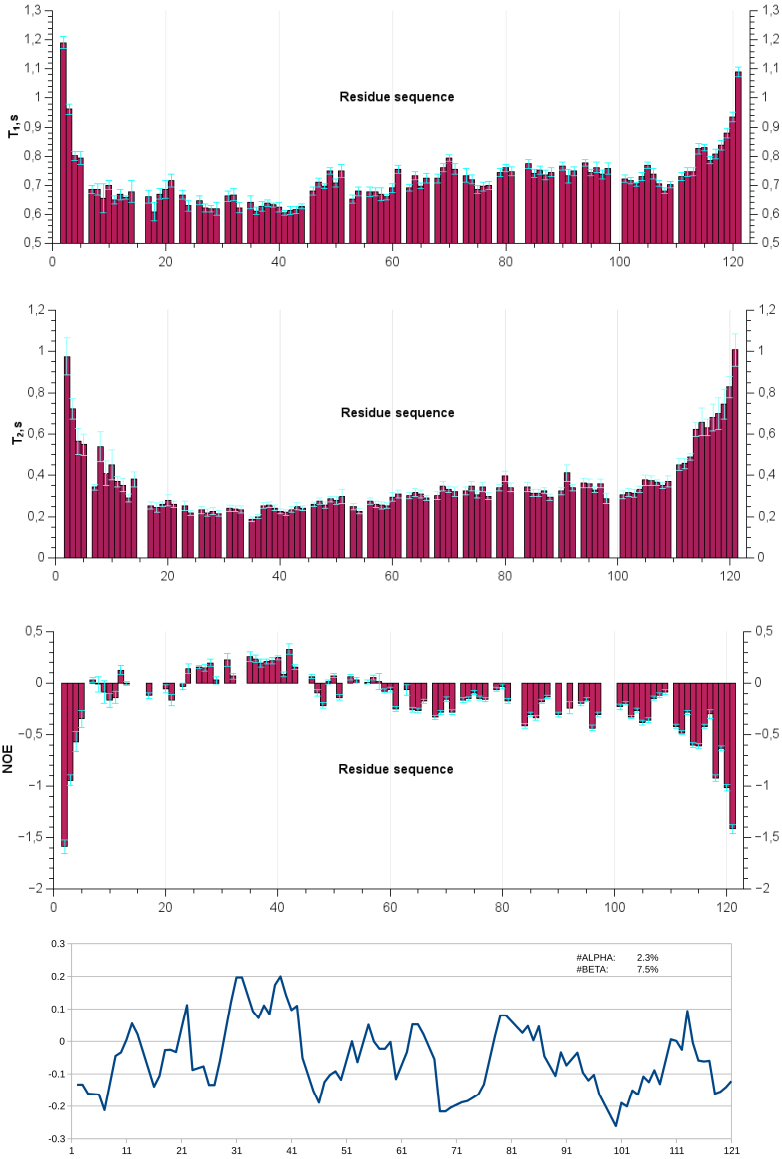

Figure 1. T_1, T_2, NOE and SSP values respectively

We identified protein polypeptide chain fragments which differ in their local mobility. The comparison of the relaxation values and the data of SSP method [2], applied to predict a residual structure by using experimental chemical shift data, allowed to distinguish more structured fragment of peptide back-bone chain which is at N-terminus. Also it is shown that the fragment demonstrate the tendency to configure alpha helical structure.

Acknowledgements

This work is supported by the Russian Science Foundation (grant #14-14-00922).

References

1. Teng, Quincy. Structural biology: practical NMR applications. Springer Science & Business Media, 2012.
2. Richter, V. A., Vaskova, A. A., Koval, O. A., & Kuligina, E. V. (2015). Antitumor Potential of Lactaptin. Biol Med (Aligarh) S, 2, 2
3. O.Chinak, A.Yunusova, A.Shernyukov, I.Pyshnaya, E.Kuligina, O.Koval, A.Nushtaeva, V.Richter, Lactaptin – membrane-active peptide with cell-penetrating properties. Biotechnology: state of the art and perspectives IX international congress, Congress proceedings, 20-22 February, 2017, Moscow, P 568-571.
4. PD Dr. Beat Vögeli. Supplementary Material to the script. The Nuclear Overhauser Effect in NMR. Structure and Dynamics Analysis. Frühjahrssemester 2015. Eidgenössische Technische Hochschule Zürich.

The determination of the relaxation properties of the emulsion consisted of proxyl type nitroxide radicals proposed as MRI contrast agent

Sergey S. Ovcherenko[1,2], Andrey V. Shernyukov[1,2], Evgeniy V. Tretyakov[1], Rui Tamura[3], Elena G. Bagryanskaya[1]

[1]N. N. Vorozhtsov Novosibirsk Institute of Organic Chemistry of Siberian Branch of Russian Academy of Sciences
[2]Novosibirsk State University
[3]Kyoto University Graduate School of Human and Environmental Studies
E-mail: ovcherenkoserjy@gmail.com

Introduction

One of the most important applications of Nuclear Magnetic Resonance is Magnetic Resonance Imaging (MRI). The major goal of MRI is to obtain the high resolution images of organism tissues with the purpose of diseases diagnosis. Usually insufficient image contrast in the areas of interest impedes the interpretation of experimental data that does not provide unambiguous diagnosis. In such cases to improve the quality of images contrast agents are used.

Contrast agents (CA) are substances which change relaxation properties of the observed nuclei [1]. The evaluation of contrast agents efficiency in MRI is the values of relaxivity r_1 and r_2 [1] which demonstrate their properties to decrease the relaxation times T_1 and T_2 of water protons per unit concentration. The using of contrast agents in MRI is the way of the contrast enhancement of the regions contained unhealthy tissues. Unhealthy tissues such as a cancer tumor metabolically differ from healthy tissues and facilitate increasingly contrast agent accumulation in itself that leads to a high contrast of the obtained images for further diagnosis.

The majority of contrast agents in MRI for medical applications are paramagnetic gadolinium ions based complexes or superparamagnetic iron oxides (magnetite Fe_3O_4) [1,2]. Paramagnetic metal ions such as Gd^{3+} cannot be applied in ionic shape as CA because of biodistribution (their accumulation in bones, liver and spleen) and high toxicity. Thus, they are used in the form of their chelate complexes which provide high thermodynamic and kinetic stability *in vivo* and support a save biodistribution in a living organism. Chelate complexes based on Gd^{3+} and Mn^{2+} demonstrate the similar values of r_1 and r_2 relaxivities and are used to obtain T_1- weighted images. However, the application of such CA is possible only at low concentration values to decrease the toxic level. The superparamagnetic iron oxide based CA at magnetic field in MRI have 1000 times larger magnetic moment than ordinary paramagnetic CA. The contrast properties of such superparamagnetic particles depend on their particle size and allow using of them to obtain both of T_1 and T_2 weighted images. However, there are some drawbacks of such CA associated with unusual magnetic susceptibility artifacts demonstration. These artifacts produce dark signals that may not only be misleading but also result in incorrect interpretation of the T_2 -weighted magnetic resonance (MR) images.

Recently, Tamura et al. [2] proposed to use robust metal-free magnetic nanoemulsions consisting of a biocompatible nonionic surfactant (compound **1**, Fig. 1) and hydrophobic, low molecular weight nitroxide radicals of proxyl type (racemic compounds **2** or **4**, Fig. 1). The nanoemulsions showed high colloidal stability, low cytotoxicity, enough reduction resistance to excess ascorbic acid, and sufficient contrast enhancement in the proton longitudinal relaxation time (T_1) weighted MR images in PBS *in vitro* (and preliminarily *in vivo*). The possibility to use such emulsions for targeted drug delivery systems visible by magnetic resonance (MR) imaging was demonstrated. Using surfactant **1** and fairly water-soluble radical **4** the stable nanoemulsion did not arise. The most suitable nanoemulsion contained water-insoluble radicals **2** (n=18), where in both the flexible, interdigitated layer structure of long

alkyl chains and the CH–p and/or CH–O interactions between neighboring cyclic nitroxide radical moieties greatly contribute to the remarkable stability of the nanoemulsions. The average particle diameter of the emulsion was 17 nm. However, relaxivity values of the emulsion were an order of magnitude less than that of typical Gd (III)-based complex agent in deionized water and comparable for ordinary water-soluble small mononitroxide molecules.

In this work we investigated relaxation properties of the nanoemulsion consisted of nitroxide radicals **3** (as surfactant) and **4**. In addition, we obtained relaxation parameters of these individual radicals to reveal possible cooperative effects (synergism).

Relaxation measurements

The average particle size diameter of investigated emulsion according to DLS data was 138.6 nm (Fig. 2).

We measured T_1 and T_2 relaxation parameters (at 4.7T) of the emulsion and solutions of individual compounds. The results are shown on (Table 1). To take into account the possible influence of dissolved oxygen in relaxation process we showed that upon the preparation of the emulsion (ultrasound treatment and keeping at 95 ^{0}C) the oxygen removes and therefore an additional degassing does not require. So, to neglect dissolved oxygen influence we used the same procedure of preparation for the solutions of individual compounds.

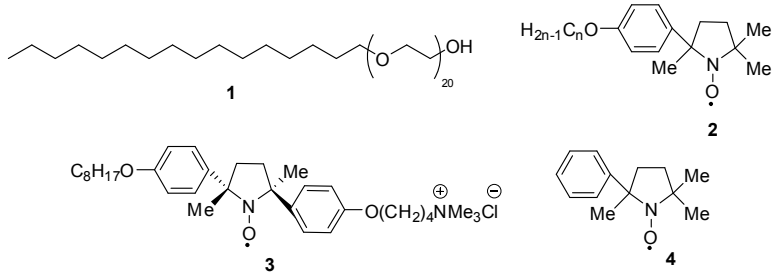

Figure 1. Nitroxide radicals

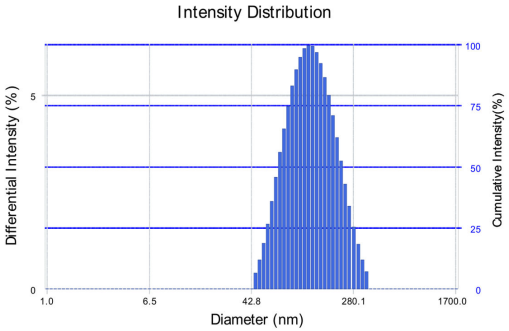

Distribution Results (Contin)	
Average diameter (nm)	Std. Dev.
138.6	61.0

Cumulants Results		
Diameter	(d)	: 115.3 (nm)
Polydispersity Index	(P.I.)	: 0.162
Diffusion Const.	(D)	: 4.434e-008 (cm²/sec)

Figure 2. DLS data of emulsion

Table 1. T_1, T_2 values of emulsion and solutions depended on concentration.

Concentration, $x10^{-3}$M	T_1, s	T_2, s
Radical **3**		
10.42	0.826±0.033	0.559±0.021
1.00	2.500±0.209	
0.33	2.831±0.218	
0.11	3.007±0.223	
Radical **4**		
50.12	0.813±0.032	0.535±0.039
4.94	1.151±0.080	
1.65	2.038±0.184	
0.55	2.788±0.352	
0.18	3.070±0.370	
Emulsion, **3** ($10x10^{-3}$M) and **4** ($50x10^{-3}$M)		
Native	0.347±0.018	0.256±0.002
Diluted 1:2	0.512±0.024	0.383±0.026
Diluted 1:30	2.071±0.173	1.526±0.024
H_2O		
Native	2.693±0.210	
After ultrasound treatment and keeping at 95^0C	3.080±0.247	
After freeze-pump procedure	3.090±0.240	1.499±0.117

We demonstrated the stability of the emulsion upon dilution in deionized water and the absence of the additional appearance of the new relaxation properties of the emulsion in comparison with its individual compounds. Furthermore we showed that the relaxation properties of the obtained emulsion were worse than as if nitroxide radicals contained in the emulsion were completely dissolved. However, the nanoemulsions of such type could be better choice as CA due to the fact of stability to biodistribution.

References

1. Geraldes, Carlos F. G. C.; Laurent, Sophie (2009). "Classification and basic properties of contrast agents for magnetic resonance imaging". Contrast Media & Molecular Imaging. **4** (1): 1–23.
2. Kota Nagura, Yusa Takemoto, Satori Moronaga, Yoshiaki Uchida, Satoshi Shimono, Akihiko Shiino, Kenji Tanigaki, Tsukuru Amano, Fumi Yoshino, Yohei Noda, Satoshi Koizumi, Naoki Komatsu, Tatsuhisa Kato, Jun Yamauchi, and Rui Tamura. Preparation of robust metal-free magnetic nanoemulsions encapsulating low-molecular-weight nitroxide radicals and hydrophobic drugs directed toward MRI-visible targeted delivery. Chem. Eur. J. 2017, 23, 1 – 9.

Determination of the fine structure of the spiro-carboheterocycle using NMR spectroscopy and X-ray diffraction analysis

M. M. Pavchenko[1], V. V. Pelipko[1], K. A. Lyssenko[2], S. V. Makarenko[1], R. I. Baichurin[1]

[1]*Herzen State Pedagogical University of Russia, Department of Organic Chemistry, Center of collective use at the Faculty of Chemistry "Instrumental methods for the study of nitro compounds, coordination, biologically active substances and nanostructured substances" 48 Moyka River Embankment, Saint Petersburg 191186, Russia*
E-mail: kohrgpu@yandex.ru
http://kohrgpu.ru, http://ckpo.herzen.spb.ru/?page=organic-chemistry
[2]*A. N. Nesmeyanov Institute of Organoelement Compounds of Russian Academy of Sciences, 119991 Moscow, Russian Federation. ul. Vavilova 28*
https://ineos.ac.ru/

Alkyl 3-bromo-3-nitroacrylates, like Michael acceptors, to produce the carbo- and heterocycles in the reactions with CH acids [1]. The interaction of ethyl 3-bromo-3-nitroacrylate with the phenylmethylpyrazolone leads to the synthesis of a spiro-carboheterocycle – ethyl 4-methyl-2-nitro-7-oxo-6-phenyl-5,6-diazaspiro[2.4]hept-4-ene-1-carboxylate **1**.

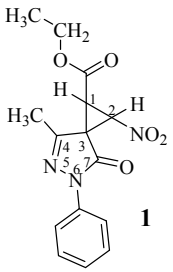

1

The rigidly fixed structure of the molecule of this compound makes it a very attractive object for study using the NMR spectroscopy involving homo- and heteronuclear experiments. Its ^{1}H and ^{13}C NMR spectra contain only one set of signals and indicate the diastereohomogeneity of the synthesized substance. The observed vicinal *J*-coupling constsnts between the methine protons of the cyclopropane ring (C^1H: 3.95 ppm, d, $^{3}J_{H^1H^2}$ = 6.3 Hz; C^2H: 5.25 ppm, d, $^{3}J_{H^1H^2}$ = 6.3 Hz) shows the *trans* configuration of these protons, which is consistent with the literature data for structurally similar compounds [2, 3]. The performed assignment of the signals is confirmed by the results of the ^{1}H-^{1}H dqf-COSY (Fig. 1), ^{1}H-^{13}C HMQC и HMBC.

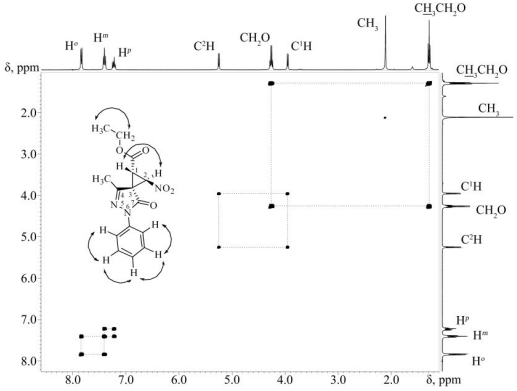

*Figure 1. ^{1}H-^{1}H dqf-COSY spectrum of compound **1** ($CDCl_3$)*

The results of ^{1}H-^{1}H NOESY (obtained with a variable value of mix. time) demonstrate the interaction of the proton C^1H and protons CH_3 of the heterocycle group (Fig. 2), which indicates what these protons in close proximity to each other.

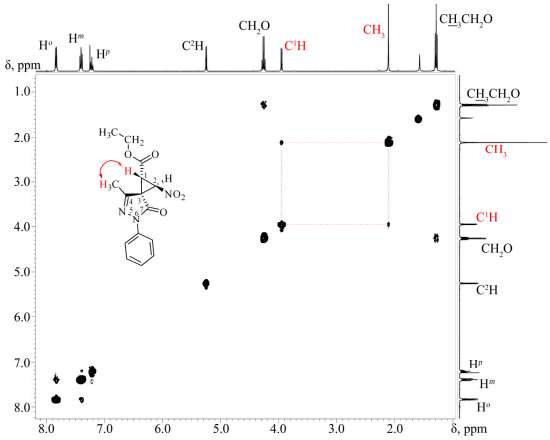

*Figure 2. ^{1}H-^{1}H NOESY spectrum of compound **1** ($CDCl_3$)*

The results of X-ray diffraction analysis performed for compound **1** confirm the conclusions of the NMR spectroscopy data (Fig. 3). Taking into account the NMR spectroscopy and X-ray diffraction analysis data, the resulting compound can be assigned the configuration of *rel*-1R, 2S, 3S.

Thus, the capabilities of the NMR spectroscopy for establishing the structure of compound have been demonstrated by studying of the synthesize spiro-carboheterocycle. In this case, the experimental data obtained confirmation in the results of the investigation of the same substance by X-ray diffraction analysis.

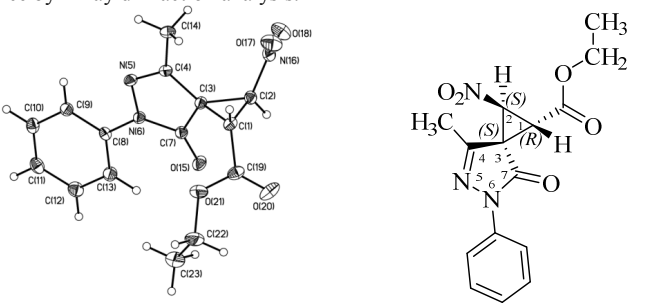

*Figure 3. Molecular structure of compound **1***

The studies were carried out in the center of collective use at the Faculty of Chemistry of the Herzen State Pedagogical University of Russia on the Jeol ECX-400A spectrometer at 399.78 (^{1}H) MHz at standard experiment settings, using a solvent signal as internal standard.

References

1. A. I. Pekki, S. V. Makarenko, K. V. Altukhov, V. M. Berestovitskaya. – *Rus. J. Gen. Chem.*, 80, 1048-1049 (2010).
2. A. J. Gordon, R. A. Ford. The Chemist's Companion. New York: Wiley, 1972.
3. E. Pretsch, P. Buehlmann, C. Affolter. Structure determination of organic compounds. Berlin: Springer-Verlag, 2000.

^{1}H, ^{13}C, ^{15}N NMR spectroscopy in the study of the structure of alkyl 3-nitropropanoates containing one asymmetric carbon atom in the structure

V. V. Pelipko, R. I. Baichurin, E. M. Leontyeva, M. A. Kuritcyna, S. V. Makarenko

Herzen State Pedagogical University of Russia, Department of Organic Chemistry, Center of collective use at the Faculty of Chemistry "Instrumental methods for the study of nitro compounds, coordination, biologically active substances and nanostructured substances"
48 Moyka River Embankment, Saint Petersburg 191186, Russia
E-mail: kohrgpu@yandex.ru
http://kohrgpu.ru, http://ckpo.herzen.spb.ru/?page=organic-chemistry

Alkyl 3-nitroacrylates are highly active substrates in the Michael reaction with representatives of CH-acids [1-3]. According to the previously described procedure [1], we synthesized adducts of alkyl-3-nitroacrylates and non-enolizing CH-acid – *N,N*-dimethylbarbituric acid.

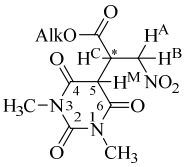

Alk = CH_3CH_2 (**1**), CH_3 (**2**)

The aim of this work was to study the structure of the obtained adducts **1, 2** by ^{1}H, ^{13}C, and ^{15}N NMR spectroscopy, including heterocorrelation experiments.

The structural feature of the molecules of the substances **1, 2** is the presence of a chiral (asymmetric) carbon atom in their molecule, which causes the protons of the $CH_2OC(O)$ and CH_2NO_2 groups to display the diastereotopic effect in ^{1}H NMR spectra (Fig. 1).

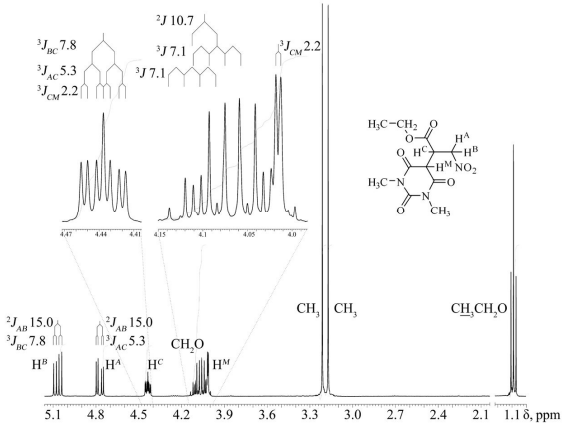

*Figure 1. ^{1}H NMR spectrum of compound **1** (CD_3CN)*

Indeed, the methylene's protons of the ester fragment form two doublets of quartets at 4.04 and 4.10 ppm (^{2}J 10.7, ^{3}J 7.1 Hz) in the NMR ^{1}H spectrum of the compound **1**. The protons of the CH_2NO_2 group and the H^C and H^M protons gave rise to an *ABCM* spin system in NMR ^{1}H spectra of substances **1, 2**: the signals of methylene protons are resonated as two doublets of doublets at 4.75-4.77 and 5.05-5.07 ppm ($^{2}J_{AB}$ 15.0-15.1, $^{3}J_{AC}$ 5.3, $^{3}J_{BC}$ 7.8 Hz), proton H^C – doublet of doublets of doublets at 4.44-4.45 ppm ($^{3}J_{CM}$ 2.2-2.3, $^{3}J_{AC}$ 5.3, $^{3}J_{BC}$ 7.8 Hz), proton H^M – doublet at 4.02-4.06 ppm ($^{3}J_{CM}$ 2.2-2.3 Hz). This assignment of the signals was also confirmed by the ^{1}H–^{1}H dqf-COSY data (Fig. 2).

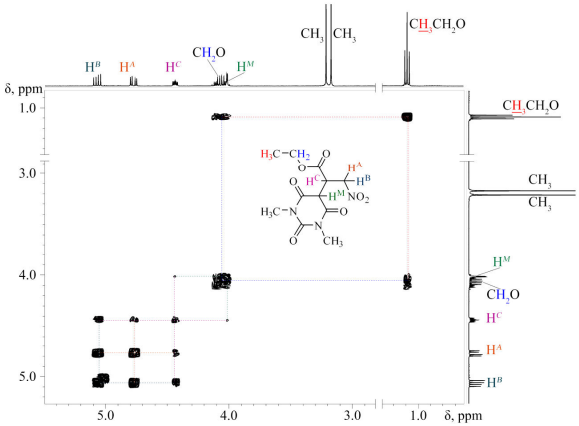

*Figure 2. ^{1}H-^{1}H dqf-COSY spectrum of compound **1** (CD_3CN)*

The NMR of ^{13}C-{^{1}H} spectra of adducts **1, 2** contained signal from all structural fragments, including those of the amide groups (C^2) at δ_C 151.45-151.46 ppm, (C^4, C^6) at δ_C 166.37-167.50 ppm and carbonyl of ester groupe at δ_C 169.56-170.27 ppm.

Additional confirmation of the presented assignment is the results of the ^{1}H-^{13}C HMQC experiment. The ^{1}H–^{13}C HMQC spectrum of **1** (Fig. 3) showed cross-peaks between magnetically nonequivalent methylene protons of the ester ethoxy group (4.04, 4.10 ppm) and the carbon nucleus resonating at δ_C 62.20 ppm, protons of the CH_2NO_2 group (4.77, 5.07 ppm) and the carbon nucleus resonating at δ_C 73. ppm, as well as between H^C (δ 4.44 ppm)/CH^C (δ 41.28 ppm) and H^M (δ 4.02 ppm)/CH^M (δ 48.89 ppm).

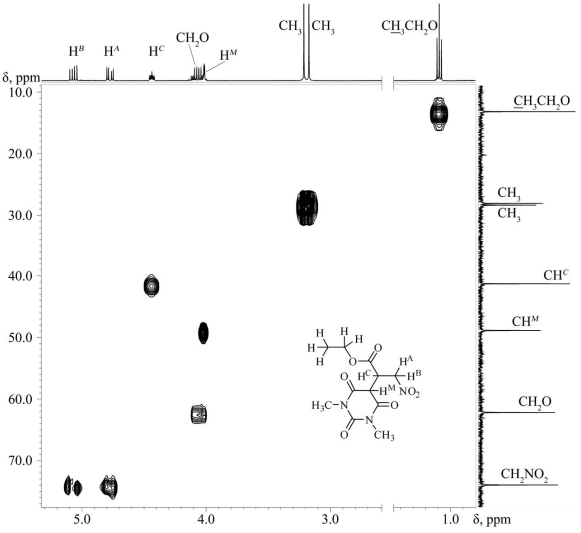

*Figure 3. ^{1}H-^{13}C HMQC spectrum of compound **1** (CD_3CN)*

Assignment of signals of carbonyl carbon atoms confirm the results ^{1}H-^{13}C HMBC experiment. In the spectrum of compound 1 (Fig. 4) only signals of two methyl groups CH_3 (δ 3.17, 3.21 ppm) showed cross-peaks with C^2 (δ 151.45 ppm), protons of the CH_2O group (δ 4.04, 4.10 ppm) demonstrated a cross-peak with the most downfield signal of the carbon atom C=O (δ 169.56 ppm).

The ^{1}H-^{15}N HMBC experiment allows to determine the chemical shift of nitrogen nucleus by the example of adduct **2** (Fig. 5).

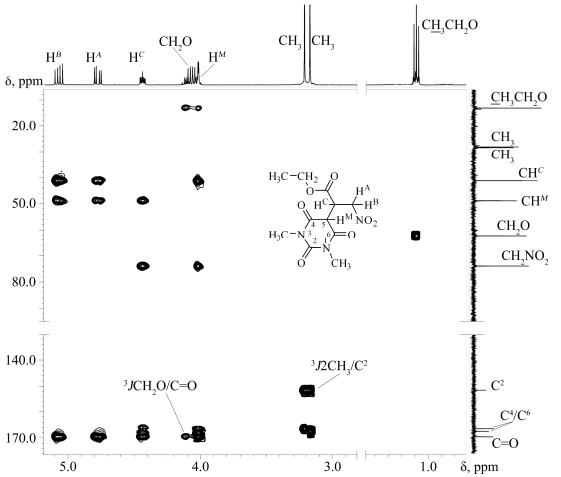

*Figure 4. ^{1}H-^{13}C HMBC spectrum of compound **1** (CD_3CN)*

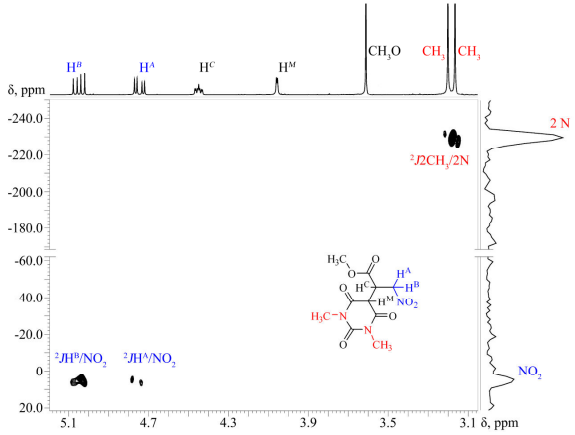

*Figure 5. ^{1}H-^{15}N HMBC spectrum of compound **2** (CD_3CN)*

Thus, the presence of cross-peaks of the methylene protons of the CH_2NO_2 group (δ 4.75, 5.05 ppm) with a signal at 4.87 ppm allows to ascribe the latter to the nitrogen atom of the nitro group, and the cross-peaks of the protons of the methyl groups (δ 3.17, 3.20 ppm) and

the signal at -229.77 ppm determine it as a signal of the nitrogen atoms of the *N,N*-dimethylbarbituric acid's substitute, which agrees with the literature data [4, 5].

Thus, the study of compounds **1, 2** containing in the structure one asymmetric carbon atom using a complex of homo- and heterocorrelation experiments of NMR spectroscopy makes it possible to fully describe their structure and to assign the signals of the atoms ^{1}H, ^{13}C, ^{15}N of all important fragments of the molecule.

The studies were carried out in the center of collective use at the Faculty of Chemistry of the Herzen State Pedagogical University of Russia on the Jeol ECX-400A spectrometer at 399.78 (^{1}H), 100.53 (^{13}C) and 40.52 (^{15}N) MHz at standard experiment settings, using a solvent signal as internal standard. The chemical shifts of ^{15}N were determined with respect to CH_3NO_2.

References

1. V. V. Pelipko, S. V. Makarenko, R. I. Baichurin, V. M. Berestovitskaya, K. S. Kovalenko. – *Rus. J. Org. Chem.*, 53, 1799-1808 (2017).
2. J. C. Anderson, A. S. Kalogirou, G. J. Tizzard. – *Tetrahedron*, 70, 9337-9351 (2014).
3. A. S. Smirnov, S. V. Makarenko, V. M. Berestovitskaya, A. I. Pekki, K. S. Kovalenko. – *Rus. J. Org. Chem.,* 42, 1242-1243 (2006).
4. G. J. Martin, M. L. Martin, J.-P. Gouesnard. ^{15}N-NMR Spectroscopy. Book serie: NMR Basic Principles and Progress. Vol. 18. Berlin: Springer-Verlag, 1981.
5. T. M. Klapötke, B. Krumm, R. Moll. – *Chem. – Eur. J.,* 19, 12113-12123 (2013).

^{1}H NMR and ESR studies of the mechanism of gallstones formation

Alina A. Pichugina[1], Larisa V. Tsyro[1], Felix G. Unger[2]

[1]Institute of Natural and Technical Sciences, Surgut State University, Lenina avenue 1, Surgut, Russian Federation
[2]Chemical Faculty, National Research Tomsk State University, Lenina avenue, 36, Tomsk, Russian Federation
E-mail: alina.com9@mail.ru
http://www.surgu.ru

Introduction

Gallstones are organomineral aggregates (OMA), which have a layered structure formed by organic and inorganic compounds [1, 2]. To date, many studies have been carried out on the composition of gallstones, such as X-ray phase analysis, IR spectroscopy, and scanning electron microscopy [3-5]. These methods allow you to identify in the gallstones such compounds as cholesterol, calcium salts, as well as the presence of pigment, whose composition by these methods is difficult to determine. Therefore, the use of such methods as electron spin resonance (ESR) and nuclear magnetic resonance (^{1}H NMR) is topical. Thus, by the ESR method, it is possible to establish the presence of free radicals in the gallstones, and by the ^{1}H NMR method to study in more detail the organic component of these stones. The data of these methods allow to study in more detail the mechanism of formation of gallstones, according to the authors of the work [6], all the processes taking place in a living organism are of a radical nature. In this connection, the establishment of the presence of diamagnetic and paramagnetic molecules in the gallstones will make it possible to understand the mechanism of their formation.

Results

In Fig. 1 shows the ESR spectra of gallstones, from which it can be seen that they differ in shape, so the selection of individual sites is conditional. In this connection, it is not always easy to identify the radicals from the observed spectra, but a comparison of the ESR spectra makes it possible to identify common features.

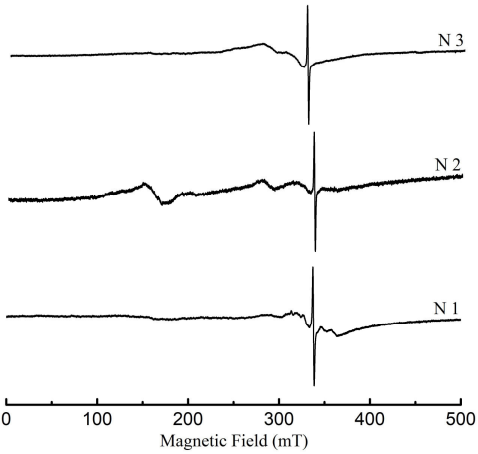

Figure 1. ESR spectra of gallstones

According to the interpretation of the obtained ESR spectra of gallstones, they contain the center of high-spin iron (g ~ 4.2), the spin centers of copper and manganese in the phase of rhodochrosite (g ~ 2.5-2.1), as well as free radicals (g ~ 2.0), which can be bilirubin crystals. Despite the fact that in a sample of gallstones, the set of spin centers is almost identical, but their ESR spectra differ. The difference consists in various intensity of signals that points out the different number of the spin centers and also width and position of peaks that can be explained with differences in an environment of the spin centers.

For a more detailed description of the spin characteristics of gallstones, the pigment part of the gallstone was separated from the cholesterol (Fig. 2).

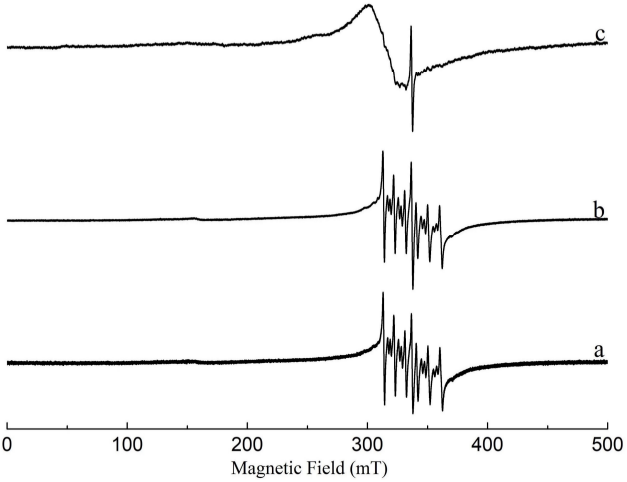

Figure 2. ESR-spectra: a - sample N 1; b - pigment part of sample N 1; c - cholesterol part of sample N 1

According to the studies, the pigment and cholesterol parts contain a different number of spin centers (Tab. 1). As can be seen from table 1, in the pigment part of the spin centers, it is approximately 10 times larger in comparison with the cholesteric, in spite of the fact that the pigment part is only 3.75 wt. % of the total mass of the stone.

Table 1. The number of spin centers in the pigment and cholesterol parts of gallstones

Sample	C_{SC}, spin/g in the pigment part	C_{SC}, spin/g in the cholesterol part	Residue, wt. %
N 1	$7.0 \cdot 10^{20}$	$2.4 \cdot 10^{19}$	4.3
N 2	$2.3 \cdot 10^{19}$	$7.6 \cdot 10^{18}$	2.6
N 3	$4.4 \cdot 10^{19}$	$7.5 \cdot 10^{18}$	4.4
N 4	$8.4 \cdot 10^{19}$	$1.2 \cdot 10^{19}$	3.7

Analysis of ^{1}H NMR spectra showed the presence in the gallstones of the structure of cholesterol $C_{27}H_{46}O$. According to the X-ray phase analysis (XRD) data, the investigated gallstones consist of 45 wt. % of cholesterol and 55 wt. % of desmosterol. Simulation ^{1}H NMR spectrum was conducted desmosterol whose structure and chemical shifts are shown in Fig. 3b.

Desmosterol is a molecule that precedes the formation of cholesterol. When comparing the chemical shifts in the structure of desmotselol with the obtained ^{1}H NMR spectra of gallstones, it was found that desmosterol is absent in them. This fact indicates that desmosterol passes into another structure, which at this stage of the study is difficult to assume.

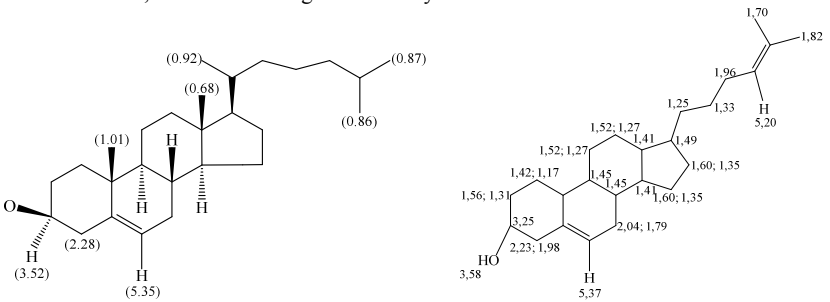

a) *b)*

Figure 3. The structures of cholesterol (a) and desmosterol (b)

Thus, on the basis of the obtained ESR and ^{1}H NMR data, it is established that particles with open (paramagnetic) and closed (diamagnetic) spin orbitals are present in the gallstones. These particles are involved in the processes that occur during the formation of gallstone.

References

1. N. G. Venneman, K. J. Erpecum. – *Gastroenterology Clinics of North Ametica,* 39 (2), 171-183 (2010).
2. A. A. pichugina, L. V. Tsyro, F. G. Unger. – *Journal of Applied Spectroscopy,* 84 (6), 1024-1029 (2018).
3. S. Pramanik, S. Ghosh, A. Roy, R. Mukherjee, A. K. Mukherjee. – *Z. Kristallogr.,* 231 (2), 97-105 (2016).
4. G. Liu, D. Xing, H. Yang, T. Wu. – *Journal of Molecular Structure,* 616, 187-191 (2002).
5. T. Qiao, R.-H. Ma, X.-B. Luo, Z.L. Luo, P.-M. Zheng, L.-Q. Yang. – *Microscopy Research and Technique,* 76, 443-452 (2013).
6. F. G. Unger, L. V. Tsyro, A. A. Pichugina, D. A. Afanasiev, S. A. Kiselev. – *Herald of the Bauman Moscow State Tech. Univ., Nat. Sci.,* 4, 107-122 (2016).

Magnetic hyperpolarization and alternative ways of MRI signal amplification

Yu. A. Pirogov

Lomonosov Moscow State University, Moscow, Russia
E-mail: yupi937@gmail.com

Magnetic hyperpolarization of nuclei allows enlarging magnetic resonance signals on 4-5 orders and provides especially high velocity, contrast and spatial resolution of MRI scanning. Using such approach is most important for visualization of internal frames of respiratory ways and revealing oncological pathologies – usual MRI methods are became unreal, because lungs tissues contain too little protons forming MRI scanner reply. Filling respiratory ways by hyperpolarized gases xenon, helium or krypton allows fine visualizing shape of gas media contact with lungs tissues. In addition, nuclei hyperpolarization of nuclei containing in medicine preparations (for instance, ^{13}C, ^{29}Si, and others) is applied for detection of preparation localization in internal organs by them targeted delivery to pathological zone. There are two main hyperpolarization methods – laser and so named dynamic nuclear polarization, each of which is connected with creating special bulky expensive devices and applicating very unprofitable therapy procedures. Therefore searching other effective ways of MRI visualization are undertaking and have also successful solutions of indicated tasks. One of such approaches is application of fluorocarbon compounds (emulsions of Perftoran® type or gases SF6, perfluorocyclobutan and others), which after adjusting scanner on Larmor frequency give powerful signal filtered due to fluorine atoms absence in organism from background noise usual at proton MRI.

Investigations on the ^{19}F nuclei were carried out with help of devices in the Center of collective using "Biospectrotomography" and supported by RFBR grant No. 17-02-00465 A.

Preparation and Characterization of Polysulfone/Pluronic F127 ultrafiltration membranes

T. Plisko[1], A. Penkova[2], K. Burts[1], S. Vasin[2], A. Bildyukevich[1]

[1]Institute of Physical Organic Chemistry of the National Academy of Sciences of Belarus, 13 Surganov street, 220007 Minsk, Belarus.
[2]St. Petersburg State University, 7/9 Universitetskaya nab. St. Petersburg 199034, Russia.
[3]Damietta University, Damietta, Egypt.

Block-copolymers of polyethylene oxide (PEO) and polypropylene oxide (PPO) (Pluronic, Poloxamer, Tetronic) were found to be the promising polymer matrix modifiers due to the different affinity for the solvents of PPO (hydrophobic) and PEO (more hydrophilic) parts of the molecule, which results in their good dispersion in hydrophobic and hydrophilic matrices. Recently, a polymer, such as Pluronic™, polyethylene oxide (PEO)–polypropylene oxide (PPO)–PEO triblock copolymers, has been widely used to increase the antifouling properties of polymer membranes.

In the present work the influence of Pluronic F127 addition to the casting polysulfone (PSF) solution on the structure, performance and physico-chemical properties of ultrafiltration membranes was studied. The effect of Pluronic F127 concentration on the phase state, viscosity, turbidity and viscous flow parameters of PSF-Pluronic F127-N, N-dimethylacenamide (DMAA) solutions was investigated. Flat-sheet ultrafiltration PSF/Pluronic F127 membranes were prepared via phase inversion technique using water as a coagulant. The hydrophilic-hydrophobic balance of the selective layer, structure and composition of PSf/PluronicF127 membranes were characterized by water contact angle measurements, scanning electron microscopy (SEM), nuclear magnetic resonance (NMR), small-angle X-ray scattering (SAXS), atomic force microscopy (AFM). The antifouling properties of the membranes were evaluated in the long-lasting experiments on ultrafiltration of bovine serum albumin solution. It was shown that the introduction of Pluronic F127 into the casting solution reduces contact angle of the membrane selective layer, significantly improves flux and antifouling stability of ultrafiltration membranes.

This work was supported by Russian Foundation for Basic Research [grant No. 17-58-04067] and Belarussian Republican Foundation for Fundamental Research [grant №X17PM-083]. The experimental work was facilitated by equipment from Resource Centers: for Nano technology, Magnetic Resonance Research Centre, X-ray Diffraction Methods, Thermal Analysis and Calorimetry, Chemical Analysis and Materials Research Centre and GEOMODEL at St. Petersburg State University.

Effect of dendrimer generation on the kinetics of peptide complex formation

Elena Popova[1], Valeriy Bezrodniy[2], Igor Neelov[2]

[1]Research Institute of Hygiene, Occupational Pathology and Human Ecology, St. Petersburg, Russian Federation
[2]ITMO University, St. Petersburg, Russian Federation
E-mail: arabka2008@mail.ru

Introduction

Dendrimers are the macromolecules with regular star-like ("star-burst") branched structure. Dendrimers usually have constant spherical shape, constant size and a constant number of charged groups under normal conditions. Lysine dendrimers are important class of dendrimers [1-7].

Therapeutic Semax peptide [8] was selected as a model peptide in this study because it belongs to a class of regulatory peptides and has an antioxidant, antihypoxic and neuroprotective properties. Semax peptide is used for acute ischemic stroke prevention, during traumatic brain injury treatment, recovery of a patient after a stroke, in the case of optic nerve disease and glaucoma optic neuropathy.

The goal of the study was to determine whether there are any differences in kinetics of complexes formation and equilibrium structure of complexes formed by dendrimers of different generations with the same number of Semax peptide molecules.

Systems, consisting of dendrimers of 3rd, 4th and 5th generations and 16 molecules of Semax peptide were chosen (Table 1).

Table 1. Characteristics of dendrimers and their complexes with Semax peptide

System	MM_{dend}, Da	The number of charged groups	The number of hydrogen bonds	Time of complex formation, ns
G3 + 16 Semax	4095	32	36	30
G4 + 16 Semax	8229	64	40	30
G5 + 16 Semax	16496	128	50	40

Modeling and Calculation Method

Modeling was performed using the molecular dynamics method for systems consisting of one lysine dendrimer of different generations (G=3-5) with positively charged NH3+ end groups, 16 Semax peptides (with charge -1 each), water molecules and chlorine counterions in a cubic cell with periodic boundary conditions. The initial conformation for peptide with internal rotation angles of $\varphi = -135°$, $\psi = 135°$, $\theta = 180°$ was modelled by Avogadro chemical editor. The structures were optimized in vacuum using molecular mechanics of AMBER force field. Further energy minimizations and simulations were performed using the GROMACS 4.5.6 software package and AMBER_99SB-ildn force fields. The potential energy of this force field consists of valence bonds and angles deformation energy, internal rotation angles, van der Waals and electrostatic interactions. The procedure of molecular dynamics simulation used for lysine dendrimers and polyelectolytes has been described earlier in [1-5]. In all calculations the normal conditions (temperature 300 K, pressure 1 ATM) were used.

Results and Discussion

The time dependences of the gyration radius for systems of dendrimers of different generation (G = 3-5) and 16 molecules of peptides are presented in Figure 1. It is shown that

dendrimer complexes of 3rd generation and 4th generation with 16 Semax molecules are formed within approximately 30 ns. At the same time, there are small fluctuations in 40 ns that are, most likely, connected with the process of redistribution of peptide positions in complexes. In the case of a dendrimer of the 5th generation and 16 peptides, the complex was formed at 40 ns. It can be concluded that the generation of dendrimers does not have a significant impact on the rate of complexes formation.

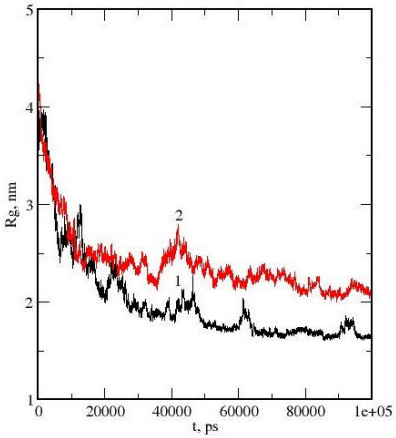

Figure 1. Time dependence of gyration radius. System of dendrimer G3 and 16 Semax peptides (1); G4 and 16 Semax peptides (2)

In equilibrium state the size *Rg* of G3 and 16 Semax complex is larger (1,15 times) than the size of the dendrimer. The sizes of two other complexes (G4 and 16 Semax, G5 and 16 Semax) are slightly larger than the sizes of dendrimers G4 and G5 in 1,24 and 1,05, respectively (see Table 2 It is quite natural, since it correlates with the molecular weight of the complexes increase compared to the molecular weight of the individual dendrimer. The size of the third complex is 1.47 times larger than the size of the first complex and 1.1 times larger than the size of the second complex.

Table 2. Eigenvalues R_g^{11}, R_g^{22}, R_g^{33} of tensor of inertia in dendrimers and dendrimer-peptide complexes

System	R_g^{11}, nm	R_g^{22}, nm	R_g^{33}, nm	R_g, nm	R_g^{33}/R_g^{11}
Dendrimer (G3)	0,98	1,224	1,316	1,444	1,34
G3 and 16 Semax	1,236	1,340	1,512	1,663	1,22
Dendrimer (G4)	1,32	1,488	1,616	1,812	1,24
G4 and 16 Semax	1,528	1,768	2,156	2,248	1,41
Dendrimer (G5)	1,628	1,96	2,02	2,344	1,22
G5 and 16 Semax	1,768	2,032	2,168	2.452	1,23

Information about the internal structure of the equilibrium complex could be obtained using radial density distribution of different groups of atoms relatively center of inertia of system. These radial distribution functions (not normalized) are shown on Fig. 2. They were calculated using *g_rdf* function of GROMACS.

Fig. 2 demonstrates that dendrimer (curve 2, Fig.6) is located in the center of the complexes and peptides (curve 1, Fig. 6) mainly on the surface of complex in all systems with 16 peptides and sometimes penetrate inside the complex. At the same time, the penetration of peptides into the center of the complex decreases with the increase in the number of dendrimer generations.

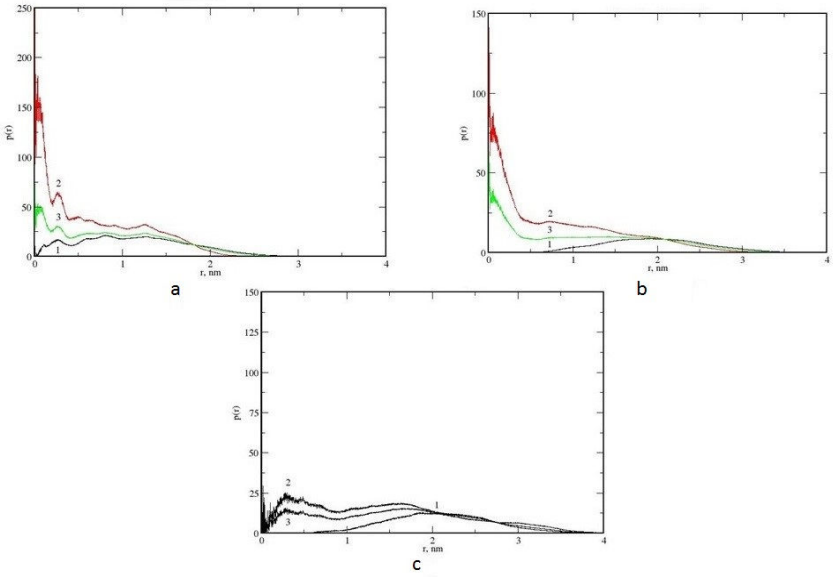

Figure 2. Radial distribution p(r) curves: dendrimer G3 and 16 Semax (a), dendrimer G4 and 16 Semax (b), dendrimer G5 and 16 Semax (c). Distribution curves: peptide atoms (1); dendrimer atoms (2); all atoms of complex (3)

Acknowledgements

This work was partly supported by grant 074-U01 of Government of RF and RFBR grants 16-03-00775 and 15-33-20693mol_a_ved. Computing resources on supercomputers "Lomonosov" were provided by supercomputer center of Moscow State University [9].

References

1. S. Falkovich, D. Markelov, I. Neelov, A. Darinskii, Are structural properties of dendrimers sensitive to the symmetry of branching? Computer simulation of lysine dendrimers, J. Chem. Phys. 139 (2013) 064903.
2. I.M. Neelov, D.A. Markelov, S.G. Falkovich, M.Yu. Ilyash., B.M. Okrugin, A.A. Darinskii, Mathematical modeling of lysine dendrimers. Temperature dependencies, Vysokomolec. Soed. Ser. A, 55, 963–970 (2013) (Polymer Science Series C, 55 (2013) 154-161).
3. I. Neelov, S. Falkovich, D. Markelov, E. Paci, A. Darinskii, H. Tenhu, in: Dendrimers in Biomedical Applications, Eds. London: Royal Society of Chemistry,2013, p. 99–114.

4. I.M. Neelov, A. Janaszewska, B. Klajnert et al, Molecular properties of lysine dendrimers and their interactions with Ab-peptides and neuronal cells, Current Medical Chemistry, 20 (2013) 134–143.
5. D.A. Markelov, S.G. Falkovich, I.M. Neelov, M.Yu. Ilyash, V.V. Matveev, E. Lahderanta, P. Ingman, A.A. Darinskii. - *Physical Chemistry and Chemical Physics*, 17, 3214–3226 (2015).
6. O.V. Shavykin, I.M. Neelov, A.A. Darinskii, Is the manifestation of the local dynamics in the spin-lattice NMR relaxation in dendrimers sensitive to excluded volume interactions? Phys. Chem. Chem. Phys., 18 (2016) 24307-24317.
7. B. Okrugin, I.Neelov, F.M.Leermakers, O.Borisov, Structure of asymmetrical peptide dendrimers: insights given by self-consistent field theory, Polymer 125(2017) 292-302
8. I.M. Neelov, E.V Popova, D.N. Khamidova, I.I. Tarasenko, Complexes of Lysine Dendrimers of 2nd Generation with Semax and Epithalon Peptides. Molecular Dynamics Simulation, International Journal of Biochemistry Research, 2 (2017)28-33
9. V. Sadovnichy, A. Tikhonravov, V. Voevodin, V. Opanasenko Contemporary High Performance Computing: From Petascale toward Exascale, Boca Raton, 2013

Characterization of complex superparamagnetic colloids by electron magnetic resonance (EMR) and second-harmonic magnetic response (M2)

V. A. Ryzhov[1], I. A. Kiselev[1], O. P. Smirnov[1], Yu. P. Chernenkov[1], V. V. Deriglazov[1], Ya. Yu. Marchenko[2], B. P. Nikolaev[2], Yu. V. Bogachev[3]

[1]*NRC "Kurchatov Institute" PNPI, Gatchina, Russia*
[2]*Research Institute of Highly Pure Biopreparations, St. Petersburg, Russia*
[3]*S-Petersburg State Electrotechnical University "LETI", St. Petersburg, Russia*
E-mail: deriglazov_vv@pnpi.nrcki.ru

Introduction

Magnetic nanoparticles (MNP) are widely adopted in technical, environmental and biomedical applications. Specifically, liquid solutions of magnetite-based MNP are employed in disease diagnostics as contrast agents in magnetic resonance imaging and in tumor treatment including hyperthermia and drug delivery. To prevent toxicity, oxidation, and aggregation, MNP are coated with some, mostly organic, shell. This may affect the relevant magnetic properties and, besides, the aggregation still may occur resulting in the formation of colloidal complexes. A comprehensive characterization of the solutions is vitally important for the correct implementation of the corresponding medical procedures.

In this study, an aqueous colloidal solution of nanosize (~10 nm) dextran-coated MNP was studied by EMR combined with the unconventional M2 technique exploiting magnetic response on the second harmonic in longitudinal geometry of magnetic fields. Both the EMR and M2 signals as functions of the external magnetic field were treated with the formalism based on the Gilbert-Landau-Lifshitz equation for the stochastic dynamics of superparamagnetic particles. By transition electron microscopy and dynamic light scattering, the colloid was shown to form aggregates consisting of ~10 - 100 MNP. From M2 measurements, MNP inside the aggregates were found to be spatially magnetically correlated at a relatively short distance, due to dipole-dipole (d-d) coupling. A set of parameters featuring the magnetic behavior of the colloid were extracted including the in-aggregate anisotropy and d-d energies, the magnetic correlation radius, the longitudinal relaxation time and many others. The joint employment of these two techniques enables to quantify separately the system of aggregates and the constituting MNP themselves. The idea exploits the fact that each technique operates in essentially different ranges of the dc magnetic field and the frequency of the ac field. At rather low dc fields of the order 100 Oe used in the M2 measurements, the MNP due to d-d coupling exhibit a collective response characteristic for the aggregates, whereas at the EMR dc fields higher than ~1 kOe, the d-d coupling is broken and each MNP responds independently. At the same time, at the ac frequencies ~10 MHz, the M2 nonlinear response is particularly strong making this technique perfectly well available for characterizing superparamagnetic systems, while the X-range EMR frequencies ~10 GHz are most informative in the dc field range above the d-d coupling field.

Experimental data

The EMR spectra were recorded with the special homemade X-range spectrometer operating at the frequency 8.54 GHz and supplied with the cylindrical two-mode balanced cavity with TE_{111}-type of electromagnetic oscillations [1]. The dc magnetic field was directed along the cylinder *z*-axis. The sample was placed at the bottom of the cavity where it was affected by the linearly polarized ac field directed along the *x*-axis perpendicular to the dc field (excitation *xz*-plane). The detection *yz*-plane was perpendicular to the excitation one and, thus,

the detected signal was proportional to the gyrotropic component of the susceptibility tensor χ_{yx} corresponding to the *y*-component of the induced magnetic moment.

The EMR signals proportional to the mixture of the dispersion χ'_{yx} - and absorption χ''_{yx} parts of the magnetic susceptibility $\chi = \chi' + i\chi''$ were registered as functions of the dc magnetic field ranging from 260 to 6400 Oe (Fig.1, left).

The real and imaginary parts of the second-harmonic magnetic response M_2 were simultaneously measured in the parallel dc and ac fields (Fig.1, right). The dc field was scanned back-and-forth symmetrically within ±300 Oe with the round-up cycles 0.125 – 4 s and with high representativity of 2048 *H*-points in each scan. The amplitude h_0 = 13.8 Oe of the ac field with the frequency 15.7 MHz ensured the condition $M_2 \sim h_0^2$.

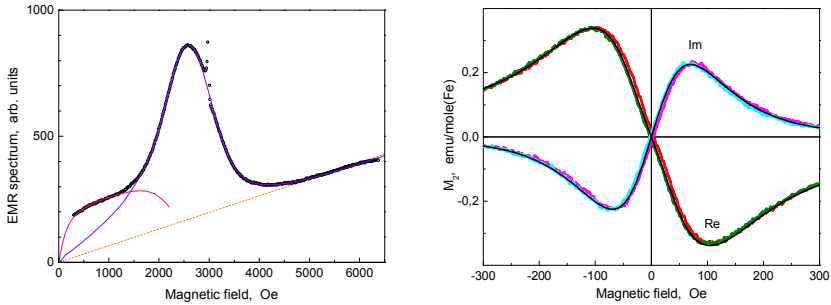

Figure 1. ***Left:*** *EMR spectrum (circles), the sharp peak at 3 kOe is the nitroxyl radical signal used as a calibration witness, the solid curves are best fits for magnetically correlated (H<1250 Oe, red) and independent (H>1650 Oe, blue) particles with the crossover at 1430 Oe, the straight dashed line is the background Hall signal.*
Right: *real and imaginary parts of the nonlinear magnetic response, the filled circles (red and magenta) are the direct scan, the open circles (green and cyan) are the reverse scan and the solid curves are the simultaneous best fit*

All the experimental dependences (Fig.1) were fitted with the functions inferred within the formalism implying a numerical solution of the Fokker-Planck equation for the kinetics of superparamagnetic particles. In Fig.1 (left), two field regions exist where the signal is described in different ways with the crossover at H_c = 1430 Oe. For $H < H_c$, the signal is well fitted with the parameters obtained from the M2 data (right) valid for the aggregates whereas for $H > H_c$, the EMR data fit yields the parameters characterizing independent MNP constituting the aggregates. The crossover is due to the break of d-d coupling by the dc field. The crossover field was estimated to fall into the interval 1120 – 1490 Oe covering the observed H_c.

The crossover is accompanied by abrupt change of the magnetization relaxation dynamics. With increasing the dc field over H_c, the longitudinal relaxation time rises by five times. This effect should be accounted for and can be used in practical applications of MNP colloids. For instance, probing the latter by magnetorelaxometry or any other suitable technique may specify whether the MNP are in the aggregated or nonaggregated state.

References

1. V. A. Ryzhov, E. I. Zavatskii, V. A. Solov'ev, I. A. Kiselev, V. N. Fomichev, V. A. Bikineev. – *Tech. Phys.*, **40**, 71 (1995) [*Zh. Tekh. Fiz.*, **65**(1) 133-145 (1995)].

Optimization of bacterial expression of MdmX N-terminal domain for NMR studies

Vladislav A. Salikov[1], Dmitry A. Luzik[1], Sevastyan O. Rabdano[1], Ivan S. Podkorytov[1] and Nikolai R. Skrynnikov[1,2]

[1]Laboratory of Biomolecular NMR, SPbSU, 199034, 7/9 Universitetskaya nab., St. Petersburg
[2]Department of Chemistry, Purdue University, 47907, 560, Oval Drive, West Lafayette IN, USA.
E-mail: vladislav.salikov@inbox.ru
http://bio-nmr.spbu.ru

Human MdmX protein is known as a negative regulator of the p53 tumor suppressor [1]. Therefore, MdmX is a highly relevant target for anticancer molecular therapy, and inhibition of p53-MdmX interaction is an important objective in this field. In this study we investigated the binding of MdmX N-terminal domain (22-111) with synthetic p53-based high-affinity peptide P4. Of particular interest is the interaction with the (specially modified) P4 peptide that is capable of covalently binding to the target MdmX domain.

To characterize this interaction, we seek to express and purify a domain of interest and assess its structural state by NMR spectroscopy.

In present work, we transformed *E.Coli* Rosetta strain by pET28a(+) plasmid with a synthetic gene encoding the protein of interest. Also, we performed optimization of the expression protocol for ^{15}N labeled MdmX in *E coli* by varying several experimental parameters. The best combination of parameters to induce the expression of the protein was determined to be: OD_{600}=0.6, 1 mM IPTG, 18°C post-induction temperature. Expression levels under different conditions were evaluated by SDS-PAGE. Prior to NMR investigation of the protein, MdmX was purified using Ni-affinity chromatography with further removing of His6-tag by means of thrombin cleavage.

Structural state of MdmX (22-111) was evaluated by ^{1}H-^{15}N HSQC spectroscopy using the data deposited in Biological Magnetic Resonance Bank for comparison (BMRB entry 16893). The obtained spectrum was found to be in good agreement with the BMRB spectrum.

In conclusion, we successfully expressed and purified the recombinant N-terminal domain of MdmX, recorded and processed the NMR spectrum and therefore confirmed the correct folding of our protein. This makes it possible to further investigate protein-peptide interaction involving MdmX.

Acknowledgements

This work was supported by the RSF grant 15-14-20038. All NMR measurements were performed at the Center for Magnetic Resonance in the Research Park of St. Petersburg State University.

References

1. Ghosh, M., Huang, K. & Berberich, S.J. 2003, "Overexpression of Mdm2 and MdmX fusion proteins alters p53 mediated transactivation, ubiquitination, and degradation", Biochemistry, vol. 42, no. 8, pp. 2291-2299.

Influence of the asymmetry of branching on the structural properties of dendrimers. Brownian dynamics simulation

Oleg V. Shavykin, Ivan V. Mikhailov[2], Igor M. Neelov[1], Anatoly A. Darinskii[2]

[1]St. Petersburg National Research University of Information Technologies, Mechanics and Optics (ITMO University
[2]Institute of Macromolecular Compound of Russian Academy of Sciences
E-mail: kupala-89@mail.ru

Introduction

Dendrimers are a class of regular hierarchically branched macromolecules. Due to the compact shape and the large number of terminal functional groups the dendrimers are of interest to a wide range of applications [1]. As a rule, each branch point gives rise to two spacers. The majority of dendrimers have spacers with the same contour length. However there are dendrimers with the asymmetry of branching, i.e. the spacers arising from the branch point have different lengths. As a characteristic of this asymmetry one can use the ratio $A = S_2/S_1$ of the contour lengths of the long S_2 and the short S_1 spacers. In contrast to dendrimer with the symmetrical branching there are only few works, where the impact of the asymmetry of branching on structural characteristics of dendrimers has been studied theoretically. In particular, dendrimers with the relatively small A were simulated by using full-atomic [2-6] and coarse-grained [7] models. For such dendrimers the effect of the asymmetry on the dendrimer conformation and the internal structure occurred to be rather weak. Dendrimers with larger values of A were considered in [8] on the base of the approximate numerical self-consistent field (SCF) method. It was shown that the large asymmetry has a weak influence on the dendrimer size but is manifested significantly in the internal dendrimer structure.

In the present work we perform the direct simulation of the coarse-grained dendrimer models by using the Brownian dynamics (BD) method in the broad range of asymmetry of branching. To reveal the effect of the asymmetry the dendrimers with different A but with the same average spacer length $\langle S \rangle = (S_1+S_2)/2$ were considered. Both global and local structural characteristics of dendrimers were calculated and their dependence on A was established.

Model

We use the coarse grained bead-spring model of a dendrimer at the good (athermal) solvent conditions. The number of generations G was varied from 2 to 8. The parameter of the asymmetry A was varied from 1 to 11 by keeping constant the average spacer length $\langle S \rangle = 6$.

Size and shape

As the characteristics of the dendrimer size we use the mean-squared distance R_e from the dendrimer center to terminal monomers:

$$R_e = \left(\langle \frac{1}{N_t} \sum_{i=1}^{N_t} (r_c - r_i)^2 \rangle \right)^{1/2}$$

and the gyration radius R_g:

$$R_g = \left(\langle \frac{1}{N} \sum_{i=1}^{N} (r_c - r_i)^2 \rangle \right)^{1/2},$$

Here r_i, r_c are coordinates for the i-th (terminal for R_e) monomer unit and the center of mass of a dendrimer respectively. Figure 1a shows the dependence R_e on the generation number G for dendrimers with different asymmetry of branching. It is seen that R_e shows a very weak sensitivity to the change of A. This result is in agreement with that obtained by the SCF

approach [8]. As to the gyration radius R_g we see some effect of the asymmetry: the slope of the dependence of the characteristic ratio R_g/R_e. on G decreases with an increase of A (fig. 1b). The maximal difference between values of R_g/R_e corresponding to the symmetrical (A=1) and strongly asymmetric (A=11) cases is observed at small G and disappears at large G.

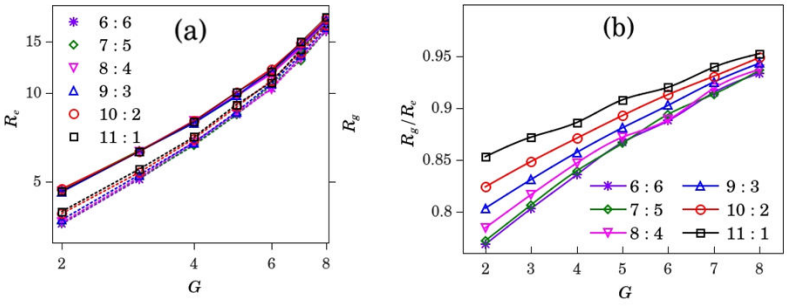

Figure 1. (a) The size characteristics of the dendrimer Re (solid lines) and Rg (dotted lines) as a function of G for all systems; (b) The characteristic ratio Rg/Re versus the number of generations G. The results for dendrimers with the different branching asymmetry (A = 6 : 6; 7 : 5; 8 : 4; 9 : 3; 10 : 2; 11 : 1) are shown

The dendrimer shape is characterized by the parameter a of the shape anisotropy, which is calculated by using the formula:

$$a = 1 - 3\frac{I_x I_y + I_x I_z + I_y I_z}{(I_x + I_y + I_z)^2}$$

where I_x, I_y, I_z are the eigenvalues of the gyration tensor. For the sphere $a = 0$.

Fig. 2a shows that this parameter deceases with G demonstration the transition to spherical shape. Similar to the size the dendrimer shape is also weakly sensitive to the asymmetry of branching. Small effect is seen for dendrimers with low G.

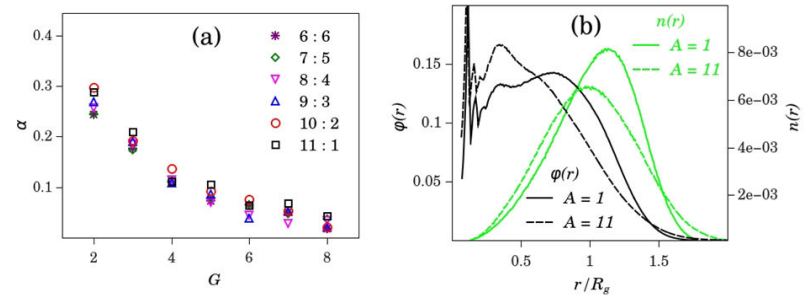

Figure 2. (a) The anisotropy of the dendrimer shape as a function of the generation number. (b) The radial volume fraction profile of monomer units (left ordinate) and the distributions of the terminal monomer units (right ordinate, normalized by total number of terminal points) for dendrimers with G = 8 at the branching asymmetry A = 1 and A = 11

Internal structure

As the characteristics of the internal dendrimer structure we use the radial distributions the volume fraction of monomer units $\varphi(r)$ and of the number of terminal monomers $n_t(r)$.

Radial distribution of the volume fraction of monomer units is given by the expression:

$$\varphi(r) = \frac{n(r)}{V(r)},$$

where $n(r)$ is the number of monomer units in the spherical layer around the dendrimer center with the radius r and the thickness Δ, and $V(r)$ is the volume of this layer. Fig. 2b shows that the asymmetry of branching significantly affects the radial density profile. By the asymmetry increase it changes the shape from the convex to the concave one. In the same time the distribution of terminal monomer units shifts towards the dendrimers center as compared to symmetrical dendrimers. These results are also in agreement with theoretical predictions of the SCF method.

Conclusions

Brownian dynamics simulations show that the asymmetry of branching has small effect on the global characteristics of dendrimer such as the size and shape but influence significantly on the internal dendrimer structure.

Acknowledgements

The research is carried out using the equipment of the shared research facilities of HPC computing resources at Lomonosov Moscow State University [9]. O.V. Shavykin and I. M. Neelov are grateful to the grant of the Government of Russian Federation 074-U01 for the support.

References

1. M. Frechet, D. Tomalia, Dendrimers and Other Dendritic Polymer, Wiley, England, 2001.
2. S. Falkovich, D. Markelov, I. Neelov, A. Darinskii, Are structural properties of dendrimers sensitive to the symmetry of branching? computer simulation of lysine dendrimers, J. Chem. Phys. 139 (2013) 064903.
3. I.M. Neelov, D.A. Markelov, S.G. Falkovich, M.Yu. Ilyash., B.M. Okrugin, A.A. Darinskii, Mathematical modeling of lysine dendrimers. Temperature dependencies, Vysokomolec. Soed. Ser. A, 55, 963–970 (2013) (Polymer Science Series C, 55 (2013) 154-161).
4. I. Neelov, S. Falkovich, D. Markelov, E. Paci, A. Darinskii, H. Tenhu, in: Dendrimers in Biomedical Applications, Eds. London: Royal Society of Chemistry, 2013, p. 99–114.
5. I.M. Neelov, A. Janaszewska, B. Klajnert, M. Bryszewska, N. Makova, D. Hicks, H. Pearson, G.P. Vlasov, M.YuIlyash, D.S. Vasilev, N.M. Dubrovskaya, N.L. Tumanova, I.A. Zhuravin, A.J. Turner, N.N. Nalivaeva, Molecularproperties of lysine dendrimers and their interactions with a-peptides and neuronal cells, Current Medical Chemistry, 20 (2013) 134–143.
6. D.A Markelov, S.G. Falkovich, I.M. Neelov, M.YuIlyash, V.V Matveev, E. Lahderanta, P. Ingman, A.A. Darinskii, Molecular dynamics simulationof spin-lattice nmr relaxation in poly-l-lysine dendrimers. Manifestation of the semiflexibility effect, Physical Chemistry Chemical Physics, 17(2015) 3214–3226.
7. I.V.Mikhailov, A.A. Darinskii Does symmetry of branching affect the properties of dendrimers? Polymer Science. Series A, 56 (2014) 534–544.
8. B. Okrugin, I. Neelov, F. M. Leermakers, O. Borisov, Structure of asymmetrical peptide dendrimers: insights given by self-consistent field theory, Polymer 125 (2017) 292–302.
9. V.Sadovnichy, A.Tikhonravov, V.Voevodin, V.Opanasenko Contemporary High Performance Computing: From Petascale toward Exascale, Boca Raton, 2013.

Study of Local Orientation Mobility in Lysine Dendrimers by NMR method

Nadezhda N. Sheveleva[1], Denis A. Markelov[1,2], Mikhail A. Vovk[1], Maria E. Mikhailova[1], Irina I. Tarasenko[3], Igor M. Neelov[3], Erkki Lähderanta[4]

[1]St. Petersburg State University, 7/9 Universitetskaya nab., St. Petersburg, 199034 Russia,
[2]St. Petersburg National Research University of Information Technologies, Mechanics and Optics (ITMO University), Kronverkskiy pr. 49, St. Petersburg, 197101 Russia.
[3]Institute of Macromolecular Compounds, Russian Academy of Sciences, Bolshoi Prospect 31, V.O., St. Petersburg, 199004 Russia.
[4]Laboratory of Physics, Lappeenranta University of Technology, Box 20, 53851 Lappeenranta, Finland
E-mail: shevelevann@gmail.com

Dendrimers are a class of macromolecules with a three-dimensional, nanoscale hyperbranched structure. The local orientation mobility of groups in dendrimers is an important parameter for drug and gene delivery, synthesis of nanoparticles, and others [1].

We study the local orientation mobility in peptide dendrimers with and without side fragments in the inner segments. The G =2 generation peptide dendrimers, Lys-2Lys and Lys-2Gly, were specially synthesized for these purposes. The samples dissolved in heavy water were studied by the ^{1}H NMR spin-lattice relaxation method. We measure temperature dependences of T_{1H} in range from 283 to 343 K. Hydrodynamic radii and effective densities of dendrimers under study were estimated by diffusion measurements. Particular attention is given to NMR active CH_2-N groups, which have separate and highly resolved peaks for inner and terminal segments in the spectrum of the dendrimers. A detailed analysis of temperature dependences of $1/T_{1H}$ for inner and terminal CH_2-N groups is presented. On the one hand, the dendrimers have different hydrodynamic radii and, as a result, the effective densities. On the other hand, the mobilities of groups in inner segments of these dendrimers are practically equal. Also the orientational mobility of the groups in the side fragments coincides with the mobility of the terminal groups [2]. Consequently, these experimental data are in a good agreement with MD simulations [3-5] and analytical theory [6] and confirm that T_{1H} relaxation in semiflexibile dendrimers is not sensitive to volume effects [7]. These data widen our understanding of local orientation mobility in hyperbranched peptide dendrimers and can be applied in further research.

References

1. Neelov, I.; Falkovich, S.; Markelov, D.; Paci, E.; Darinskii, A.; Tenhu, H. In *Dendrimers in Biomedical Applications*; Klajnert, B and Peng, L and Cena, V, Ed.; The Royal Society of Chemistry, 2013; pp 99–114.
2. Markelov, D. A.; Dolgushev, M.; Lähderanta, E. In *Annual Reports on NMR Spectroscopy*; Webb, G. A., Ed.; Academic Press, 2017; Vol. 91, pp 1–66.
3. Neelov, I. M.; Markelov, D. A.; Falkovich, S. G.; Ilyash, M. Y.; Okrugin, B. M.; Darinskii, a. a. *Polymer Science Series C* **2013**, *55* (1), 154–161.
4. Markelov, D. A.; Shishkin, A. N.; Matveev, V. V; Penkova, A. V; Lähderanta, E.; Chizhik, V. I. *Macromolecules* **2016**, *49* (23), 9247–9257.
5. Markelov, D. A.; Falkovich, S. G.; Neelov, I. M.; Ilyash, M. Y.; Matveev, V. V.; Lähderanta, E.; Ingman, P.; Darinskii, A. A. *Phys. Chem. Chem. Phys.* **2015**, *17* (5), 3214–3226.
6. Grimm, J.; Dolgushev, M. *Physical Chemistry Chemical Physics* **2016**, *18* (28), 19050–19061.
7. Shavykin, O. V; Neelov, I. M.; Darinskii, A. A. *Phys. Chem. Chem. Phys.* **2016**, *18*, 24307–24317.

Development of a standard base for the "medium" and "strong" constant field's magnetic induction measurement

V. Ya. Shifrin[1], D. I. Belyakov[1], D. D. Kosenkov[1,2], and A. E. Shilov[1]

[1]NIL-2205, VNIIM of the D.I. Mendeleyev, Saint-Petersburg
[2]Faculty of Control Systems and Robototechnics, ITMO University, Saint-Petersburg
E-mail: V.Ya.Shifrin@vniim.ru

The main objective of the study is the expansion of the field of metrological support for measurements of the magnetic quantities basic unit - magnetic induction (MI) directly based on the state primary standard GET12-2011 [1], from $1 \cdot 10^{-6}$ - $1 \cdot 10^{-3}$ T to $1 \cdot 10^{-6}$ - 1 T.

There are fundamental limitations connected with the inconsistency of the measurement ranges realized on the basis of existing quantum measurement methods within the limits $1 \cdot 10^{-6}$ - $1 \cdot 10^{-3}$ T and $1 \cdot 10^{-3}$ - $2 \cdot 10^{-2}$ T. This fact did not make it possible to directly transfer the unit size from GET12-2011 to all measurement areas in the range from $1 \cdot 10^{-6}$ to 1 T in previous years.

In the previous two years, the procedure of transferring the unit of MI size from the state standard GET 12-2011 [2] to working teslameters was developed in the range from 1 mT to 1 T.

At the first stage of the MI transfer procedure, the conversion coefficients of the quantum cesium magnetometer (QCM) were determined by comparing it with the GET 12-2011 in the range of 0.8-1.5 mT.

In Fig. 1 there is a block diagram of the measuring system for transferring the MI unit from the GET 12-2011 to the QCM.

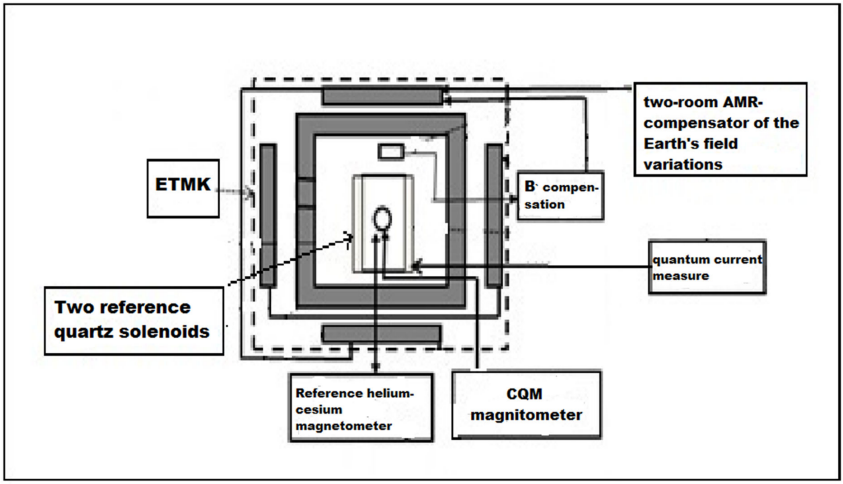

Figure 1. Structural diagram of the measuring system for transferring the MI unit from the GET 12-2011 to the CMC

The measuring system in the MI reproduction mode consists of the following six main components from the composition of the GET12-2011 and, collated with the reference helium-cesium magnetometer EGM, the QCM magnetometer: two reference quartz solenoids fed by a quantum measure of the current; standard three-component MI (ETMK) with a system for generating the Earth's magnetic field compensation currents; two-room AMR-compensator of

variations of the Earth's field; the reference helium-cesium magnetometer and compensator of industrial noise. ETMK with a current generation system provides compensation of the Earth's magnetic field, the current intensity quantum measure generates a direct current in the series-connected windings of standard quartz measures.

At the second stage of transmitting a MI unit in the measurement range of 8-25 mT, the NMR-teslameter designed for these experiments is calibrated by comparing it with the QCM using a quantum MI comparator.

In Fig. 2 there is a block diagram of the quantum comparator MI for the range 8-25 mT.

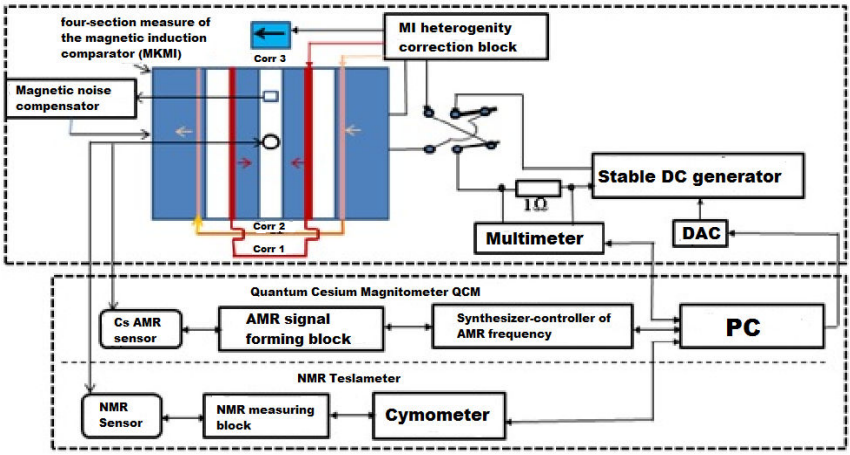

Figure 2. Structural diagram of a quantum comparator of a unit of magnetic induction of a constant field of 1-25 mT

The main elements of the created comparator are: atomic magnetic resonance quantum cesium magnetometer QCM; four-section measure of the magnetic induction comparator (MKMI) with additional windings for homogeneity correction, stable constant current generator GPT with follow-up control system; NMR tesla meter. At the last stage of transferring a unit of MI to the strong field, consistent comparisons of NMR-Teslameter's measuring transducers covering a number of measurement subbands overlapping the range of 0.02-1 T and calibrating the working NMR-Teslameters with the developed experimental NMR-Teslameter sample in the comparator electromagnet.The results of the studies described above make it possible to transfer the MI unit directly from the GET 12-2011 SI operating in the $1 \cdot 10^{-3}$ - 1 T range with the total standard uncertainty within $(1...2) \cdot 10^{-6}$.

Studies to determine and refine the components of the conversion coefficient of QCM according to the above procedure continue.

References

1. V. Ya. Shifrin, V.N. Khorev, V.N. Kalabin, S.L. Voronov, A.E. Shilov, Measuring Technology, 2012, No. 7, pp. 3-7.
2. DI Belyakov, VN Khorev, AE Shilov, V.Ya. Shifrin, Measuring Technology, 2017, No. 12, pp. 28-31.

0212-0201 mixed-phase of Sr-Ca-Cu-O superconductor: influence of doping on the material properties

A. Sklyarova[1], T. Naito[1], S. Shinoda[1], V. I. Chizhik[2] and H. Suematsu[1]

[1]Extreme Energy-Density Research Institute, Nagaoka University of Technology, 1603-1 Kamitomioka, Nagaoka 940-2188, Japan
[2]St. Petersburg State University, 7/9 Universitetskaya nab., St. Petersburg, 199034, Russia
E-mail: asklyaro@vos.nagaokaut.ac.jp

In this work growth of $(Sr,Eu)_2CaCu_2O_y$ and $Sr_2Ca(Cu,Fe)_2O_y$ polycrystalline materials under 5GPa have done. For the growth condition optimization, non-enriched raw powders of SrO_2, $CaCO_3$ Fe_2O_3, Eu_2O_3 and CuO were synthesized and mixed in a glove box. The raw powders were sealed into a gold capsule, which is place in a pressure media, rapidly heated up to 875 - 1050°C and kept for 1 h.

It is difficult to obtain a pure 0212 phase of Sr-Ca-Cu-O and secondary phases, which are inevitable for the high pressure synthesis, can appear. Because of sample inhomogeneity, a number of interesting and important effects in Fe and Eu-substituted samples can be observed. One of them is a magnetic ordering appearing below 20 K in samples with Cu substituted by Fe. This ordering effect is shown in Fig.1, where the distortion of the magnetic susceptibility curves both in ZFC and FC regimes takes place.

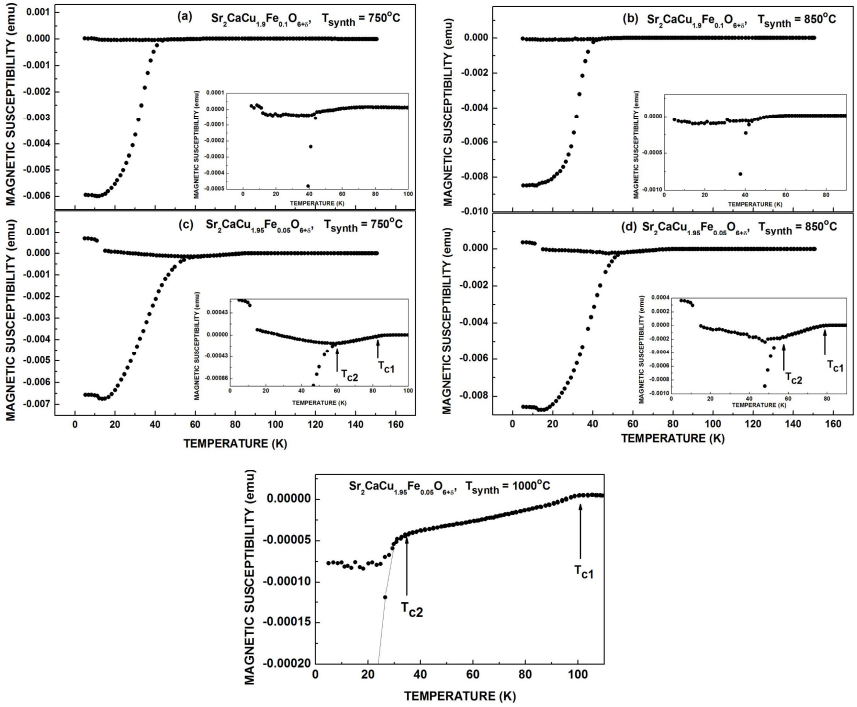

Figure 1. Magnetic susceptibility vs. temperature in ZFC and FC (10 Oe) regimes for the Fe-substituted samples synthesized at different temperatures. The insets show the transition region in more details [1]

Another effect appeared in the fairly homogeneous samples with Sr by Eu substitution: low-temperature measurements gave the complex structure of superconducting dome.

We think that the hyperfine properties study can clarify the observed effects and the spectroscopic methods were possible to use for the local environment investigation. For $Sr_2CaCu_2O_y$, with our preliminary experiments reveal that the oxygen content can be controlled by precise post annealing in a thermo balance in a wide range from $y = 5.00$ to 5.42. Using these data, the coordination number for Sr is determined and enables us to compare the local environment obtained by Mössbauer spectroscopy.

Acknowledgements

A part of this work was supported by RFBR (grant #16-32-50007).

References

1. A. Sklyarova, S. Shinoda, T. Nagumo, V. I. Chizhik, V. V. Matveev and H. Suematsu "Observation of low-temperature magnetic ordering in mixed-phase Sr-Ca-Cu-O superconductors substituted by iron", Supercond. Sci. Technol., vol. 29, p. 085001, 2016.

NMR study of reorientational motion in borohydrides of $Mg(BH_4)_2$

Alexey V. Soloninin[1], Alexander V. Skripov[1], Olga A. Babanova[1], Torben R. Jensen[2], Yaroslav Filinchuk[3]

[1]Institute of Metal Physics, Ural Division of the Russian Academy of Sciences, S. Kovalevskoi 18, Ekaterinburg 620990, Russia
[2]Center for Materials Crystallography, Interdisciplinary Nanoscience Center (iNANO), and Department of Chemistry, Aarhus University, Langelandsgade 140, DK-8000 Aarhus C, Denmark.
[3]Institute of Condensed Matter and Nanosciences, Universite catholique de Louvain, Place L. Pasteur 1, B-1348 Louvain-la-Neuve, Belgium
E-mail: alex.soloninin@imp.uran.ru

Introduction

Magnesium borohydride $Mg(BH_4)_2$ containing 14.9 mass % of hydrogen is considered as one of the most promising materials for hydrogen storage. X-ray and neutron diffraction studies of the crystal structures of $Mg(BH_4)_2$ have revealed an unexpected structural complexity of this material. The low-temperature (α) phase of $Mg(BH_4)_2$ has the hexagonal symmetry (space group $P6_122$). The unit cell of α-$Mg(BH_4)_2$ contains 330 atoms [1]. Above 463 K, α-$Mg(BH_4)_2$ irreversibly transforms to the orthorhombic high-temperature (β) phase (space group *Fddd*). The unit cell of β-$Mg(BH_4)_2$ contains 704 atoms. The characteristic feature of the cubic γ phase (space group *Id*-3*a*) is a three-dimensional set of interpenetrating channels. The empty volume in the structure of the γ phase amounts to 33% [2]. The amorphous $Mg(BH_4)_2$ obtained by pressure collapse of the porous γ-$Mg(BH_4)_2$ is a distinct and a stable form of magnesium borohydride, with one of the highest volumetric hydrogen densities of 145 g/L [3]. The aim of the present work is to study the H jump motion in different phases of $Mg(BH_4)_2$ using ^{1}H and ^{11}B NMR measurements of the spectra and spin-lattice relaxation rates over wide ranges of temperature (82-443 K) and resonance frequency (14-90 MHz).

Experimental results

The temperature dependences of the proton spin-lattice relaxation rates R_1^H measured at three resonance frequencies for α-$Mg(BH_4)_2$ are shown in Figure 1. For the relaxation mechanism due to nuclear dipole-dipole interaction modulated by atomic motion, $R_1^H(T)$ typically exhibits a frequency-dependent maximum. This maximum is expected to occur at the temperature at which the atomic jump rate τ^{-1} becomes nearly equal to the resonance frequency ω. As can be seen from Figure 1, the observed temperature dependence of R_1^H for α-$Mg(BH_4)_2$ shows two well-separated peaks; both the positions and the amplitudes of these peaks depend on the resonance frequency. Such a behavior suggests a coexistence of at least two atomic jump processes with different characteristic rates τ_i^{-1}. First of all, we use a 'two-peak' model including two types of jump motion and a Gaussian distribution of activation energies. However, the R_1^H drop between the peaks predicted by this model appears to be too strong. This suggests the presence of an additional jump process giving rise to an extra relaxation rate peak at intermediate temperatures. We use a 'three-peak' model including three types of jump motion and a Gaussian distribution of activation energies for the fastest jump process. The results of this fit are shown by red solid lines in Figure 1 and the values of activation energies are presented in Table 1. The feature of the local environment of BH_4 groups is their nearly linear coordination by two Mg atoms. Such an unusual coordination of BH_4 groups immediately suggests that different values of E_{ai} can be related to different types of reorientation of the same

BH_4 group. In fact, the rotation around the 2-fold axis connecting B and Mg atoms does not break any Mg – H bonds; therefore, this type of motion should correspond to the lowest value of E_a. The rotation around two other 2-fold axes of a BH_4 tetrahedron breaks all the Mg – H bonds and should be associated with the highest value of E_a. The intermediate value of E_a can be ascribed to the rotation around the 3-fold axes, since such a rotation breaks half of the Mg – H bonds.

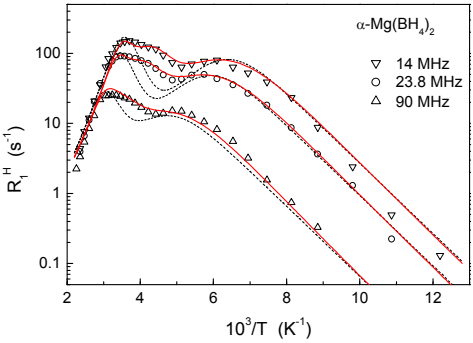

Figure 1. Proton spin-lattice relaxation rates measured at 14, 23.8 and 90 MHz for α-$Mg(BH_4)_2$ as functions of the inverse temperature. The dashed lines show the simultaneous fits of the 'two-peak' model to the data. The red solid lines show the simultaneous fits of the 'three-peak' model to the data

The $R_1^H(T)$ peak for β-$Mg(BH_4)_2$ is shifted to considerably lower temperatures with respect to both $R_1^H(T)$ peaks for α-$Mg(BH_4)_2$. This means that the reorientational motion of BH_4 groups in β phase is generally much faster than in α phase. More precisely, the distribution of H jump rates in β phase is shifted to higher rates with respect to that in α phase. The significant distribution width for β-$Mg(BH_4)_2$ may result from the antisite disorder and the considerable spread in B – Mg distances [2]. Comparison of the fit parameters for γ- and β-$Mg(BH_4)_2$ shows that the average activation energy E_a for the γ phase is considerably larger, and the distribution width ΔE_a is smaller than for the β phase. The reorientational motion of BH_4 groups in different phases of $Mg(BH_4)_2$ cannot be described it terms of a single activation energy. This may be related to the differences in coordination of the BH_4 groups. It should be noted that the ^{11}B spin-lattice relaxation rate measurements in borohydrides usually give essentially the same information on the parameters of reorientational motion as the R_1^H measurements.

The position of the $R_1^H(T)$ peak for the amorphous $Mg(BH_4)_2$ (Figure 2) differs significantly from the corresponding positions for all the crystalline $Mg(BH_4)_2$ phases. In fact, for the amorphous $Mg(BH_4)_2$ the $R_1^H(T)$ maximum at $\omega/2\pi = 14$ MHz is observed near 190 K, while for the crystalline α-, β-, and γ-phases the $R_1^H(T)$ maxima at the same frequency occur near 290 K, 120 K, and 270 K, respectively. This means that the amorphous phase of $Mg(BH_4)_2$ exhibits its own distinct dynamics of BH_4 reorientations. As can be seen from Figure 2, the experimental $R_1^H(T)$ data for the amorphous $Mg(BH_4)_2$ exhibit significant deviations from the

standard behavior. First, the high-temperature slope of the $R_1^H(T)$ peak appears to be steeper than the low-temperature one. Second, the frequency dependence of R_1^H at the low-temperature slope is much weaker than the expected ω^{-2} dependence. These features are consistent with the presence of a broad distribution of H jump rates, which can be expected for the amorphous system.

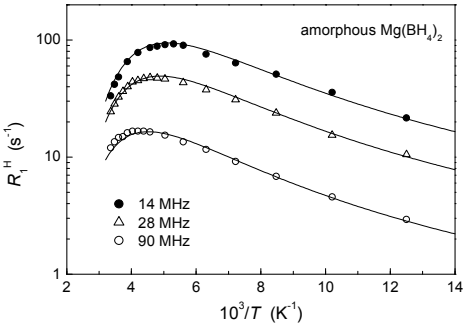

Figure 2. Proton spin-lattice relaxation rates measured at 14, 28, and 90 MHz for the amorphous $Mg(BH_4)_2$ as functions of the inverse temperature. The solid lines show the simultaneous fit of the model with a Gaussian distribution of the activation energies to the data

Table 1. Activation energies for BH_4 reorientations in different phases of $Mg(BH_4)_2$

Compound	activation energy E_a or $\overline{E}_a$ (meV)	dispersion of the E_a distribution, ΔE_a (meV)
α-$Mg(BH_4)_2$	116 (6), 298 (12), 362 (5)	10 (4)
β-$Mg(BH_4)_2$	138 (5)	36 (3)
γ-$Mg(BH_4)_2$	276 (5)	19 (4)
amorphous $Mg(BH_4)_2$	234 (9)	100 (10)

Acknowledgements

This work is supported by the Russian Federal Agency of Scientific Organizations under Program "Spin" No. 01201463330.

References

1. A. V. Skripov, A. V. Soloninin, O. A. Babanova, H. Hagemann, Y. Filinchuk. – *J. Phys. Chem. C*, 114, 12370−12374 (2010).
2. A. V. Soloninin, O. A. Babanova, A. V. Skripov, H. Hagemann, B. Richter, T. R. Jensen, Y. Filinchuk. – *J. Phys. Chem. C*, 116, 4913−4920 (2012).
3. V. Ban, A. V. Soloninin, A. V. Skripov, J. Hadermann, A. Abakumov, Y. Filinchuk. – *J. Phys. Chem. C*, 118, 23402−23408 (2014).

Molecular mobility of polylactide investigated by electronic paramagnetic resonance

Yulia V. Tertyshnaya, Ludmila S. Shibryaeva, Anatoliy A. Popov

Emanuel Institute of Biochemical Physics RAS, Moscow, Russia
E-mail: terj@rambler.ru
www.ibcp.chph.ras.ru

Introduction

The EPR method is one of the widely used methods for determining structural and kinetic parameters in chemistry. Although to control the structure of polymers EPR is not as popular as other methods, for instance thermal ones. In this work, the EPR method was applied to study molecular mobility in polymers, in particular polylactide and its blends of with low density polyethylene before and after exposure to different environmental factors. Polylactide is a promising polymer that can be used in various fields of industry. There are many works studying its structure and properties [1, 2]. In this paper, the authors study the influence of distilled and natural seawater on PLA with varying degrees of crystallinity. Crystallinity is one of the decisive characteristics that determines the diffusion process and hydrolytic activity of the polymer in general [3]. However, it should be noted the contribution of the amorphous phase of the polymer, which may have a different packing density of macromolecules, and therefore, with approximately the same degree of crystallinity of the polymers, the diffusion coefficient will differ.

Experimental

Preparation of Samples

PLA samples with similar characteristics were chosen for our study: PLA1 4032D (Nature Works, United States) with a number-average molecular weight of 1.9×10^5 g/mol, density of 1.24 g/cm3, and a melt flow index (MFI) of 3–4 g/10 min; PLA2 Hycail HM 1011 (Finland) with a number-average molecular weight of 1.7×10^5 g/mol, density of 1.24 g/cm3, and MFI of 2–4 g/10 min. However, the crystallinity of PLA1 and PLA2 differed almost twofold. We studied the PLA1 and PLA2 films with a thickness of 100–110 μm obtained by pressing on a laboratory press at T = 185–190°C followed by cooling in air.

Electronic Paramagnetic Resonance

The molecular mobility in the amorphous phase was studied by the spin probe method on an automated EPR spectrometer (EPR-B, Semenov Institute of Chemical Physics, Russian Academy of Sciences, Moscow). The probe was stable nitroxide 2,2,6,6- tetramethylpiperidine-1-oxyl. The radical was introduced in the films from vapors at 50°C to a concentration

not exceeding 10–3 mol/L. The EPR spectra were recorded in the absence of saturation, which was checked according to the dependence of the signal intensity on the microwave field strength. The correlation time of probe rotation (τ) was calculated from the EPR spectra by the equation (1):

$$\tau = 6.65 \times 10^{-10} \Delta H^{+} \left(\sqrt{I^{+}/I^{-}} - 1 \right), \quad (1)$$

where ΔH^{+} is the width of the low-field component of the spectrum, and I^{+}/I^{-} – is the intensity ratio of low- to high-field components, respectively. The measurement error was ±7%.

Results

An EPR study of the molecular mobility of polylactide showed [4] that PLA2 had a denser amorphous phase: the correlation time of the probe was higher than that of other samples.

Consequently, the diffusion of water is determined not only by crystallinity, but also by the molecular structure of the amorphous part of the polymer. The EPR spectra recorded after reaching the equilibrium concentration of water do not differ in shape from the spectra of the initial PLA1 and PLA2 samples and represent a triplet [3]. A different situation is observed after 120 days of hydrolytic treatment. Figure 1 shows the EPR spectra of PLA1 and PLA2 after 120 days of treatment with sea water. The spectra are triplets for both types of polylactide, as they are for the original samples.

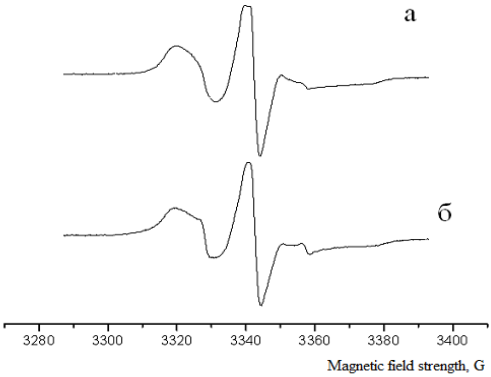

Figure 1. EPR spectrum of (a) PLA2 and (b) PLA1 after treatment with sea water for 120 days at T = 23°C

After the treatment with distilled water, the EPR spectra of PLA1 and PLA2 differ. The spectrum is a triplet for PLA2 and a singlet for PLA1 (Fig. 2).

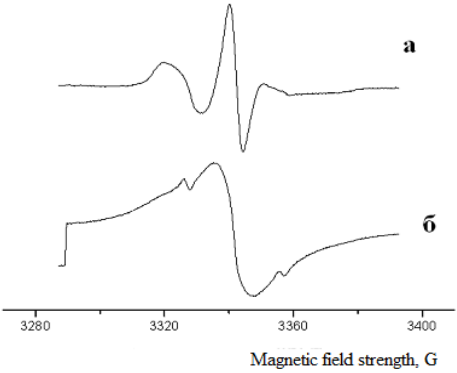

Figure 2. EPR spectrum of (a) PLA2 and (b) PLA1 after treatment with distilled water for 120 days at T = 23°C

The presence of a singlet may be explained by several factors. For example, when the destruction begins, pores are formed, and the radical “slips” through them. On the other hand,

this may be due to the increased density of the amorphous part of the polymer due to the formation of water associates and the impossibility for the radical to penetrate there. The experimental correlation times (τ) slightly decreased after the aqueous medium for both PLA types (Table 1).

Table 1. Correlation times in the samples after their treatment with an aqueous medium after the introduction of the radical at T = 50 ^{0}C.

Sample	$\tau \times 10^{10}$сек, original	$\tau \times 10^{10}$сек, distill. water	$\tau \times 10^{10}$сек, sea water
PLA1	10.2	----	9.1
PLA2	58.5	42.8	50.7

As is known, the polymers can contain water homogeneously dissolved in the form of individual molecules. This water can act as a plasticizer and increase the segmental mobility of the amorphous phase of the polymer. If water associates stabilized by hydrogen bonds are formed, they can hinder the motion of macromolecule segments. It follows from the foregoing that the effect of water on the structure and molecular dynamics of PLA is ambiguous.

In the case of PLA1 after treatment with distilled water, it was impossible to determine because, as noted above, a singlet was obtained. After the experiment with sea water, τ of PLA1 was close to τ of the starting sample. In this case, immobilization, which appears due to associates in the vicinity of ester groups, neutralizes plasticization, which leads to chain mobility in the amorphous phase.

So, under the action of a water medium, a set of factors such as the nature of the polymer, crystallinity, and density of the amorphous phase determines the transport properties of the polymer, thereby changing its molecular mobility and structure of polymers.

Acknowledgements

This study was performed using the instruments of the New Materials and Technologies Multiaccess Center (Emanuel Institute of Biochemical Physics, Russian Academy of Sciences, Moscow).

References

1. Yu.V. Tertyshnaya, S.G. Karpova, A.A. Popov. – *Rus J of Phys Chem B,* 11**(3),** 531-537 (2017).
2. Yu.V. Tertyshnaya, A.V. Lobanov, A.V. Khvatov. – *Rus J of Phys Chem B,* 11**(5),** 828-832 (2017).
3. E. Olewnik-Kruszkowska. – *Polym. Degrad. Stab,* **129**, 87-95 (2016).
4. Yu.V. Tertyshnaya, S.G. Karpova, O.V. Shatalova, A.V. Krivandin, L.S. Shibryaeva – *Polymer Science. Series A,* 58 **(1)**, 50-56 (2016).

Research of kern of an electronic spin resonance method

Larisa V. Tsyro[1], Alina A. Pichugina[1], Felix G. Unger[2]

[1]Institute of Natural and Technical Sciences, Surgut State University, Lenina avenue 1, Surgut, Russian Federation
[2]Chemical Faculty, National Research Tomsk State University, Lenina avenue, 36, Tomsk, Russian Federation
E-mail: larisa.tsyro@yandex.ru
http://www.surgu.ru

Introduction

At present, several geochemical systems, for example, the gas-oil-water-collector system which can be considered from positions of quantum chemistry of heterogeneous systems and questions of origin of oil are described [1, 2]. The debatable nature of oil origin models periodically leads to their analysis. By the ESR, NMR methods it is established that asphaltenes represent nearly 100% of the molecules containing unpaired electrons [3]. Precipitation of various water systems has shown that they are concentrates of paramagnetic molecules. Similarly and breeds of a collector (kern material) contains a large number of molecules with unpaired electrons. From all the above it follows that further study of oil-bearing areas should be carried out to compare the results of the analysis of oils containing well rocks and the results of the analysis of precipitation isolated from the water part of this system [1, 2]. In this paper, more attention is paid to the study of the last part of the system "gas-oil-water-collector" – reservoir rock.

Research Methods

As objects of a research samples of kerns of 45 fields of the Tomsk region have been chosen. Samples differ in the depth of the core and in the rocks. Among the examined deposits, it is possible to identify deep rocks with depths from 3000 m to 3300 m; medium-deep - from 2000 m to 3000 m; not deep deposits - from 1300 m to 2000 m. Soapstone, sandstone, aleurolite, coal and the interstratifying breeds generally occur among samples.

The electron spin resonance (ESR) method was used to analyze the cores. Preliminary preparation consisted of grinding a core sample in ball mills. The powder thus obtained was placed in an ampoule made of quartz glass, the ampoule was placed in the resonator of an ESR spectrometer. A spectrometer of the SE/X brand operating in the X-band was used. The device was tuned (the corresponding microwave modulation was selected), the spectrum was recorded. Conditions of spectrum shooting: a) field width 700 mT; b) sweep time 16 min; c) ν 9 GHz; d) the sensitivity was selected depending on the sample. Microwave modulation was selected in such a way that saturation would not occur for the sample.

Results

Consideration of a large number of kern spectra obtained by the ESR method for various rocks and deposits allows us to conclude that the nature of the spin centres in rocks. For all spectra, close forms of the lines are observed. This is due to the fact that the chemical composition of different rocks differs insignificantly, the kern materials differ in the degree of cementation. The ESR spectra of all rock types have a high intensity, a wide line and a rather complex and unresolved species. A more or less resolved hyperfine structure manifesting as a sextet indicates the presence in the rock of particles with a nuclear spin of 5/2 (for example, manganese, aluminum, magnesium, oxygen isotopes, etc.). The hyperfine structure of a narrow peak in the region g=2 in such samples can not be obtained because of the duration of the lattice spin-relaxation processes, as evidenced by the low microwave saturation power of this absorption peak. At the same time, short relaxation times are characteristic for the carriers of

all other signals, the saturation parameters for which are attained only at very high microwave power of the klystron.

In the kern material collections there are several deposits in which the cores are selected in a wide range of depths from 1300 m to 2900 m. For such deposits, it is necessary to separately consider the change in the concentration of spin centers as a function of the depth of occurrence (Fig. 1).

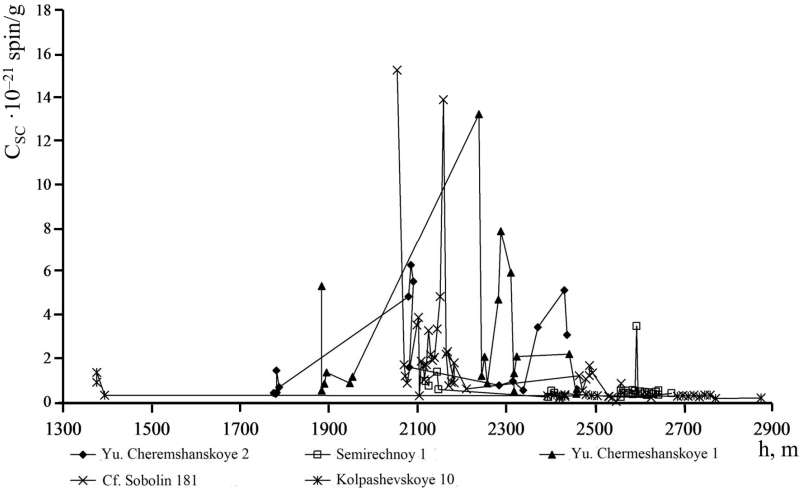

Figure 1. The change in C_{SC} for fields with a set of kerns in a wide range of depths

The figure clearly shows the area of the maximum value of the C_{SC} - this is an interval from 2000 m to 2300 m. In the area of more than 2300 m, the value of the C_{SC} decreases. The increase in C_{SC}, "bursts" of concentration occur for some samples of mudstone and sandstone, which are probably more friable than the rest of the samples. Thus, it can be stated that for most rocks the concentration of spin centers decreases with increasing depth of the kern.

Figure 2 shows an example of a spectrum with a pronounced singlet line with g-factor 2, which is manifested by the presence of free radicals of the organic matter of the kern.

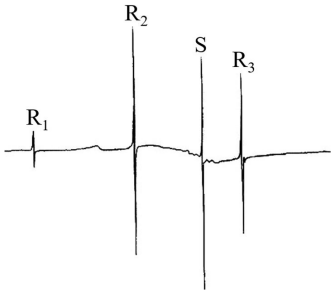

Figure 2. Spectrum No. 209 of the Core sample of the Kolpashevskoye deposit 10:
R_1, R_2, R_3 - position of peaks of reference rubies,
S - position of the line of the singlet of free radicals

The concentration of spin centers for the free radical singlet in the entire depth interval is of the order of 10^{18} spin/g. In the deep region, there is an increase in the spin centers for the free radical singlet for some samples - coal interbedded rocks. For these samples, the value can reach 10^{20} spin/g. The latter is a consequence of the fact that carbon will contribute to the singlet. Examples of samples with the characteristic under consideration are given in Table 1.

Table 1. These concentrations of spin centers for the free radical singlet (C^s_{SC}) for kerns of different deposits and rock types

Sample	Field	Rock	Depth of occurrence	$C^s_{SC} \cdot 10^{-18}$, spin/g
1	Archinskoye	Coarse argillite	3050.0–3055.0	1.6
2	Nizhne-Taboganskoye	Coarse argillite	2738.0–2739.0	18.7
3	Kalinous	Alyurolite	2818.0–2822.0	4.1
4	Kalinous	Argillite	2549.0–2557.0	2.0
5	Kalinous	Coal	2930.0–2936.0	226.0
6	Kalinous	Coal	2936.0–2941.0	626.7
7	North-Kalinove	Argillite	2636.0–2646.0	2.7
8	North-Kalinove	Argillite	2709.0–2713.0	7.6
9	North-Kalinove	Argillite	2690.0–2697.0	1.5
10	North-Kalinove	Interlocking clay, Alyurolite	2697.0–2705.0	2.5
11	North-Kalinove	Argillite	2592.0–2597.0	4.0
12	North-Kalinove	Argillite	2579.0–2605.0	2.8
13	North-Kalinove	Argillite	2608.0–2612.0	2.1

1. Spin properties are inherent in all sedimentary rocks irrespective of their type (argillite, aleurolite, sandstone, interlocking rock).
2. It was established that the concentration of spin centers of different rock types corresponds to a value of the order of 10^{21} spin/g. The change in the concentration of spin centers as a function of the depth of occurrence is dynamic, but there is a tendency to decrease with increasing depth, which is due to the compaction of the rock, which leads to the establishment of additional chemical bonds through overlapping and population of closed spin-orbitals by electron pairs.
3. The presence of organic matter in rocks with a concentration in the entire depth interval of the order of 10^{18} spin/g is shown.

Investigation of kern material is also necessary for studying the geological structure of deposits, determining reserves, drawing up schemes for development of deposits and searching for methods of influencing reservoirs. Therefore, the search for a possible correlation of traditional geophysical data with the data obtained by modern physicochemical methods, one of which is the ESR method, continues to be relevant.

References

1. L. N. Andreeva, L. V. Tsyro, S. Ya. Aleksandrova, F. G. Unger – *Chemistry of Oil and Gas: Proceedings of the VI International Conference. Tomsk: Publishing House of the Optics and Atmosphere of the SB RAS,* 1, 90-92 (2006) (in Russian).
2. L. N. Andreeva, L. V. Tsyro, S. Ya. Aleksandrova, F. G. Unger – *Chemistry of Oil and Gas: Proceedings of the VI International Conference. Tomsk: Publishing House of the Optics and Atmosphere of the SB RAS,* 1, 92-95 (2006) (in Russian).
3. L. N. Andreeva, L. V. Tsyro, S. Ya. Aleksandrova, F. G. Unger. – *Geochemistry,* 6, 670-678 (2004) (in Russian).

Theoretical analysis of the impact of the spin echo pulse sequence on a J-coupled two-spin system

K. V. Tyutyukin, S. A. Shubin, V. V. Frolov

St. Petersburg State University, 1, Ulyanovskaya str., St. Petersburg, 198504, Russian Federation
E-mail: kos101@mail.ru

Introduction

When the 90^0-τ-180^0-τ-echo pulse sequence is executed on the ω_{0H} frequency and the additional 180^0 pulse is applied to phosphorus simultaneously with 180^0 ^{1}H pulse, one can obtain a MR image of ^{1}H not coupled to phosphorus via indirect spin-spin coupling. By subtracting this image from a total proton distribution, we obtain an image of ^{1}H nuclei coupled to ^{31}P. Thus, we map the spatial distribution of components containing phosphorus in the sample.

Taking into account the fact that gyromagnetic ratio of ^{1}H is 2.5 times higher than that for ^{31}P, and, generally, NMR signal intensity is proportional to γ^3, one gains ca. 16-fold in intensity. Accordingly, it is expedient to obtain MR images of ^{1}H spins coupled to ^{31}P nuclei, obtaining the distribution of phosphorus in the sample as the result. The experimental result is shown in Figure 1.

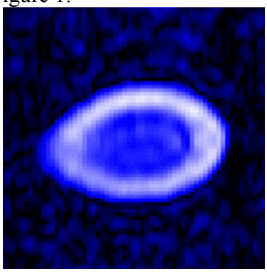

Figure 1. MR image with suppression of the signal from phosphorus in a sample of water-trimethyl phosphate

Theoretical calculation

The initial state of two-spin system H-P (equilibrium state), in the presence of a constant magnetic field B_0 applied in the z direction, is described by the reduced density operator. The density operator is written as a combination of the identity matrix and the matrix of the operator I_z.

$$\rho_0 = \begin{pmatrix} \frac{n}{2} + \Delta & 0 \\ 0 & \frac{n}{2} - \Delta \end{pmatrix} = \frac{n}{2}\begin{pmatrix} 1 & 0 \\ 0 & 1 \end{pmatrix} + 2\Delta \begin{pmatrix} \frac{1}{2} & 0 \\ 0 & -\frac{1}{2} \end{pmatrix} = \frac{n}{2}\mathrm{E} + 2\Delta I_z$$

$$E = \begin{pmatrix} 1 & 0 \\ 0 & 1 \end{pmatrix}$$

$$\rho_0 = I_z + S_z$$

I_z is the projection operator of spin H onto the z axis,
S_z is the projection operator of spin P onto the z axis.
The Hamiltonian of the spin-spin interaction, takes the following form:

$$H_{is} = 2\pi J S_z I_z$$

The total Hamiltonian in the rotating frame, taking into account the inhomogeneity of the static field B_0 and the chemical shift, can be written as follows:

$$H_{full} = \omega(r) I_z + 2\pi J S_z I_z + \omega_{cs} I_z$$

$\omega(r)I_z$ - Hamiltonian describing the inhomogeneity of the static field in the sample,
$\omega_{cs}I_z$ - proton chemical shift Hamiltonian,
$2\pi JS_zI_z$ - Hamiltonian of indirect spin-spin interactions.
As a result of the action of 90^0 pulses on ^{1}H spins, the density matrix takes the following form:

$$\rho_1 = e^{-iH_{rf}t_{90}}\rho_0 e^{iH_{rf}t_{90}} = I_x + S_z$$

$H_{rf} = B_1\gamma I_y$ - Hamiltonian of RF interaction
To calculate the resulting signal, we use the Average Hamiltonian Theory. For this purpose, we calculate the effective Hamiltonian in a frame of reference associated with the RF interaction, before and after the 180^0 pulse.
Let us consider the effect of two 180 pulses on ^{1}H and a pulse of arbitrary duration on ^{31}P on the total Hamiltonian of the internal spin-spin interactions.
The effective Hamiltonian of the system before applying two pulses is

$$H_{full} = \omega(r)I_z + 2\pi JS_zI_z + \omega_{cs}I_z$$

In the reference frame, which is connected with the RF interaction, which is described by the Hamiltonian. The Hamiltonian of the RF interactions can be written as follows

$$H_{rf} = \omega_{1I}I_x + \omega_{1S}S_x$$

Where we assume that $\omega_{1i}I_x$ and $\omega_{1s}S_x$ are much larger than all internal interactions in the Hamiltonian H_{full}. Thus, during the RF irradiation, internal interactions are ignored.
Upon the transfer to the reference frame associated with the RF-interaction, the internal Hamiltonian in the new interaction frame is calculated in accordance with expression:

$$\widetilde{H}_{int} = U_{ext}^{\dagger}(t)H_{int}U_{ext}(t) - iU_{ext}^{\dagger}(t)\frac{d}{dt}U_{ext}(t)$$

$U_{ext}(t) = e^{-iH_{rf}t_{\mathrm{p}}}$ - propagator of the RF-interaction H_{rf}
$\widetilde{H}_{full2} = U_{ext}^{\dagger}H_{full}U_{ext}$ - Hamiltonian of the system after 180^0 and X^0 pulses.

$$\widetilde{H}_{full2} = e^{iH_{rf}t_p}(\omega(r)I_z + 2\pi JS_zI_z + \omega_{cs}I_z)e^{-iH_{rf}t_p}$$
$$= e^{iH_{rf}t_p}(\omega(r)I_z + \omega_{cs}I_z)e^{-iH_{rf}t_p} + e^{iH_{rf}t_p}(2\pi JS_zI_z)e^{-iH_{rf}t_p}$$

Consider two terms individually:
The first term after substitution of Hint becomes:

$$\widetilde{H}_{full2}^{(1)} = e^{iH_{rf}t_p}(\omega(r)I_z + \omega_{cs}I_z)e^{-iH_{rf}t_p}$$

$H_{rf} = \omega_{1I}I_x + \omega_{1S}S_x$ - since RF-interactions, applied to nuclei of different types, do not affect each other or, in other words, the corresponding operators I_x and S_x commute, the effect of the two pulses can be considered separately. Therefore, the exponential operator in the expression can be divided into the product of two exponential operators. Therefore, in order to analyze the influence of a 180^0 pulse on the chemical shift Hamiltonian and the inhomogeneity of the field, we can confine ourselves to that part of the preceding equation that contains the operators of the hydrogen nuclei.

$$\widetilde{H}_{full2}^{(1)} = e^{iH_{rf}t_p}(\omega(r)I_z + \omega_{cs}I_z)e^{-iH_{rf}t_p} = e^{i\pi I_x}(\omega(r)I_z + \omega_{cs}I_z)e^{-i\pi I_x}$$
$$e^{i\pi I_x}I_z e^{-i\pi I_x}(\omega(r) + \omega_{cs})$$
$$(I_z\cos(\pi) + I_y\sin(\pi))\,(\omega(r) + \omega_{cs})$$
$$-(\omega(r)I_z + \omega_{cs}I_z)$$

Thus, after 180^0 pulses on protons, parts of the Hamiltonian linear in I_z change sign to the opposite.
Let us consider the he second term in Eq.
Since both terms in $H_{rf} = \omega_{1I}I_x + \omega_{1S}S_x$ commute with each other, then

$$\widetilde{H}_{full2}^{(2)} = e^{iH_{rf}t_p}(2\pi JS_zI_z)e^{-iH_{rf}t_p} = e^{i\omega_{1S}t_pS_x}e^{i\pi I_x}(2\pi JS_zI_z)e^{-i\pi I_x}e^{-i\omega_{1S}t_pS_x} =$$
$$2\pi Je^{i\pi I_x}(I_z)e^{-i\pi I_x}e^{i\omega_{1S}t_pS_x}(S_z)e^{-i\omega_{1S}t_pS_x}$$
$$\widetilde{H}_{full2}^{(2)} = 2\pi J(I_z\cos(\pi) + I_y\sin(\pi))(S_z\cos(\omega_{1S}t_p) + S_y\sin(\omega_{1S}t_p))$$

$$\tilde{H}_{full2} = -(\omega(r)I_z + \omega_{cs}I_z) + 2\pi J(I_z\cos(\pi) + I_y\sin(\pi))(S_z\cos(\omega_{1S}t_p) + S_y\sin(\omega_{1S}t_p))$$
$$\tilde{H}_{full2} = -(\omega(r)I_z + \omega_{cs}I_z) + 2\pi J(-I_z)(S_z\cos(\omega_{1S}t_p) + S_y\sin(\omega_{1S}t_p))$$

If in the experiment the angles of rotation of the pulses in both channels equal to 180^0, then the Hamiltonian does not change. And then throughout the entire experiment the effective (average) spin Hamiltonian is equal: $\bar{H} = \frac{(H_{full}\tau + \tilde{H}_{full2}\tau)}{2\tau}$

$$\bar{H} = \frac{2\pi J S_z I_z\tau - 2\pi J I_z\big(S_z\cos\omega_{1S}t_p + S_y\sin\omega_{1S}t_p\big)\tau}{2\tau}$$
$$\bar{H} = \pi J[S_z I_z + I_z\big(S_z\cos\omega_{1S}t_p + S_y\sin\omega_{1S}t_p\big)]$$

in the case of 180^0 pulses, the last expression equals to $2\pi J S_z I_z$.

Thus, as a result of the action of this pulse sequence, the chemical shifts and inhomogeneity of the static magnetic field B_0 are averaged (spin echo), while the effective average Hamiltonian of the spin-spin interactions does not equal to zero in general.

Let us consider the effect of the average Hamiltonian on the density matrix.

$\rho_1 = I_x + S_z$ – density matrix after a 90^0 pulse

$$\rho_2 = U_{\text{evol}}\rho_1 U_{\text{evol}}^{\dagger}$$
$$U_{\text{evol}} = e^{-i\bar{H}t}$$
$$\rho_2 = e^{-i2\pi J I_z S_z 2\tau}\rho_1 e^{i2\pi J I_z S_z 2\tau}$$

Let us Consider the effect of the Hamiltonian on the hydrogen part of the density matrix. In this case, the term of the density matrix describing the state of the phosphorus nuclei, S_z, is excluded from consideration, since the operator S_z commutes with the average spin Hamiltonian ($[S_z, 2I_zS_z]$=0). Consequently, the orientation of the spins of the phosphorus nuclei does not change its orientation.

Since there are three operators for which the cyclic commutation relation is fulfilled: I_x, $2I_yS_z$, $2I_zS_z$, then we can write:

$$\rho_{\text{final}} = e^{-i\pi J 2I_z S_z 2\tau} I_x e^{i\pi J 2I_z S_z 2\tau} + S_z$$
$$\rho_{\text{final}} = I_x\cos(2\pi J\tau) + 2I_yS_z\sin(2\pi J\tau) + S_z$$

The observed signal can be calculated according to the following equation:

$$S(t) = Tr\big\{(I_x(\cos(2\pi J\tau) + 2I_yS_z\sin(2\pi J\tau)) + S_z)(I_x + iI_y)\big\}.$$

Since in the experiment only the first term is directly detected, for minimization of the observed signal from the coupled ^{31}P-^{1}H pairs, the following condition must be fulfilled: $2\pi J\tau = \pi$, which leads to $\tau = \frac{1}{2J}$. In this case, one achieves the maximal contrast between different parts of the sample, where coupled and non-coupled subsystems are localized. The echo signal detected by the receiving RF-coil from the J-coupled spins is minimal in this case.

Summary

The results obtained in the theoretical calculations are in complete agreement with the experimental data. The maximum effect, suppression of the signal from ^{31}P, is observed with the parameters obtained by the theoretical analysis.

References

1. Malcolm H. Levitt, Spin Dynamics Basic of Nuclear Magnetic Resonance 2nd ed.
2. Laurance D. Hall, Timothy J. Norwood, and Steve C.R. Williams. Coupled-Spin-Filtered Imaging in an Inhomogeneous Magnetic Field. Journal of Magnetic Resonance 79 p.363-368 (1988).
3. A. G. Webb, S.C.R. Williams, and L. D. Hall. Generation of Coupled Spin-Only Images Using Multiple-Echo Acquisition. Journal of Magnetic Resonance 84 p.159-165 (1989).
4. Ernst R. R., Bodenhausen G., Wokaun A., Principles of Nuclear Magnetic Resonance in One and Two Dimensions. Clarendon Press, Oxford 1987. 610 Seiten: 1988.

Small-angle x-ray scattering profile of the two-domain Pax-5 protein in aqueous solution by molecular dynamics simulations

Milosh Ubovich[1], Sergei A. Izmailov[2], Andrei V. Egorov[1]

[1]Faculty of Physics, Saint-Petersburg State University, Russia
[2]Laboratory of bio-NMR, Saint-Petersburg State University, Russia
E-mail: ubovich.milosh@yandex.ru

Introduction

The two-domain Pax5 protein (see Fig. 1, PDB code 1MDM) is thought to contribute to many cancers [1]. Protein conformational dynamics are expected to be a key component in getting a deeper understanding of its function. However, no single experimental method can provide a comprehensive description of this aspect of the system behavior. In particular, the relative positioning of protein domains in proteins with significant domain mobility is difficult to quantify. In the present study the molecular dynamics (MD) simulations was used to address the issue of quantitative modeling of small-angle x-ray scattering (SAXS) profiles in aqueous solutions of the two-domain Pax5 protein.

Simulations details and results

MD simulations were performed using the Amber14 package [2] with ff14SB force field. A single Pax5 protein molecule was centered in the orthorhombic ($P2_12_12$) periodic cell with dimensions 101×79×97 Å and the rest of the cell were filled with the TIP3P water. The simulations were carried out in a *NVT* ensemble at 298 K. The system was equilibrated during the 1 ns run. Finally, the 1 μs simulation was performed. SAXS profiles were calculated using the *saxs_md* program included in the Amber package. The effect of the protein domains dynamics on SAXS profiles was given a special attention.

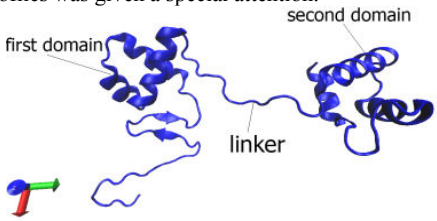

Figure 1. The structure of the Pax5 protein

Acknowledgements

The project was conducted using the computer facilities of the Laboratory of bio-NMR at Saint-Petersburg State University.

References

1. C. Perez-Borrajero, M. Okon, L. P. McIntosh. – *J. Mol. Biol.*, **428**, 2372-2391 (2016).
2. D. A. Case, V. Babin, J. T. Berryman, R. M. Betz, Q. Cai, D. S. Cerutti, T. E. Cheatham, III, T. A. Darden, R. E. Duke, H. Gohlke, A. W. Goetz, S. Gusarov, N. Homeyer, P. Janowski, J. Kaus, I. Kolossváry, A. Kovalenko, T. S. Lee, S. LeGrand, T. Luchko, R. Luo, B. Madej, K. M. Merz, F. Paesani, D. R. Roe, A. Roitberg, C. Sagui, R. Salomon-Ferrer, G. Seabra, C. L. Simmerling, W. Smith, J. Swails, R. C. Walker, J. Wang, R. M. Wolf, X. Wu, P. A. Kollman. AMBER 14, University of California, San Francisco, 2014.

High Resolution NMR Spectra and Dynamic Structure of Vinylcyclopropane

Vladislav V. Stanishevskiy[1], Dmitriy A. Cheshkov[2], Tatyana A. Ganina[1], Alla K. Shestakova[2] and Vyacheslav A. Chertkov[1]

[1]Lomonosov Moscow State University, Moscow, Russia
[2]State Research Institute of Chemistry and Technology of Organoelement Compounds, Moscow, Russia
E-mail: Stvladislav@yandex.ru

Introduction

Nowadays, the main trend in conformational dynamics reveal a tendency to studies of dynamic objects, characterized not by a discrete set of states, but by a continuous set of conformations. As parameters characterizing the conformational state of molecules in solution, we used spin couplings, which display well the fine features of intramolecular effects and are relatively weakly influenced by the medium.

Methods

As a model compound, we chose vinylcyclopropane with two rigid fragments and inhibiting some sort of hindered internal rotation of these fragments around a simple C_1-C_9 bond.

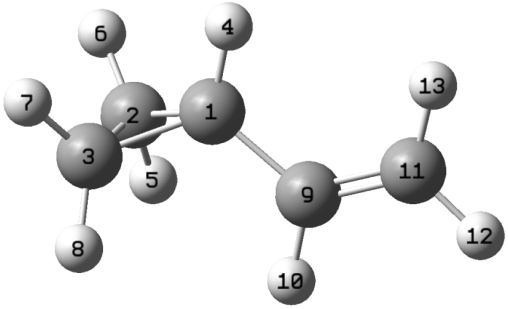

Figure 1. Structure and numbering of vinylcyclopropane

In the present work, synthesis of vinyl cyclopropane was carried out and high-resolution NMR spectra were recorded (Bruker AV-600, toluene-D_8, 303K). Analysis of the well-resolved multiplet structure in ^{1}H NMR spectra performed using the recently developed ANATOLIA program package [1] in frameworks of the total lineshape analysis approach [2, 3].

We have used the approach developed in our laboratory [4, 5], based on the description of the conformational dynamics of molecules in the framework of a model of the large amplitude vibrations, and on the use of spin-spin coupling constants for characterization of the dynamic process. The method includes a series of successive stages: the construction of a potential energy surface, the calculation of the coordinates of the reaction path, the calculation of the conformational dependencies of the spin couplings measured experimentally in this study.

Results

The potential of the inhibited internal rotation around a single bond connecting the vinyl group and the three-membered ring was obtained by scanning in in terms of the Møller–Plesset

second-order perturbation theory with basis set aug-cc-PVTZ, constructing the conformational dependences of the basic spin couplings in the FPT DFT (B3LYP) approximation with basis set aug-cc- PVTZ. The values of conformationally dependent spin-spin couplings averaged over the internal rotation are calculated. It is shown that the spin-spin coupling constants calculated by this method are in good agreement with the experimental data obtained by us.

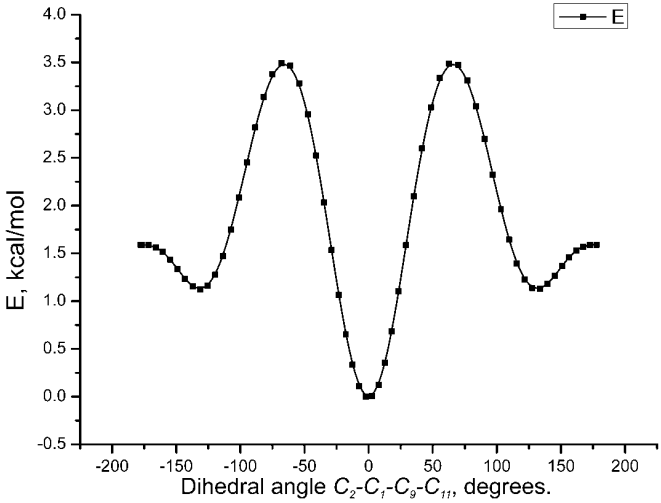

Figure 2. Potential energy surface of vinylcyclopropane

References

1. D.A. Cheshkov , K.F. Sheberstov , D.O. Sinitsyn , V.A. Chertkov– *Magn. Reson. Chem.,* **56**, 1-9 (2018).
2. V.A. Chertkov, D.A. Cheshkov, D.O. Sinitsyn– *eMagRes*, **6**, 359-368 (2017).
3. D.A. Cheshkov, D.O. Sinitsyn, K.F. Sheberstov, V.A. Chertkov – *J. Magn. Reson.,* **272**, 10-19 (2016).
4. T.A. Ganina, V.A. Chertkov – *Russ. J. Org. Chem*., **52**, 489-498 (2016).
5. T.A. Ganina, D.A. Cheshkov, V.A. Chertkov – *Russ. J. Org. Chem*., **53**, 12-23 (2017).

Poems about School

* * *

Чижик-Spinus, где ты был?
– «Я сигнал за хвост ловил!
Сделал я ему “Фурье” –
Закружилось в голове!»

Цели «Spinus»’а просты:
Дать научные мосты!
Пусть у вас здесь будет шанс
Пообщаться «в резонанс»!

В Школе здесь научат всех
Сочетать с наукой смех,
Дискотеки с Э-Пе-эР,
Я-Ка-эР и Я-эМ-эР!

В Школе много новых лиц,
Будем превращать их в птиц:
Вдруг хотя б одной из ста
Дастся «Нобель-высота»!

2010

* * *

Spinus, Spinus, where you were?
Did you dive in the Resonance world?
– “Yes! I dived with my great joy –
Resonance is a pleasant toy!”

“Spinus” school invited you
To look for a knowledge clue.
We will show the signal birth
In the field of our Earth!

If you wish to have success,
At the School achieve progress!
We will teach you all to fly
In the scientific sky!

We desire you to get
Many victories-побед!
It will be a good surprise
If you catch the Nobel prize!

2010

magnettech
by Freiberg Instruments

high performance electron paramagnetic resonance spectrometer

MiniScope MS 5000

ESR spectrometer with scientific grade performance

Next generation electron spin resonance spectroscopy (ESR). Combined state of the art electronics and extended experience of magnet and resonator engineering allow for more than a factor of two improvement in signal to noise ratio.

compact size

the ideal 'everywhere' spectrometer

45 kg, 397 x 262 x 192 mm

sensitivity & stability

outstanding sensitivity and magnetic field stability, extended data detection schemes

detection limit of 10 nM in PBS

versatile options

automated goniometer for measurement of angular dependencies, low temperature measurements, big collection of specialized sample holders and glassware, comfortable software for data handling and evaluation

autosampling for liquids, powder and solid samples

Wide field of applications

Life sciences
Nitric oxide measurement, reactive oxygen species, oxidative stress, radical generating systems, photo dynamic therapy

Food Chemistry and Pharmacy
Antioxidative features of foodstuff, radicals in foodstuff, radiation-induced radicals

Petrochemistry
Living polymers, nitroxide quantification, radicals in varnish, UV stability of scratch resistant varnish

Environmental Toxicology
Generation of radicals by particles

Alanine Dosimetry
Alanine dosimetry (tablets, thin films)

Separation of Radicals
EPR/HPLC coupling

Biophysical Features
Oxymetry, membrane fluidity, pH in microenvironment, viscosity, phase partition

Bioinorganic Chemistry
Bioinorganic transition metal compounds, fenton chemistry, effect of heavy metal ions on living tissue

Cosmetic
Radical protection factor, protection features of UV-filters in creme, shampoo, etc.

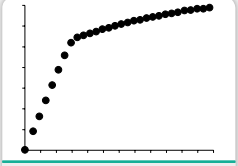
Kinetic of ROS generation by xanthine / xanthine oxidase

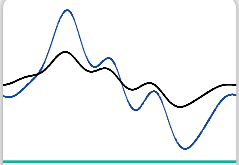
Basal (black) and stimulated (blue) NO generation by rat aorta

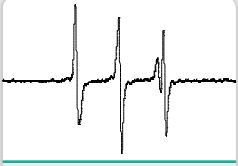
TEMPO in a two phase system oil/water


Spectrum of an Alanine tablet irradated with 5 Gy

Technical specification

Microwave	MS 5000	MS 5000X
Operating frequency	X-band	X-band
Sensitivity	5 x 10^9 spins/0.1 mT (5 x 10^9 spins/G)	3 x 10^9 spins/0.1 mT (3 x 10^9 spins/G)
Signal to noise ratio	(600:1)	(1000:1)
Microwave power	1 µW – 100 mW	1 µW – 100 mW
Concentration sensitivity	50 pM	10 pM
Field sweep range	650 mT (6500 G)	660 mT (6600 G, wider ranges on request)
Field homogeneity	± 5 µT (50 mG) within sample region	± 5 µT (50 mG) within sample region
Field stability	1.0 µT/h (10 mG/h)	1.0 µT/h (10 mG/h)
Sweep resolution (field and time)	≥ 125,000 points	≥ 250,000 points
Reference standard	optional: Integrated and motorized	optional: Integrated and motorized
Magnetic field range	0 to 650 mT (0 to 6500 G)	-10 to 650 mT (-10 to 6500 G, wider ranges on request)

Accessories

Autosampler for powder and solid samples

automated handling of up to 23 samples in quarz tubes 3–6 mm diameter, precise hight positioning within resonator for highest reproducibility.

Autosampler for liquids

Automatic liquid sample transfer for spectrometers of the MiniScope series, Autosampler and integrated peristaltic pump, software controlled. Software for kinetic measurements, including automatic data acquisition and data evaluation. Single or multiple chemicals, optional: automated component mixing and temperature control.

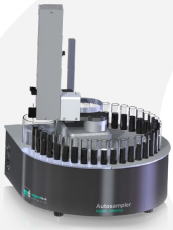

Temperature Controller – TC H04

Temperature range 93 – 473 K. Liquid nitrogen storage, measurement with cavity integrated nitrogen dewar.

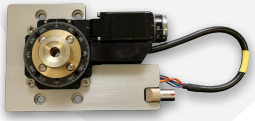

Automated Goniometer

Fully automated angular rotation of sample, step size 0,1° to 180°. Each measurement of a new spectrum starts with an automated readjustment of the spectrometer for best measurement performance.

Dewars

To manually cool the samples.

Bio Temperature Controller

For temperatur stabilization of biological systems like tissue samples.
Temperature range: 293 – 350 K.

Glassware

50 µl capillaries, flat cell and special holder SH-P, tissue cell, sample tubes, finger dewar, etc.

Tissue Cells

For tissue samples.

Highlights

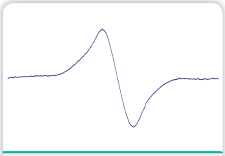

1 µM TEMPO (one line)

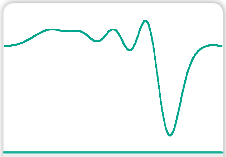

SOD mimetic Cu (II) complex

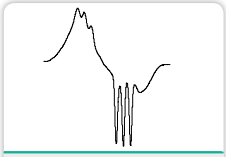

NO-Hemoglobin

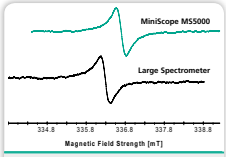

Weak pitch: P = 12 mW, modulation = 0.2 mT

Detection limit
10 nM in PBS

Available standards
Chromium and Manganese
Wide magnetic field range
(30 – 650 mT)

Ultra fast and stable auto frequency control
No spikes due to liquid nitrogen bubbles

Sensitivity of MS 5000 bench top spectrometer compared to large stationary spectrometer with universal TE 102 cavity

Software – ESRStudio

ESRStudio is the most modern and dynamic software for ESR measurements with convenient workflow based user interfaces.

Highlights:

- Most advanced operating and data evaluation software
- Modern and user friendly user interfaces
- User/application based customization
- Advanced scientific capability
- Work flow for automated spectrum evaluation
- Automated report generation for convenient research work
- Versatile optimization of parameters like signal amplitude, phase of magnetic field modulation etc.

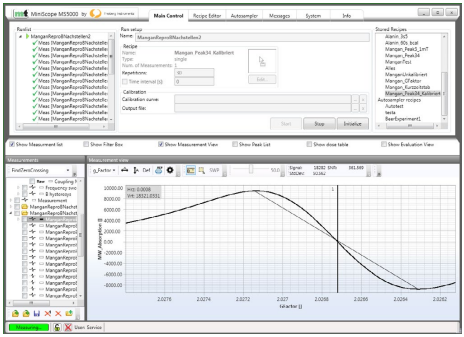

Contacts

Magnettech GmbH
Ernst-Augustin-Str. 12
D-12489 Берлин, Германия
Тел.: +49 30 6780 2526
Факс: +49 30 6322 4101
E-mail: sales@magnettech.de
www.magnettech.de

Официальный дистрибьютор в России:
ООО «Промэнерголаб»
107392 Москва, Россия, ул. Просторная, д. 7
Тел./Факс +7 (495) 221-12-08
8 800 234-12-08
E-mail: info@czl.ru
www.czl.ru

VQZ Bonn Zertifiziert DIN EN ISO 9001

Europa fördert Sachsen. EFRE Europäischer Fonds für regionale Entwicklung

Author Index

Notes

Notes

Magnetic Resonance and its Applications

Abstracts book

Saint Petersburg State University
April 1-6, 2018

Подписано в печать 21.03.2018. Формат 60 × 84 1/16.
Бумага офсетная. Verdana. Печать цифровая.
Усл. печ. л. 16,27. Тираж 150 экз. Заказ № 454.

Отпечатано в Издательстве ВВМ .
198095, Санкт-Петербург, ул. Швецова, 41.

Schedule of Spinus-2018

	01.04.18 Sunday	02.04.18 Monday	03.04.18 Tuesday	04.04.18 Wednesday	05.04.18 Thursday	06.04.18 Friday	07.04.18 Saturday
08:45 – 10:00		BREAKFAST				9:10-10:30 BREAKFAST	BREAKFAST
10:00 – 11:30		**Registration 30** **Opening 10** **Chizhik 30** ***GROUP PHOTO 20***	**Fujara 40** Privalov 20 Chertkov 15 Ryzhov 15		**Cabal 40** Svyatova 15 Mikhailovskaya 15 Drozdov20	**Vasiliev 40** Mozzhukhin 20	**Departure**
11:30 – 12:00		COFFEE BREAK			COFFEE BREAK		
12:00 – 14:00		**Papavassiliou 40** **Varela 40** **Dvinskikh 40**	**Rameev 40** **Fraissard 40** **Michel 40**		Schepkens 20 Dallons 20 Kumaravel 20 **Skrynnikov 40** Kharkov 20	Atta 20 Krylova 15 Pokochueva 15 Marchenko 15 Ievlev 15 Babanova 20 Okrugin 20	
14:00 – 15:30		LUNCH			LUNCH		
15:30 – 17:00		Bystrov 15 Baranauskaite 15 Shuvarakova 15 Dolgorukov 15 Mamadazizov 15 Zorin 20	Oral blitz reports of young scientists (5min x 14) Lahderanta 20		Oral blitz reports of young scientists (5min x 18)	Dolgushev 20 Shpotya 20 Zinkevich 20 Kosenkov 15 Neronov 15	
17:00 – 17:30	**Registration of participants**	COFFEE BREAK			COFFEE BREAK		
17:30 – 19:00		Izmailov 15 Rabdano 15 Semisalova 20 Grunin 20 Kachala 20	**POSTER SESSION I**		**POSTER SESSION II**	Kulagina 20 **Samoson 40** **Awarding Closing**	
19:00 – 20:00		DINNER				DINNER	
20.00	**Welcome**	**Cultural and sporting activities**		**Round table Chairman: Sergeyev**	**CONFERENCE DINNER**		